Quantifying Lake System Dynamics

By

Daniel James Herron

B.Sc. (Hons.) University of Liverpool

A thesis submitted in fulfilment of the requirements for
the Degree of Doctor of Philosophy of
the University of London

Department of Geological Sciences
University College London
University of London

October 2001

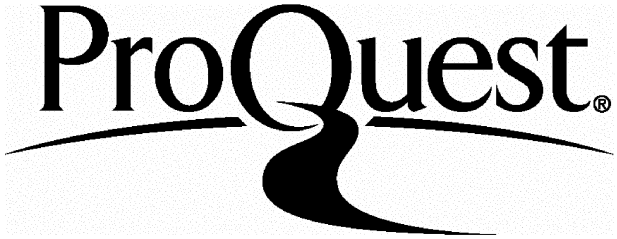

Abstract

Analysis of thickness time series, generated from varved sediments originating from lakes in the Arctic, USA, Finland, Germany and Poland, and intermittently spanning the last ca. 15,000 cal yrs BP, reveals a range of system dynamics. Lake sedimentation leading to varve formation can be considered in terms of the quantity and stratigraphic position of the sedimentary deposit. The amount of sediment deposited is statistically represented by gamma and log-normal distributions. This suggests sedimentation is characterised by a series of random depositional events that are added and multiplied over time, respectively. Phase portraits qualitatively indicate scale invariance. Power spectra, autocorrelation functions and fluctuation analysis quantitatively confirm scale invariance over all resolvable orders of magnitude, with exponents in the range ca. $H = 0.6$ to 0.9. Crossovers occur in the power spectra on ca. 100 yrs timescales for some lakes, indicating the possible presence of changes in dominant timescales of large scale climatic processes. Deviations from established relations between scaling exponents, and differences from the AR(1) null hypothesis, both based on random walk processes, indicate the role of other underlying scaling mechanisms, such as (self-organised) critical phenomena and/or multiscaling. E-folding times calculated from waiting time analysis indicates lake systems are characterised by two states, characterising the "main" dynamics on decadal timescales, and the "extreme" dynamics up to centennial timescales. The e-folding times for the main system processes compare well with some of those calculated from the autocorrelation function and AR(1) process, again indicating the presence of other complex dynamics. Effectively, lakes are threshold systems with random forcing on different timescales. No relations were isolated for correlations between basic physical parameters and statistical exponents, indicating the individualistic nature of lake systems. This is confirmed by the lack of spatial correlation between averaged, but unshifted lake systems. This is attributed to insufficient atmospheric spatiotemporal smoothing, the thermal regime of lakes displaying a greater response to slower long term processes, rather than faster shorter term processes, and to the occurrence of extreme events, which ultimately control the emergence of correlation, up to and beyond centennial timescales.

Acknowledgements

The completion of this Ph.D. thesis owes as much to the efforts of other people as it does to my own. Considering the traditional ups and downs of conducting research, together with my own particular personality traits, it is no mean feat that I find myself in a position to be able to thank those people. Firstly, for setting me on the road of research I'd like to thank Jurgen. I also owe a huge debt to the data contributors, Heikki and Josef in particular. In addition, the analysis of this data could not have been possible without the colossal help of Peter, and the final presentation owes much to the equally impressive design skills of Holger. Beyond the tangible object that is my thesis, many others have played an equally important role in ensuing its completion. Fellow research students have made the path to completion a much smoother ride. I am particularly indebted to; Dave, Ossie, Valentina, Dave, Rhodri, and Alex, as well as Dave, Matt, Kate, Danny, Sean, Arthur, Dave and Louise. The efforts of Ron, Leisa, and Celine made the administrative aspects of the research all the easier. Light, and not so light relief was provided by; Stephen, Russell, Chris, Paul, Rob, Mook, Mike, Alison, Salwa, Georgia, Michele, Shermayne, Shirley, Vassilis, and Franck; and to the numerous significant others. I would especially like to thank my mam and dad, Jean and Joe, who have been unstinting in their emotional and financial support throughout the Ph.D., as they have been before and will no doubt be after. Without the collective efforts of these people there would quite simply be no thesis, and for that I am very thankful.

Contents

List of Figures

List of Tables

Chapter 1

Introduction

1.1 Overview and Aims

It is the aim of this study to apply the qualitative concepts of general systems theory, together with robust time series analysis in order to quantify temporal and spatial lake system dynamics, in particular aspects of sedimentation. General systems theory has been advocated as the theoretical framework for describing observations and thus developing knowledge of natural systems [1], [2], [3], [4]. General systems theory is based on the premise that all systems possess four properties; (i) wholeness and order, (ii) adaptive self-stabilisation, (iii) adaptive self-organisation, (iv) intra- and inter-systemic hierarchies [3]. Or, stated more simply, natural systems are; (i) wholes with irreducible properties, (ii) maintain themselves in a changing environment, (iii) create themselves in response to self-creativity in other systems, and (iv) are co-ordinating interfaces in nature's hierarchy [4]. General systems theory has been successfully applied in ecology [5], [6] and geomorphology [7], [8], [9], [10], [11], [12]. Below we outline the dynamics of natural systems and lake systems, including the generation of the time series analysed in this study.

1.2 Natural System Dynamics

1.2.1 Structure, Thresholds and Feedbacks

Natural systems are structured sets of interconnected objects, forming an entity embedded in an environment [13],[11]. Natural systems are characterised by; (i)

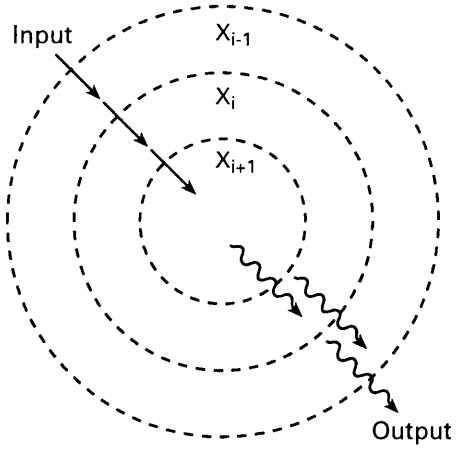

Figure 1.1: Schematic diagram illustrating the arrangement of hierarchy in an open natural system. Each level (X_i) has a thermodynamic input (straight arrow) and output (curly arrow), and dissipation of energy. After [5].

hierarchically arranged subsystems and system components, or elements [14], [15], [16], [17] (see Figure 1.1.), (ii) coupling between fast varying local variables, and slow varying global variables [18], [19], [20], [21], and (iii) strong internal interactions - self-organisation processes [22], where global phenomena can emerge through synergistic processes [23], [24], [25], and weak external interactions with the surrounding environment.

These system dynamics can be characterised from a holistic perspective, i.e., whole, or reductionist, i.e., components. Generally, the notion of "whole" is primary in relation to the notion "system". Consequently, as Koestler [26], recognised that each hierarchical level is both part and whole of the system, so that each system is at the same time both a self-contained whole to its subordinated subsystems and a dependent part of its supersystem.

The two main system mechanisms are thresholds and feedbacks [27]. Thresholds are boundaries beyond which change occurs through the action of internal or external processes (see Figure 1.11.) [28], [29], [30]. It is recognised that although thresholds are easily conceptualised, they are difficult to identify and quantify [31]. Feedback mechanisms are classified as positive, which amplify processes, or negative, which dampen processes [27] (see Figure 1.2.). They operate in accordance with response and relaxation times, comprising a range of system parameters that

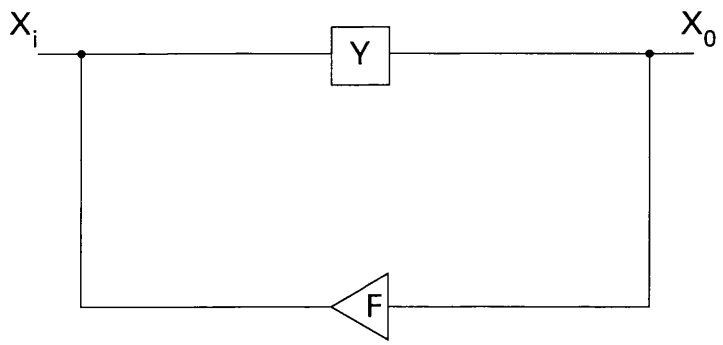

Figure 1.2: Schematic diagram illustrating system feedback. X_i is the imput, X_o is the output, Y is the transfer fucntion, and F is the feedback.

interact additively and multiplicatively [32].

The response time is the time it takes a system to respond to a change of an input [13]. The relaxation time is the time it takes for a system to return to an equilibrium state following a perturbation, often characterised by a particular fraction, e.g., $1/e$ [34]. These can create an instantaneous or lagged system response in time and space. Typically, linear dynamics are characterised by an instant response, and proportional causes and effects, while nonlinear dynamics are characterised by a lagged response, and non-proportional causes and effects (see Figure 1.3.). The simplest way to observe linear and nonlinear phenomena is in the dynamics of a particle oscillating in a double well potential (see Figure 1.3.).

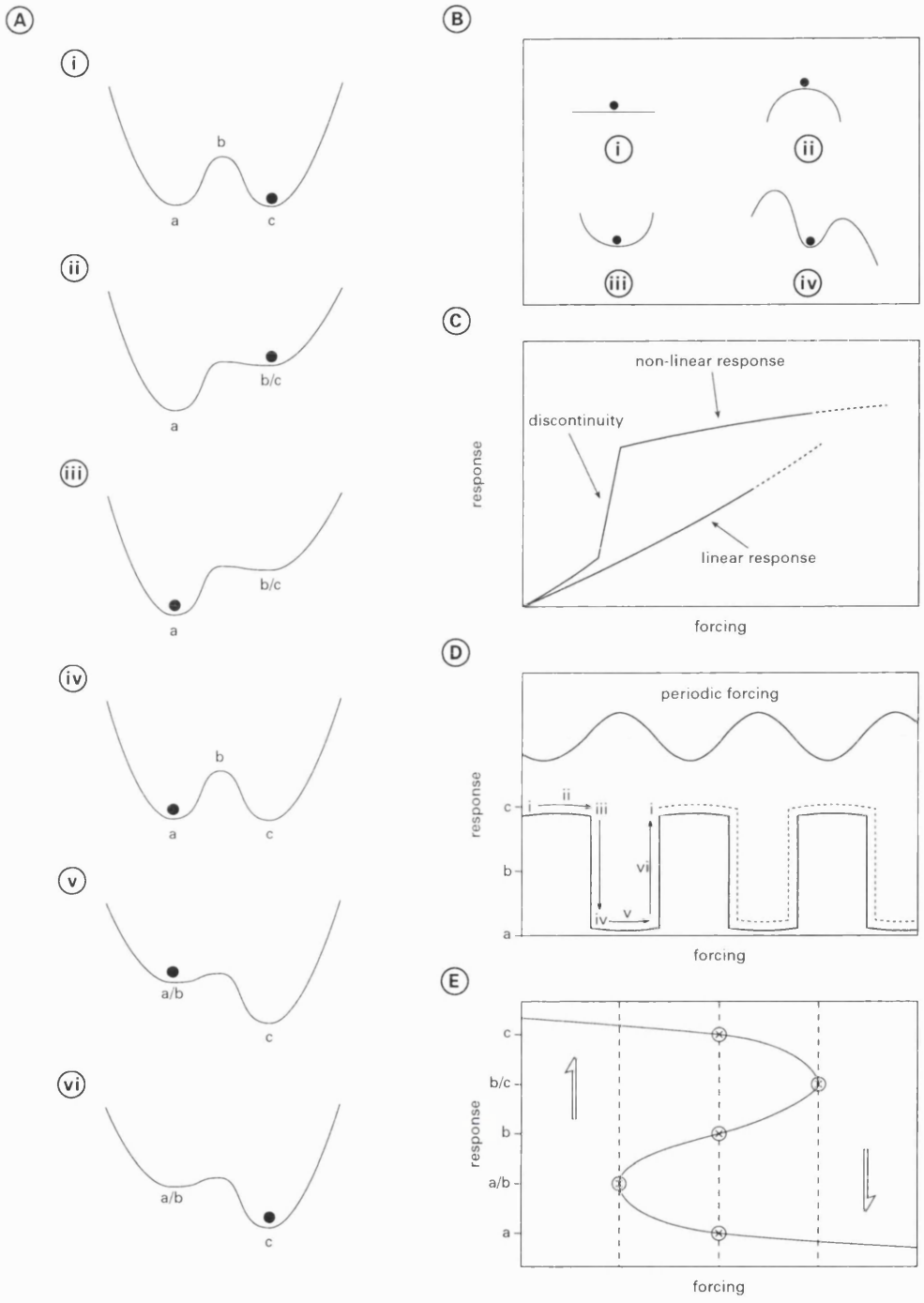

Figure 1.3: Schematic diagram illustrating the dynamics of a double well potential. B.i. object in neutral equilibrium, B.ii. object in unstable equilibrium, B.iii. object in stable equilibrium, B. iv. object in metastable equilibrium. C. a linear response is proportional to the forcing mechanism, while a nonlinear response is non-proportional, and is characterised by discontinuities. A. and D. show the (linear) response and evolution of a particle in a double well potential under the influence of a periodic forcing (sine curve). E. shows the classical (nonlinear) hysteresis (lag between application/removal of a force) curve of A. and D. Adapted from [35].

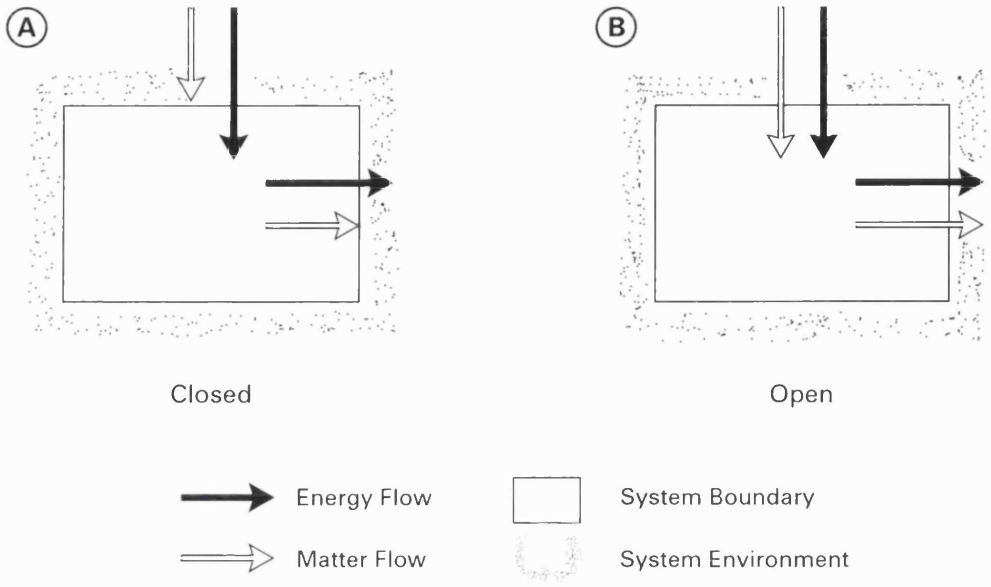

Figure 1.4: Schematic diagram illustrating the types of natural systems. A. closed systems are characterised by the input and exchange of only energy with the environment. B. open systems are characterised by the input and exchange of energy and matter with the environment. After [33].

1.2.2 Thermodynamics

As natural systems consist of a very large number of elementary entities possessing internal energy, they can be described thermodynamically; (i) isolated systems - these do not allow the transfer of either matter or energy across their boundaries, (ii) adiabatically isolated systems - here the transfer of heat (and also of matter) across the boundaries is excluded, but not the transfer of other forms of energy, (iii) closed systems - only the transfer of matter is excluded, (iv) open systems - the passage of energy together with the molecules of some (but not necessarily all) matter [36] (see Figure 1.4.).

System change is represented by entropy, given as, $dS = dS_i + dS_e$, where dS is the total change of entropy in the system, dS_i is the entropy change produced internally by irreversible processes and dS_e is the entropy transported externally across the system boundaries. In an isolated system, dS increases or remains constant, as it is uniquely determined by dS_i, which necessarily grows as the system performs work (work may be reversible, whereas entropy grows as irreversible processes, e.g.,

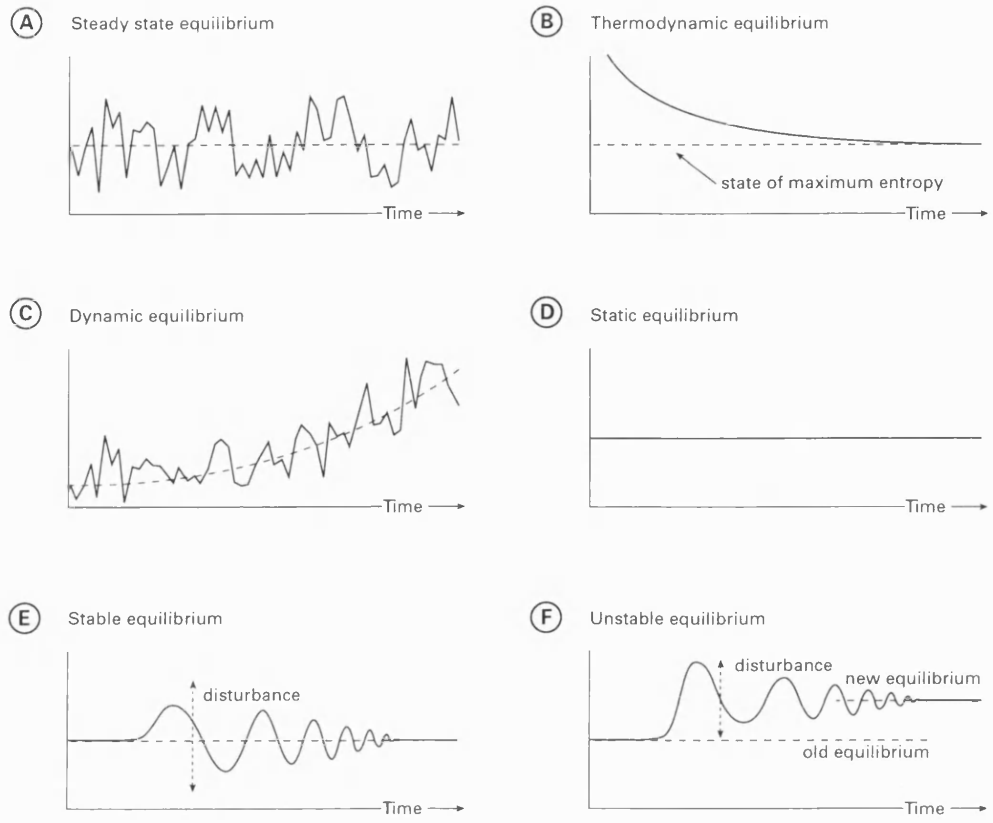

Figure 1.5: Schematic diagram illustrating the types of equilibrium. A. steady state equilibrium. B. thermodynamic equilibrium. C. dynamic equilibrium. D. static equilibrium. E. stable equilibrium. F. unstable equilibrium. After [27].

friction). All available energy is degraded and all concentrations of matter are dissipated. The system ceases to undergo change when the entropy reaches its maximum. The system has then reached an equilibrium state (see Figure 1.5.) corresponding to the state of maximum particulate disorder [37].

However, natural systems are not isolated systems, as their boundaries let through energy. When the system receives a boundary flow of free energy from its environment, dS_e it can offset the entropy produced within the system dS_i and may even exceed it. Thus, dS in an open system need not be positive, and can be zero or negative. So if $dS = 0$ then the system is in a steady state. However, conditions when $dS_e = dS_i$ are rare for any extended period of time, and systems are thus metastable, i.e., fluctuating around the states that define their steady states, rather than settle into them without further variation. However, if $dS < 0$, then the sys-

tem will move away from equilibrium. Here externally derived free energy, dS_e will lead to the storage and cycling of matter, energy, and information (characterised by a quantity - "extent" and a quality - "content" [38]), which move the system further from equilibrium. This is reflected in decreased internal entropy, dS_i and increased internal order and organisation, dS_o (an arrangement of selected parts so as to promote a specific function). Entropy change in such a system is given as, $dS_e - dS_i < 0$ [37], i.e., the entropy produced by irreversible processes within the system is shifted as boundary outputs into the environment. This is reflected in decreased organisation and increased entropy of the environment [39]. Prigogine [24], termed natural open systems out-of-equilibrium as "dissipative structures". In natural systems, matter can be viewed in terms of local processes, and energy in terms of global processes.

1.2.3 Phase Space and Almost Intransitivity

The state of a natural system at any instant in time is described by the state variables in n-dimensional phase space. As natural systems are open and dissipative (as opposed to conservative - Hamiltonian systems with divergent trajectories), system evolution is generally characterised by trajectories in phase space, contracting and eventually converging to some bounded subset, i.e., an attractor [40]. There are four types of attractor; (i) point attractors, which lead to a steady solutions, (ii) limit cycles, which lead to periodic solutions, (iii) torus attractors, which lead to quasiperidic solutions, and (iv) strange attractors, which lead to aperiodic (chaotic) solutions (see Figure 1.6.).

Quantifying natural system evolution is dependent on the notion of stationarity. In natural systems an ensemble average of an infinite number of realisations is often not available, and they are typically represented by only one realisation, i.e., one time series. However, if the time series is sufficiently long, and in a finite time the system passes through all the possible states accessible to it, then it can be shown that where $T \rightarrow \infty$, the time average $\bar{x}_T$ is equivalent to the ensemble average, and the infinite limit can be relaxed, i.e., ergodicity [41]. In such circumstances, systems are described as stationary, and the system is termed transitive (see Figure 1.8.)

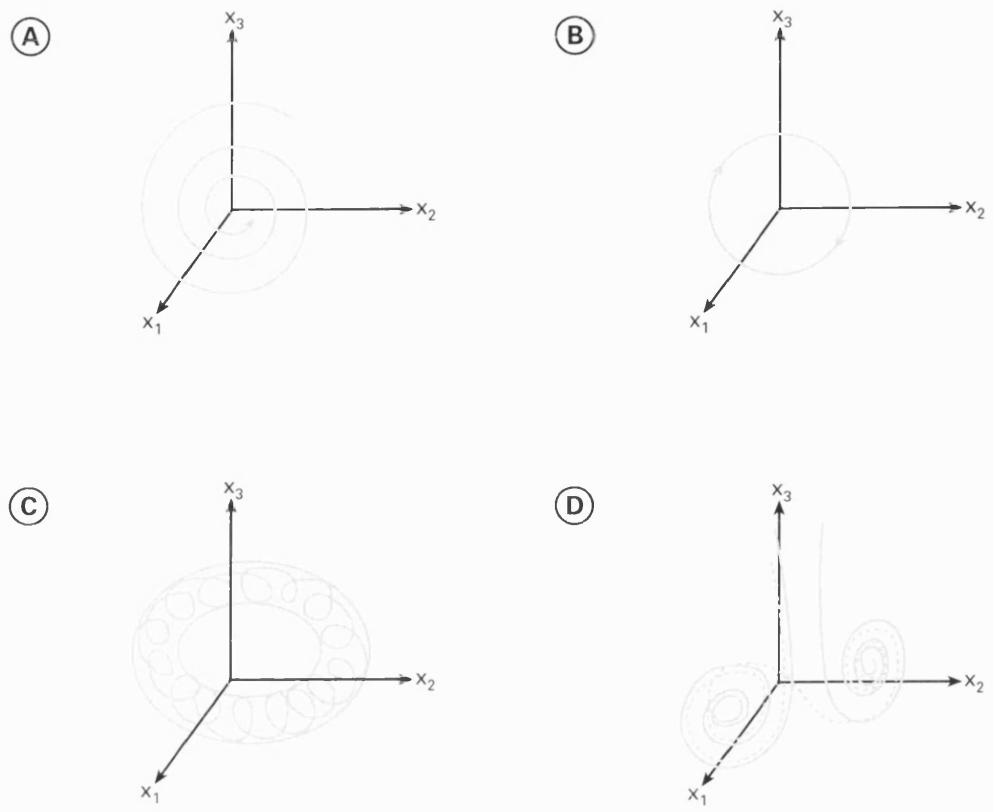

Figure 1.6: Schematic diagram illustrating the types of attractors. A. point (damped harmonic oscillator), B. limit (driven harmonic oscillator), C. torus, D. strange (switching basins).

[42]. However, it is possible that during the course of its evolution, a transitive system may possess different sets of statistics, which are defined over a finite time interval. These shifts from one state to another are termed bifurcations (see Figure 1.7.).

Effectively, bifurcations represent the exceedence of a threshold, characterised by stepwise reorganisation [43], with each new system configuration characterised by a solution of the system equations [44], [40]. In principle, it is possible that the state of natural systems after a long time could end up in one of several steady states, i.e., intransitive (see Figure 1.8.), though such a scenario is considered doubtful [45], [42].

As such, many natural systems are considered "almost intransitive", i.e., in a continual state of transient adjustment [44], [11], [39] (see Figure 1.8.). Almost

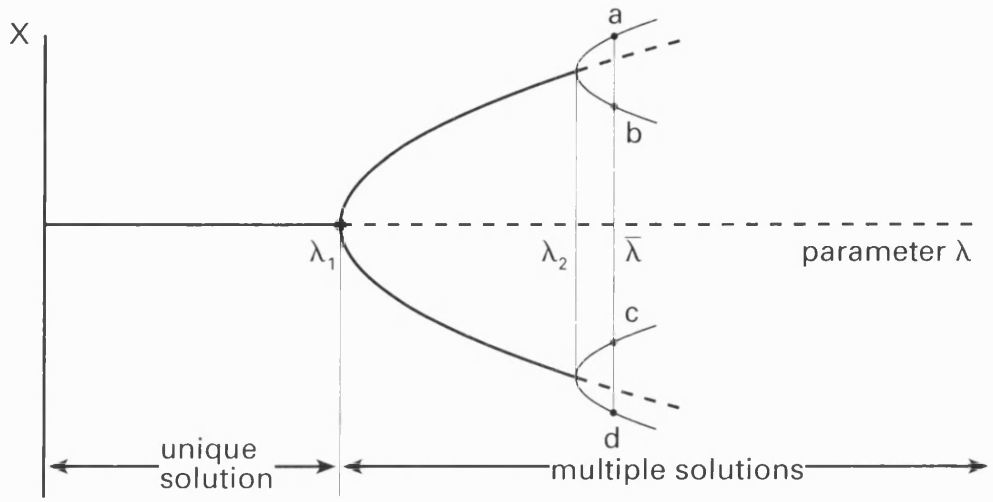

Figure 1.7: Schematic diagram illustrating the concept of bifurcation. New branches of a parameter are generated at values $\lambda_1, \lambda_2, \lambda_3, ...$, referred to as bifurcation points. These yield a range of possible states, branches (a) to (d) for the value $\lambda = \bar{\lambda}$. After [40].

intransitivity has been invoked in climatology [46], [47], [48], ecology [49], [50], and solar activity [51]. These various types of system evolution can be characterised by single and double well potentials and related attractors (see Figure 1.9.)

1.2.4 Statistical Distributions

The dynamics of natural systems appear in time series and statistical distributions and are represented by relations between the statistical moments, in particular between the mean and variance (see Figure 1.10.). Typically, these are nonlinear relations, i.e., a small change in the mean can result in a large change in the frequency of extremes [52]. The variance exerts most influence over the frequency of extreme values [53]. Changes in the mean and variance represent the crossing of system thresholds, where the system behaviour (sensitive to internally and/or externally generated forcing) is governed by critical levels, which determine the output of the system as robust or responsive (see Figure 1.11.) [54], [55]. Such system variability is essentially on all temporal and spatial scales (see Figures 1.12. and 1.13., respectively), and the perception of any form of system dynamics, particularly response time, is scale dependent.

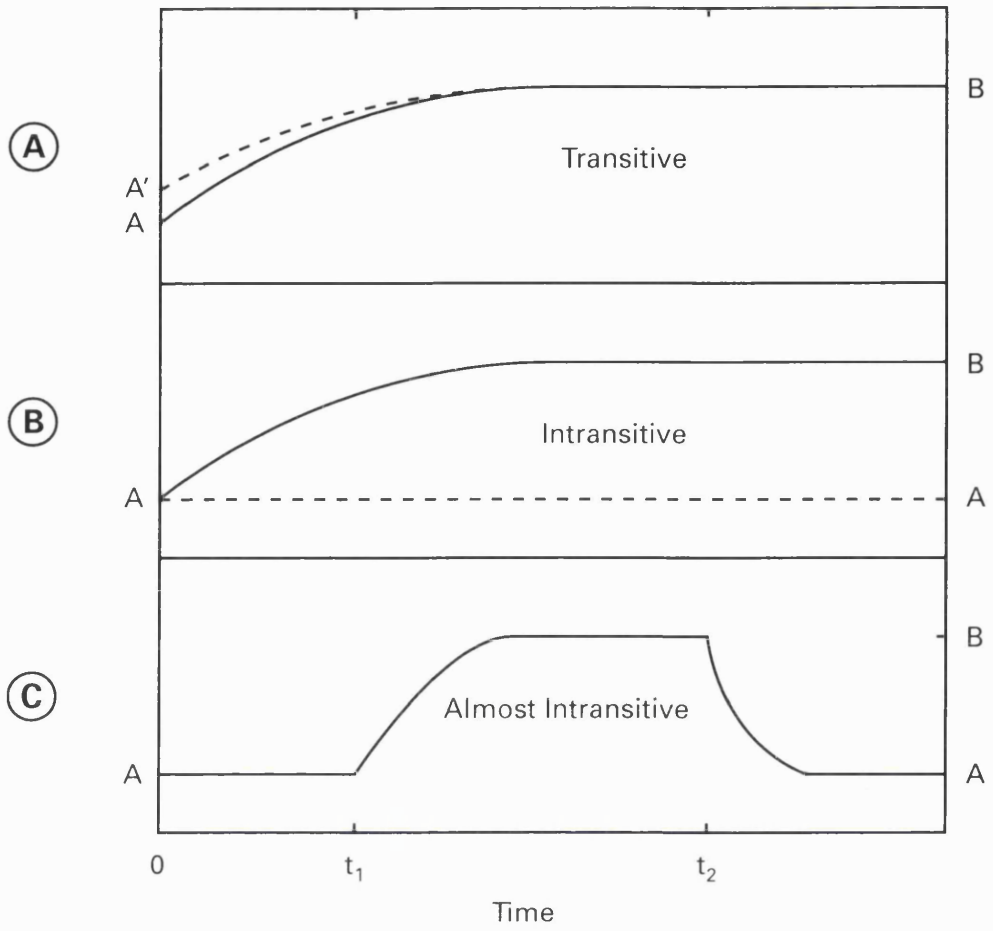

Figure 1.8: Schematic diagram illustrating the forms of natural system evolution. A. a transitive system is characterised by two different initial states A and A' which evolve into the same equilibrium state B. B. an intransitive system is characterised by two or more alternative equilibrium states A and B for the same boundary conditions. C. an almost intransitive system is characterised by intransitive behaviour for a given period of time, shifting (e.g., at time t_1 - caused by forcing) to an alternative state B where it may remain until a time t_2. Then after returning to state A it may remain there or undergo further shifts. After [42].

Natural systems yield a range of statistical distributions (e.g., power-law, stretched exponential, and/or log-normal distributions). Power laws are very common in nature [60]. They represent scale invariant dynamics, also termed scaling, persistence, dependence, serial (long) term (range) correlation, memory, self-affine, self-similar, and 1/f noise. This statistical similarity/affinity incorporates variability and transitions at all temporal and spatial scales, from which a straightforward connection

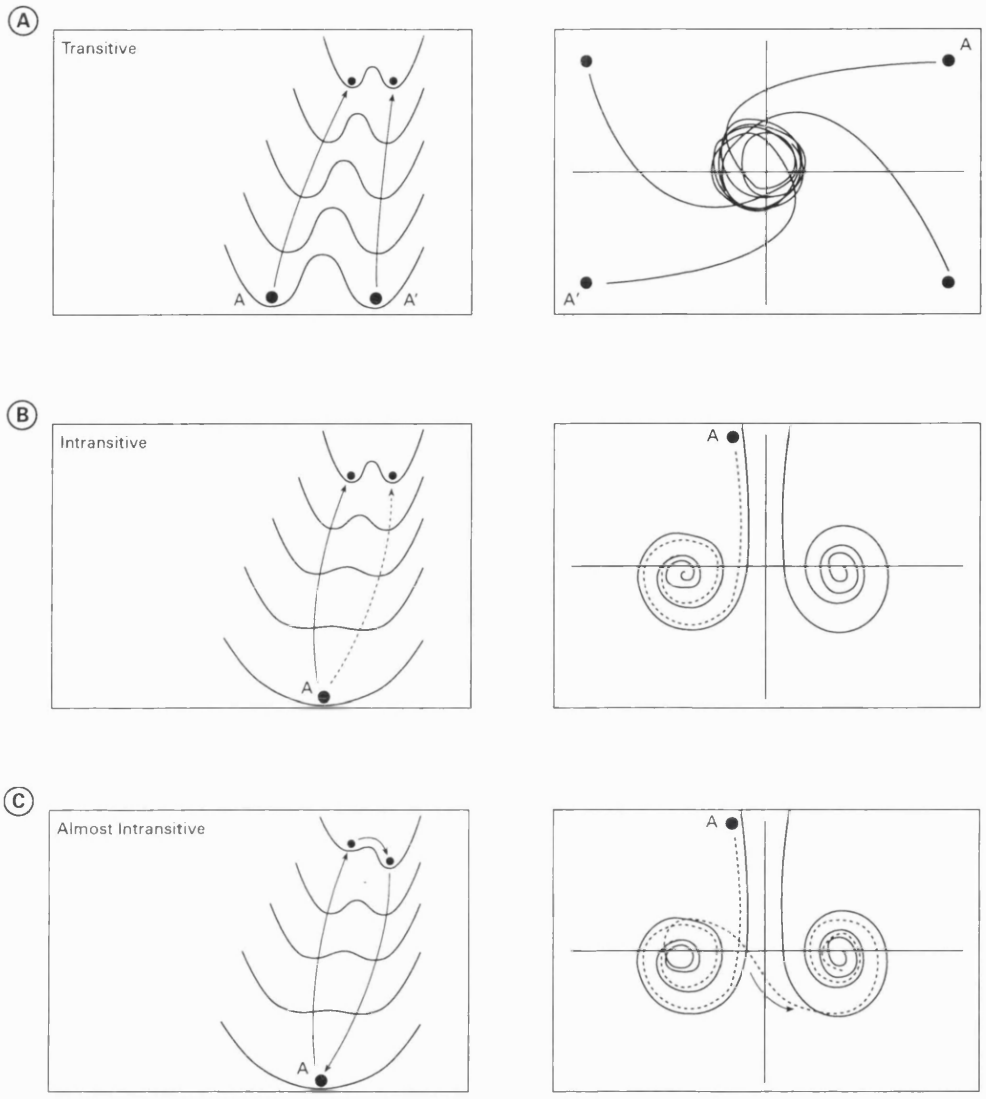

Figure 1.9: Schematic diagram illustrating the evolution of dynamics of single and double well potentials and related attractors. This figure relates the evolution of the system type, effectively, single and double well potentials and associated attractors with that of the evolution of natural systems. A. the initial conditions for A and A' are different, but the evolve with the same double well potential to what is effectively the same attractor. B. a single well evolves into a double well, but the particle does transgress the barrier, thereby staying in one attractor configuration. C. a single well evolves into a double well, which is represented by an evolution toward an attractor, and switching to another by transgressing the lower barrier. This configuration is stable. Adapted from [35].

can be made to fractal geometry [61]. Scale invariance is inherently linked to uni-

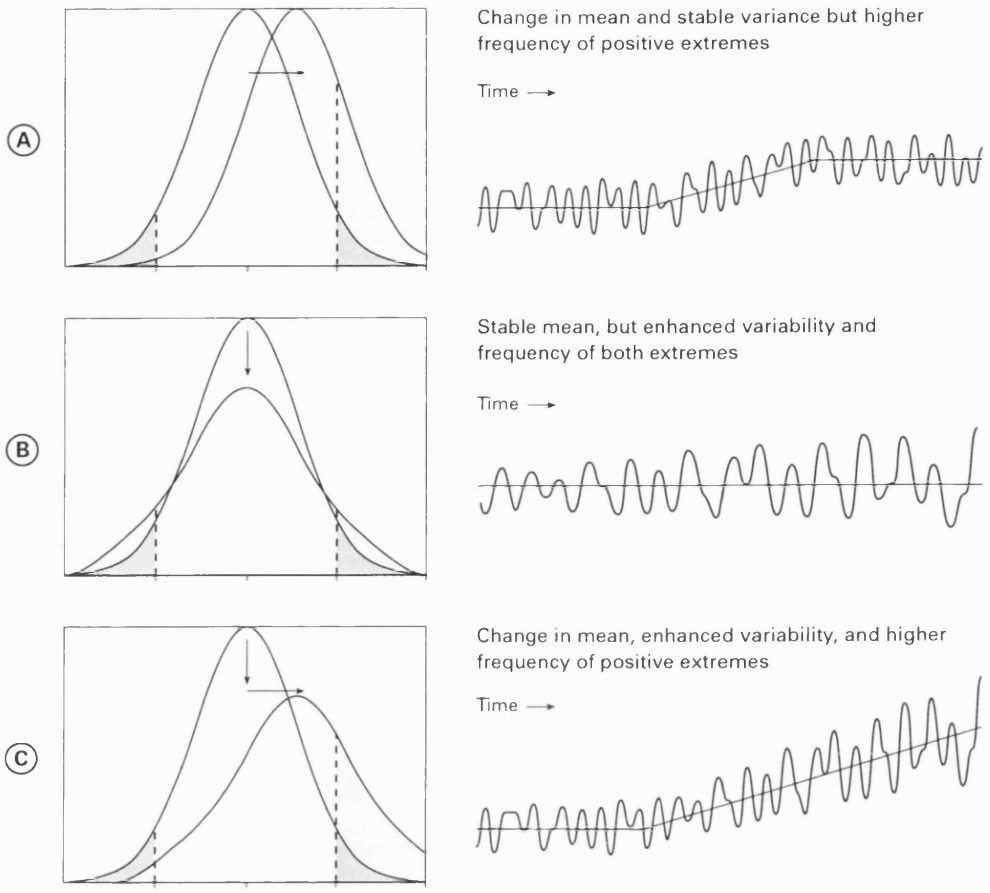

Figure 1.10: Schematic diagram illustrating the relations between forms of time series and probability density functions. The solid lines represent a notional frequency distribution, in this case Gaussian. The shading indicates the extreme parts of the distribution, representing events in the tails of the distribution that occur infrequently. A. if there is a shift in the mean this will produce a number of positive extreme events. B. if the variance changes, then extreme events are produced at both ends of the frequency distribution. C. if the mean and variance change at the same time, then the occurrence of extremes is more complex. Adapted from [56], [57].

versality, where macroscopic system parameters are not dependent on microscopic features, i.e., independent of scale (time and space), and whose properties are shared by seemingly disparate natural systems [62]. In the strictest statistical sense, scaling should occur over infinite orders of magnitude. However, in reality scaling may not occur over an infinite range, as natural systems are characterised by processes that may not interact over all timescales [63]. In addition, system fluctuations, such as

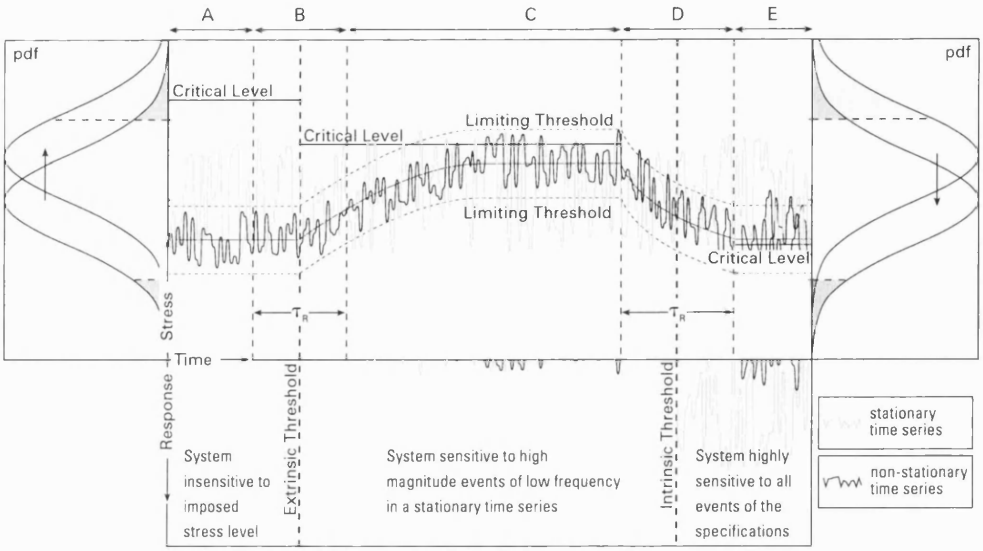

Figure 1.11: Schematic diagram illustrating the relationships between stress-response and thresholds mechanisms. System response is represented by a series of critical levels. These change after every threshold crossing. At the extrinsic threshold, the stress exceeds a critical level to cause a change in the number of events, which will exceed the threshold value. At the intrinsic thresholds, change is not related to increase in stress but to an internal mechanism that changes resistance but has a similar response. The pattern for both a stationary and a non-stationary series is shown. Zones A, C, and E represent robust behaviour, where system dynamics are repeatedly crossing intrinsic thresholds, but overall the system response is stable within limiting thresholds. Zones B and D represent responsive behaviour, where in response to externally imposed change, system dynamics move across extrinsic threshold to new process regime. System dynamics in A, C, and E are replaced by new dynamics created in C and E respectively. The response time (τ_R) is proportional to sensitivity. Adapted from [54], [55].

scaling are affected by the ratio of system size to its boundary [24].

1.3 Lake System Dynamics

1.3.1 Lake Response to Environmental Variability

Lake systems respond hydrologically and thermally to environmental variability [124]. The hydrological response of lakes to climate forcing is manifested primarily in lake level variations and fluid flow dynamics [125]. The local moisture balance is given as, (precipitation - evaporation ($P - E$)), and the local hydrological balance

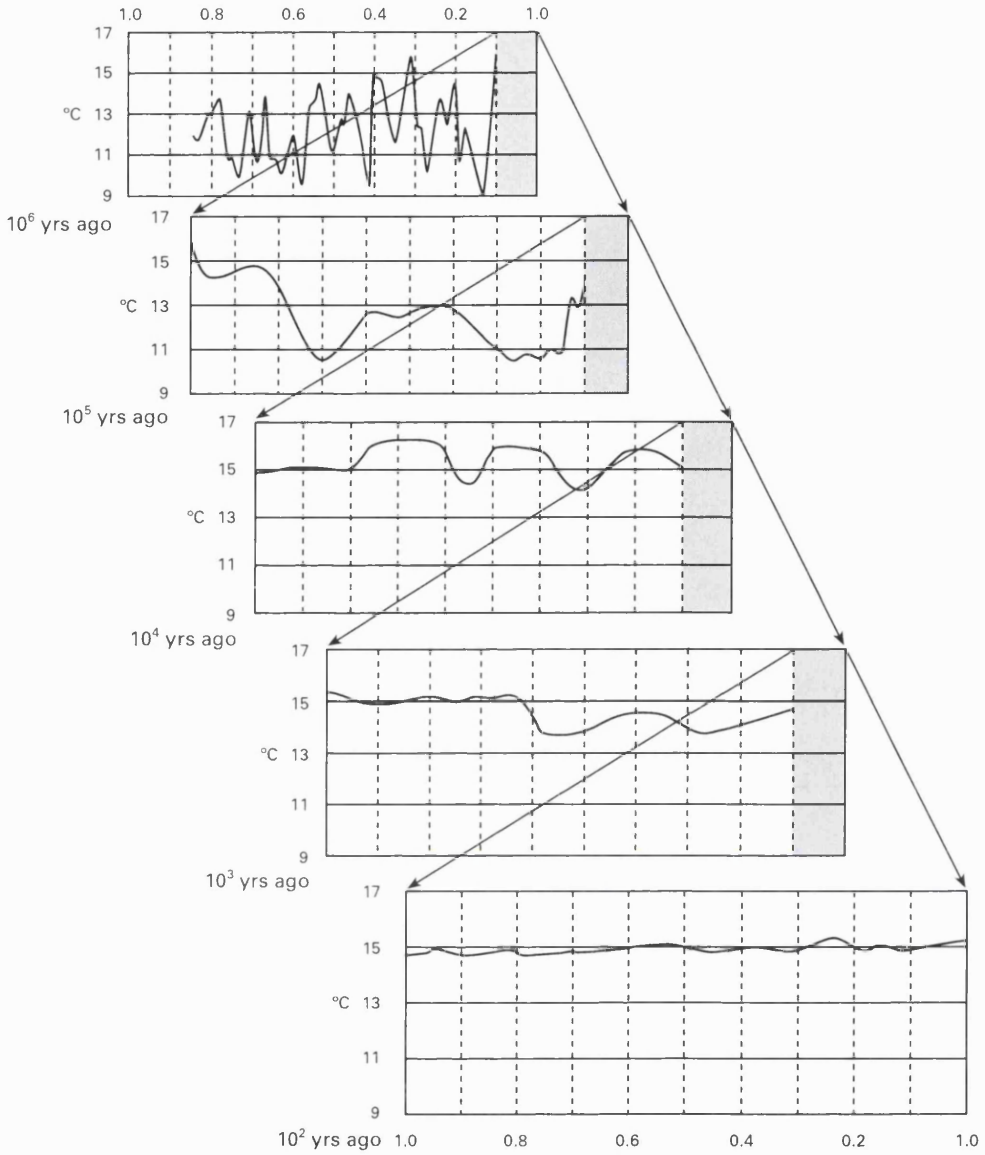

Figure 1.12: Schematic diagram illustrating the scales of temporal variation. The timescale ranges from decadal (lowest panel) to ma yrs (top panel). Each successive panel, from the back to the front, is an expanded version (expanded by a factor of 10) of one-tenth of the previous column. Thus, higher-frequency climatic variations are "nested" within lower-frequency changes. Note that the temperature scale (representing global mean annual temperature) is the same on all panels. It is worth pointing out that local temperatures show much larger variance on diurnal and seasonal timescales than on any other including 10^5 to 10^6 years. After [58].

is given as [(precipitation + runoff $(P + R)$) - (evaporation + discharge $(E + D)$)] [126]. The magnitude and rate of the hydrological response is dependent on the hy-

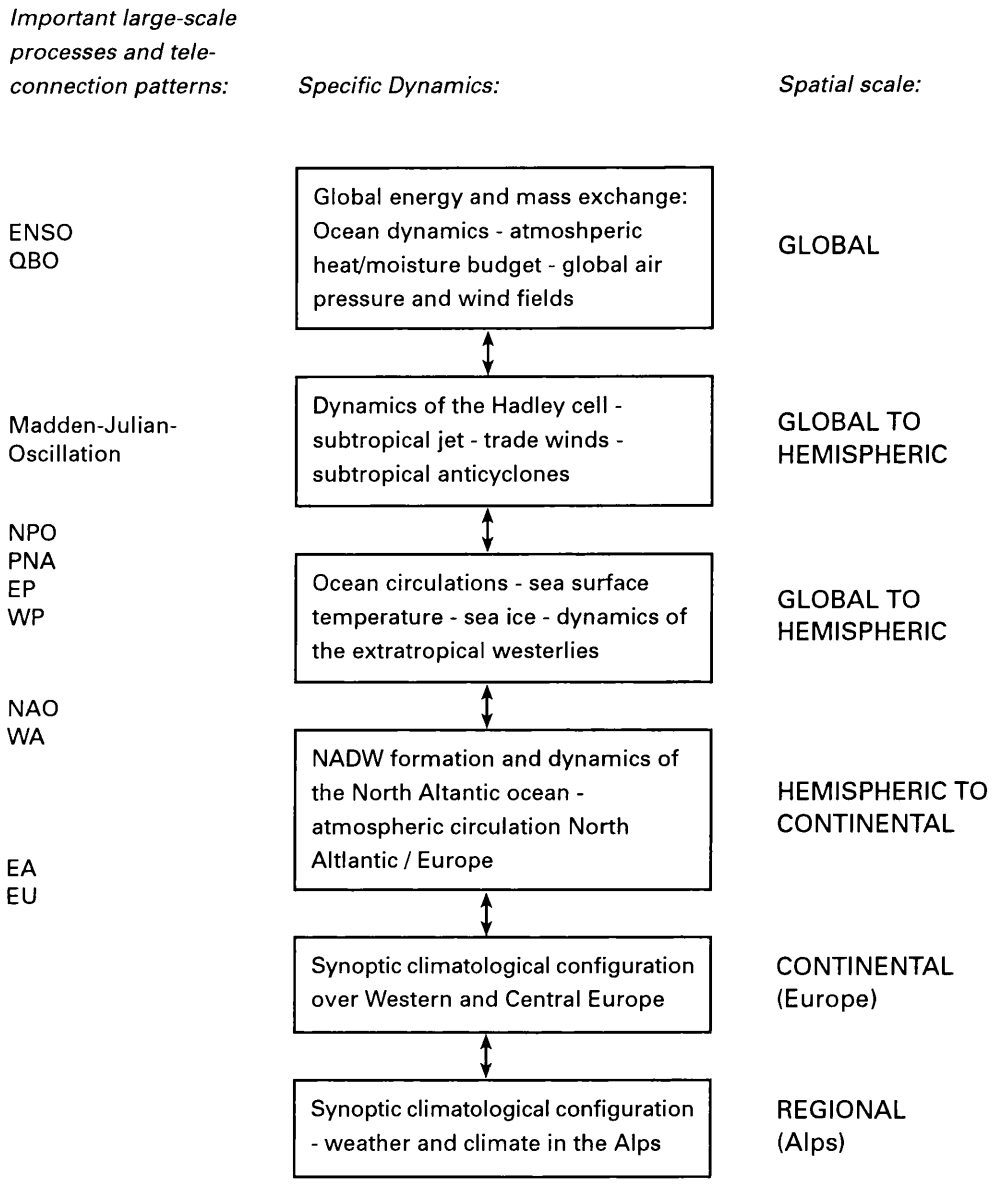

Figure 1.13: Schematic diagram illustrating the scales of spatial variation. Interactions patterns, both downscaling and upscaling are shown for the global change and the effects in the Alpine region. Abbreviations: EA Eastern Atlantic Pattern; ENSO El Nino-Southern Oscillation; EP Eastern Pacific Pattern; EU Eastern European Pattern; $NADW$ North Atlantic Deep Water; NAO North Atlantic Oscillation; NPO North Pacific Oscillation; PNA Pacific North American Pattern; QBO Quasi-Biennial Oscillation; WA West Atlantic Pattern; WP West Pacific Pattern. After [59].

drological setting, i.e., lake basin status as open or closed systems. Typically, closed

lakes respond to changes in the $P - E$ balance more rapidly than open systems, due to ground water inputs in closed systems being more passive than atmospheric and catchment inputs in open systems [126]. The evolution of lakes is often characterised by phases of open and closed dynamics [127]. The main driving mechanisms of hydrological flow patterns are point-sourced river influxes, wind-driven progressive surface waves, turbidity currents, and seasonal changes in air temperature [125]. These processes create temporally and spatially intermittent active confines of energetic flow throughout the thermal density stratification, including the surface mixed layer, the boundary layers on the lake sides and bottom, and patches in the interior [128]. The thermal response of lakes is manifested in the generation of thermal density stratification. The size and morphology of the lake basin determines the extent of the thermal density stratification and resistance to mixing [127]. The seasonal cycles in the energy budget, and in particular the penetration of solar radiation directly affect the lake surface temperature and subsurface temperature [129]. These in turn produce water density gradients, which create the vertical temperature profile. The epilimnon is the upper, warm oxygenated and circulating layer, the metalimnon is below, and the hypolimnon is the lower cooler and relatively undisturbed layer, which maybe anoxic [127].

1.3.2 Lake Sediment Origin and Deposition

Lakes are efficient natural settling basins for allochthonous (externally derived) and autochthonous (internally derived) particles [130]. Under certain environmental conditions, such particles may form annually laminated sediments, also known as varves. These are invaluable archives of (palaeo)environmental variability, with an exact and independent (of radiometric and radiocarbon methods) chronology [131], [132]. The formation of varves is dependent on several important factors; material in suspension, lake morphology, and lake stratification [131]. Suspended sediment in the water column is derived from allochthonous and autochthonous sources. Allochthonous particles originate from catchment process (e.g., river discharge, catchment run-off and glacial activity), and atmospheric processes (e.g., precipitation and wind) [133]. Autochthonous particle formation is controlled by temperature and precipitation.

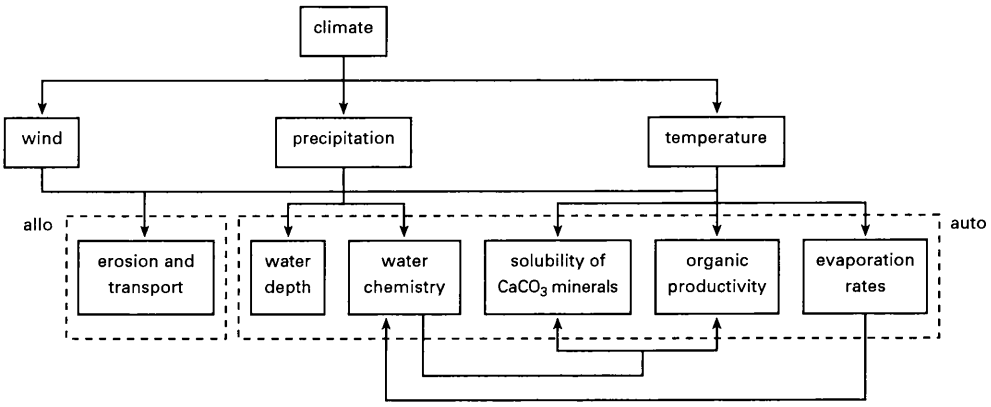

Figure 1.14: Schematic diagram illustrating the concepts of hierarchy in varve forming processes. Varve particle formation is displayed as a hierarchical process. In particular, the figure highlights the interaction between the processes controlling both allochthonous and autochthonous particle formation.

Temperature influences the solubility of carbonate minerals, organic productivity, and evaporation rates, which influence water chemistry, and thus autochthonous organic productivity. Precipitation controls water depth and water chemistry, and thus affects organic productivity and carbonate mineral precipitation (see Figure 1.14.) [120], [134]. The morphometry of the basin, (e.g., shape, size, and orientation) influences the hydrological flow patterns, which ultimately determine whether sediments remain undisturbed for varve formation [125]. Favourable characteristics include; flat bottom, deep, bedrock basin, a small drainage area, and no significant inflow [131], [135]. Thermal density stratification aids varve preservation by dampening the hydrological flow patterns. Varves are known to form in monomictic (thermal stratification only exists in one season - summer), dimictic (two seasons), and meromictic (more than two seasons) lakes [136], [135]. Although these conditions are conducive to varve formation and preservation, the principle driving mechanism is the seasonal cycle of sedimentation, where sediment deposited during one year must include two or more macro- or microscopically distinguishable seasonally deposited layers [132]. These originate from the annual cycle of seasons, which is the dominant oscillation in lake sediments (diurnal forcing may be as large, but response times of lake temperatures are too long for it to have any effect).

A general model can be outlined for varve formation. Spring and summer is char-

acterised by temperature warming, melting any snow that may have accumulated in the catchment and on the lake surface over the winter. The melt-water discharge and related erosion leads to the influx of particulate matter, which forms a distinctly light coloured fine sand to silt mineral rich lower layer. This minerogenic layer may also be rich in planktonic diatoms and chrysophyte cysts. The spring and summer is characterised by increased biological activity in the lake water column and catchment. Phytoplankton dynamics, (e.g., diatom blooms) begin in spring after any ice melt and continue into the summer. These are often associated with concomitant high inputs of dissolved silica into the lake [137]. Darker amorphous organic matter may also form, composed of plant fibres, algae, and pollen [136]. Also, lighter layers may form due to authigenic calcite crystal growth. The calcite is precipitated if the lake is supersaturated with calcium carbonate, as a result of algae and bacteria photosynthetic uptake of dissolved CO_2, which is itself temperature dependent [137]. In addition, dolomite and aragonite, as well as siderite crystals may form. These particles form the lower laminae of the varve. Autumn and winter is characterised by the cessation of algal activity and carbonate precipitation due a reduction in water temperature. In the calm waters fine-grained clay and silt material (comprising organic detritus, diatom frustules, faecal pellets, iron sulphides, plant debris, and clay minerals - which has been in suspension during the year) settles out during this quiescence, forming a quite distinct dark, almost black layer [136]. These particles form the upper laminae of the varve. "Structural extras" exist within this depositional framework [138]. Typically, allochthonous material is the dominant source, originating from rainstorms or turbidity currents, often occurring in autumn [138], whereas wind derived material is a year round process. In addition, authigenic chemical precipitates, such as iron and $CaCO_3$, and biogenic or autochthonous extras, such as algal blooms (both seasonally and non-seasonally specific) may also occur [138].

1.3.3 Review of Lake Sediments and System Dynamics

Lake sediments, and in particular varve thickness variations are sensitive to a range of linear and nonlinear environmental fluctuations [139], [50]. In Baldeggersee,

Switzerland, dark laminae thickness and total varve thickness are correlated with annual precipitation, whereas light laminae thickness is correlated with summer precipitation [132]. Conversely, varve thickness fluctuations in Nicolay Lake, Nunavut, Canada are sensitive only to rainfall [140]. Varve thickness variations in Lake Silvaplana, in the Swiss Alps are also correlated with mean summer temperatures, but can only be fully explained by the additional factors of summer precipitation and the number of days with snow per year [141]. Similarly, in Lakes Paajarvi, Paijanne, and Pyhajarvi, in Finland, varve thickness variations are controlled by both temperature and precipitation [142]. In addition, varve thickness is correlated with summer temperature in three small glacier-fed lakes, in the Southern Canadian Cordillera [143], as well as in Lake C2-8 in the Canadian Arctic [144], and Upper Soper Lake, Baffin Island, where dark laminae thickness is correlated with average summer temperature [145]. Interestingly, in Holzmaar, Germany, varve thickness was found to correlate with spring temperatures, as well as pollen, indicating a link between landscape openness and sediment delivery [133], [146].

In Lake Kassjon, northern Sweden, diatom fluctuations reveal a 20 yr lag with respect to a regional dendrochronological temperature proxy record, which is attributed to temperature changes driving biogeochemical processes in the catchment [147]. Scale invariance has been isolated in a range of varve thickness time series. In their classic studies, Hurst [118], and Mandelbrot and Wallis [119], isolated scaling by applying the rescaled range method. Scale invariance was also isolated in minerogenic fluctuations in Holzmaar, Germany, from 3000 to 10,000 cal yrs BP [12]. In addition, in studies of Lake Ojibway, Canada [148], various New England lakes, USA [149], and Lake Gosciaz, Poland [150], autoregressive (AR) models isolated long temporal correlation in varve sedimentation.

1.3.4 Time Series Construction

Lake Name and Grid Reference	Altitude (m.a.s.l.)	Area (km^2)	Depth (μ) (m)	Volume (m^3)	Catchment Area (Km^2)
Belauersee, 54 06 N, 10 56 E	29	1.14	9	10.26	4.47
Buchsee, 48 04 N, 12 10 E	493	0.08	0.8	0.06	2.5
C2-8, 82 50 N, 78 00 W	2	1.8	43.4	77.94	26.6

Deep, 47 41 N, 95 23 W	421	0.1	20	2	25
Degersee, 47 44 N, 09 29 E	495	0.33	5.4	1.8	1.37
Donard, 66 40 N, 61 21 W	450	0.36	10	3.6	7.8
Elk, 47 15 N, 95 15 W	427	1.01	11.2	11.3	2
Gosciaz, 52 30 N, 10 20 E	64	0.45	5	2.25	5.88
Hamelsee, 52 46 N, 09 19 E	20	0.07	2.3	0.16	0.25
Heinalampi, 63 07 N, 27 39 E	90	0.03	8	0.24	3.6
Illmensee, 47 52 N, 09 22 E	747	0.76	7.8	5.93	8
Karhun'lpi, 62 19 N, 30 20 E	92	0.03	10	0.3	22
Meerfelder, 50 06 N, 06 45 E	337	0.25	9.2	2.3	5.76
Muttelsee, 47 37 N, 09 40 E	492	0.08	2.8	0.22	0.36
Paajarvi, 60 46 N, 24 03 E	103	13.1	15.2	199.1	244
Paijanne, 62 15 N, 26 00 E	78	85.6	21.3	1823.3	320
Pyhajarvi, 60 30 N, 27 01 E	40	12.9	21	270.9	460
Pyoreal'pi, 62 15 N, 30 29 E	76	0.04	18	0.72	9
Ristijarvi, 63 37 N, 28 57 E	106	0.29	20	5.8	3.5
Schleinsee, 47 37 N, 09 39 E	474	0.18	6.4	1.15	0.6
Siethenersee, 52 16 N, 13 13 E	41	0.3	2.8	0.84	1.5
Tervalampi, 61 41 N, 29 22 E	94	0.02	11	0.22	1.7

Table 1.1: Summary of lake parameters in this study.

The thickness time series in this study originate from a range of sources (see Figure 1.15. and Table 1.1.). Dr's Salonen (Paijanne, Pyhajarvi, Paajarvi), Hughen (Donard), Lamoureux (C2-8), Goslar (Gosciaz), Brauer (Meerfelder Maar), Slawinski (Deep), and Anderson (Elk) provided existing thickness time series. The remaining time series were generated by the author from core surface and thin section photographs, provided by Dr Heikki Simola, of the University of Joennsu, Finland (Ristijarvi, Pyorealampi, Tervalampi, Heinalampi, and Kaarhunpaanlampi) and Dr Josef Merkt, of the German Geological Survey, Hannover, Germany (Belauersee, Buchsee, Degersee, Hamelsee, Illmensee, Muttelsee, Schleinsee, and Siethenersee). The annual nature of the varves was verified by the author, as well as by Dr's Merkt and Simola (see Figures 1.16. to 1.21. and Table 1.2.). In terms of the lake basin geology, the US lakes, Finnish lakes, and Lake C2, in the Arctic, lie totally with glacial deposits (moraines, etc), as do the northern German lakes of Belauersee, Hamelsee, and Siethenersee. Lake Meerfelder Maar lies in a volcanic provence while the southern German lakes, Buchsee, Illmensee, Muttlesee, Degersee, and Schleinsee, lie in a

metamorphic provence associated with the Alps.

An important component of varve identification and subsequent time series analysis, is the minimum thickness value. The general consensus is that ca. 0.20 mm is the most appropriate [151], [152], [153], and as such was applied in this study (although variations exist from author to author). The reasoning for the 0.2 mm lower limit is based on the "typical" thickness of a distinctive seasonal laminae. For example, a spring diatom layer composed of only four to five medium sized diatoms would already be ca. 0.2 mm thick [151], and considering the fragile nature of diatoms this may not be preserved [153]. Similarly, the upper limit of a particle size of a winter layer composed of fine-grained organic detritus is ca. 0.2 mm. Thus, if little more than this is deposited during the year, seasonally distinct layers are not possible, and the potential varves would be thinner than the grain of the matrix [152]. Also, such sublaminae would consist of only one line of silt particles, and there is no environment so calm as to preserve such a deposit [153]. In addition, a thin layer may represent only one part of a varve. This is not unusual, for example, if minerogenic influx is ceasing due to catchment conditions. This makes it very difficult to see the limit between the summer diatom blooms of two succeeding years [153].

In order to generate varve thickness time series, the existing core surface and thin section photos were enlarged using a flat bed scanner and measured with a standard ruler. Each original photo had an overlap of ca. 10% in order to maintain continuity between respective photos. Varve counts were then made on the enlarged images in three single vertical axis, left, centre, and right. Where a disturbance occurred on one axis, an adjoining axis was counted to provide continuity. The recorded thickness was the mean of three measurements for total varve thickness. Although counting errors are minimal where the boundaries of the individual varves can be clearly identified, the estimated thickness error is ca. 10% (see Figures 1.22. to 1.28. and Table 1.3.). In chapter two we highlight the methods applied to analyse the generated varve thickness time series. All numerical analysis was carried out using existing IDL programming code.

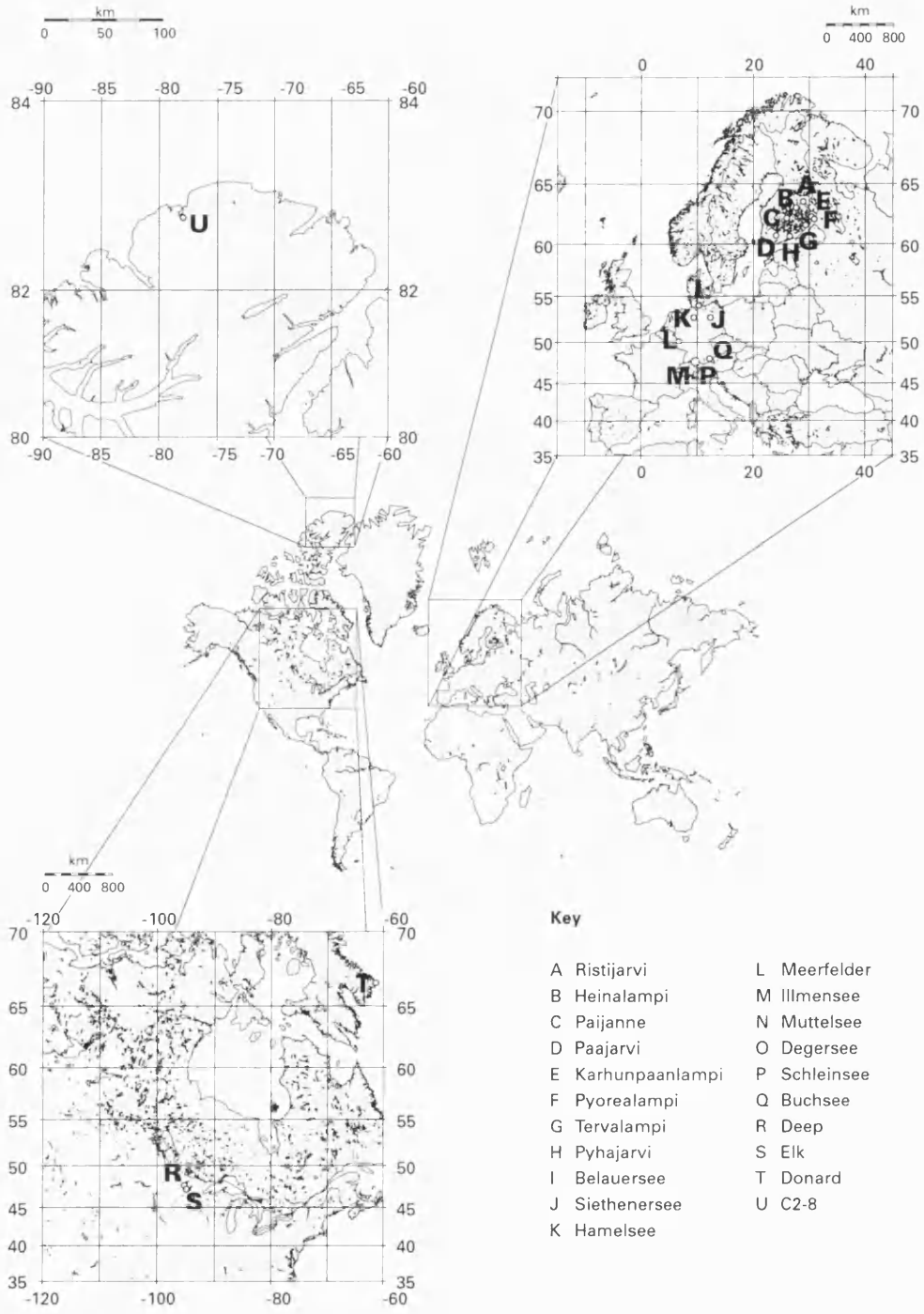

Figure 1.15: Map illustrating the location of the lakes in this study.

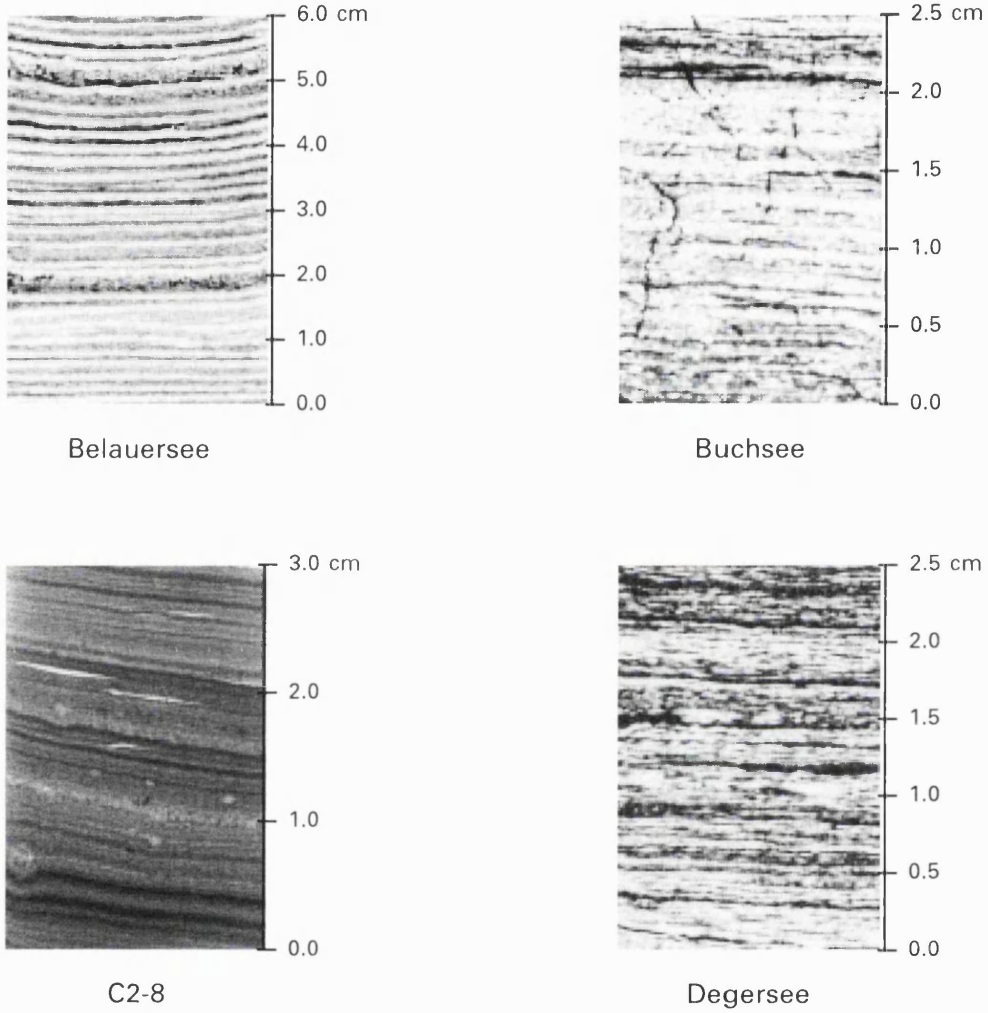

Figure 1.16: In Belauersee each varve generally consists of two layers: (i) a light mostly calcitic layer precipitated in summer; (ii) a dark layer rich in organic detritus deposited in winter. In Buchsee each varve generally consists of two layers: (i) a white calcite layer precipitated in summer; (ii) a dark organic layer deposited in winter. In Lake C2-8 each varve generally consists of two layers: (i) a light spring/summer coloured silt and fine sand lower layer; (ii) a finer darker winter upper layer. In Degersee each varve generally consists of two layers: (i) light summer layer beginning with chrysophyte cysts, followed by diatoms, and calcite crystals; (ii) a mainly organic layer containing the chrysophyte cysts of the next spring in its upper part.

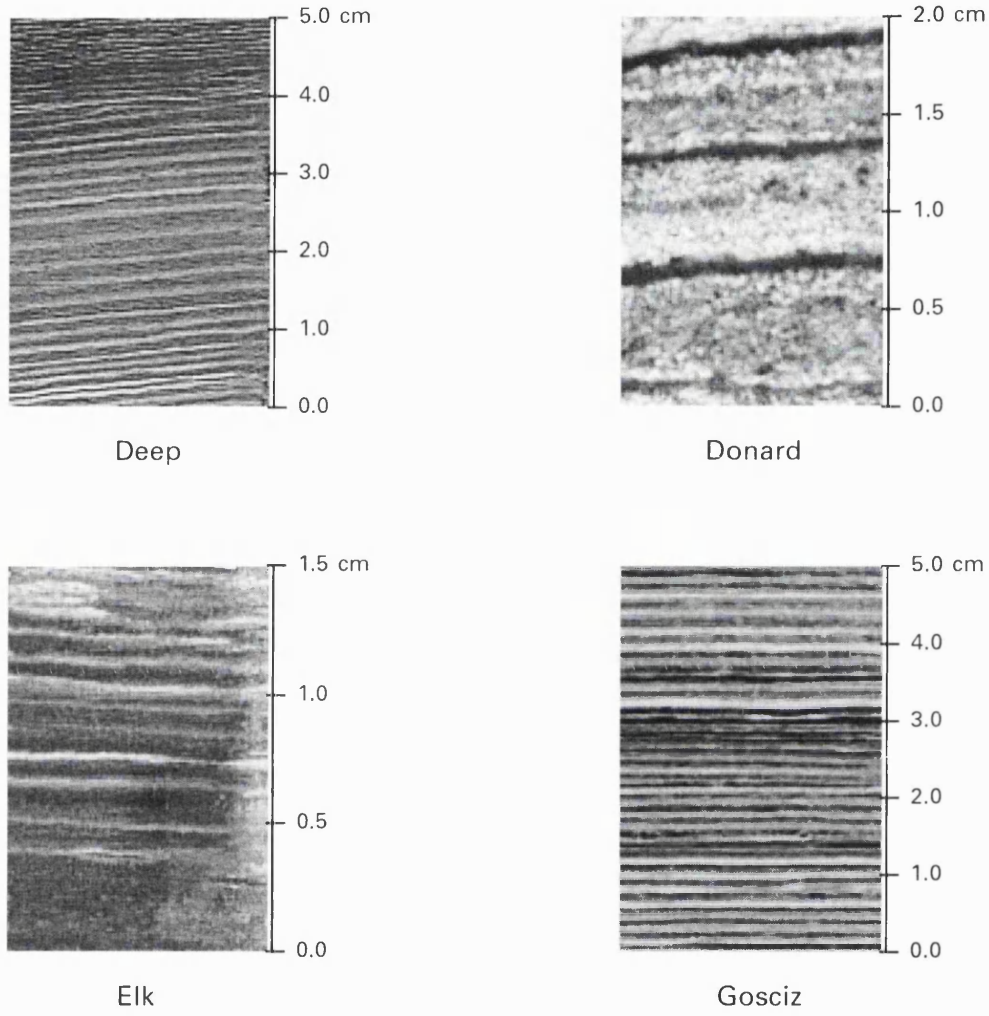

Figure 1.17: In Lake Deep each varve generally consists of two layers: (i) a light calcitic layer precipitated through photosynthesis in summer; (ii) a darker clastic and organic debris deposited in other seasons. In Lake Donard each varve generally consists of two layers: (i) a light spring/summer layer composed of fine sand to silt mineral grains; (ii) a dark winter layer composed if clay mineral grains. In Elk Lake each varve generally consists of two layers, but with significant variation in the sequence: (i) spring/summer layers consist of organic matter, diatoms, carbonate aggregates, dolomite, aragonite, (ii) autumn/winter layers consists of ferric iron, iron manganese, and clay/silt. In Lake Gosciaz each varve generally consists of two layers: (i) a light mostly calcitic layer precipitated in summer; (ii) a dark layer rich in organic detritus deposited in winter.

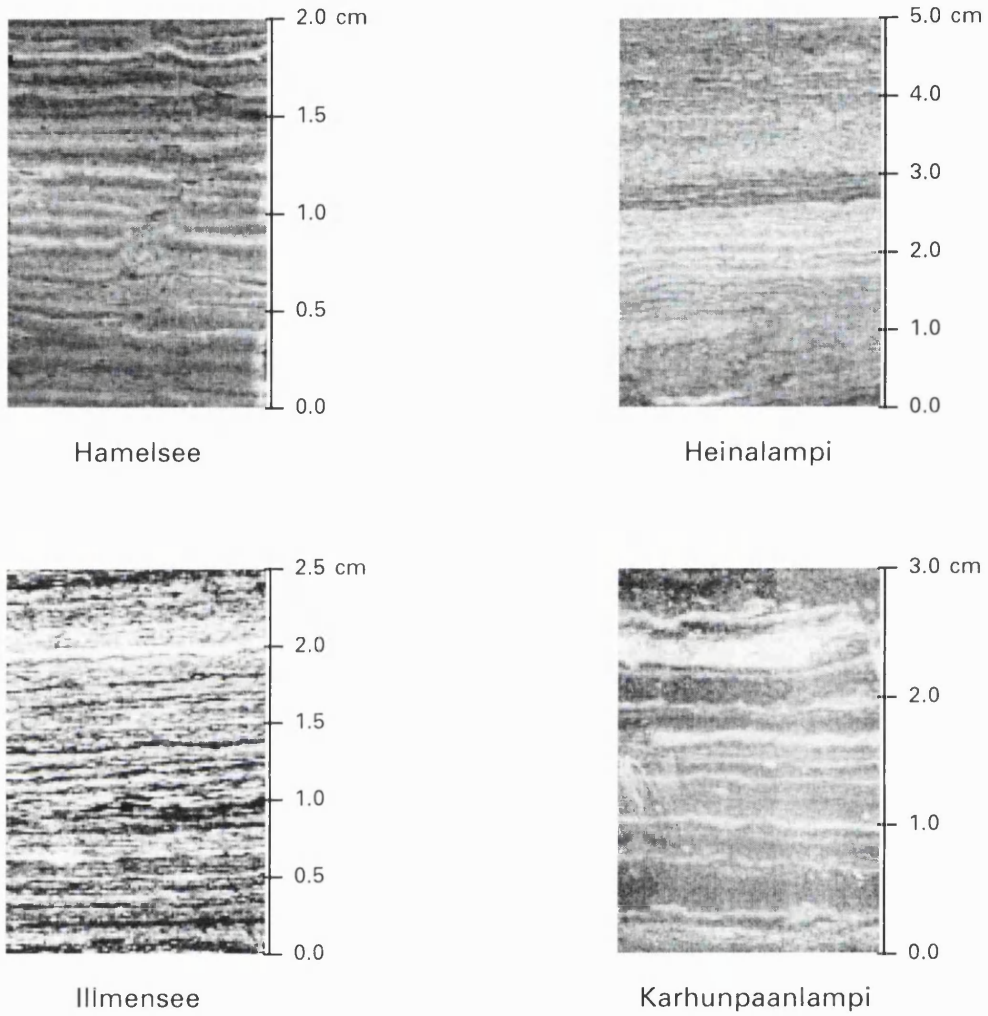

Figure 1.18: In Hamelsee each varve generally consists of two layers: (i) an autumn and winter layer consisting of coarse particles (including clay, silt and sand, which are mostly at its end and near the summer); (ii) The upper part of the layer may contain diatom frustules and chrysophyte cysts occurring in the lake during the late winter and spring. Siderite crystals are also present in the summer layer. In Lake Heinalampi each varve generally consists of two layers: (i) an organic rich summer layer consisting of planktonic diatoms; (ii) a diatom poor, silty autumn-winter-spring layer, with chryosophyte statospores. In Illmensee each varve generally consists of two layers: (i) light summer layer with diatoms, chrysophyte cysts, calcite crystals; (ii) a mainly organic layer deposited in the winter. In Lake Karhunpaanlampi each varve generally consists of two layers: (i) a light spring/summer coloured minerogenic lower layer; (ii) a brown detrital winter upper layer.

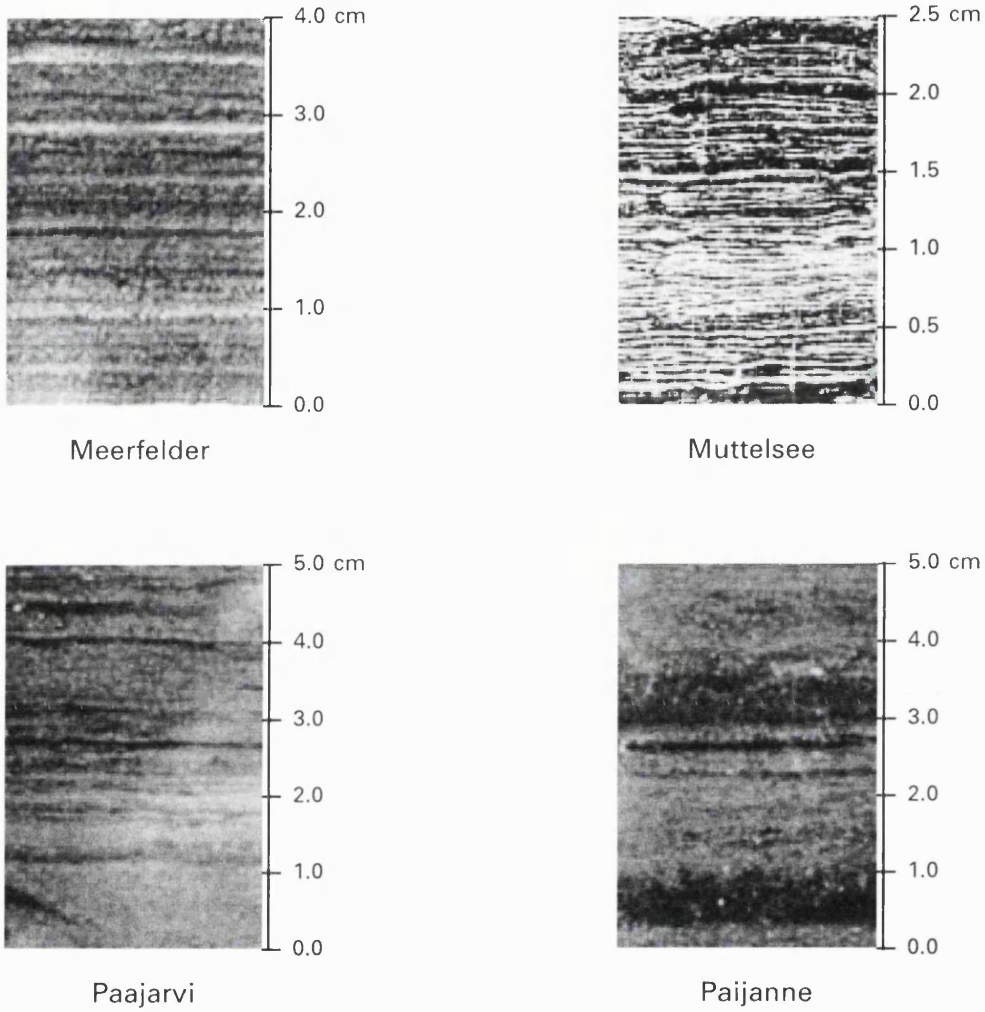

Figure 1.19: In Meerfelder Maar each varve generally consists of two layers, but with significant variation in the sequence: (i) spring/summer layers consist of amorphous organic matter, with chrysophyte cysts diatoms, slightly graded silt layer, (ii) autumn/winter layers consist of siderite, vivianite, allochthonous minerogenic matter, plant debris, clay, amorphous organic matter. In Muttelsee each varve generally consists of two layers: (i) light summer layer with diatoms, chrysophyte cysts, calcite crystals; (ii) a mainly organic layer deposited in the winter. In Lake Paajarvi each varve generally consists of two layers: (i) light, thick summer layers mainly of minerogenic material but rich in diatoms; (ii) a thin dark winter layers containing more organic material and iron sulphides. In Lake Paijanne each varve generally consists of two layers: (i) light, thick summer layers of mainly minerogenic material, also rich in diatoms; (ii) thin, dark winter layers richer in organic material and iron sulphates.

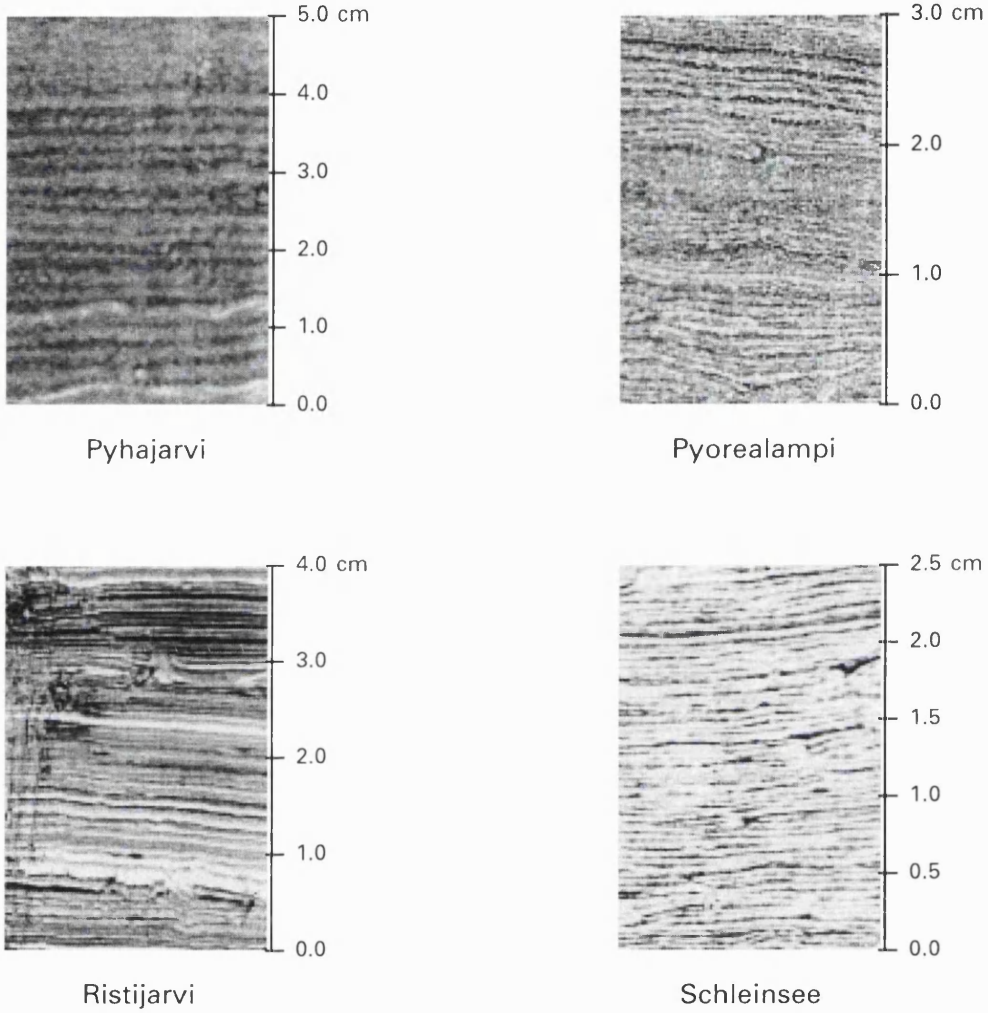

Figure 1.20: In Lake Pyhajarvi each varve generally consists of two layers: (i); light, thick summer layers composed almost entirely of diatom layers showing seasonal succession in places; (ii) thin, dark winter layers richer in organic material and iron sulphates. In Lake Pyorealampi each varve generally consists of two layers: (i) a light spring/summer coloured silt and fine sand lower layer; (ii) a finer brown organic winter upper layer. In Lake Ristijarvi each varve generally consists of two layers: (i) a thick green summer layer consisting of planktonic diatoms; (ii) a dark winter layer composed of organic detritus. In Schleinsee each varve generally consists of two layers: (i) a white calcite layer precipitated in summer; (ii) a dark organic layer deposited in winter.

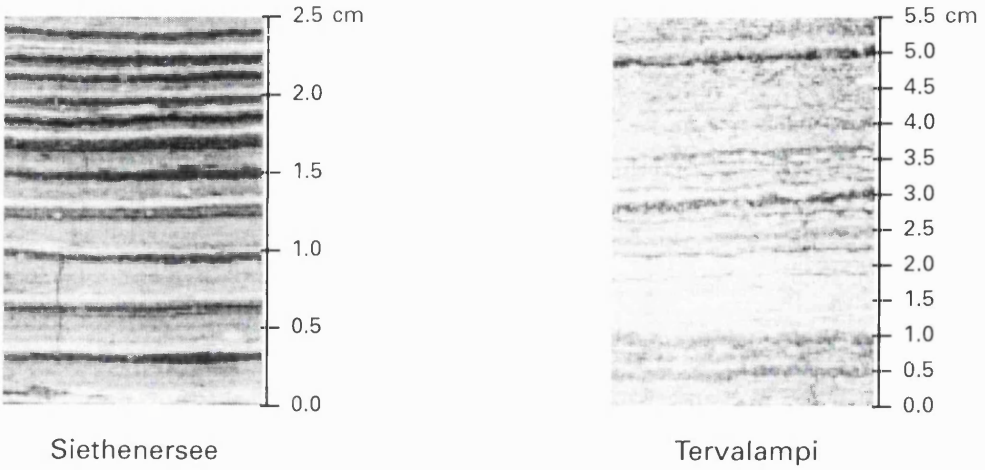

Figure 1.21: In Siethenersee each varve generally consists of two layers: (i) a white calcite layer precipitated and deposited in summer; (ii) a dark organic layer deposited in winter. In Lake Tervalampi each varve generally consists of two layers: (i) a light spring/summer coloured silt and fine sand lower layer; (ii) a finer darker winter upper layer.

The varve chronologies for some lakes were not counted from the sediment water-interface (i.e., not "nailed" chronologically to the present day), but were "floating". In such instances, the chronology was anchored primarily by tephra layers. The most notable are; the LCR tephra at 9407 cal yrs BP [151], the Saksunarvatn tephra at 10,090 cal yrs BP [154], and the Laacher See Tephra (LST) at 12,880 cal yrs BP [155]. Intermittent radiocarbon dates were used where available for extra clarification of the tephra based chronology [151]. Belauersee was anchored by the notable "Elm decline", dated at 5660 cal yrs BP [151]. Only single cores from each lake were available for study. In addition, in this study we focus only on the varve thickness time series, as availability of varve geochemical and physical data was limited, and not viable for time series analysis. Evidence suggests that human activity has been a feature of some of the lakes in this study, particularly in the recent sediments of the Finnish lakes. In addition, with respect to the preservation of varves, the lake basins are not affected by vegetation, or large depth variations, which may cause resuspension.

Lake	Varve Age (cal yrs BP)	Length (yrs)	Depth (m)	Investigator
Belauersee	2783-8165	5382	11.382-21.59384	Herron/Merkt
Buchsee	12,231-12,998	768	14.76-15.15804	Herron/Merkt
C2-8	-42-280	323	0-0.06549	Lamoureux
Deep	7644-10,487	2844	29.8989-32.8	Slawinski
Degersee	7447-9509	2063	21.395-21.94723	Herron/Merkt
Donard	-42-1198	1241	0-0.96454	Hughen
Elk	-23-10,246	10,224	0-21	Anderson
Gosciaz	3197-12,861	9665	0-9.8638	Goslar
Hamelsee-a	7798-11,527	3730	16.26024-18.82398	Herron/Merkt
Hamelsee-b	12,622-13,299	678	19.63364-20.09454	Herron/Merkt
Heinalampi	-33-349	383	0-0.40531	Herron/Simola
Illmensee	7224-9513	2290	19.665-20.42998	Herron/Merkt
Karhunpaanlampi	-37-180	218	0-0.83203	Herron/Simola
Meerfelder-a	11,000-11,584	585	6.91-7.24	Brauer
Meerfelder-b	11,636-13,540	1905	7.30-8.9	Brauer
Muttelsee	12,589-13,036	448	14.9-15.1233	Herron/Merkt
Paajarvi	-39-799	839	0-1.1329	Salonen
Paijanne	-39-1025	1065	0-1.3892	Salonen
Pyhajarvi	-40-592	633	0-1.0954	Salonen
Pyorealampi	-42-2042	2085	0-1.43764	Herron/Simola

Ristijarvi	-39-5550	5590	0-5.27028	Herron/Simola
Schleinsee	6226-10,245	4020	19.67-21.00889	Herron/Merkt
Siethenersee	12,620-13,107	488	23.95-24.90024	Herron/Merkt
Tervalampi	-30-136	167	0-0.27704	Herron/Simola

Table 1.2: Summary of time series parameters in this study.

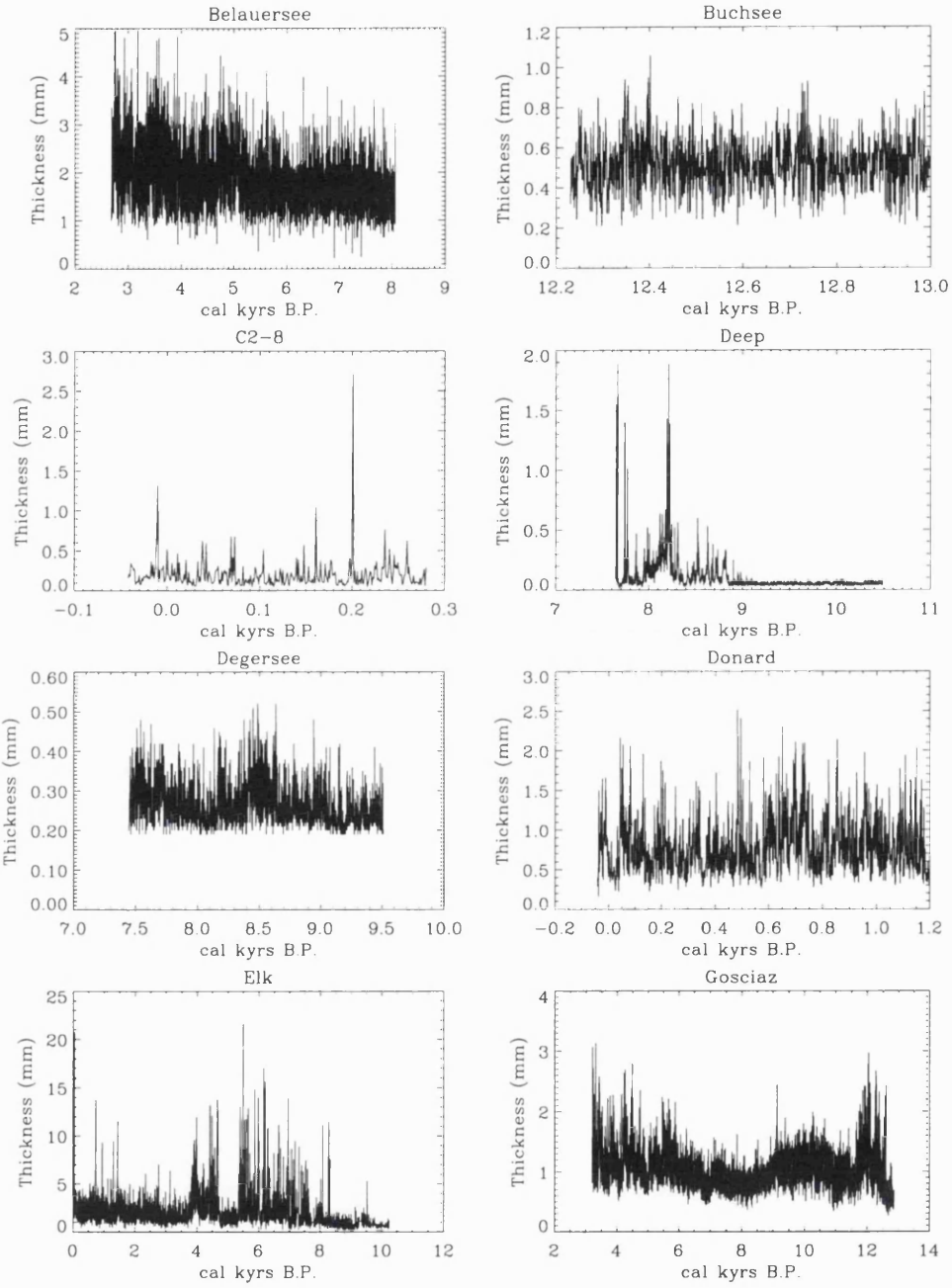

Figure 1.22: Figure illustrating the varve thickness time series from: Belauersee, Buchsee, C2-8, Deep, Degersee, Donard, Elk, and Gosciaz.

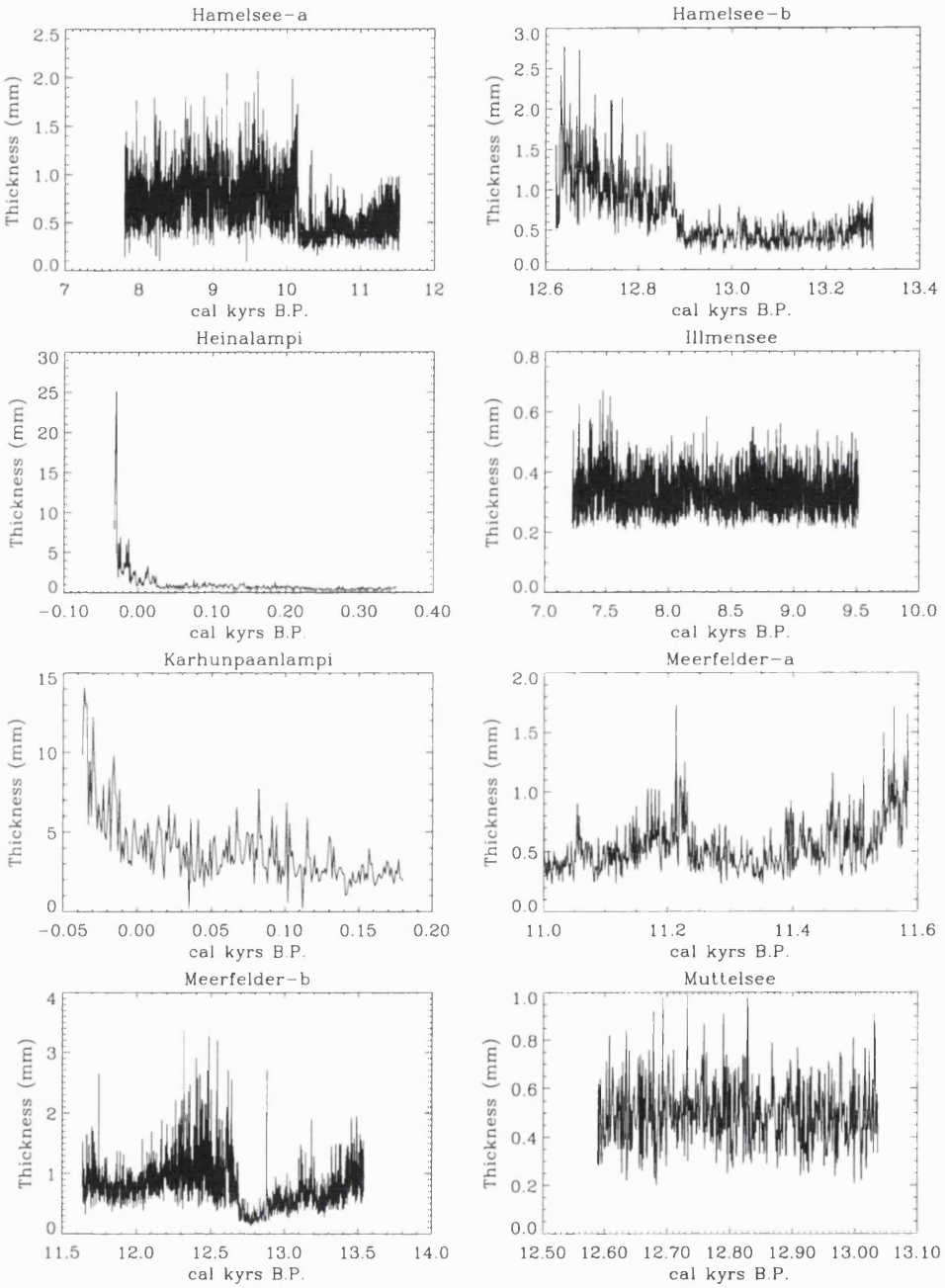

Figure 1.23: Figure illustrating the varve thickness time series from: Hamelesee-a, Hamelsee-b, Heinalampi, Illmensee, Karhunpaanlampi, Meerfelder-a, Meerfelder-b, and Muttelsee.

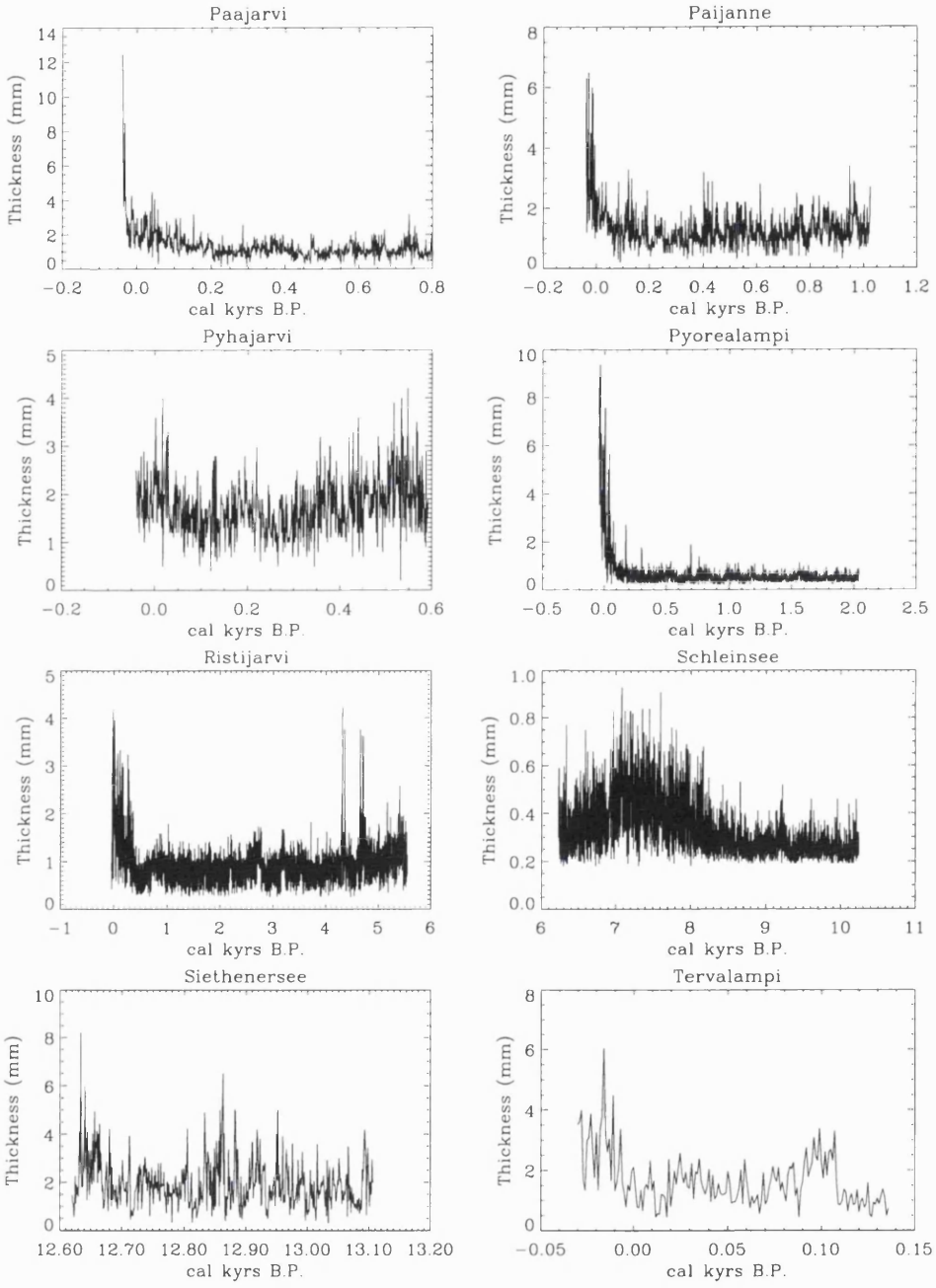

Figure 1.24: Figure illustrating the varve thickness time series from: Paajarvi, Paijanne, Pyhajarvi, Pyorealampi, Ristijarvi, Schleinsee, Siethenersee, and Tervalampi.

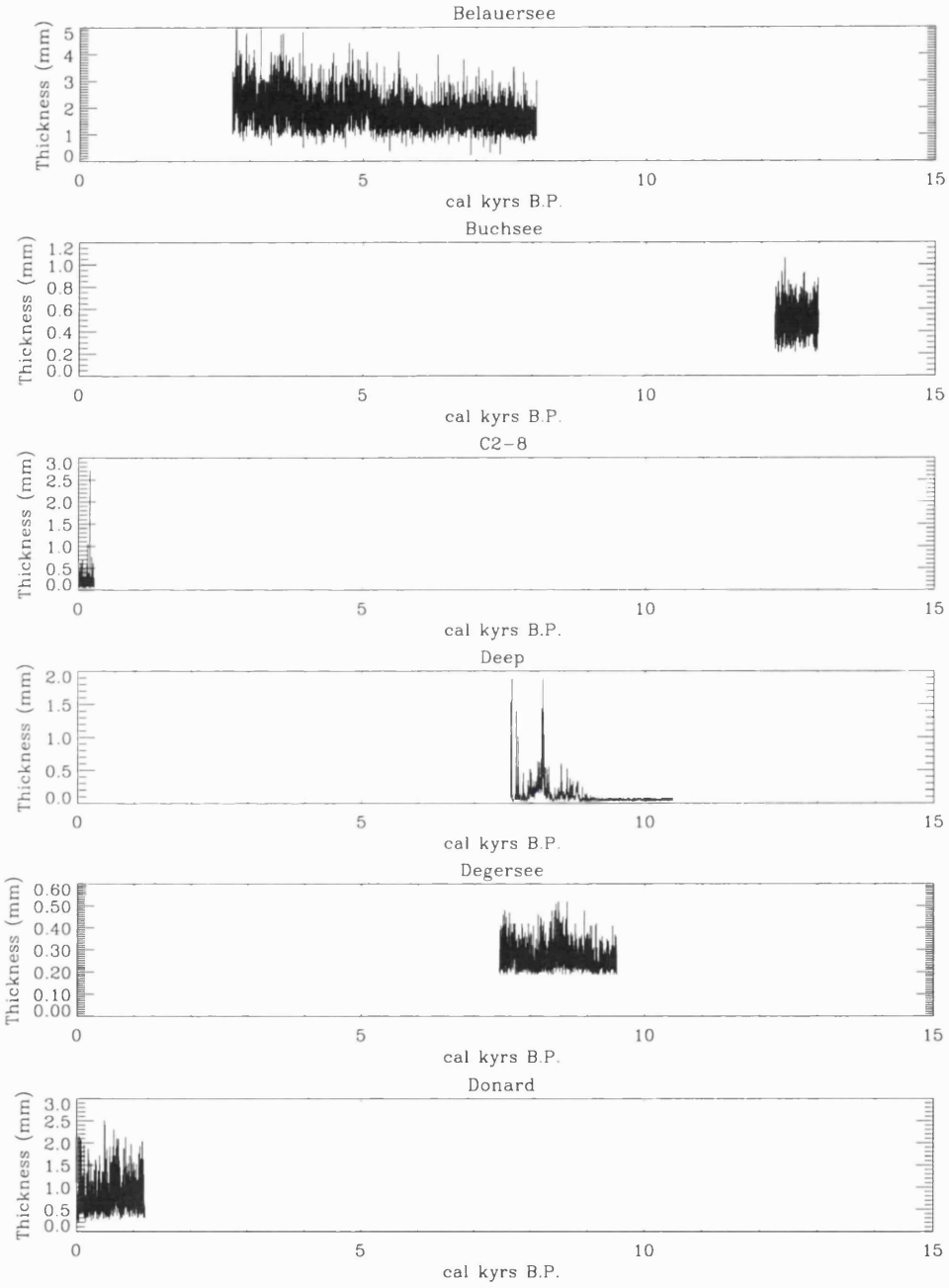

Figure 1.25: Figure illustrating the varve thickness time series from: Belauersee, Buchsee, C2-8, Deep, Degersee, and Donard.

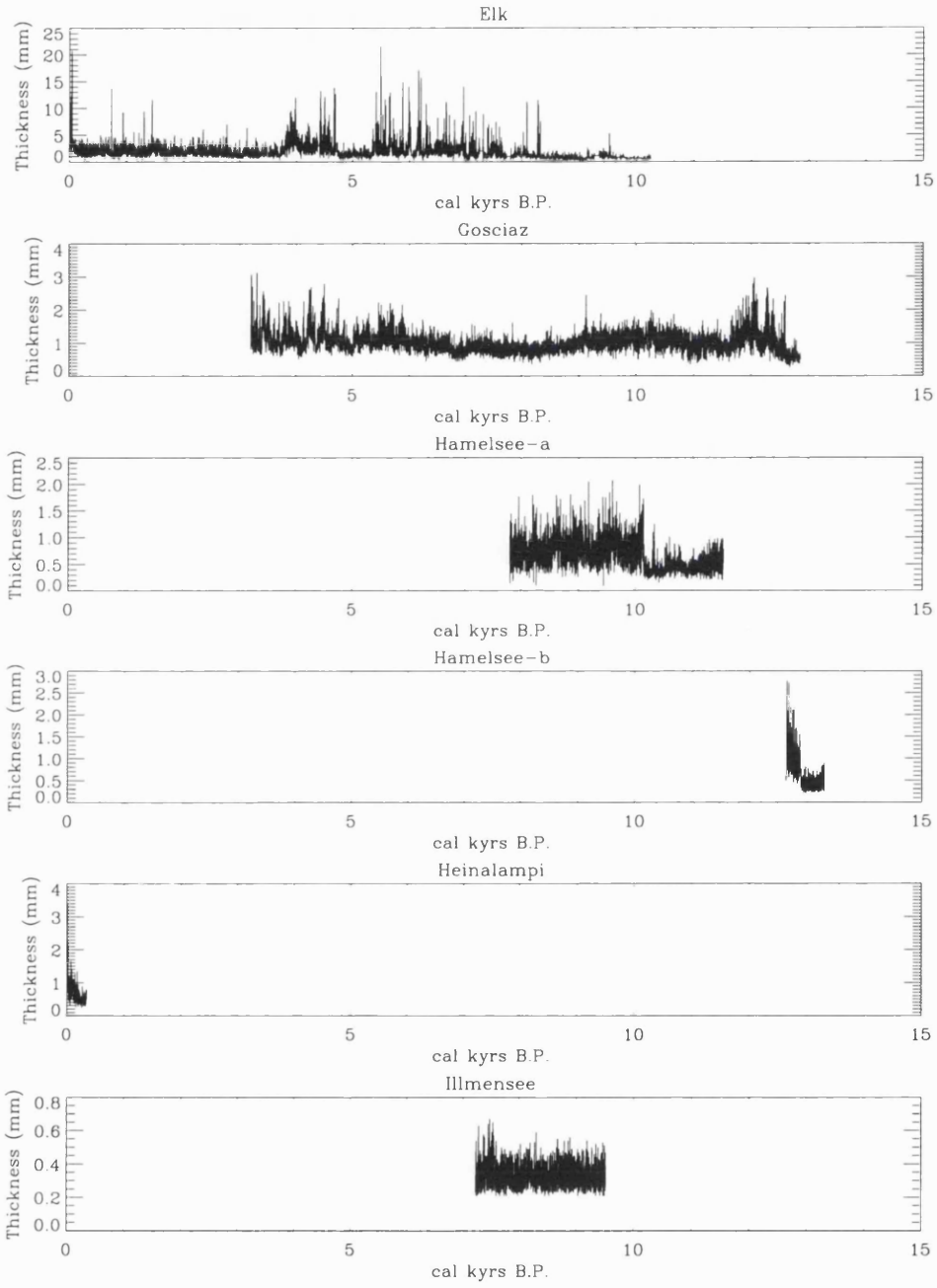

Figure 1.26: Figure illustrating the varve thickness time series from: Elk, Gosciaz, Hamelesee-a, Hamelsee-b, Heinalampi, and Illmensee.

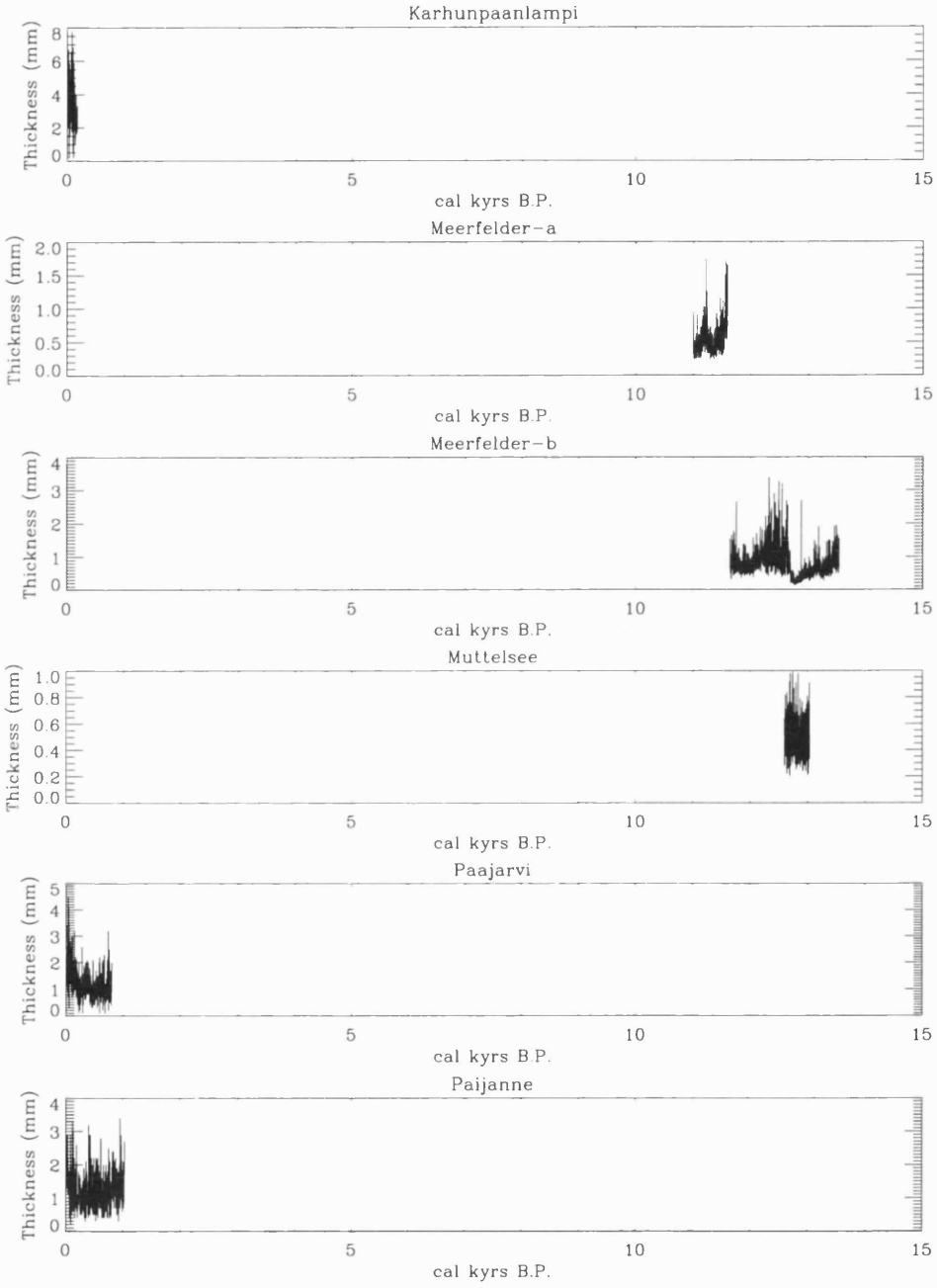

Figure 1.27: Figure illustrating the varve thickness time series from: Karhunpaanlampi, Meerfelder-a, Meerfelder-b, Muttelsee, Paajarvi, and Paijanne.

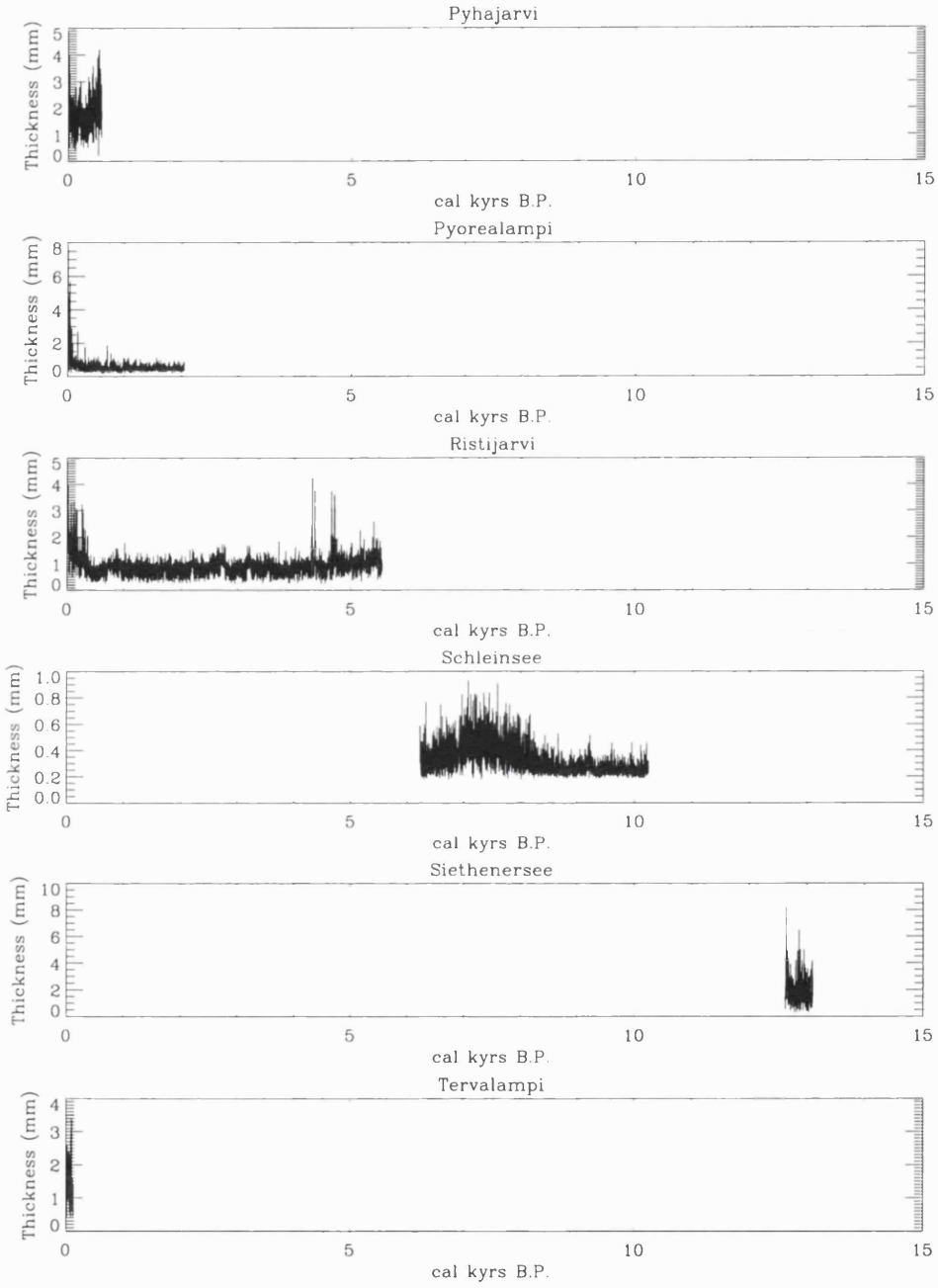

Figure 1.28: Figure illustrating the varve thickness time series from: Pyhajarvi, Pyorealampi, Ristijarvi, Schleinsee, Siethenersee, and Tervalampi.

Lake	μ	Min.	Max.	σ^2	γ_1	γ_2
Belauersee	1.9	0.22	4.96	0.37	0.83	4.48
Buchsee	0.52	0.21	1.06	0.02	0.27	2.87
C2-8	0.2	0.05	2.72	0.04	7.13	80.39
Deep	0.1	0.02	1.89	0.01	6.18	63.77
Degersee	0.27	0.19	0.52	0.003	1.1	4.06
Donard	0.78	0.16	2.51	0.137	1.27	4.78
Elk	1.89	0.08	21.64	2.009	3.57	26.73
Gosciaz	1.02	0.26	3.13	0.1	1.17	6.17
Hamelsee-a	0.69	0.09	2.07	0.08	0.68	3.57
Hamelsee-b	0.68	0.19	2.78	0.17	1.58	5.97
Heinalampi	1.06	0.24	25.19	3.74	8.7	94.97
Illmensee	0.33	0.21	0.67	0.01	0.64	3.42
Karhunpaanlampi	3.82	0.18	14.09	4.64	1.95	8.29
Meerfelder-a	0.55	0.23	1.73	0.05	1.61	7.16
Meerfelder-b	0.8	0.13	3.39	0.16	1.56	7.69
Muttelsee	0.5	0.2	0.99	0.02	0.55	3.25
Paajarvi	1.35	0.1	12.5	0.83	5.76	58.23
Paijanne	1.3	0.2	6.5	0.41	2.61	16.94
Pyhajarvi	1.73	0.2	4.2	0.37	0.71	3.94
Pyorealampi	0.69	0.2	9.38	0.6	6.13	49.3
Ristijarvi	0.94	0.25	4.24	0.14	2.33	14.92
Schleinsee	0.33	0.18	0.93	0.01	1.3	4.7
Siethenersee	1.94	0.3	8.23	1.03	1.46	7.09
Tervalampi	1.66	0.44	6.04	0.77	1.48	6.37

Table 1.3: Summary of time series statistics in this study. Mean - μ, Minimum - min., Maximum - max., standard deviation - σ^2, Skewness - γ_1, Kurtosis - γ_2.

Chapter 2

Method

2.1 Preprocessing

2.1.1 Sampling

Natural systems are characterised by variability on all timescales. As such an inherent problem of generating a time series from natural systems is that the sampling resolution, Δt, rarely matches the actual resolution. Such undersampling manifests itself in the power spectrum, whereby high frequency components beyond the Nyquist frequency, $\lambda_N = \pi\Delta t$, can "fold-back" contaminating spectral components, i.e., aliasing [156]. In this study, although sub-seasonal variability is apparent, the annual nature of the sampling is thought to sufficiently capture the variability under investigation.

2.1.2 Stationarity

Typically, natural systems display non-stationary signatures. The two main forms of non-stationarity in a time series are trends and abrupt changes. A trend is represented by a parameter changing in a continuous and systematic manner, comprising all the frequency components whose wavelength is greater than the length of the observed series. The harmonics that characterise a trend are inversely proportional to frequency. So when a trend is transformed into a contribution to the power spectrum, it will subsequently be inversely proportional to the square of the frequency. This will influence the low frequency range of the power spectrum, and mask variability at higher frequencies [157].

A time series in which there is a single abrupt change of a statistical moment, constitutes a basic example of non-stationarity. Abrupt changes occur between one or more regimes, when the period of the change is substantially shorter than states before and after this change [158]. In this study, the time series are not detrended, as any trends that exist (along with the cyclic and noise components) are considered valuable statistical components of natural system variability. In addition, the time series are not partitioned according to abrupt changes, as the mean (frequently removed in standardising) and variance are considered important natural system statistical variables. In addition, partitioning time series into stationary subsets is complicated by the scale dependent definition of abrupt change.

2.2 Quantifying Distributions

2.2.1 Mean, Variance and Covariance

A time series representing a natural system is given as, $x(t) = x_0, x_1, x_2, ..., x_T$, where $x_0, x_1, x_2, ..., x_T$, etc., are successive observations of a given parameter at equally spaced intervals at times $0, \Delta t, 2\Delta t$, etc.

Such a time series can be classified according to the underlying component parts (see Figure 2.1.), e.g.,

1. $x_t = D_t + N_t$, where D_t is a deterministic component, and N_t is a stochastic component [159].

2. $x_t = S_t + N_t$, where S_t is a signal component and N_t is a noise component [160]

3. $x_t = C_t + T_t + N_t$, where, C_t is a cyclic component, T_t is a trend and N_t is a noise component [161].

The series $x(t)$ in terms of fluctuations around a mean value $\bar{x}(t)$, defined over time T, are given as,

$$\bar{x}_T = \frac{1}{T}\sum_{t=1}^{T} x(t)$$

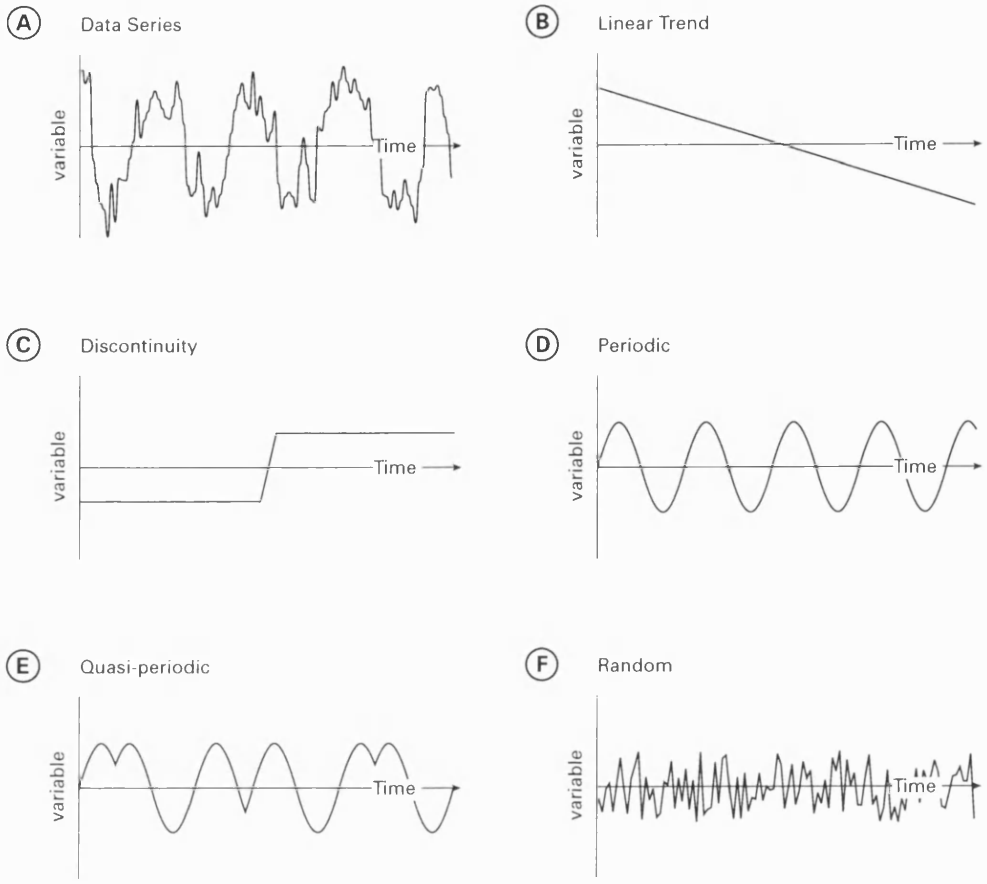

Figure 2.1: Schematic diagram illustrating hypothetical components of A. a time series. B. linear trend. C. discontinuity. D. periodic. E. quasi-periodic. F. random.

$$\lim_{T\to\infty} \bar{x}_T \equiv \langle x \rangle. \tag{2.1}$$

This is a time average, where the average is taken of the variable $x(t)$ at a given time instant t. Fluctuations of a time series around its mean is given as, $x(t) = (\bar{x} + x_0), (\bar{x} + x_1), (\bar{x} + x_2), ..., (\bar{x} + x_T)$, where $x_0, x_1, x_2, ..., x_T$, are the deviations of each successive observation about the mean $\bar{x}$. Properties of the deviations of a fluctuating signal about its mean, can be found from the higher order moments, $\langle x^n \rangle$. The variance of the time series is given as,

$$\begin{aligned} \mathrm{var}(x(t)) &= \frac{1}{T}\sum_{t=1}^{T}[x(t) - \bar{x}_t]^2 \\ &= \langle [x - \langle \bar{x} \rangle]^2 \rangle \end{aligned}$$

$$\equiv \sigma^2(x). \tag{2.2}$$

The square root of the variance is the standard deviation $\sigma(x)$, that is, the amount the values of x deviate from the mean value. The covariance is a measure of the tendency for two variables to vary together, and is defined as the ensemble average of the product of deviation of one random variable, x, from its mean with the deviation of the other variable, y, from its mean, given as,

$$\begin{aligned} \mathrm{cov}(x,y) &= \langle (x_n - \bar{x})(y - \bar{y}) \rangle \\ &= \langle xy \rangle - \langle x \rangle \langle y \rangle \\ &= \sigma^2(x) \qquad \text{when y = x.} \end{aligned} \tag{2.3}$$

Normalising with the product of the two respective standard deviations, defines the correlation between the two variables, where a value of 1 corresponds to perfect positive correlation, 0 to no correlation, and -1 to perfect negative correlation (see Figure 2.2.), given as,

$$\frac{\langle (x_n - \bar{x})(y_n - \bar{y}) \rangle}{\sqrt{\langle (x_n - \bar{x})^2 \rangle \langle (y_n - \bar{y})^2 \rangle}}. \tag{2.4}$$

2.2.2 Quantifying Scale Invariance

Scale invariance is quantified by generic quantities, i.e., scaling exponents, but they are not diagnostic in terms of identifying physical environments or processes [64]. These are calculated from best-fit regression lines in log-log plots of; autocovariance functions (α), power spectra (β), fluctuation analysis (H), and exceedence probability (D). The scaling exponents are defined below.

2.2.3 Autocovariance Function

The relationship between the fluctuations around the mean of a signal at time t and of the same signal at some future time $(t + \tau)$, can be computed from the

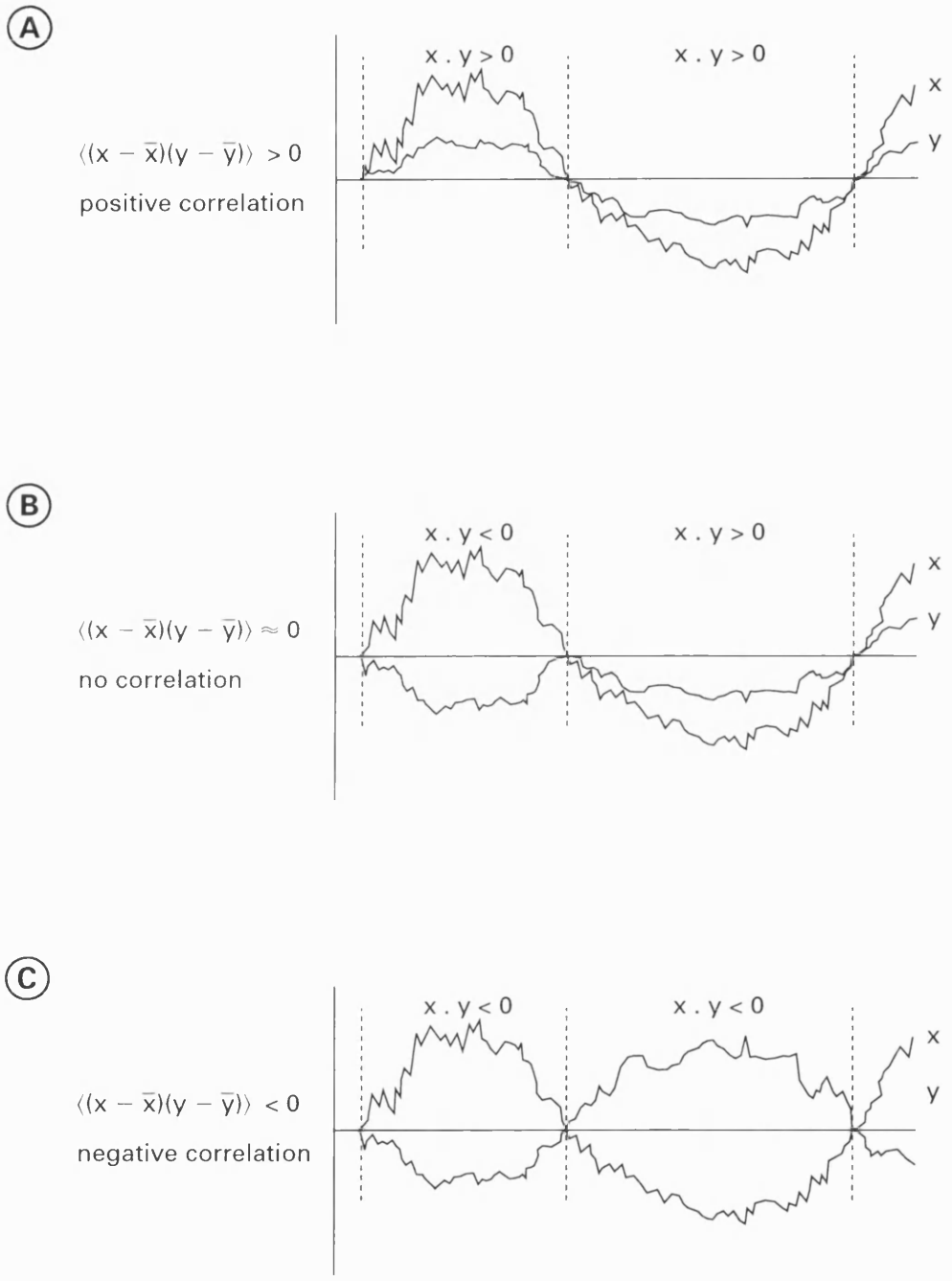

Figure 2.2: Schematic diagram illustrating the concepts of correlation with respect to two hypothetical time series x and y. A. positive correlation. B. no correlation. C. negative correlation.

autocovariance function ($c(\tau)$), i.e., the covariance between the signal $x(t)$ and the lagged signal $x(t+\tau)$, given as,

$$c(\tau) = \langle [x(t+\tau) - \langle x \rangle][x(t) - \langle x \rangle] \rangle. \tag{2.5}$$

Normalising this quantity with the variance (for $\langle x \rangle = 0$) gives,

$$\tilde{c}(\tau) = \frac{\langle x(t)x(t+\tau) \rangle}{\langle x^2(t) \rangle}, \tag{2.6}$$

$$\tag{2.7}$$

so that $\tilde{c}(0) = 1$.

For certain self-similar processes over a certain range the scaling exponent α, is given as,

$$\tilde{c}(\tau) = 1 - \lambda \tau^{\alpha}, \tag{2.8}$$

for $0 < \tau < T$ (where T is an upper limit), and $0 < \alpha$, and where λ is a constant.

2.2.4 Power Spectrum

The variance of a time series $(x_1, x_2, ...x_T)$ of finite length may be attributed to different timescales by expanding it into a finite series of trigonometric (sines and cosines) functions [159], given as,

$$x_t = A_0 + \sum_{k=1}^{T-1/2} (a_k cos \frac{2\pi kt}{T} + b_k sin \frac{2\pi kt}{T}). \tag{2.9}$$

This equation distributes the variance in the time series to the periodic components in the expansion below from Parcevals theorem, given as,

$$\frac{1}{T} \sum_{t=1}^{T} (X_t - \bar{X})^2 = \int x^2 dx = \sum (a_k^2 + b_k^2). \tag{2.10}$$

The elements $(a_k^2 + b_k^2)$ are collectively referred to as the periodogram of the finite series $X_1, ..., X_T$ when they are multiplied by $T/4$ [159]. This periodogram is the

Fourier transform of the estimated autocovariance function $c(\tau)$ evaluated at the Fourier frequencies ω_i, given as,

$$\sum_{\tau=-\infty}^{\infty} c(\tau)e^{-2\pi\tau\omega}. \tag{2.11}$$

The Wiener-Khintchin theorem states that the Fourier transform of the autocorrelation function equals the power spectrum. The estimated autocovariance function is computed from the original time series. The power spectrum is then obtained by taking the real discrete Fourier transform (DFT) of this autocovariance function. This is a function of frequency $P(\omega)$ defined at the interval $\frac{-1}{2\Delta t}, \leq \omega \leq \frac{1}{2\Delta t}$ is given as,

$$\begin{aligned} P(\omega) &= \frac{1}{N\Delta t}(X|\omega|^2) \\ \text{for } n &= 0, 1, ..., \frac{(N-1)}{2}, \end{aligned} \tag{2.12}$$

where Δt is the sampling interval, N is the number of observations, and $X(\omega)$ is the DFT which was computed using the fast Fourier transform (FFT) algorithm. This proceedure only holds for stationary time series.

For certain self-similar processes over a certain range the scaling exponent β, is given as,

$$P(\omega) \sim \omega^{-\beta}, \tag{2.13}$$

for $\omega_1 < \omega < \omega_2$.

As the low frequencies are not well represented by the short time series, the artificial sharp edges create spurious power. This problem is circumvented by applying a Hanning window and calculating the power spectrum using the FFT algorithm over a number of temporal intervals with a length shorter than the entire time series, and each of which with its own power spectrum (see Figure 2.3.). Then all these power spectra are averaged, allowing a significant increase in the accuracy of spectrum calculation without using the frequency smoothing.

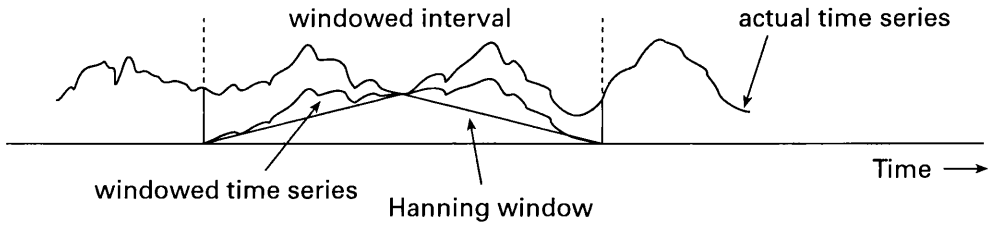

Figure 2.3: Schematic diagram illustrating the application of a Hanning window to a time series. The effect of the Hanning window is to adjust the form of the time series in order to reduce the effects of the truncation associated with finite length.

2.2.5 Fluctuation Analysis

Fluctuations of a time series $x(t)$, can be charcaterised as a random walk, calculated from the net displacement $y(t)$, and defined by the running sum,

$$y(t) \equiv \sum_{i-1}^{t} u_{(i)}. \tag{2.14}$$

A statistical quantity characterising the walk is the root mean square $(r.m.s)$ fluctuation of the average displacement. This is also known as fluctuation analysis, given as,

$$F(t) \equiv \sqrt{\langle (\Delta y(t))^2 \rangle - \langle \Delta y(t) \rangle^2}, \tag{2.15}$$

where, $\Delta y(t) \equiv y(t_0+t) - y(t_0)$, and the angular brackets indicate an average over all positions t_0 in the walk [162], [80], [76]. From this analysis, three types of system behaviour can be distinguished for $F(t) \sim t^H$, where H is a scaling exponent; (i) $H = 0.5$ (uncorrelated time series), (ii) $H > 0.5$ (positive long-range correlations), and (iii) $H < 0.5$ (negative long-range correlations) [80].

2.2.6 Exceedence Probability Analysis

Given the frequency distribution $N(x)$ of some quantity x, it is said to display scaling if it follows a power law, given as, $N(x) = Cx^{-D}$, where C is a constant, D is a scaling exponent, and N, in the case of varve sedimentation, is the number of layers with thickness greater than x [111], [123].

2.2.7 Features of Scale Invariance

In a nutshell, when α, β, and H are increasing, D decreases, representing a time series with many large values are few small values. Conversely, when α, β, and H are decreasing, D increases, representing a time series with a range of large and small values. Such exponents only hold if a system displays self-similarity over certain ranges, typically long periods. Within such ranges, crossovers may occur where one or more scaling exponents characterise the process. Relations exist for these scaling exponents for certain processes, e.g., (i) $\beta = 2H \pm 1$ [65], (ii) $\alpha = \beta - 1$ (for $p(\omega) \propto \omega^{-\beta}$ [66], (iii) $D = (5 - \beta)/2$ [67], and (iv) $H = \alpha/2$ (for stationary random processes only) [68]. For a thorough mathematical description of scaling exponent relations, see [69], [70], [71]. However, many natural processes display more complex intermittent signatures, for which other scaling relations may hold [72]. The origin of scale invariance is inherently linked to nonlinear dynamics. However, a "universal organising principle" has yet to be conclusively established, as scaling originates from many different processes [167], e.g., (i) random walk, (ii) critical phenomena, and (iii) multiscaling.

Scale invariance is independent of the distribution of random variables, i.e., Gaussian or non-Gaussian (see Figure 2.4.). Generally, additive processes lead to Gaussian processes, from the central limit theorem, whereas multiplicative processes lead to non-Gaussian processes. Furthermore, in sedimentation, there are two aspects to be considered; (i) the "quantity" of the sedimentary deposit and (ii) the stratigraphic "position" of the sedimentary deposit. Although these properties are inherently linked, they need not display the same statistical signature [73], [74]. Tables 2.1. and 2.2. review the occurrence of statistical distributions in natural systems. Overall, natural processes are represented by at least one statistical distribution. In addition, all of the atmospheric, oceanographic, palaeoclimatic and sedimentologic records display a range of scaling exponents.

Parameter	Distribution	Reference
Marine shelf deposits	$D = 0.71$ and $D = 0.80$	[104]
Shallow water carbonates	exponential	[105]
Peritidal carbonates	exponential	[106]
Peritidal carbonates	exponential	[107]

Carbonates	exponential	[108]
Peritidal carbonates	exponential	[109]
Volcaniclastic turbidites	D = 1.12	[110]
Turbidites	D = -1.39 $\pm$ 0.02	[111]
Turbidites	D = -1.16	[111]
Turbidites	D = 1	[112]
Turbidites	β = -0.29/-0.11; -0.30/-0.21; -0.34/-0.34	[73]
Turbidites	D = -0.95	[113]
Turbidites	D = 0.70 $\pm$ 0.01 and D = 1.47 $\pm$ 0.02	[114]
Turbidites	D = 1.52 $\pm$ 0.02	[114]
Turbidites	exponential	[115]
Turbidites	log-normal	[116]
Turbidites	log-normal	[117]
Lake sediment acc.	D = -1.21 and D = -1.78	[12]
Varve thickness	H = 0.77	[118]
Varve thickness	H = 0.83	[119]
Varve thickness	log-normal	[120]
Varves thickness	log-normal	[121]
Fluvial particles	weibull, log-normal and gamma	[122]
Glaciodeltaic deposits	D = 1.0, 0.8, 0.5 and β = -0.36, -0.32, -0.32	[123]
Debris flows	D = -0.49 $\pm$ 0.01	[114]

Table 2.1: Summary of distributions for sedimentary parameters (power laws are represented by scaling exponents.)

Parameter	Distribution	Reference
Temperature	β = -0.54 and α = 1.6	[75]
Temperature	β = -2	[76]
Temperature	β = -1.8	[77]
Temperature	β = -0.5	[78]
Temperature	H = 0.55	[79]
Temperature	H = 0.65 and H = 0.40	[80]
Temperature	α = 0.7 and H = 0.65	[68]
Temperature	Gaussian	[75]
Temperature	Gaussian	[68]
Rainfall	β = -0.12	[81]
Rainfall	β = -0.2 $\pm$ 0.1 and β = -0.3 $\pm$ 0.1	[82]
Rainfall	β = -0.7	[83]
Rainfall	β = - 0.52	[84]
Rainfall	gamma and weibull	[85]
Rainfall	weibull	[86]
Rainfall	gamma	[87]
Precipitation	H = 0.74 $\pm$ 0.03	[88]
Precipitation	weibull	[89]
Precipitation	gamma	[90]
Humidity	β = -0.61 $\pm$ 0.01 and Gaussian	[91]
Atmospheric circulation	H = 0.6	[92]
Cloud albedo	log-normal	[93]
Cloud condensation	gamma	[94]
Sea surface temperatures	β = -1.07 $\pm$ 0.01	[95]
Sea surface temperatures	β = -2	[96]
NAO index	β = -0.22	[97]
CO_2 - Biosphere 2	D = -1.31	[98]
CO_2 - Byrd ice core	D = -2.3	[98]
GRIP δ O^{18}	β = -1.6	[99]
GRIP δ O^{18}	β = -1.4	[100]
GRIP Ca	β = -0.6 and β = -2	[101]
Tree ring indicies	H = 0.68 $\pm$ 0.02	[88]
Tree ring indicies	β = -0.54 and β = -0.50	[84]
Fluvial discharge	β = -0.7 $\pm$ 0.3 and β = -1.6 $\pm$ 0.5	[82]
Fluvial discharge	β = -2.47 and β = -0.72	[102]
Fluvial sediment transport	β = -0.9 and H = 0.8	[65]
Fluvial sediment transport	D = -1.33 $\pm$ 0.03	[103]

Table 2.2: Summary of distributions for climatic parameters (power laws are represented by scaling exponents.)

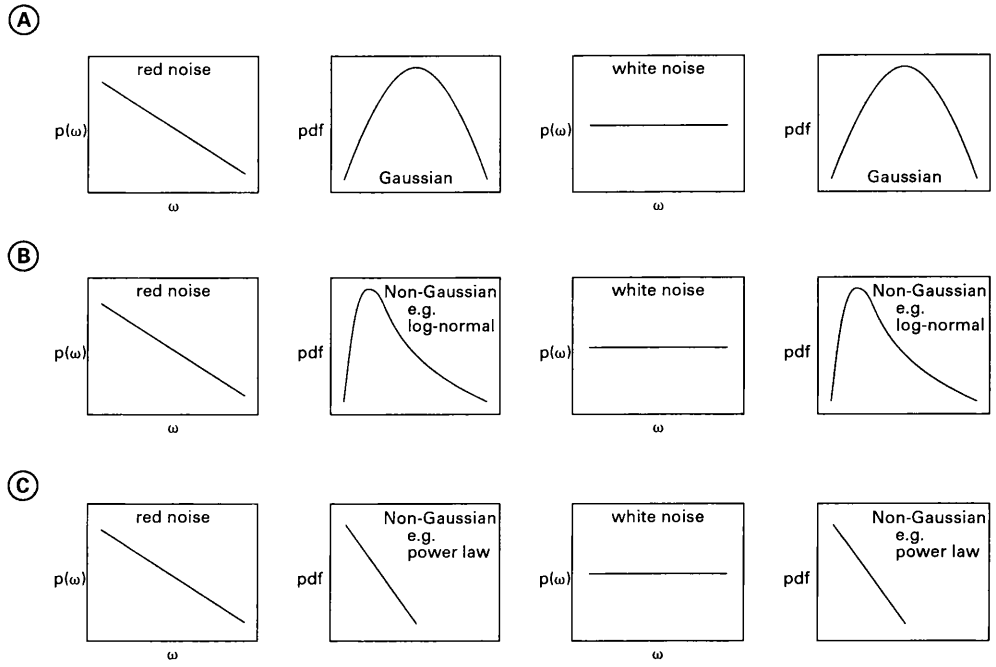

Figure 2.4: Schematic diagram illustrating the types of statistical signatures. In a range of natural systems the dynamics of the system can be measured as a quantity and as a position in time. The pdf is applied to investigate the quantity distributions, while the power spectra (and also autocorrelation functions, fluctuation analysis, etc) are applied to investigate the position distributions. A. a Gaussian quantity distribution can occur with a red or white noise power spectra (position distribution). B. a non-Gaussian, i.e., log-normal or gamma quantity distribution can occur with a red or white noise spectra (position distribution). C. a non-Gaussian, i.e., power law quantity distribution can occur with a red or white noise power spectra (position distribution).

2.2.7.1 Random Walk

We can represent the random walk evolution of a natural system by a simple analogy to coin tossing [168]. If we let the initial value of a time series $X(t)$ at $t = 0$ of the random variable be equal to zero $X(0) = 0$, and let the next variable be the outcome of tossing a coin. Then the next variable at the next instant of time has an equal probability of being greater or less than zero, and the size of the change is one unit, i.e., the outcome of a toss is $P_n = \pm 1$ (head or tail). The sum of the number of heads and tails is then, $X(t) = \sum_{n=1}^{t} P_n$ [65]. If we repeat this process indefinitely, the direction of change is random, but the value of $X(t)$ at any time depends to a large

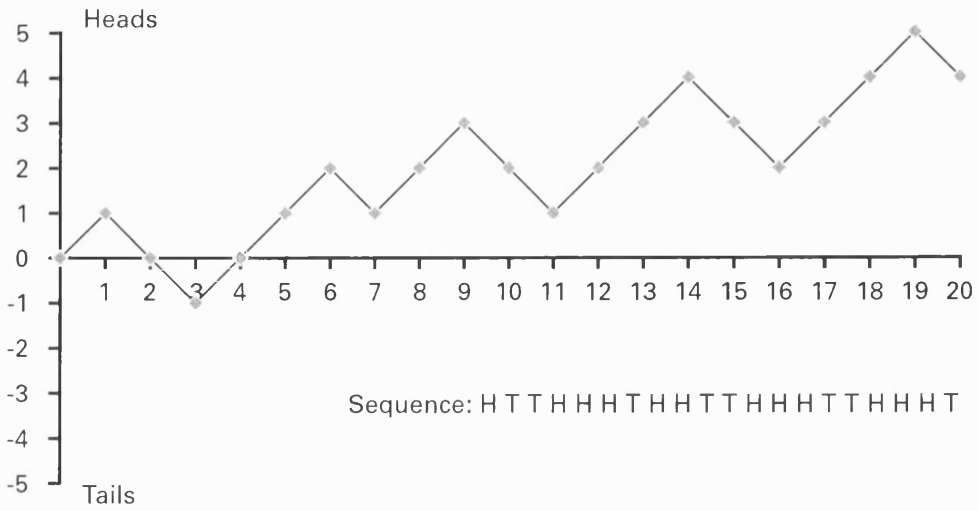

Figure 2.5: Schematic diagram illustrating random walk dynamics. The analogy of a random walk is coin tossing, whereby each toss of a coin, with outcome heads or tails is a random event. However, we would normally expect after a number of tosses for the mean of the process to occupy a position close to zero. The schematic displays this is not the case, and the position is dependent on the previous tosses.

extent of the "memory" of previous values. Thus, although we would expect the evolution of the time series to remain close the long term mean, we will have, zero average $\langle X(t) \rangle$, but, variance $\langle X(N)^2 \rangle = \sigma_\theta^2 t$. Rather than the fixed size of change of one from the coin tossing analogy, we can extend the random walk model by having the size of the increment as variable drawn from some probability distribution [169]. If the series of random variables are drawn from a probability distributions that forms a white noise, these numbers are used as the increments of the random walk, then we can produce a Brownian motion (see Figure 2.5.) [169]. The random walk model has been applied in climatology to explain the response of the ocean (slower) response to (faster) atmospheric forcing [170], [79].

2.2.7.2 Critical Phenomena

As fluctuations in an open dissipative system approach a critical point, they increase in strength at every scale [171]. Directly at the critical point, the system undergoes a phase transition (sudden changes of the macroscopic state of an entire system, caused by threshold crossing of a microscopic component [172], e.g., liquid $\rightarrow$ gas

and magnetic $\rightarrow$ non-magnetic), whereby the generally exponential fluctuations, change into a power law, via self-organisation, i.e., positive feedback mechanisms. The system then effectively exists on all time and length scales; from molecules (microscale) to the entire system (macroscale), resulting in universal behaviour, termed Self-Organised Criticality (SOC), where the system balances on the "edge of chaos" [172]. As such, system evolution, and order on the "edge of chaos" is then be dictated by a sequence of relaxation's from criticality to a new marginally stable situation. As natural systems are hierarchically arranged (where fluctuations of elements in a given level X_i are relevant to a group of elements of the previous level, $X_i - 1$), relaxations can only arise if a certain portion of the fluctuation in the above level, $X_i + 1$ has already relaxed (see Figure 1.1.) [20]. As such, the system may be susceptible to another event of different size and duration [95], which may be caused by both minor and major changes, on time scales faster than the time scale at which they are forced [111]. In addition to the power law, the other primary signatures of SOC are; (i) a large number of degrees of freedom, (ii) opposing mechanisms, preventing accommodation in any sort of equilibrium, and (iii) thresholds, where each individual unit changes abruptly its behaviour when a certain limiting value is reached (see Figure 2.6.) [95]. SOC has been suggested as the underlying dynamics of numerous natural systems including; humidity [91], sea surface temperature [95], CO_2 fluctuations [98], fluvial sediment transport [103], glaciodeltaic deposits [123], turbidite deposits [113], [111], and lake systems dynamics [12].

2.2.7.3 Multiscaling

Scaling originating from random walks and critical phenomena is termed monoscaling, and is represented by one scaling exponent. However, there are instances when several local scaling exponents are required to describe a process, i.e., multiscaling [166], which is characterised by a multiplicative cascade of singularities, representing structures of greatly varying intensities and scales (see Figure 2.7.) [174], [103], [175]. Numerous natural phenomena display multiscaling signatures, including; δ O^{18} in the GRIP ice core [100], river flows [82], [102], and rainfall [82], [81].

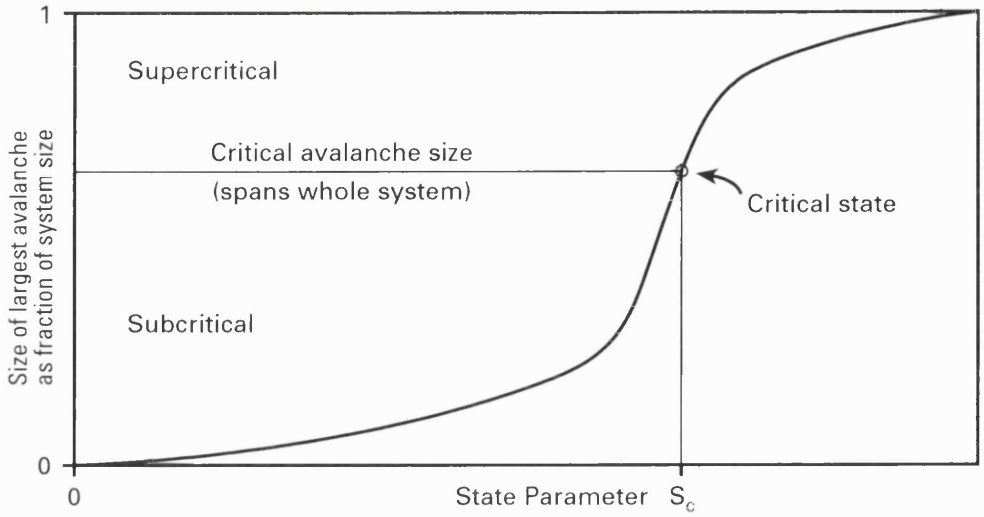

Figure 2.6: Schematic diagram illustrating self-organised critical dynamics. The critical state is the smallest value of S that allows avalanches to span the whole system. Starting from any point the system will do to the critical state, i.e., globally independent of initial conditions. After [173].

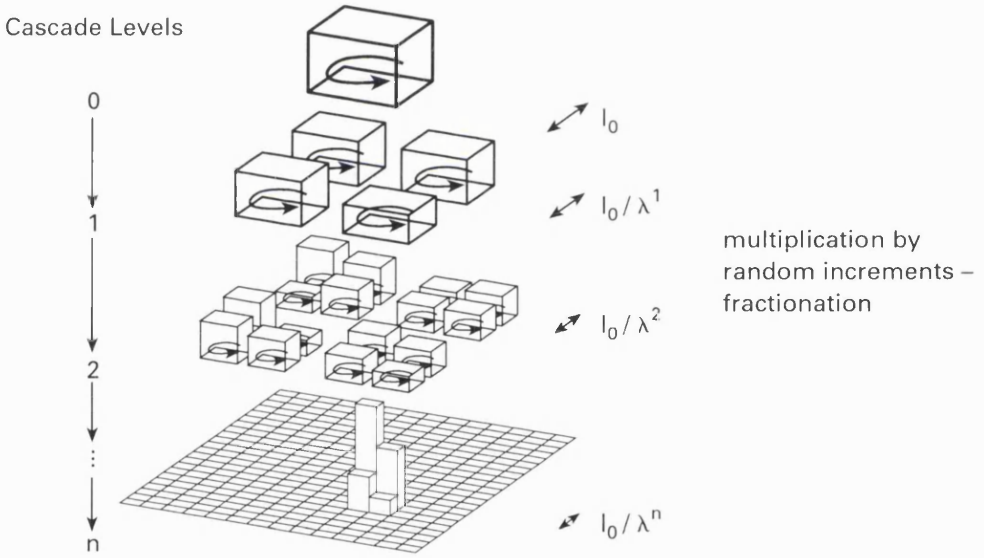

Figure 2.7: Schematic diagram illustrating multiscaling dynamics. A cascade process in 2D is characterised by partitioning of eddies into sub eddies, and related transfer of energy flux. The large scale flux of the field this multiplicatively modulates the smaller scale fluxes. After [176].

2.2.8 Probability Density and Cumulative Distribution Functions

Random variables are defined as real-valued functions on the sample space Ω, which is a list of possible outcomes of an experiment, where each item in the list is a

simple event. For example, if we throw a coin ten times, then we may be interested in the number of heads obtained rather than the precise sequence of H (head) and T (tail) which is observed. As such, random variables depend upon which event in Ω takes place when the experiment is conducted [159]. For example, suppose a coin is tossed three consecutive times, and if we let X be the number of heads obtained. The correspondence between the simple events of the experiment and the values taken by X are $\Omega = HHH, HHT, THH, TTH, THT, HTT, TTT$, where $X = 3, 2, 2, 1, 1, 1, 0$, respectively. These random variables are described as discrete or continuous.

For events described in terms of continuous random variables, the probability of an event is expressed as the integral of a probability density function (pdf) taken over the interval that describes the event. Effectively, the pdf is the probability that a random variable lies in a certain infinitesimal interval. If we let X be a continuous random variable that takes values in the interval Ω, then the probability density function for X is a continuous function $f_X(\cdot)$ defined on the real line $\mathcal{R}$ with the following properties; (i) $f_X(x) \geq 0 \forall\, x \in \Omega$, (ii) $\forall f : \int_\Omega f(x)dx = 1$, and (iii) $P(X \in (a, b)) = \int_a^b f_X(x)dx \forall\, (a, b) \subseteq \Omega$.

An equivalent description of the stochastic characteristics of a continuous random variable is given by the distribution function, frequently referred to more descriptively as the cumulative distribution function (cdf). The distribution function for X is a non decreasing differentiable function $F_X(\cdot)$ defined on the real line $\mathcal{R}$ with following properties; (i) $\lim_{x\to-\infty} F_X(x) = 0$, (ii) $\lim_{x\to+\infty} F_X(x) = 1$, and (iii) $\frac{d}{dx}F_X(x) = f_X(x)$.

The central limit theorem states that the distribution of a sum of independent and identically distributed random variables converges towards a normal distribution as the number n, of random variables increases (see Figure 2.8.) [159]. In this study we compare the distribution of the varve thickness time series with the two distributions; (i) log-normal, given as [163],

$$f(x) = \frac{1}{\sqrt{2\pi}\sigma}\frac{1}{x}\exp(-(\log(x) - \log(\theta))^2/2\sigma^2), \tag{2.16}$$

and (ii) gamma, given as [163],

$$f\alpha,\nu(x) = 1/\Gamma(\nu)\alpha^{\nu}x^{\nu-1}\exp^{-\alpha x}\,. \tag{2.17}$$

The Gaussian limit for the gamma function is given as [163],

$$\sqrt{\nu}/\alpha f((\nu + \Gamma\nu x)/\alpha) \rightarrow 1\sqrt{2\pi}\exp^{-x^2/2}\,. \tag{2.18}$$

For the gamma distribution, ν is the shape parameter, and α is the scale parameter. The mean of the gamma distribution is related to the parameters ν and α by $E(Z_k) = \nu\alpha$, and the variance by $Var(Z_k) = \nu\alpha^2$ (see Figure 2.8.). The shape parameter is dimensionless, as it governs only the "shape" of the distribution, e.g., corresponding to the exponential distribution for $\nu = 1$, with the degree of skewness decreasing as ν increases. On the other hand, the scale parameter α has no bearing on the shape of the distribution. For $\nu = 1$, the gamma function is represented by an exponential function, while for $\nu > 1$, the function is a non-symmetrical bell shaped distribution. As ν increases, the gamma density changes from a highly non-symmetrical function with large positive skewness to a broad, flat bell shaped curve. As α increases the height of the gamma density decreases [163].

2.2.9 Minimum Thickness and Probability of Detection

Natural phenomena, such as sedimentation, are characterised by finite sized events, whereas the fitted statistical distributions are based on infinitesimally small events [165]. As the minimum varve thickness in this study is ca. 0.20 mm, the fit of the statistical distribution would be truncated. We can circumvent this by applying another distribution, the probability of detection (POD). If we select varves of unit thickness as a random process x_i, where x is a stochastic variable, then they are selected from some distribution $\phi(x)$. In this study we can only detect varves $x > 0.2$, so the distribution is truncated, given as,

$$\tilde{\phi}(x) = \begin{cases} N\phi(x) & x > 0.2 \\ 0 & x < 0.2, \end{cases} \tag{2.19}$$

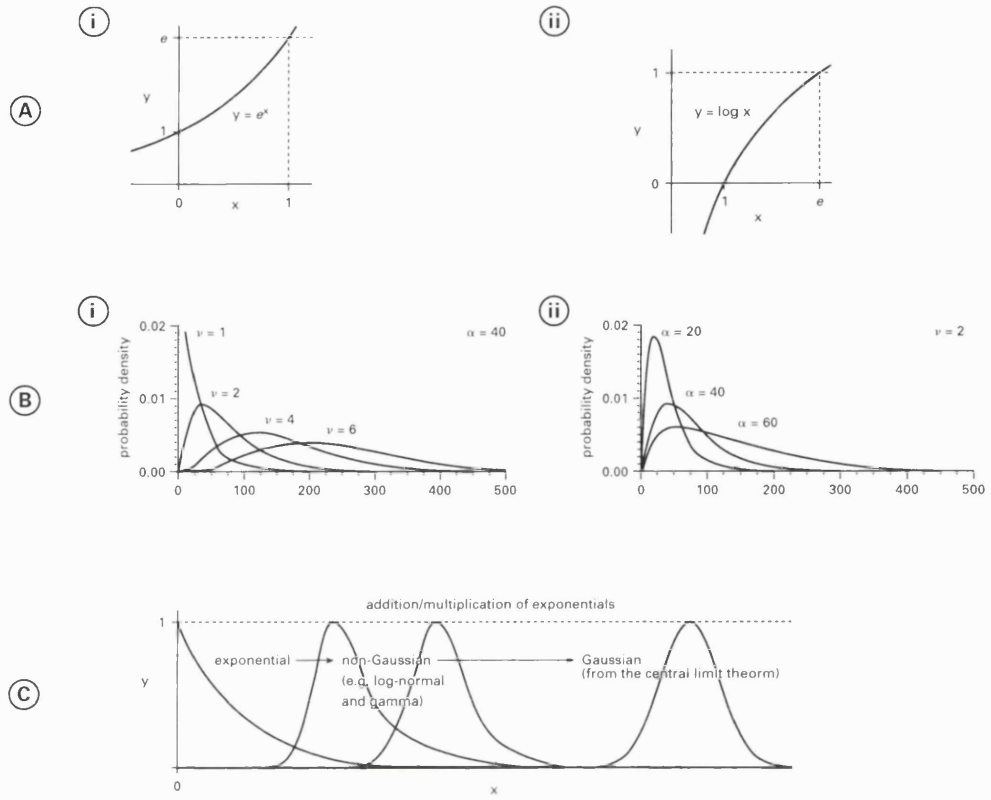

Figure 2.8: Schematic diagram illustrating illustrating various probability distributions. A. displays the link between logarithms and exponentials. After [164]. B. displays the flexibility of the gamma distribution (i) variable parameter ν with constant parameter α, and (ii) variable parameter α with constant parameter ν. After [90]. C. displays the addition and multiplication of random variables - exponentials, to form gamma and log-normal distributions. These evolve toward the normal distribution, from the central limit theorem.

where N is a normalisation constant.

This means we have applied the simple POD (see Figure 2.9.), where we say $P(x)$ is a sedimentation event, and $POD(x)$ is the probability distribution of x, is given as,

$$POD(x) = \begin{cases} 1 & x > 0.2, \\ 0 & x < 0.2. \end{cases} \tag{2.20}$$

From the POD, we have the distribution of x given as,

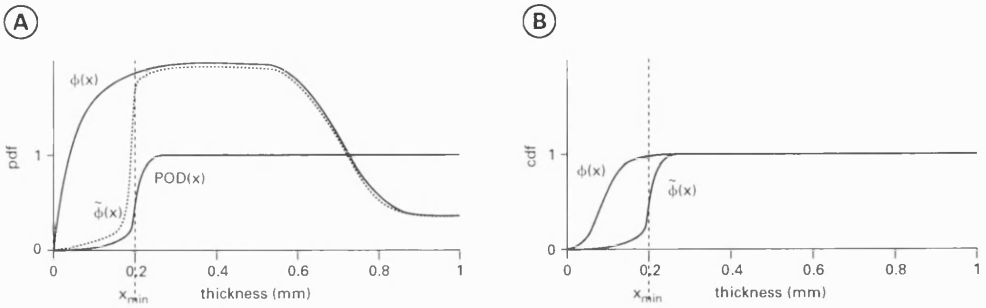

Figure 2.9: Schematic diagram illustrating the concepts of probability of detection. A. and B. display a typical fit to truncated data (in this study the minimum is 0.2mm) would be inaccurate. After [35].

$$\tilde{\phi}(x) = POD(x)\phi(x)N. \tag{2.21}$$

Integrating we have,

$$\begin{aligned} 1 &= \int \tilde{\phi}(x)dx \\ 1 &= \int_0^\infty POD(x)\phi(x)Ndx \\ 1 &= N\int_{0.2}^\infty \phi(x)dx \\ N &= 1/\int_{0.2}^\infty \phi(x)dx \\ N &= 1/\int_0^\infty POD(x)\phi(x)dx. \end{aligned} \tag{2.22}$$

2.2.10 Waiting-Time Distribution

Natural phenomena can be characterised by the time intervals between events of a unit value. In this study utilise the annual resolution of the varve thickness time series to calculate the time intervals between varves of unit thicknesses. Of particular interest are the relations between the times for "main" and "extreme" - thinner/thicker varves (see Figure 2.10.).

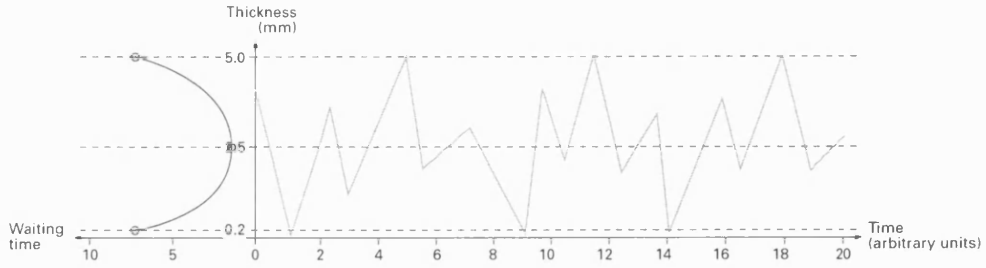

Figure 2.10: Schematic diagram illustrating the construction of waiting time distributions/ The time between varves of a unit thickness are averaged for a range of varying unit threshold values to produce a waiting time distribution curve. Effectively each period of thicker and thinner varves is an e-folding time between other thinner and thicker varves respectively. It is clear that the waiting time for the "extreme" thinner and thicker varves is longer than that for "main" values.

2.2.11 Null Hypothesis - Red and White Noise

The time series in this study are assessed with respect to white noise, i.e., random and red noise, i.e., simple random walk scaling. A white noise time series is generated by shuffling the original time series in order to create a random surrogate time series [177]. A red noise time series is generated from an AR(1) process, a discrete differential equation [178]. System dynamics, i.e., global variables can be represented by such reduced sets of differential equations, through the slaving principle, where fast system variables can become "slaved" to slow system variables and lose their status as independent dynamical variables. This allows the compression of information that is necessary to describe natural systems into a few order parameters, i.e., ordinary differential equations (ODE's) [23], [25].

There are four versions of uncoupled ODE's that can be applied to quantify system dynamics. The first is given as,

$$\dot{y} = f(y), \tag{2.23}$$

which is non-coupled, autonomous, without a constant, where $f(y)$ is some given function of y. This is the archetypal equation for deterministic dynamical systems [179]. However, for many natural systems, there is a natural discrete unit of time (e.g., one year for varves) where the evolution is described by a sequence of y_i with

index i indicating time, i.e., $y_i = y(t_i)$. The dynamical rule is expressed as an iterated function, given as,

$$y_{i+1} = f(y_i), \tag{2.24}$$

where f is a vector function with vector arguments [179].

The second is given as,

$$\dot{y} = f(y, t), \tag{2.25}$$

which is non-coupled, non-autonomous, without a constant, where $f(y, t)$ is some given function, vector or field of y, and where $y = (y_1, y_2, ...)$, and is a variable or field and time t, and initial condition $y = y_0$ at $t = 0$, y_0 being a given constant. The third is given as,

$$\dot{y} = f(y, \lambda), \tag{2.26}$$

which is non-coupled, autonomous, with a constant, where $f(y, \lambda)$ is some given function, vector or field of y and λ is a constant, or set of control parameters [180].

The fourth is given as,

$$\dot{y} = f(y, \lambda, t), \tag{2.27}$$

which is non-coupled, non-autonomous, with a constant, where $f(y, \lambda, t)$ is some given function, vector or field of y, where $y = (y_1, y_2, ...)$, and is a variable or field and time t, and initial condition $y = y_0$ at $t = 0$, y_0 being a given constant, and λ also being a constant.

The main forms of coupled ODE's that can be applied to quantify system dynamics are given as,

$$\begin{aligned} \dot{x} &= f(x, y) \\ \dot{y} &= g(x, y), \end{aligned} \tag{2.28}$$

which are coupled, autonomous, without a constant, where $x = (x_1, x_2, ...)$, $y = (y_1, y_2, ...)$ are the variables or fields, effectively, some dimension as x and y representing the system, f, g are some dimension as x, y [164]. Here we can assume that the variables y represent the slow components, and x represents the fast components [160]. As such, the fast variables would be represented in y, i.e., y is dependent on x and the slow variables would be a long time mean, $\bar{y}$ [160]. The forcing x can be considered to be a white noise, when x has forgotten its initial state over the typical time scale associated with y, and the influence of x on y can be described as a continuous random forcing, i.e., Brownian motion [160]. Here we apply an extension to the coupled equations, by explicitly involving time, t, as a variable. The dynamics of these coupled equations can be represented by a stochastic (continuous) differential and (discrete) difference equation, also known as a Langevin equation, given as,

$$dy = f(y)dt + \sigma dB, \tag{2.29}$$

$$\tag{2.30}$$

where dy and dt are the change in time t of y. However, as σdB does not physically exist, it is more legitimate to write the equation in a form involving infinitesimal small changes, given as [160],

$$dy = ydt + \sigma dB. \tag{2.31}$$

Without loss of generality we can take $y_0 = 0$ and expand $f(y)$ to the first order, given as,

$$dy/dt = -\lambda y + \sigma x, \tag{2.32}$$

and again, we can rewrite involving infinitesimal small changes, given as,

$$dy = -\lambda y dt + \sigma dB. \tag{2.33}$$

As the time series in this study are discrete y_n, where n corresponds to the discrete time index, we would use a discrete version of the Langevin equation, which is possible as differencing in discrete time corresponds to differentiation in continuous time [181], given as,

$$y_{n+1} = -\lambda y_n + \sigma \eta_{n+1}, \tag{2.34}$$

where $n = 1, ..., N$ denotes the discrete time increments in units of the sampling interval Δt, $0 \leq \lambda \leq 1$, λ is the value of the lag-one autocorrelation coefficient, describing the degree of serial correlation in the noise, and $\sigma \eta_n$ is uncorrelated zero mean Gaussian white noise sequence with variance σ^2 [178]. This is called an AR(1) (2.34) (Markov) process. The autocorrelation function is given as,

$$c(\tau) = e^{\lambda |\tau|}, \tag{2.35}$$

and the e-folding time is given as,

$$\tau = 1/\lambda, \tag{2.36}$$

which is the time it takes for the autocorrelation to change by a factor of $1/e$ when the exponent of e changes by ~ 1. This is a common way of expressing the time it takes for a system to reduce an imposed perturbation to a factor of $1/e$ of the perturbed value [75], [96], and is also the feedback timescale between the slow and fast variables [178]. Some typical e-folding times include; atmosphere - 11 days, ocean mixed layer - 7-8 yrs, deep ocean - 300-1000 yrs, mountain glaciers - 300 yrs, ice sheets - 3000 yrs, and the Earth's mantle - 30 ma yrs [182].

The power spectrum of y is the Fourier transform of the autocorrelation function, given as,

$$P_y(\omega) = \frac{2\lambda}{\omega^2 + \lambda^2}. \tag{2.37}$$

For $\omega \ll \lambda$ we have $P(\omega) \sim 1$, that is, y itself is a white noise signal on time scales long in comparison to the typical time scales of the y dynamics. For $\omega \gg \lambda$ we have $P(\omega) \sim \omega^{-2}$, which is a scaling red noise spectrum [160].

2.2.12 Attractors

2.2.12.1 Method of Delays

The method of delays allows the construction of the phase space spanned by the full set of variables $y_1, y_2..., y_n$, which represent the system dynamics. This is possible as the self-interaction between the variables in a dynamical system is such that every component of the time series contains information on the dynamics of the entire system [183]. We construct such a time series of the form,

$$y(t_i) = y(t_i), y(t_i + \tau), ..., y(t_i + (n-1)\tau), \tag{2.38}$$

where n is the embedding dimension of the vector $x(t_i)$, and τ is the delay function. We can visualise the system attractor by projecting it on the plane $y(t), y(t+\tau)$. The embedding dimension should be $\geq 2D + 1$, where D is the dimension of the manifold containing the attractor. This embedding procedure is controversial as it is only strictly valid for asymptotic limits, i.e., infinite time and infinitesimal perturbations. Whereas natural systems are characterised by non-infinitesimal perturbations and finite times [80]. The delay parameter, τ, is chosen to maintain linear independence. To date there is no preferred criteria, though values of τ that are too low lead to redundancy, i.e., excessively correlated, and values of τ to high lead to irrelevancy, i.e., no correlation. In this study we apply a value of $\tau = 2$.

- Damped Harmonic Oscillator

  A simple pendulum can be represented by a differential equation, given as,

$$d^2y/dt^2 + \omega^2 y = 0, \tag{2.39}$$

where x is the angular displacement of the pendulum from the vertical, ω is its natural frequency for small angular displacements, and t is time. This is a linear system, and is not chaotic because there is only one degree of freedom, that associated with x. Also the right hand side is a constant (zero), meaning that the system is autonomous. This can be rewritten, given as,

$$\ddot{y}(t) + \alpha_1 \dot{y}(t) + \alpha_2 y(t) = 0. \tag{2.40}$$

After a pendulum is set in motion, dampening will eventually bring the system to rest, i.e., $= 0$. Here we assume $\alpha > 0$, which corresponds to a friction (dampening) term that removes energy from the system. For a damped harmonic oscillator the attractor is the point at rest, i.e., in this case the origin. Thus a damped harmonic oscillator is described by a point cycle attractor. The dimension D of a point cycle is zero.

- Driven Harmonic Oscillator

  Any oscillator needs a source of energy to drive it (with the exception of idealised conservative systems). If the driving force is a random variable, then the system takes on the behaviour of a random process. So we can adapt the harmonic oscillator to describe the motion of a randomly disturbed pendulum, by applying a whole succession of impulses. As the impulses occur at random time instants the system will continue to oscillate, but will now exhibit irregular amplitudes and intervals [161], given as,

$$d^2y/dt^2 + \omega^2 y = \eta(t), \tag{2.41}$$

which is non-autonomous, because the time (t) has become an additional degree of freedom. This system may show chaotic dynamics according to the nature of the function $\eta(t)$. This can be written as a second order differential equation, given as,

$$\ddot{y}(t) + \alpha_1 \dot{y}(t) + \alpha_2 y(t) = \eta(t), \tag{2.42}$$

where at time t, $X(t)$ denotes the angular deviation of the pendulum, and $\eta(t)$, denotes the random impulse force acting on the pendulum, which changes with every time increment. This can be rewritten as a second order difference equation, effectively an AR(2), given as,

$$y_t + a_1 y_t - 1 + a_2 y_t - 2 = \eta(t), \tag{2.43}$$

where, $\eta(t)$ denotes the same type of purely random "white noise" process as above [161]. This forcing, $\eta(t)$, arriving at time t affects not only the value y_t, but also the values at all subsequent time points. The random process $\eta(t)$ is thus "drawn into" the system, exhibiting intrinsic stochastic behaviour [161]. A driven harmonic oscillator will lead to a limit cycle attractor. Systems characterised by limit cycle attractors are self-oscillating, and not dependent on initial conditions [184]. The stability of the oscillation is ensured by virtue of any oscillating particles outside or inside the limit cycle have the tendency to approach it, thus producing periodic movement from a non-periodic source of energy [184]. The dimension of a limit cycle is one.

- Torus

  If the trajectories from different initial conditions, which represent the evolution of the system in state space are attracted to and remain on a surface, then a torus attractor is produced [185]. The motion on the attractor is quasi-periodic, characterised by two frequencies related to the two different rotations on the torus [185]. Thus, if we know the evolution of such a system from an initial condition we can predict the evolution of the system from some other initial condition accurately [185].

- Strange

The attractors discussed above are "well-behaved" and usually correspond to systems whose evolution is predictable, and are thus also known as non-chaotic. However, for many other natural systems, the attracting set can be much more irregular, and can in fact have a dimension that is not an integer. Such sets are associated with strange attractors, which are fractal objects with self-similar properties [60].

2.2.12.2 Routes to Chaos

There are two main routes to chaos. The first route to chaos, known as the Ruelle-Takens route, is based on repeated bifurcations of attractors leading to chaos. Essentially for each of the attractor types; point, limit, torus and strange, the system approaches a critical value, then bifurcates into the next more complicated attractor until eventually chaos reigns [185]. The second route to chaos is known as period doubling (also via bifurcations) and is modelled by the logistic equation [186], [187] given as,

$$y_{n+1} = \lambda y_n(1 - y_n), \tag{2.44}$$

where y_{n+1} is a particular variable, λ is a forcing parameter, n is the iteration time step. This equation states that the next value $(y_n + 1)$ is some nonlinear function $f(y) = \lambda x(x-1)$ of the current value (y_i). This equation crucially involves feedback because the value of the state variable at a given time (y) is used to generate the values at the next time, y at $t + 1$ [188]. From this equation, stable behaviour with a single equilibrium value, oscillations between 2,4,8,16...stable states, and chaotic or incoherent behaviour are all possible. The logistic equation has been applied in ecology [186], [189], and climate [190], [191], [192], [193]. However, there are two main limitations associated with the application of the logistic equation to natural systems. Firstly, in some ecological populations a constant immigration factor inhibits the onset of chaos by a process called period reversal, prompting suggestions that chaos is fragile and easily inhibited [186], [194]. Secondly, such a model usually only captures system variability in the early stages of irregularity,

before the onset of full chaotic motions.

Chapter 3

Quantity Signatures

3.1 Introduction and Results

In this chapter we present the results from the pdf's and cdf's. Figures 3.5. to 3.7. display the pdf fits of the observed data to the POD for the log-normal (full curved line) and gamma (dashed curved line) distributions, as well as a fitted power law (full straight line). The x-axis is the varve thickness, and the y-axis is the probability density.

Generally, the observed data are fitted well by the gamma and log-normal distributions, e.g., Belauersee, Gosciaz, Ristijarvi and Schleinsee (see Table 3.1.). In addition, for all lakes in the central portion of the distribution, both the gamma and log-normal distributions, as well as the power law fit the observed data well, e.g., Belauersee, Buchsee, Elk, Gosciaz, and Hamelsee-a. Some time series, appear to be fitted equally well throughout the distribution by the power law, e.g., C2-8, Deep, Degersee, Hamelsee-b, Heinalampi, Meerfelder-a, Paajarvi, and Pyorealampi.

For the thinner varve variations, the full curved line of the log-normal distribution generally fits these data the best (with the exception of Donard which is fitted by the gamma), e.g., Belauersee, Gosciaz, and Hamelsee-a. Although these variations are noticeable, the number of data points at such values is small. In addition, there are instances when the thin varves are not adequately fitted by either distribution. For the thicker varve variations, the data is fitted equally well by both the gamma and log-normal distributions. Variations for the thicker varves are less than for the thinner varves, with exception of lakes Deep, Heinalampi, Paajarvi, Pyorealampi,

and Ristijarvi.

Figures 3.8. to 3.10. display the cdf fits of the observed data to the POD for the log-normal (full curved line) and gamma (dashed curved line) distributions. The x-axis is the varve thickness, and the y-axis is the cumulative probability density. The POD can be seen in good effect (at the 0.2 minima) in several of the lakes, e.g., Degersee, Ristijarvi, and Schleinsee. In comparison with the pdf's, less variation is seen in the cdf's (due to binning procedures), with slight deviations from the gamma and log-normal distributions seen in C2-8, Heinalampi, Paajarvi, Pyorealampi, and Ristijarvi.

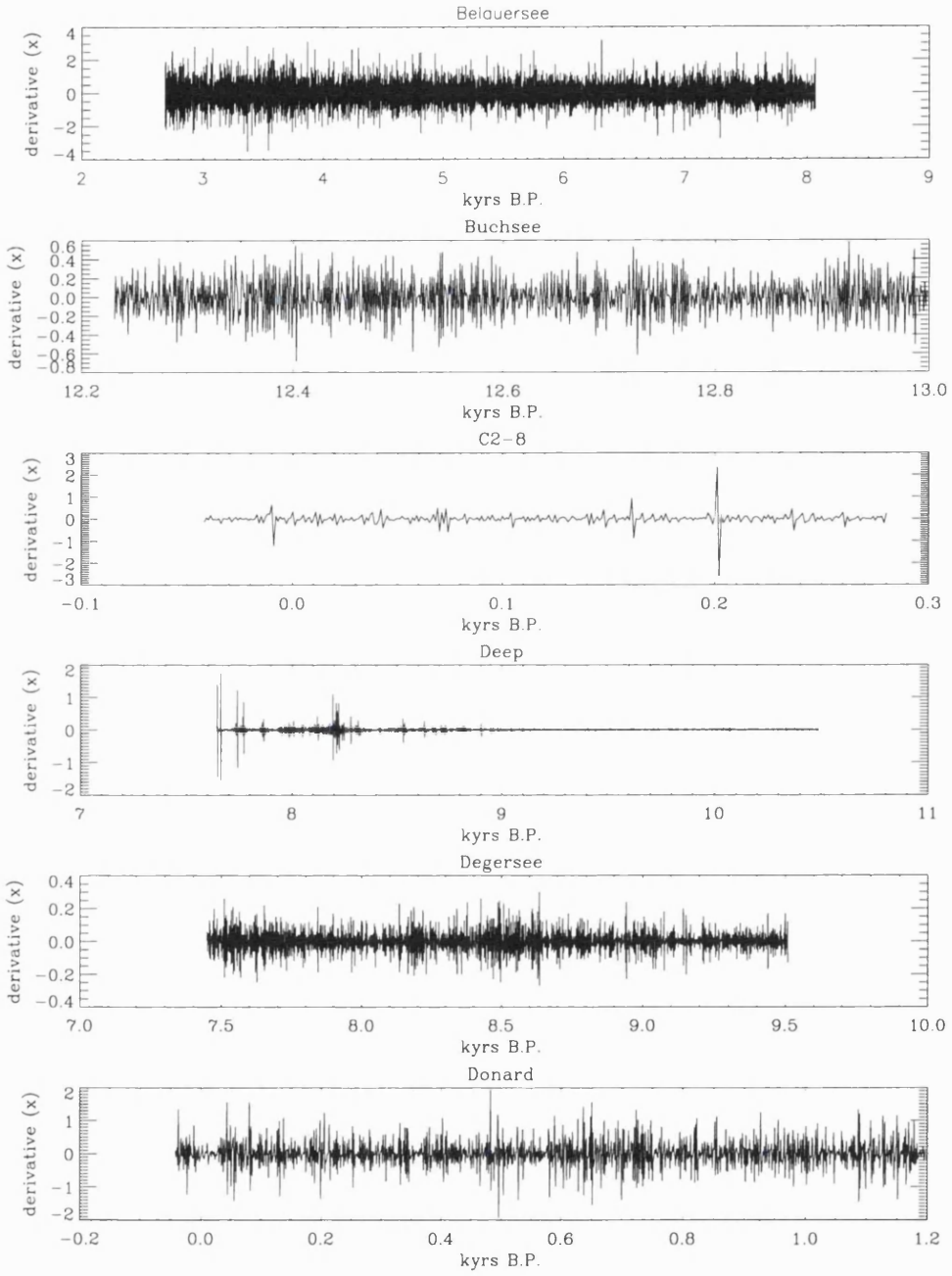

Figure 3.1: Figure illustrating the varve thickness time series from: Belauersee, Buchsee, C2-8, Deep, Degersee, and Donard.

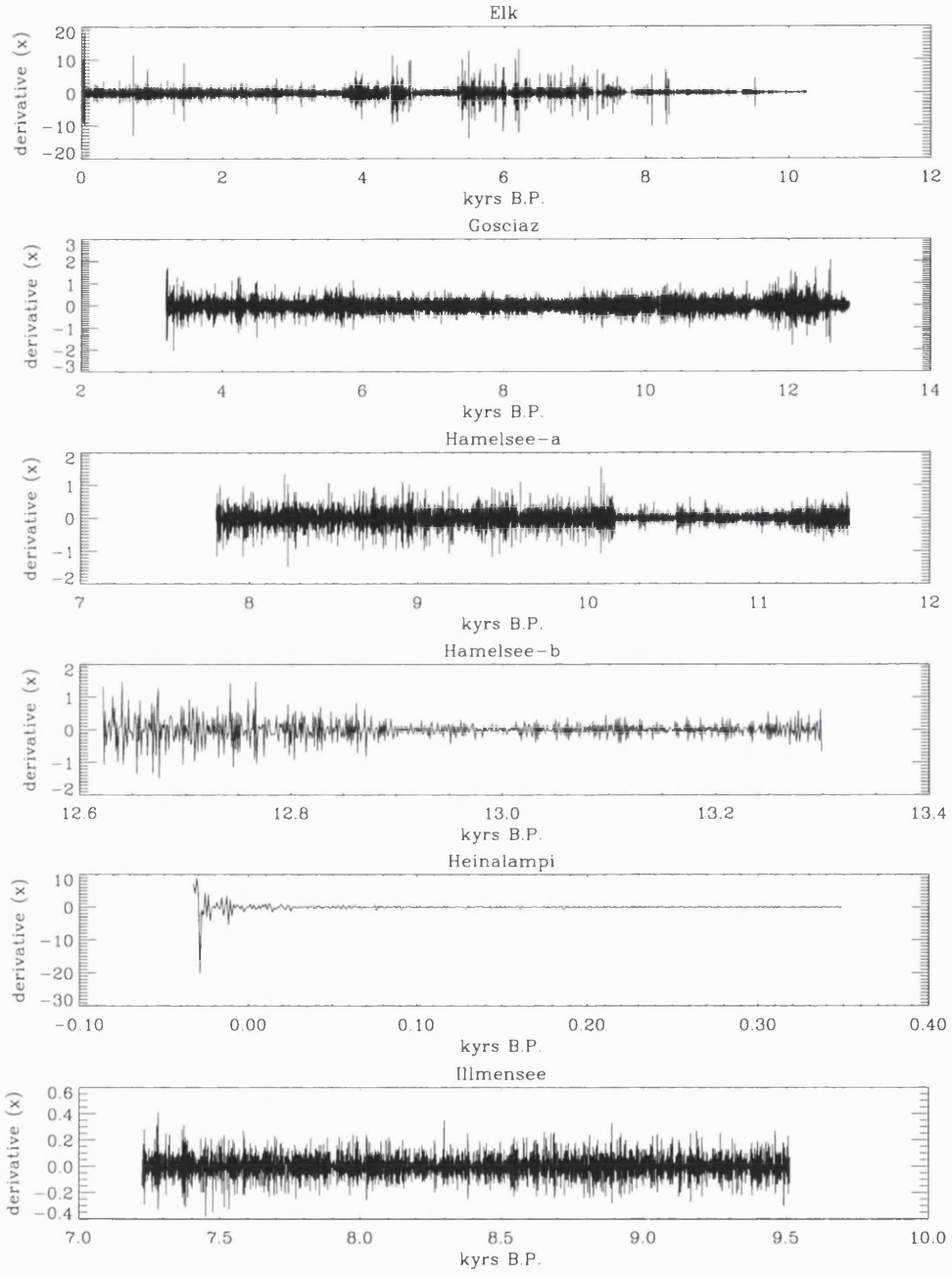

Figure 3.2: Figure illustrating the varve thickness time series from: Elk, Gosciaz, Hamelesee-a, Hamelsee-b, Heinalampi, and Illmensee.

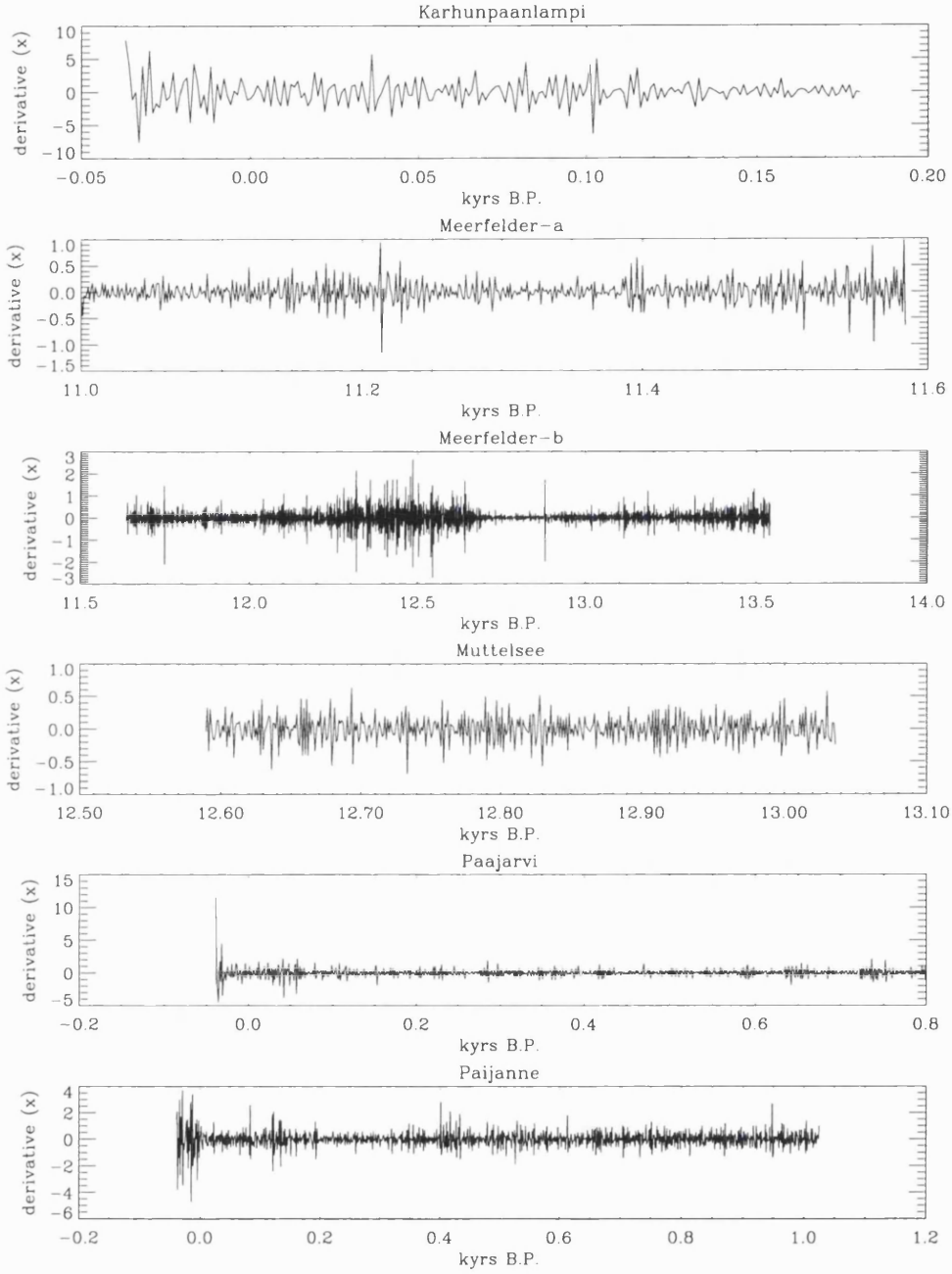

Figure 3.3: Figure illustrating the varve thickness time series from: Karhunpaanlampi, Meerfelder-a, Meerfelder-b, Muttelsee, Paajarvi, and Paijanne.

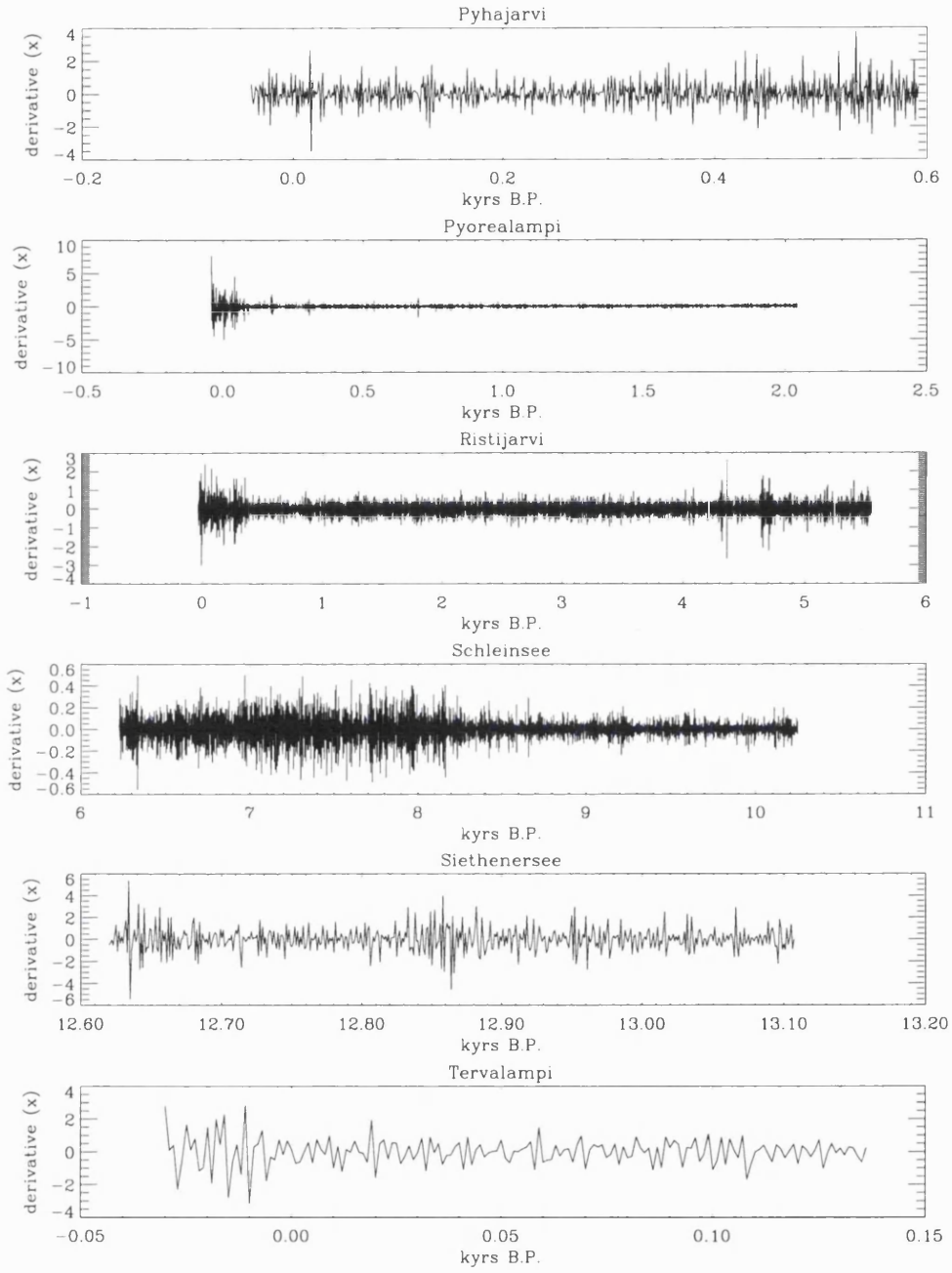

Figure 3.4: Figure illustrating the varve thickness time series from: Pyhajarvi, Pyorealampi, Ristijarvi, Schleinsee, Siethenersee, and Tervalampi.

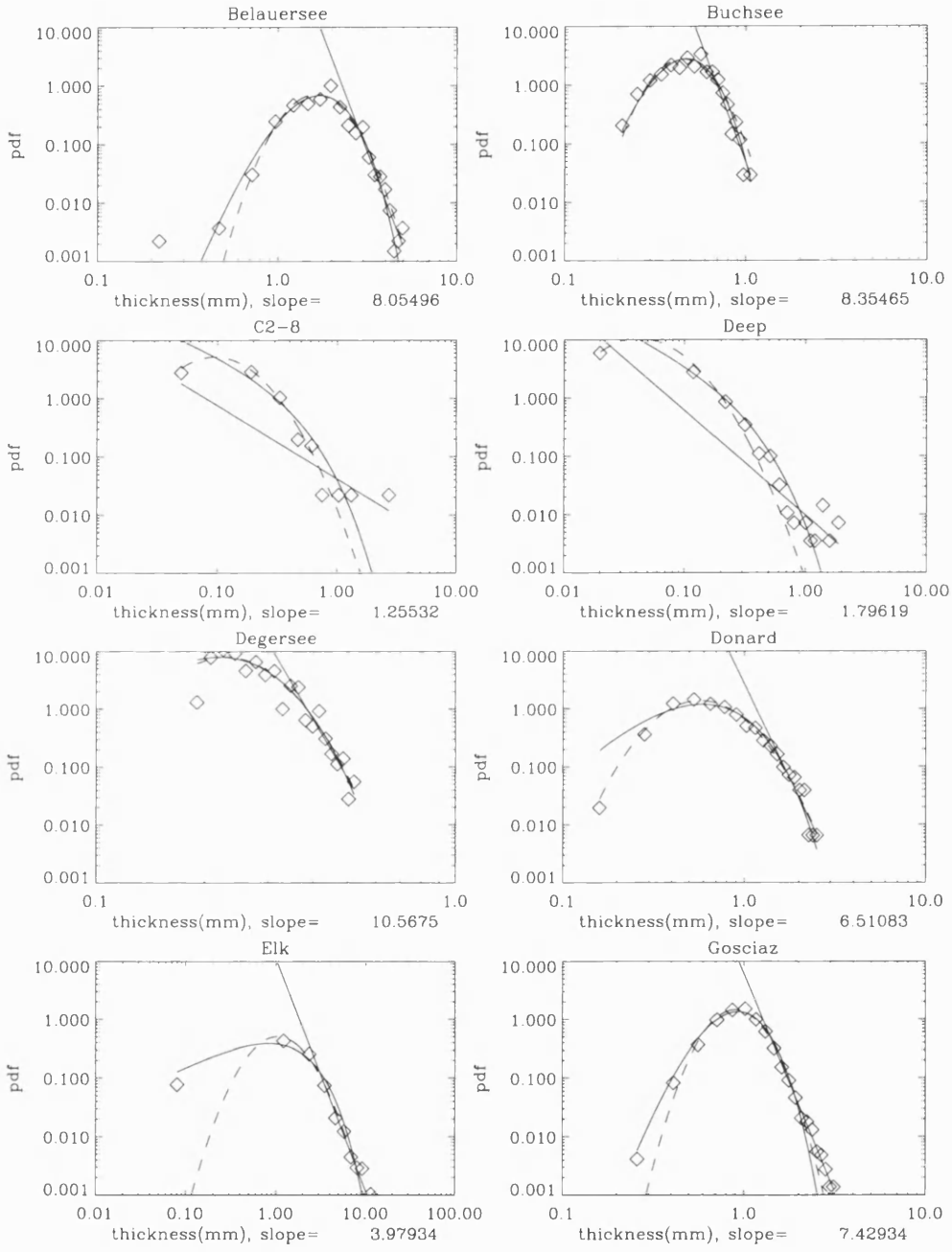

Figure 3.5: Figure illustrating the probability density function for: Belauersee, Buchsee, C2-8, Deep, Degersee, Donard, Elk, and Gosciaz.

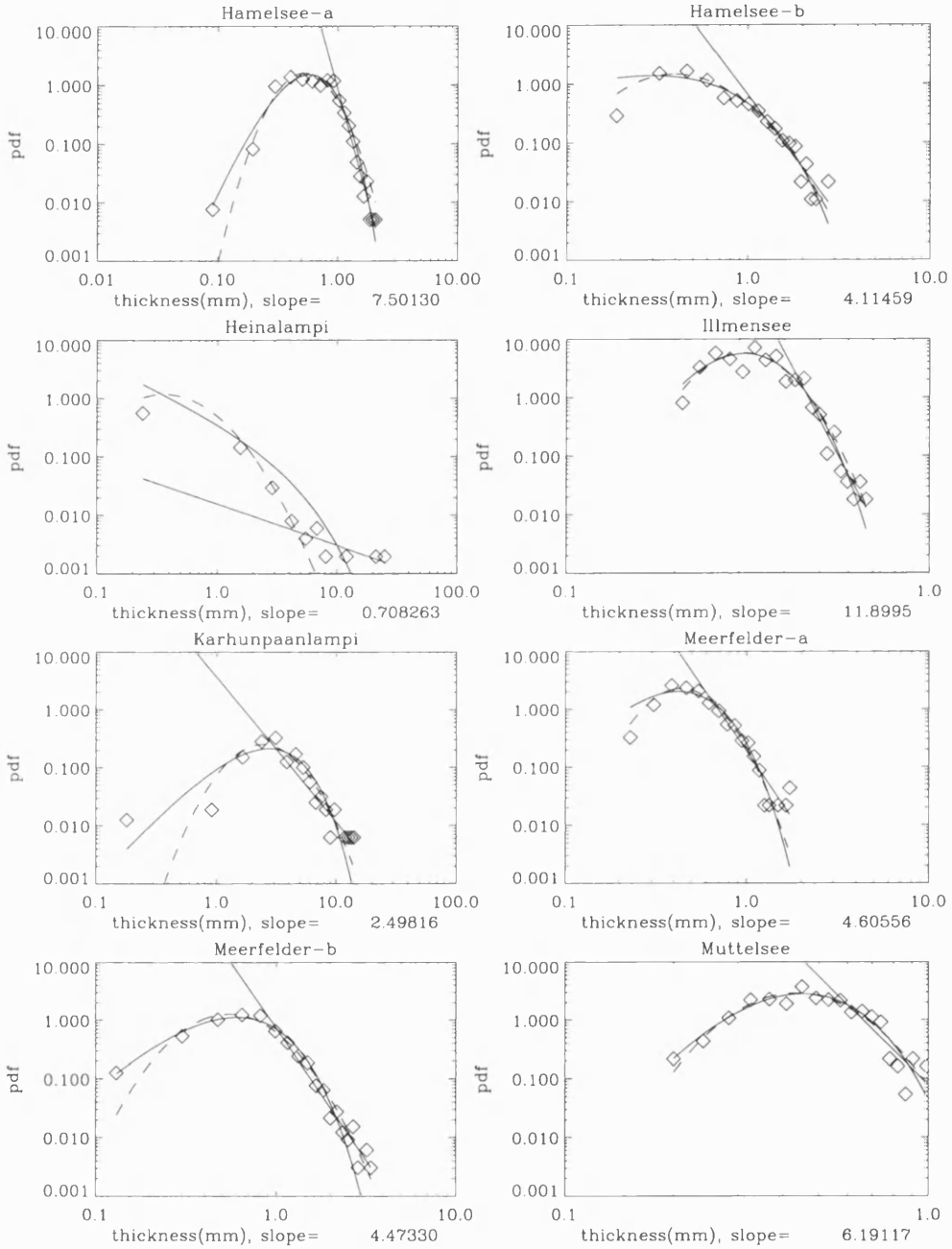

Figure 3.6: Figure illustrating the probability density function for: Hamelesee-a, Hamelsee-b, Heinalampi, Illmensee, Karhunpaanlampi, Meerfelder-a, Meerfelder-b, and Muttelsee.

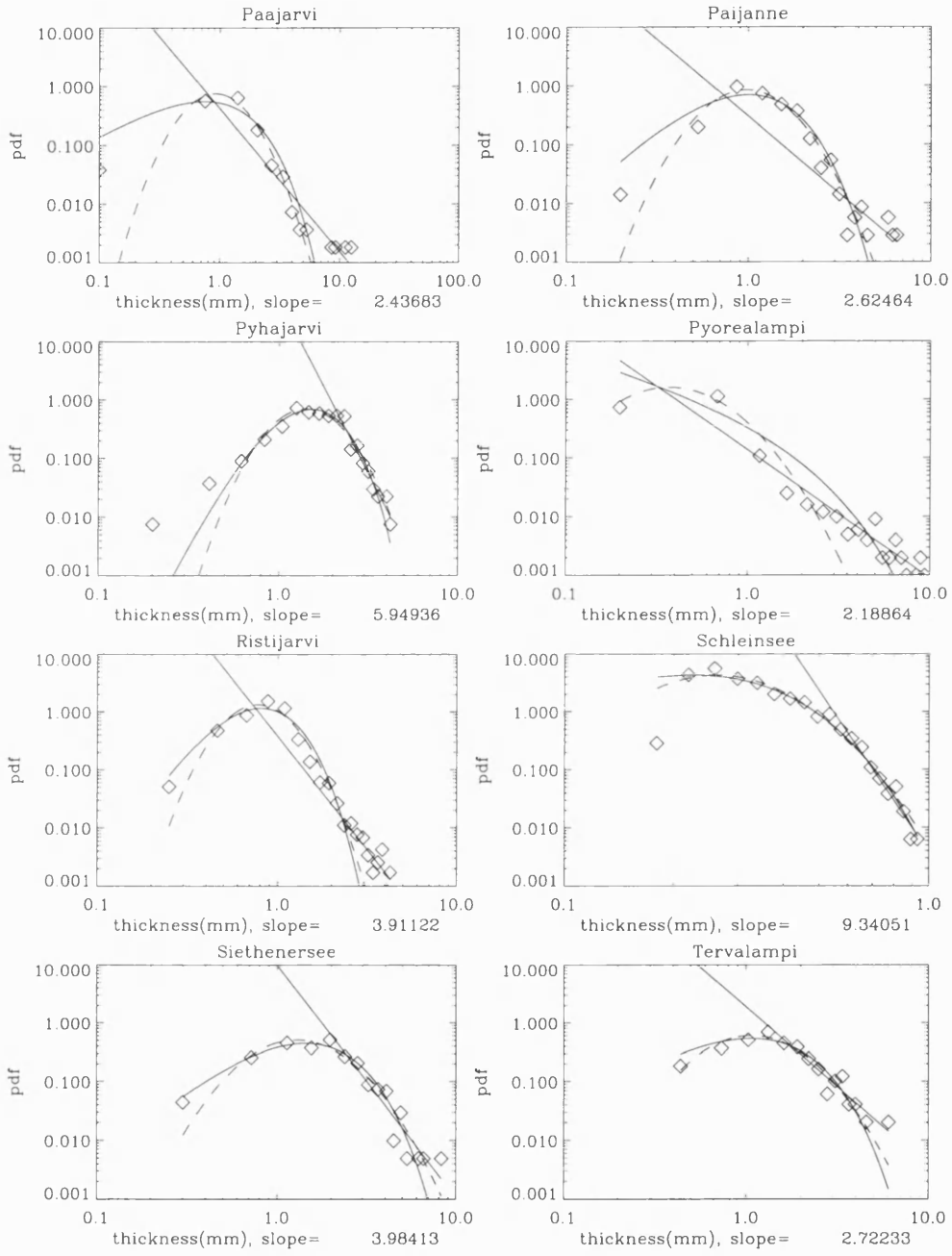

Figure 3.7: Figure illustrating the probability density function for: Paajarvi, Paijanne, Pyhajarvi, Pyorealampi, Ristijarvi, Schleinsee, Siethenersee, and Tervalampi.

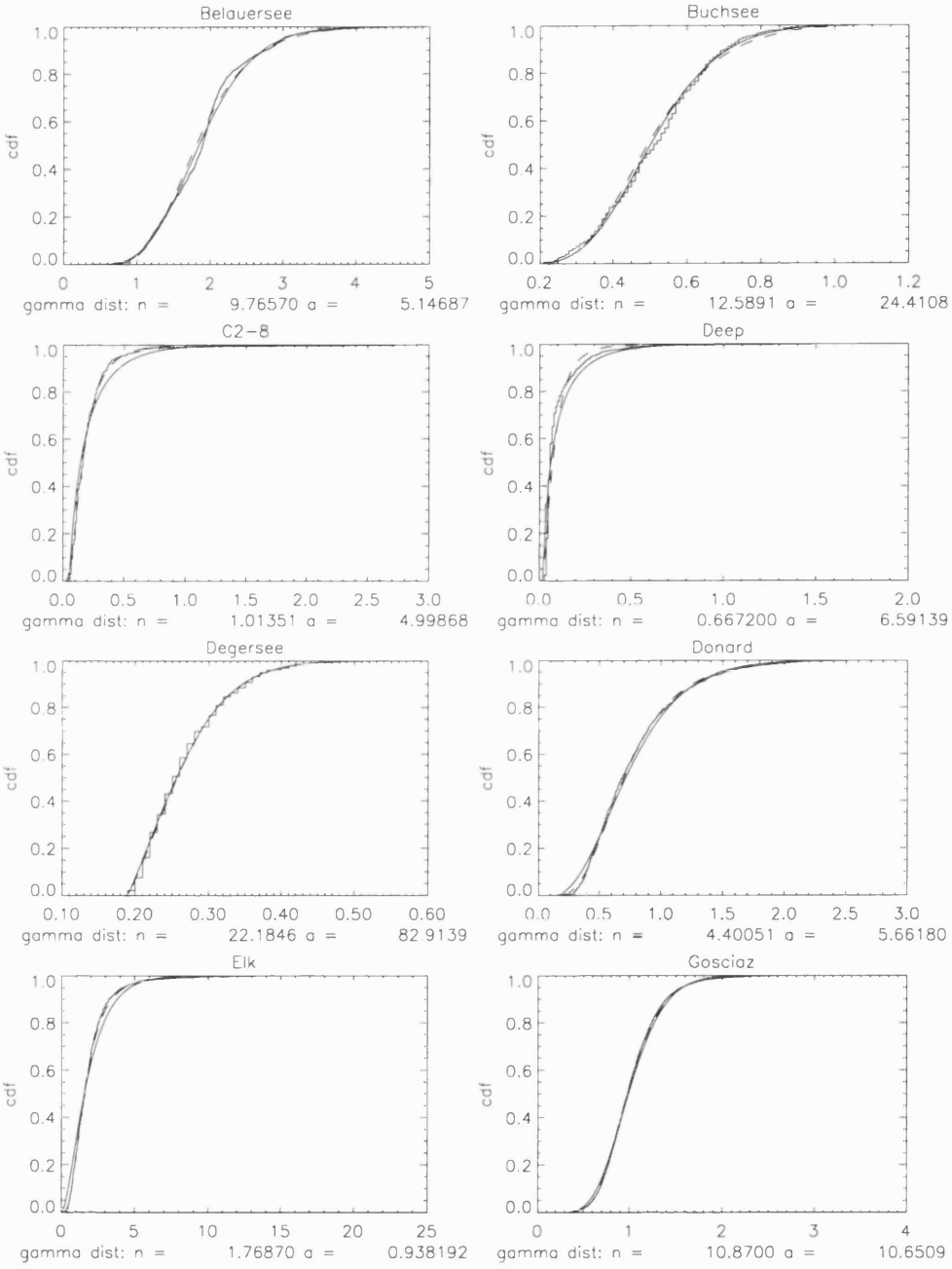

Figure 3.8: Figure illustrating the cumulative distribution function for: Belauersee, Buchsee, C2-8, Deep, Degersee, Donard, Elk, and Gosciaz.

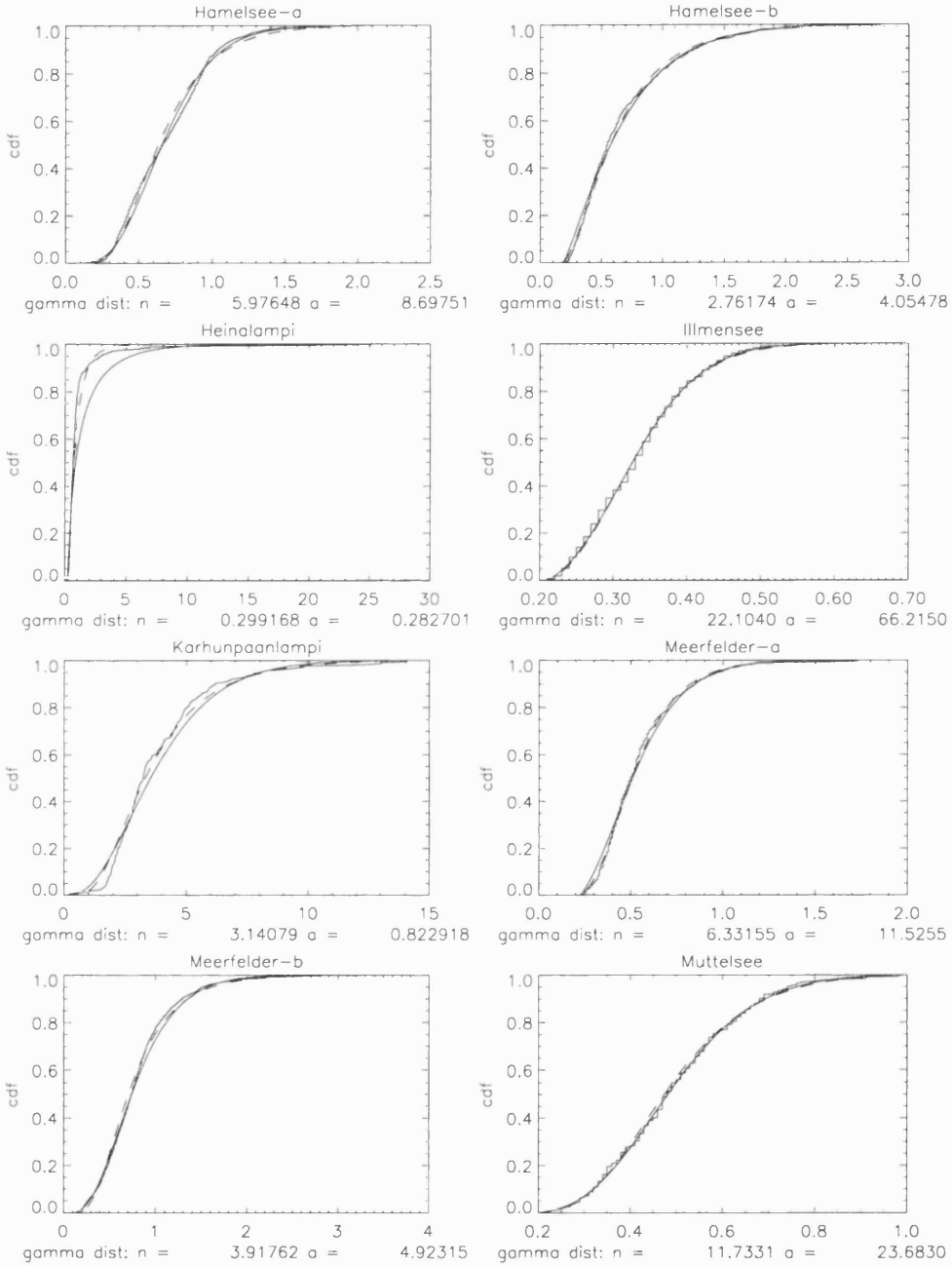

Figure 3.9: Figure illustrating the cumulative distribution function for: Hamelesee-a, Hamelsee-b, Heinalampi, Illmensee, Karhunpaanlampi, Meerfelder-a, Meerfelder-b, and Muttelsee.

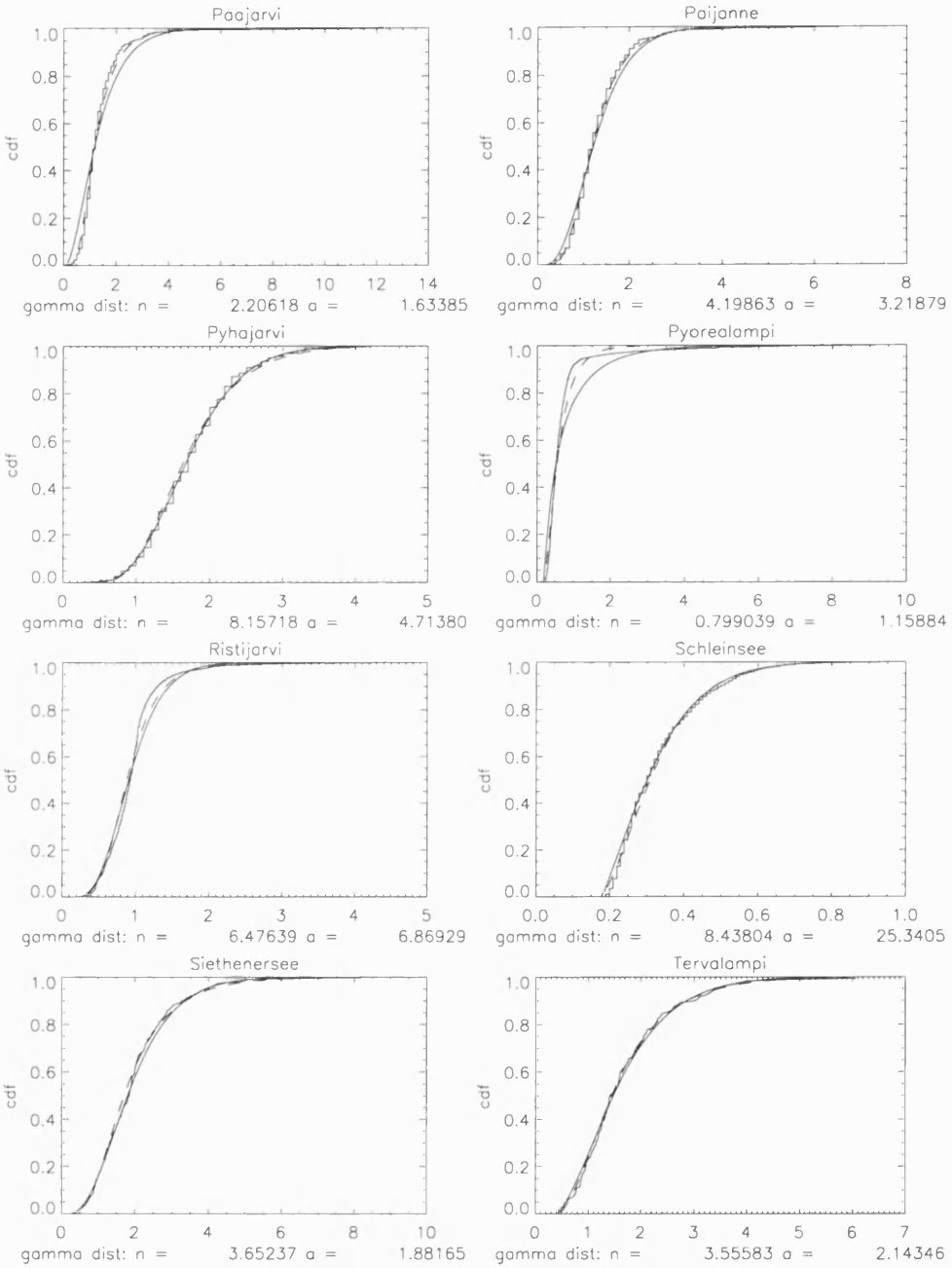

Figure 3.10: Figure illustrating the cumulative distribution function for: Paajarvi, Paijanne, Pyhajarvi, Pyorealampi, Ristijarvi, Schleinsee, Siethenersee, and Tervalampi.

Lake	Fitted Distribution	γ_ν	γ_α	$\sqrt{\nu}/\alpha$
Belauersee	Log and Gamma	9.77	5.15	0.61
Buchsee	Log and Gamma	12.59	24.41	0.15
C2-8	Log and Gamma	1.01	5	0.2
Deep	Log and Gamma	0.67	6.59	0.12
Degersee	Log and Gamma	22.18	82.91	0.06
Donard	Log and Gamma	4.4	5.66	0.37
Elk	Log and Gamma	1.77	0.94	1.42
Gosciaz	Log and Gamma	10.87	10.65	0.31
Hamelsee-a	Log and Gamma	5.97	8.70	0.28
Hamelsee-b	Log and Gamma	2.76	4.05	0.41
Heinalampi	Log and Gamma	0.30	0.28	1.95
Illmensee	Log and Gamma	22.1	66.22	0.07
Karhunpaanlampi	Log and Gamma	3.14	0.82	2.16
Meerfelder-a	Log and Gamma	6.33	11.52	0.22
Meerfelder-b	Log and Gamma	3.92	4.92	0.4
Muttelsee	Log and Gamma	11.73	23.68	0.14
Paajarvi	Log and Gamma	2.2	1.63	0.91
Paijanne	Log and Gamma	4.2	3.22	0.64
Pyhajarvi	Log and Gamma	8.16	4.71	0.61
Pyorealampi	Log and Gamma	0.8	1.16	0.77
Ristijarvi	Log and Gamma	6.48	6.87	0.37
Schleinsee	Log and Gamma	8.44	25.34	0.11
Siethenersee	Log and Gamma	3.65	1.88	1.01
Tervalampi	Log and Gamma	3.56	2.14	0.88

Table 3.1: Summary of statistical distribution exponents

3.2 Discussion

The non-Gaussian pdf's and cdf's, fitted by the gamma and log-normal distributions are similar to those highlighted in the review, where a range of natural processes are fitted by log-normal and gamma distributions, such as temperature, precipitation, as well as sediment particle size, and sedimentary deposits, e.g., turbidites and varves. The gamma distribution is the end member of the Poisson process, which describes the number of random events per interval of time or space (the exponential distribution describes the frequency distribution of spaces or gaps between those events). As such, the addition of exponential distributions (random variables) evolves towards the gamma distribution [159], [105] (see Figure 2.4.). Correlation results indicate γ_α and γ_ν exponents do not relate to any of the available physical parameters (though γ_α does correlate with β and modelled τ), indicating quantity dynamics in sedimentation are a product of a complex interplay between numerous variables (see Figures 5.4. to 5.19.). The log-normal distribution is the stable law for the multiplication of random variables (exponentials), effectively a multiplicative cascade of singularities [176],[101], [102]. As the full range of varve thickness values are fitted by the gamma and log-normal distributions, the occurrence of thin and thick varves are viewed as "extreme" events rather than as "outliers".

For the gamma distribution we can examine the statistical and physical mechanisms further by examining the shape, ν and scale, α parameters. If we take $\exp^{\alpha x}$, where α is the length of the tail, and x is the time series, then we would expect large α to be associated with strong intermittency, and conversely small α with weak or non-intermittency. Visual comparison with the time series (based on the derivative, the difference in thickness between successive varves) does not indicate any such relations (see Figures 3.1. to 3.4.). Only lakes Deep and Elk display any definite intermittent signature, which are not prolonged. In addition, there are no relations for deviations from the Gaussian limit ($\sqrt{\nu}/\alpha$) for the Gamma function (see Table 3.1.). This suggests that only bulk features of the distributions are fitted well by the gamma distribution, and that from the good fit of the log-normal distribution, the dynamics of the time series are not of purely gamma form.

As such, sedimentation can be represented by a series of random events, given as, $P(1) = x, P(2) = x^2, P(n) = x^n$, where x is a stochastic variable which is some stochastic fraction x_1 of another variable $\tilde{x}$, $x = x_1\tilde{x}$. This is expressed as, $\tilde{x} = x_2\tilde{\tilde{x}}$ and so on. Thus, we can express x as $x = x_1, x_2, ..., x_n$ where $x_1, x_2, ..., x_n$ are stochastic variables. The addition of these random variables leads to the gamma distribution. Taking the logarithm gives, $\log x = \log x_1 + \log x_2 + ... + \log x_n$. Thus, $x = \exp(\log x_1 + \log x_2 + ... + \log x_n)$. The fluctuations $\log x_1, \log x_2, ..., \log x_n$ are generally well behaved, so $\log x$ will tend to a Gaussian distribution, from the central limit theorem. Moreover, the log-normal distribution will be naturally occurring for a fractionation process under rather general conditions, and thus functionally similar to a multiplicative cascade [195].

Chapter 4

Temporal Signatures I

4.1 Introduction and Results

In this chapter we present the results of the phase portraits, exceedence probability analysis, power spectra, autocorrelation functions, and fluctuation analysis.

Figures 4.1. to 4.3. display the phase portraits for the lakes in this study. The x-axis and y-axis are varve thickness, plotted with respect to a lag of 2 between data points within each time series. The basic feature of correlation is clear in each plot, with the attractor only filling a portion of the available phase space (an uncorrelated random time series which would fill the space more fully). Excursions from the main portion of the attractor, typically fanning out from the origin, e.g., Deep, Elk, and Pyorealampi, indicate the occurrence of extreme events.

Figures 4.4. to 4.6. display the exceedence probability for each lake. The x-axis is the varve thickness and the y-axis is the exceedence probability. Generally, it is clear that, in agreement with the pdf's, a power law only fits part of the data, mainly the central portion. In most cases the form of the distribution is curvi-linear. There are variations, with the upper part fitted well in C2-8, Deep, Degersee, Heinalampi, Pyorealampi, and Schleinsee, and the lower part is fitted well in C2-8, Heinalampi, Kaarhunpaanlampi, Paajarvi, and Paijanne.

Figures 4.7. to 4.9. display the power spectra for the lakes in this study. The x-axis is the frequency and the y-axis is the power. Generally, it is clear in all plots that a best fit line can be applied, though some are represented by two scaling regimes, i.e., Belauersee (ca. 100 yrs), Degersee (ca. 100 yrs), Gosciaz (ca. 120 yrs),

Hamelsee-a (ca. 80 yrs), Meerfelder-b (ca. 100 yrs), Ristijarvi (ca. 60 yrs), and Schleinsee (ca. 120 yrs).

Figures 4.10. to 4.12. display the autocorrelation function for the lakes in this study. The x-axis is the lag that the time series is shifted relative to itself, and y-axis is the autocorrelation. Seven of the lakes do not allow the calculation of a scaling exponent, e.g., Buchsee, Donard, and Tervalampi. The remaining lakes are best fit by the power law, with slight areas of non-coverage in the lower lag years, e.g., Belauersee, Degersee, and Pyhajarvi.

Figures 4.13. to 4.15. display the fluctuation analysis for the lakes in this study. The x-axis is the root mean square deviation, and the y-axis is the length of the time series. Generally, all lakes display scaling signatures. Slight deviations from the best fit line are apparent for most lakes, and always for the (length related) upper section.

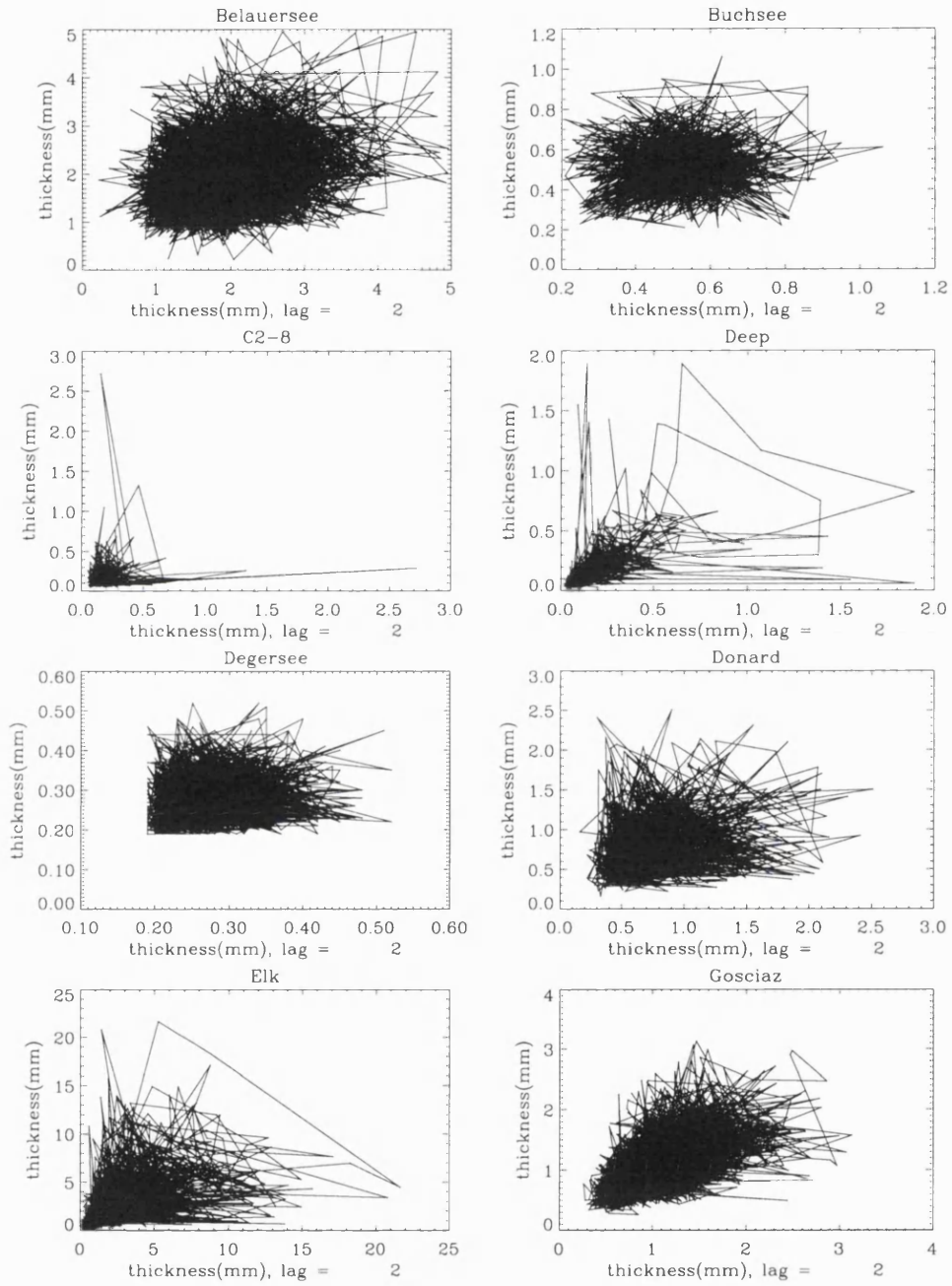

Figure 4.1: Figure illustrating the phase portraits for: Belauersee, Buchsee, C2-8, Deep, Degersee, Donard, Elk, and Gosciaz.

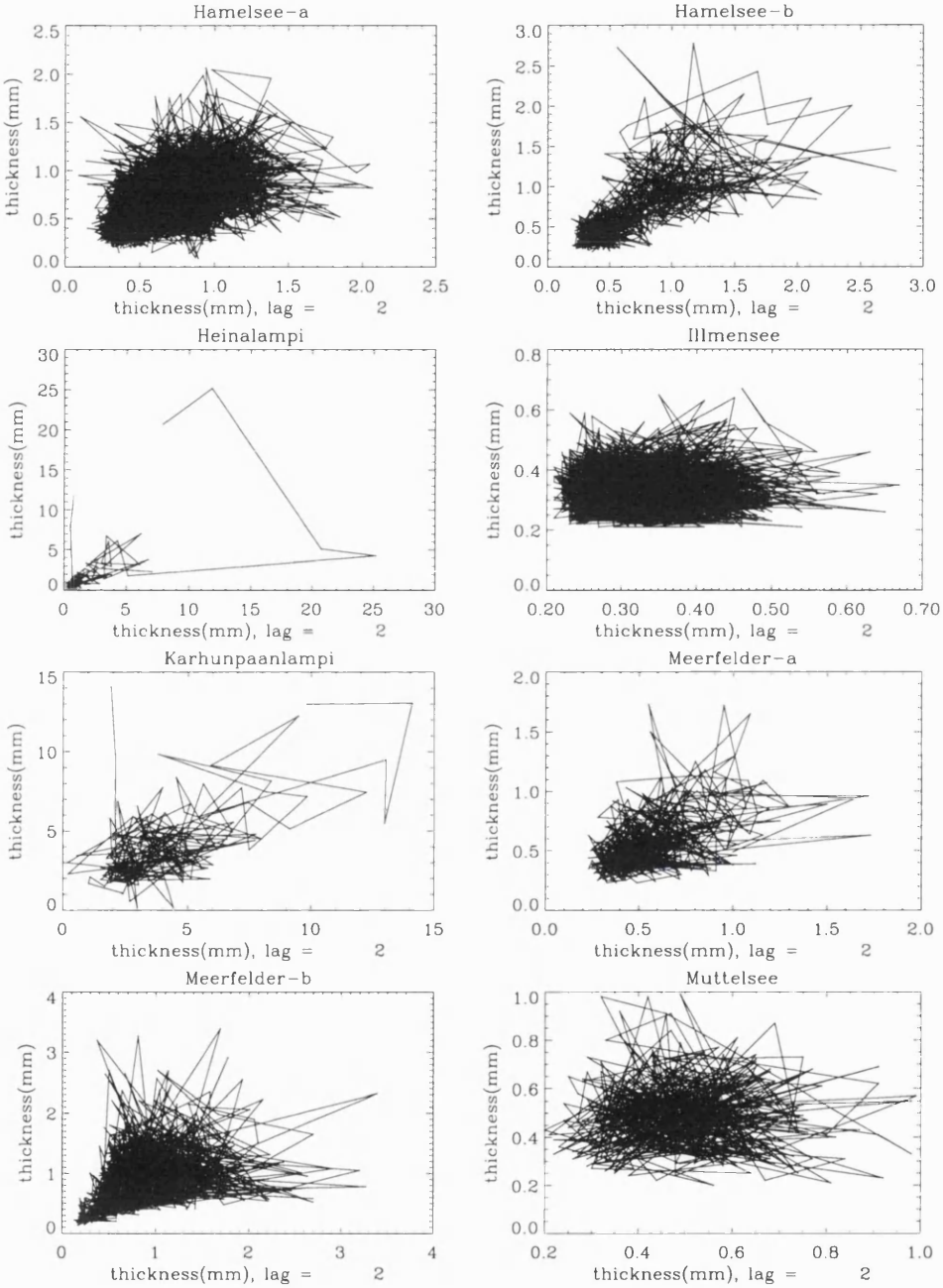

Figure 4.2: Figure illustrating the phase portraits for: Hamelesee-a, Hamelsee-b, Heinalampi, Illmensee, Karhunpaanlampi, Meerfelder-a, Meerfelder-b, and Muttelsee.

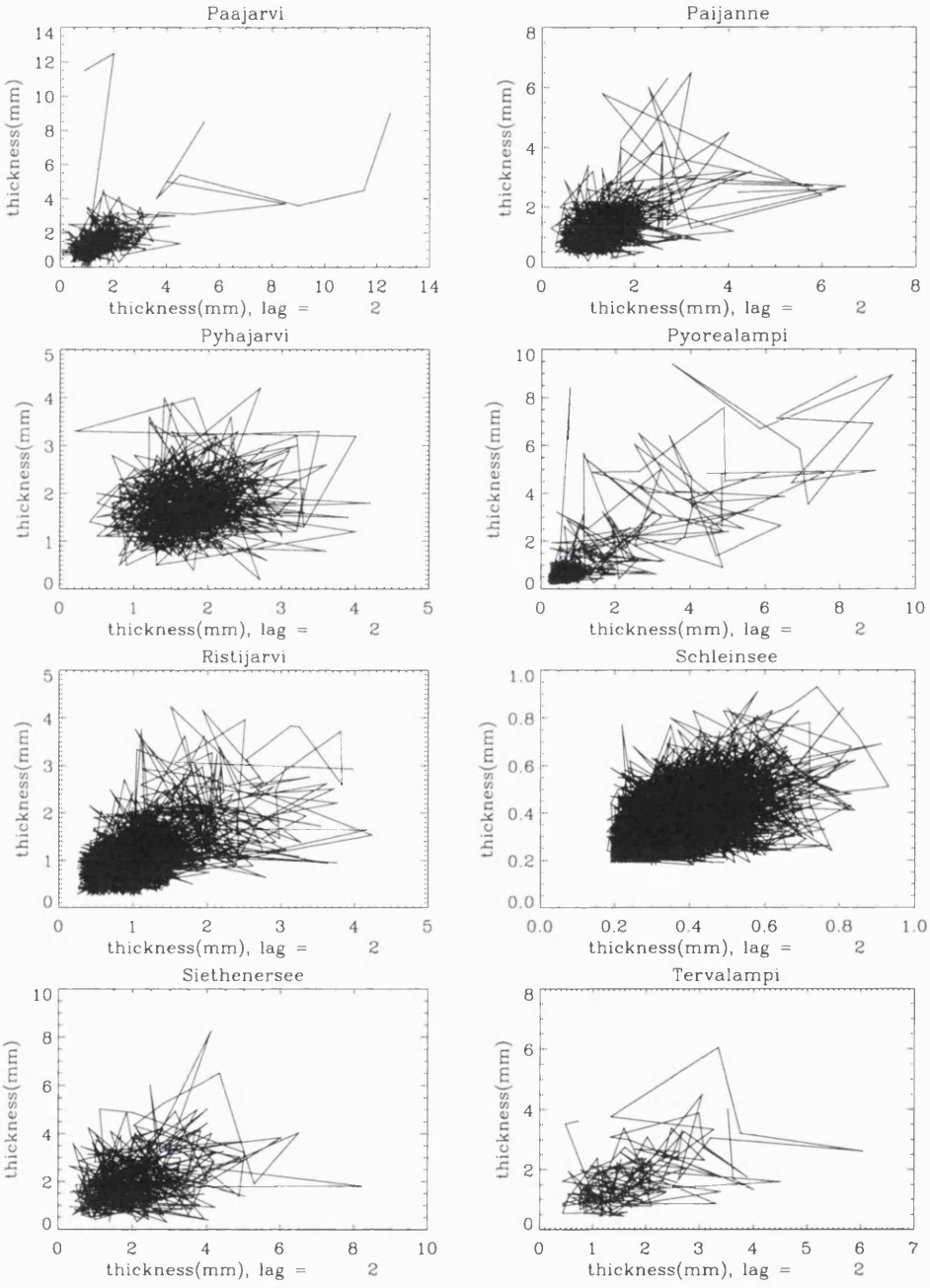

Figure 4.3: Figure illustrating the phase portraits for: Paajarvi, Paijanne, Pyhajarvi, Pyorealampi, Ristijarvi, Schleinsee, Siethenersee, and Tervalampi.

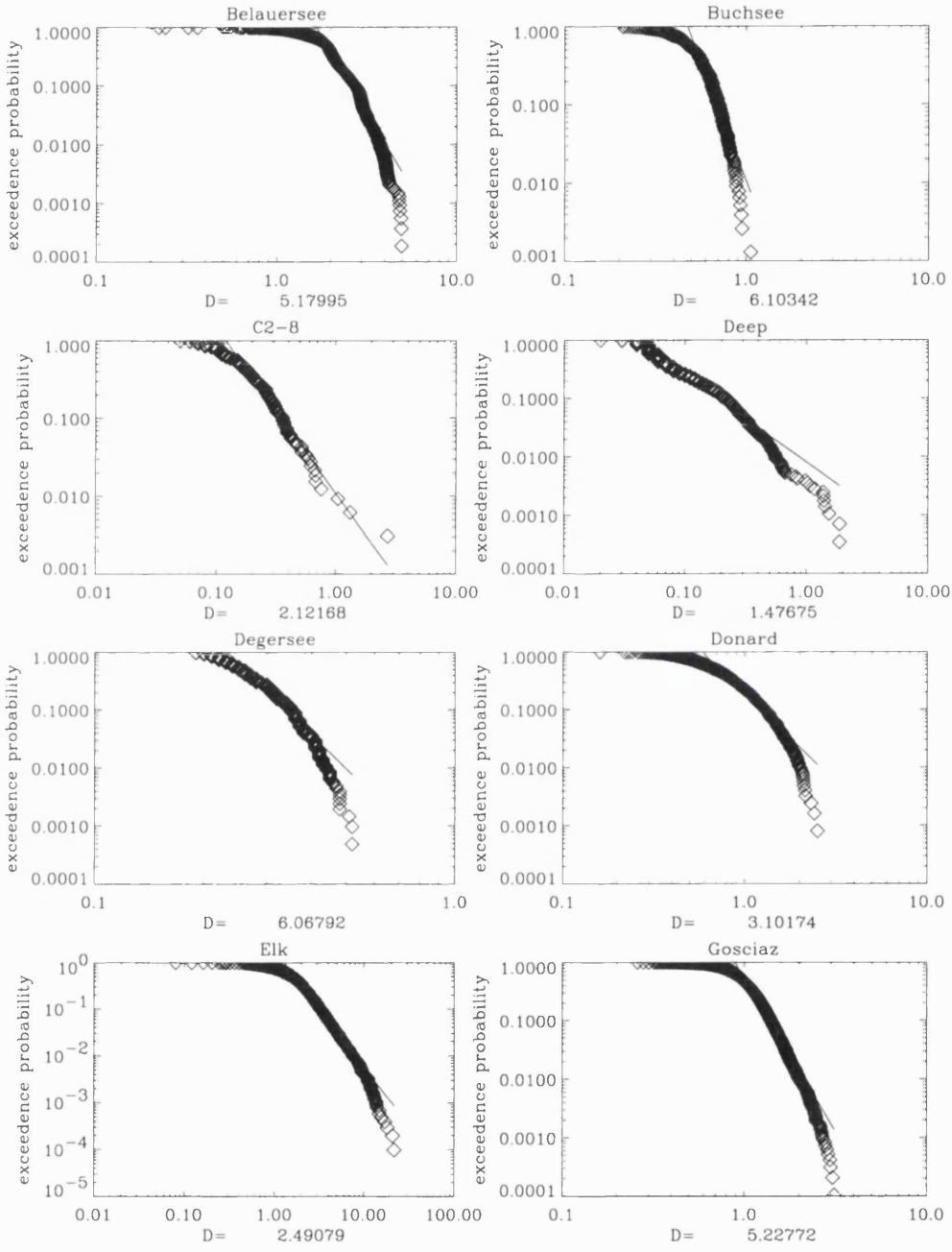

Figure 4.4: Figure illustrating the exceedence probability analysis for: Belauersee, Buchsee, C2-8, Deep, Degersee, Donard, Elk, and Gosciaz.

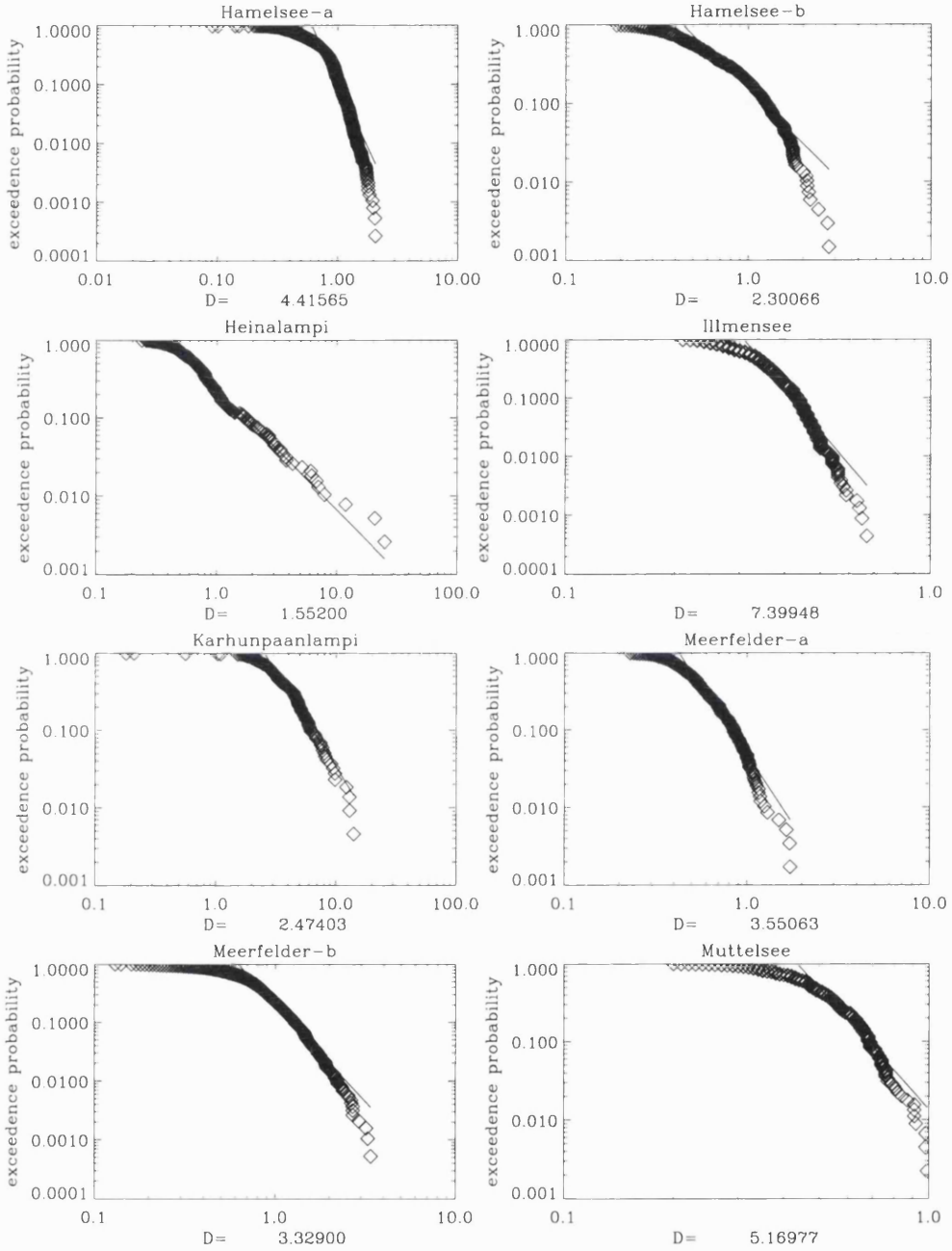

Figure 4.5: Figure illustrating the exceedence probability analysis for: Hamelesee-a, Hamelsee-b, Heinalampi, Illmensee, Karhunpaanlampi, Meerfelder-a, Meerfelder-b, and Muttelsee.

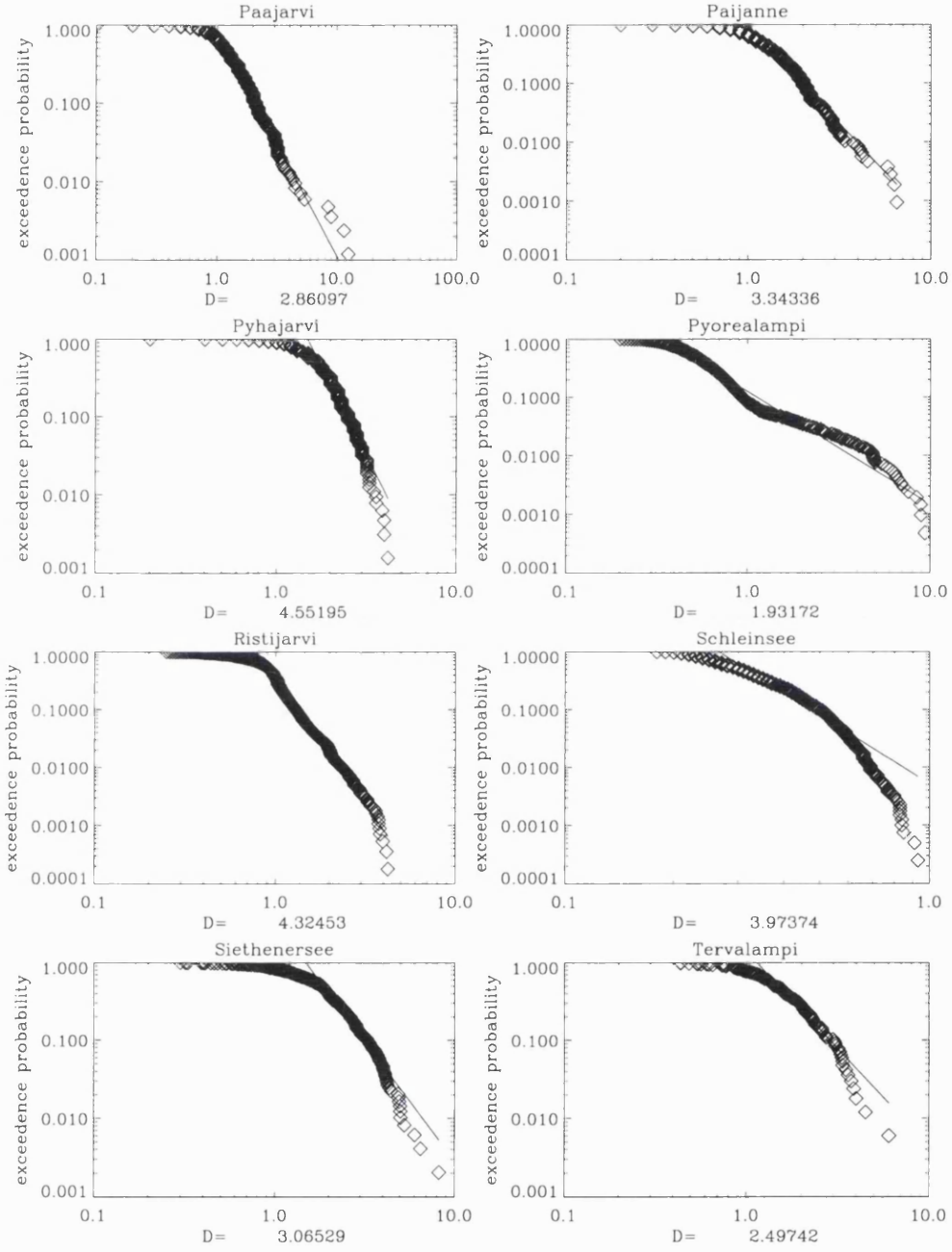

Figure 4.6: Figure illustrating the exceedence probability analysis for: Paajarvi, Paijanne, Pyhajarvi, Pyorealampi, Ristijarvi, Schleinsee, Siethenersee, and Tervalampi.

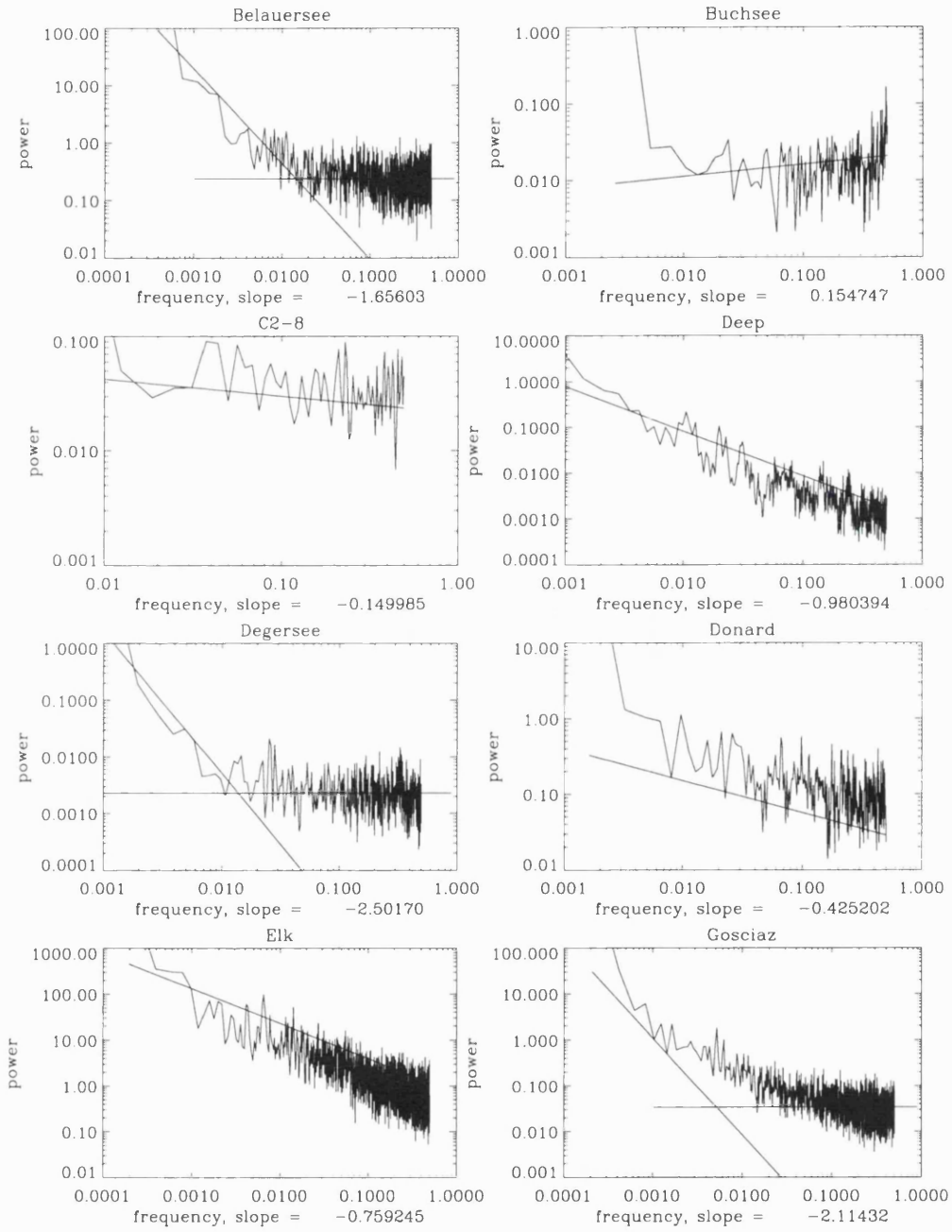

Figure 4.7: Figure illustrating the power spectra for: Belauersee, Buchsee, C2-8, Deep, Degersee, Donard, Elk, and Gosciaz.

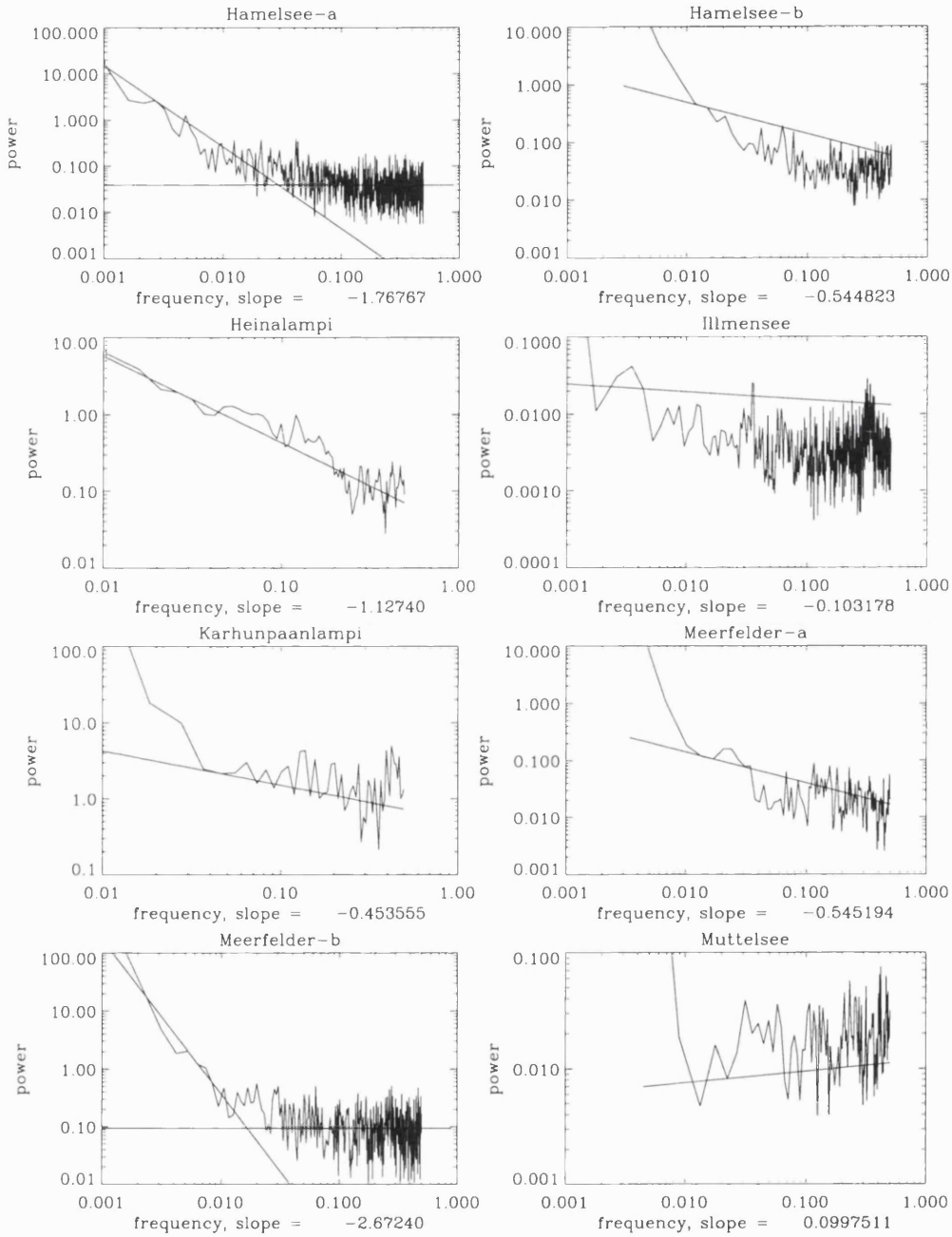

Figure 4.8: Figure illustrating the power spectra for: Hamelesee-a, Hamelsee-b, Heinalampi, Illmensee, Karhunpaanlampi, Meerfelder-a, Meerfelder-b, and Muttelsee.

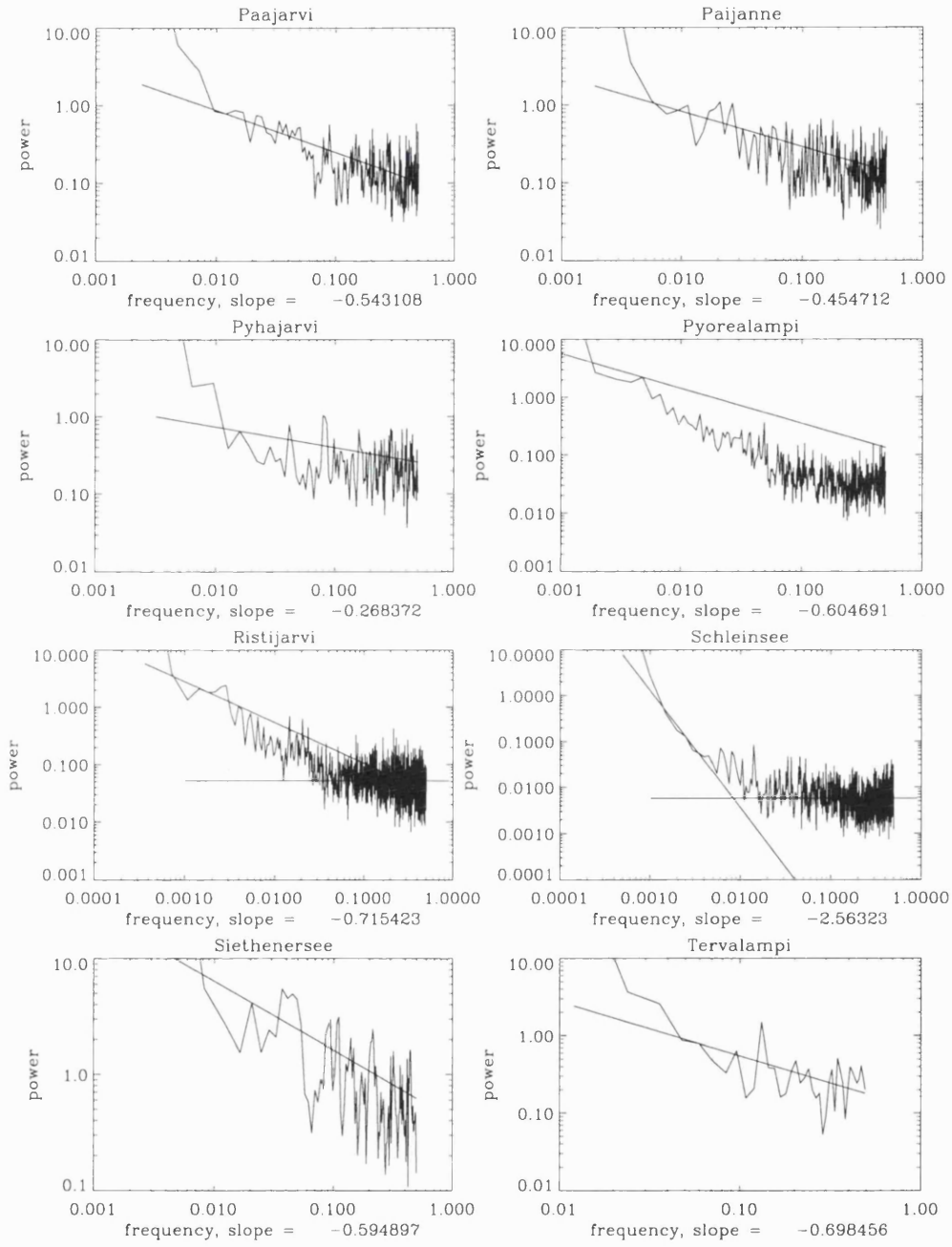

Figure 4.9: Figure illustrating the power spectra for: Paajarvi, Paijanne, Pyhajarvi, Pyorealampi, Ristijarvi, Schleinsee, Siethenersee, and Tervalampi.

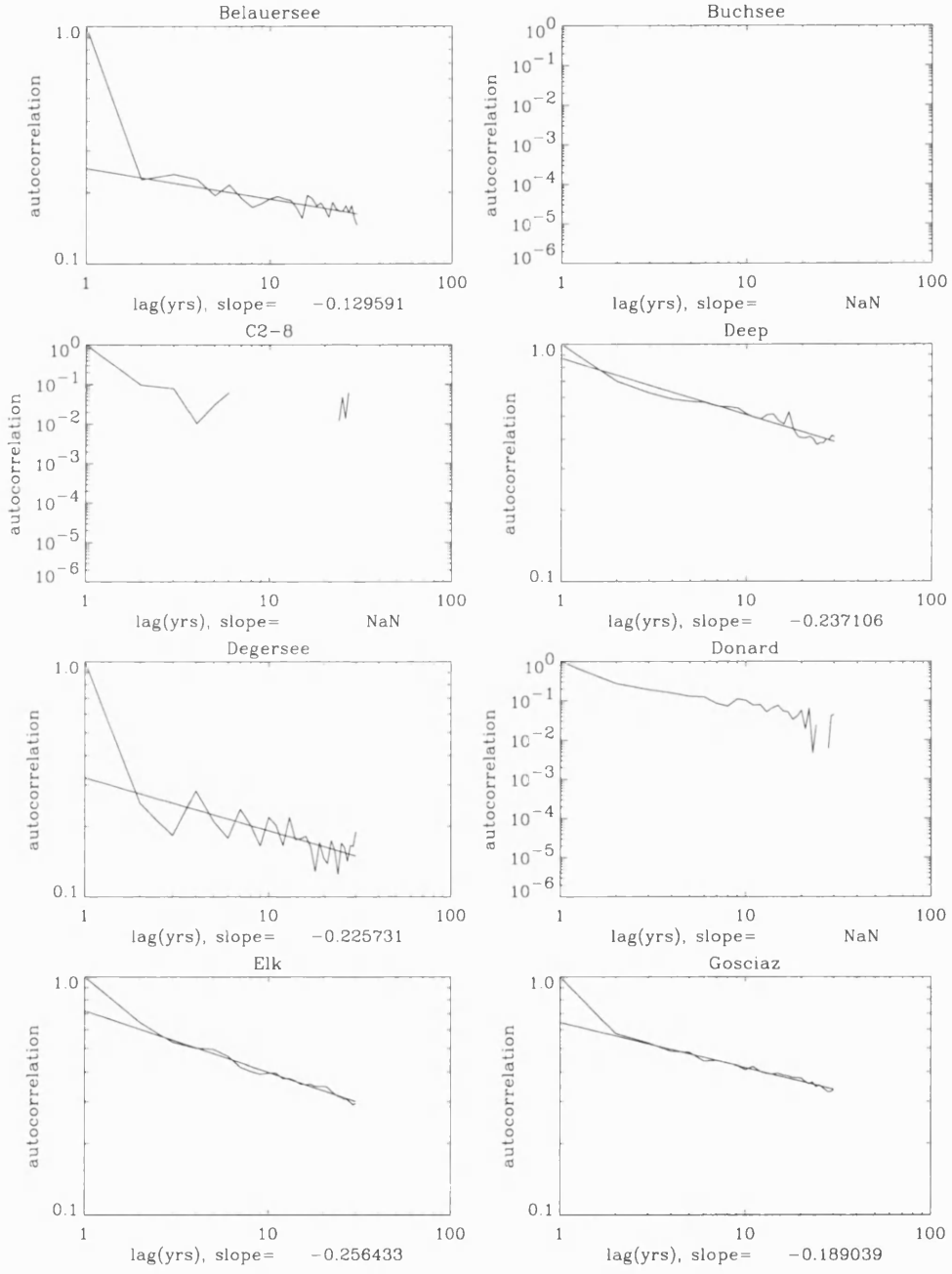

Figure 4.10: Figure illustrating the autocorrelation functions for: Belauersee, Buchsee, C2-8, Deep, Degersee, Donard, Elk, and Gosciaz.

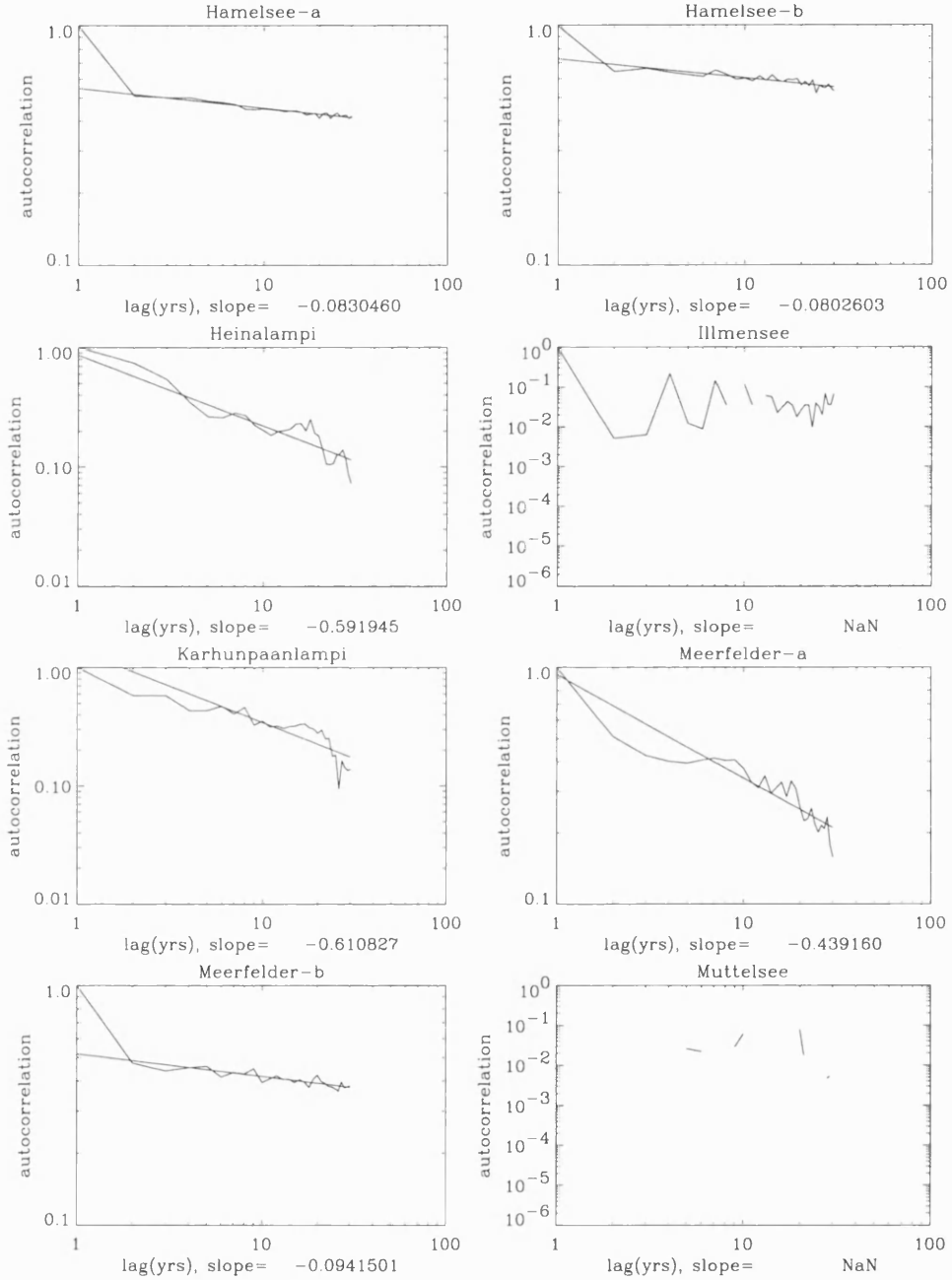

Figure 4.11: Figure illustrating the autocorrelation functions for: Hamelesee-a, Hamelsee-b, Heinalampi, Illmensee, Karhunpaanlampi, Meerfelder-a, Meerfelder-b, and Muttelsee.

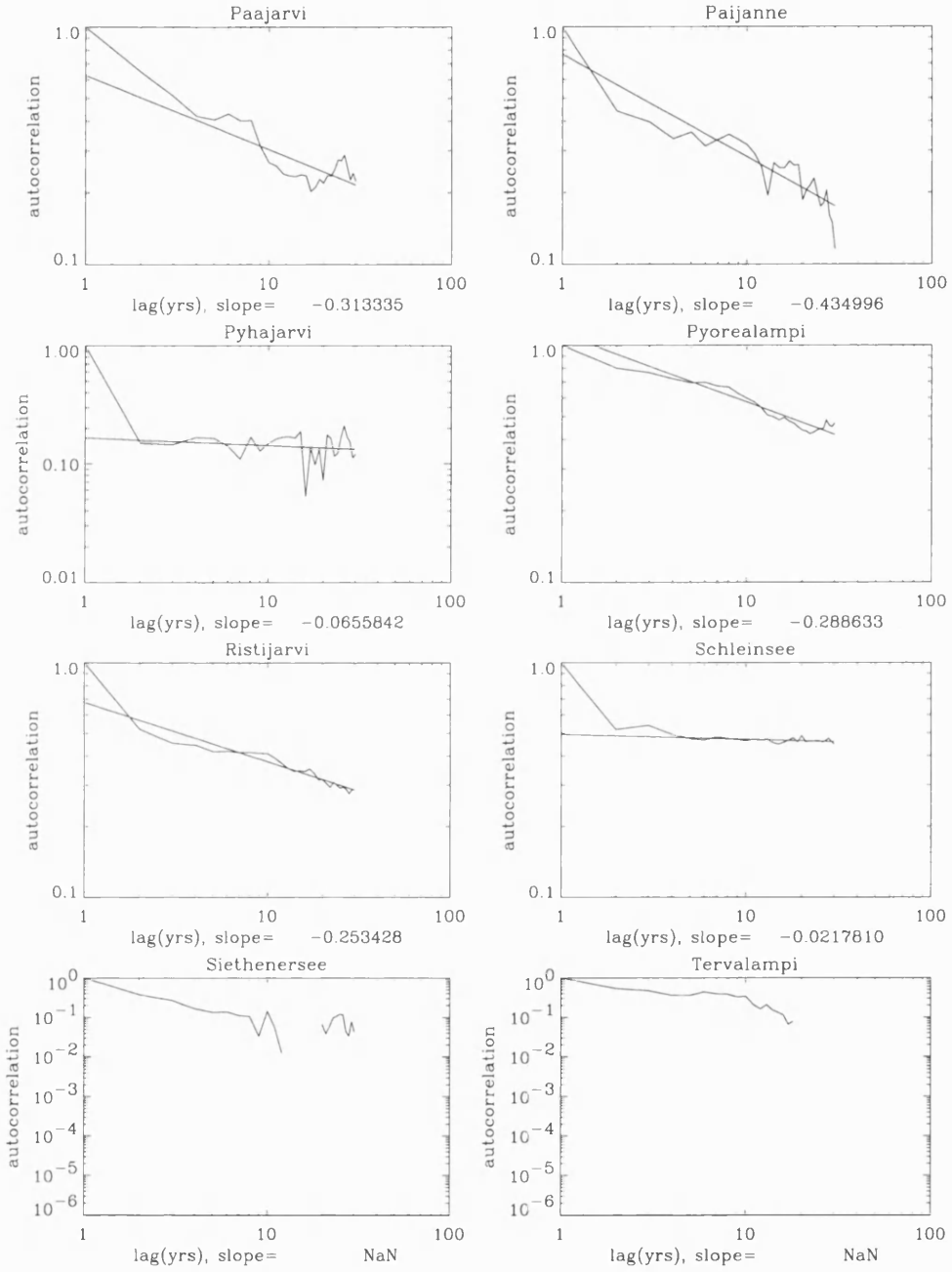

Figure 4.12: Figure illustrating the autocorrelation functions for: Paajarvi, Paijanne, Pyhajarvi, Pyorealampi, Ristijarvi, Schleinsee, Siethenersee, and Tervalampi.

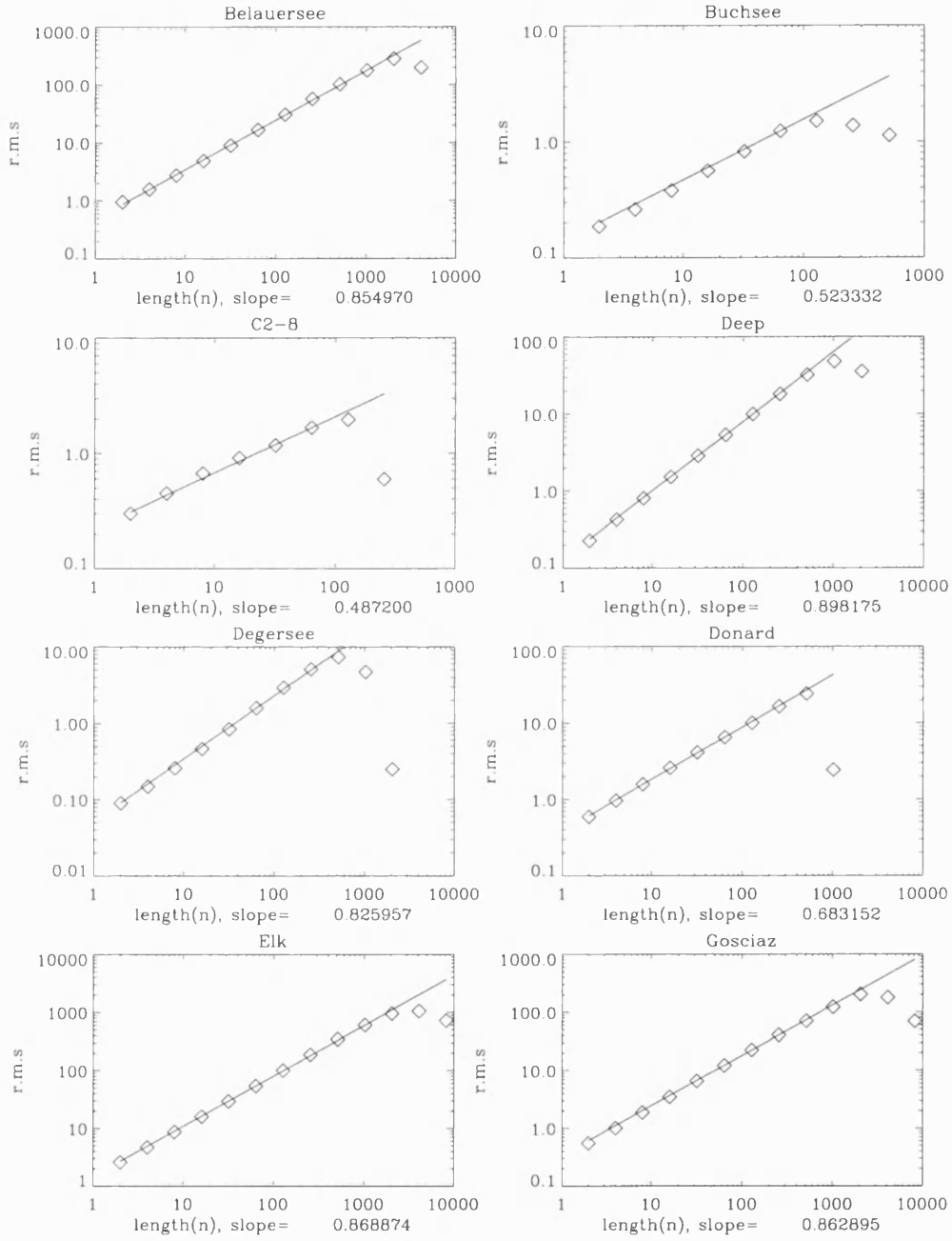

Figure 4.13: Figure illustrating the fluctuation analysis for: Belauersee, Buchsee, C2-8, Deep, Degersee, Donard, Elk, and Gosciaz.

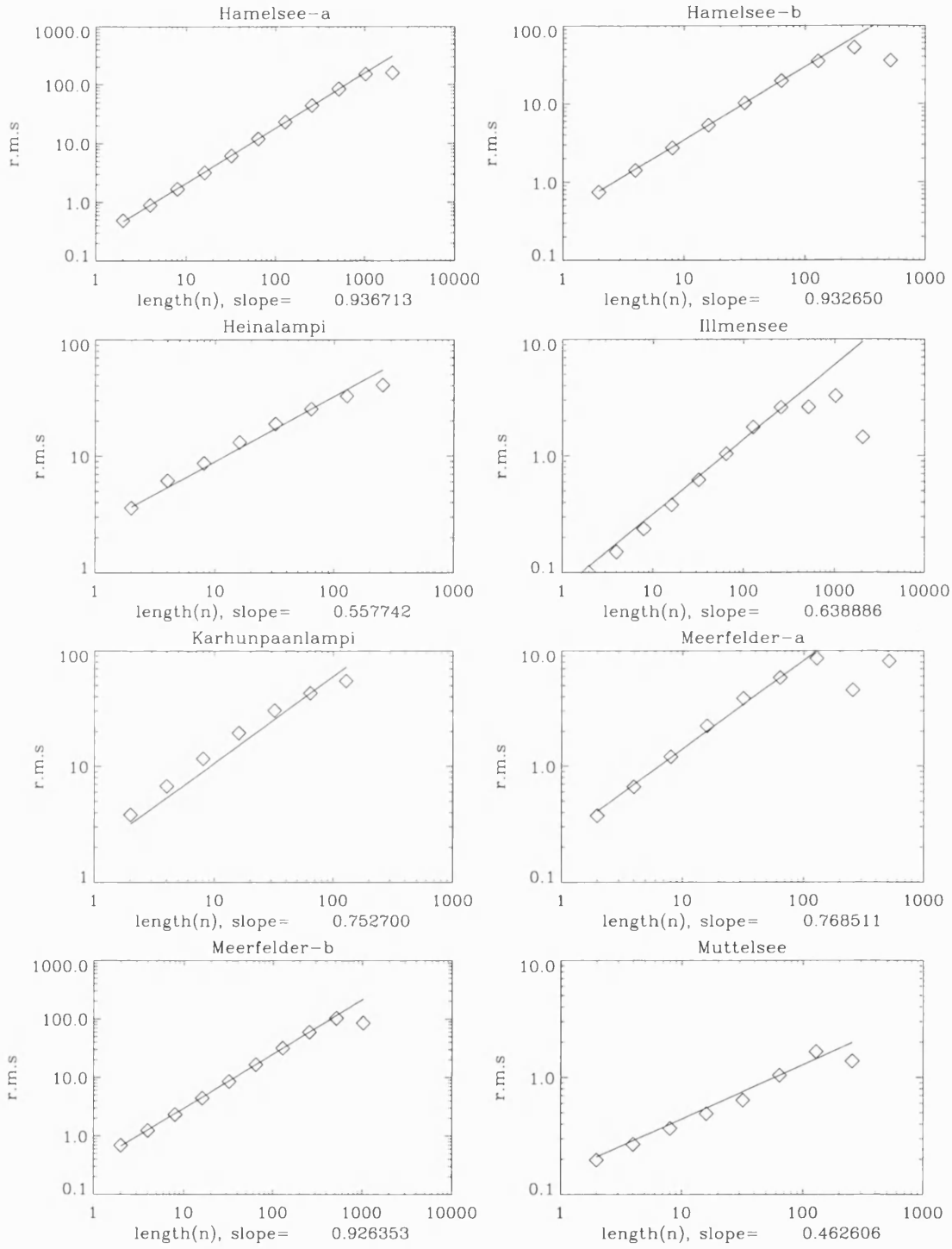

Figure 4.14: Figure illustrating the fluctuation analysis for: Hamelesee-a, Hamelsee-b, Heinalampi, Illmensee, Karunpaanlampi, Meerfelder-a, Meerfelder-b, and Muttelsee.

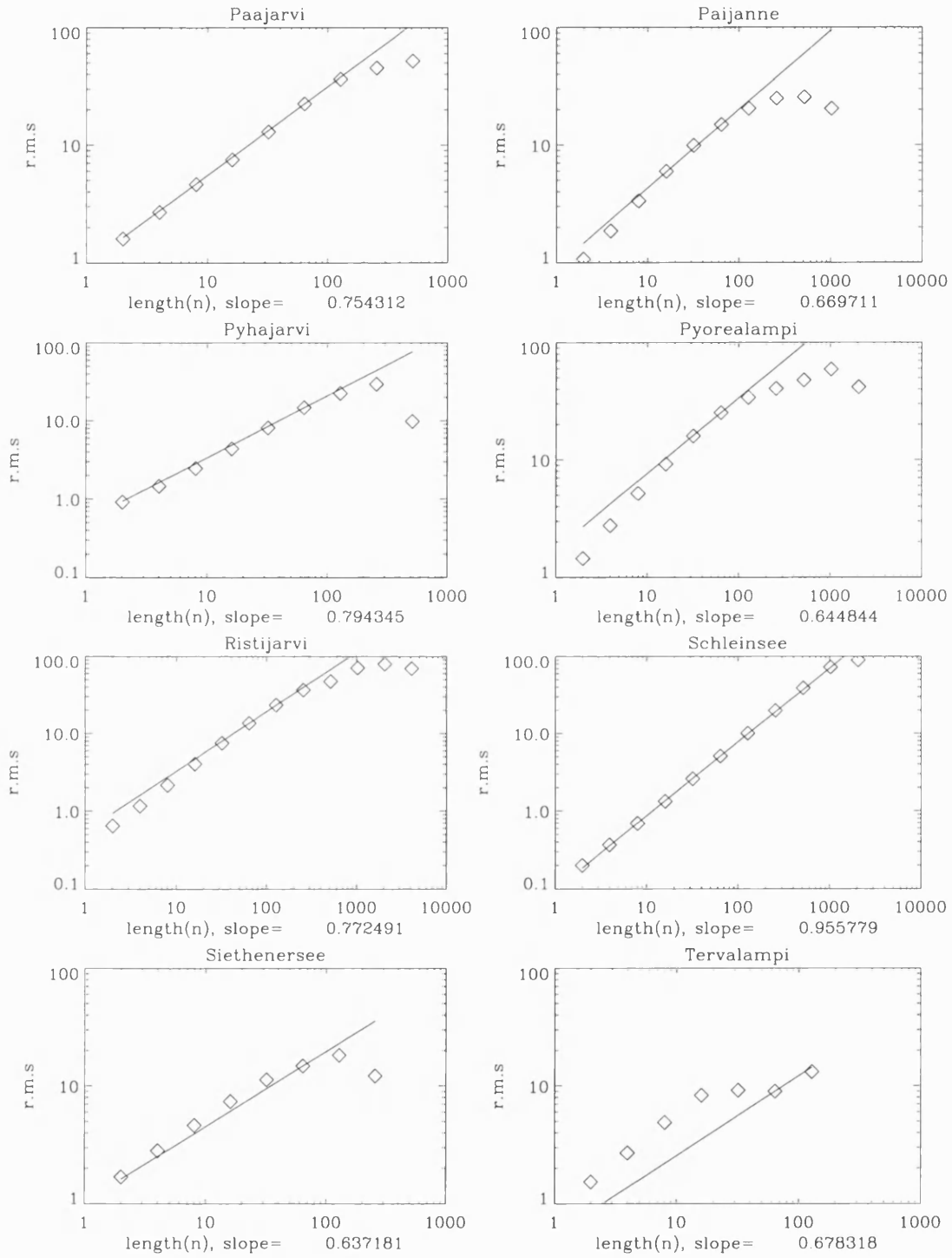

Figure 4.15: Figure illustrating the fluctuation analysis for: Paajarvi, Paijanne, Pyhajarvi, Pyorealampi, Ristijarvi, Schleinsee, Siethenersee, and Tervalampi.

Lake	β	α	H
Belauersee	-1.66	-0.13	0.85
Buchsee	0.15	non-scaling	0.52
C2-8	-0.15	non-scaling	0.49
Deep	-0.98	-0.24	0.90
Degersee	-2.5	-0.23	0.83
Donard	-0.43	non-scaling	0.68
Elk	-0.76	-0.26	0.87
Gosciaz	-2.11	-0.19	0.86
Hamelsee-a	-1.77	-0.08	0.94
Hamelsee-b	-0.55	-0.08	0.94
Heinalampi	-1.13	-0.59	0.56
Illmensee	-0.1	non-scaling	0.64
Karhunpaanlampi	-0.46	-0.61	0.75
Meerfelder-a	-0.54	-0.44	0.77
Meerfelder-b	-2.67	-0.09	0.93
Muttelsee	0.10	non-scaling	0.46
Paajarvi	-0.55	-0.31	0.75
Paijanne	-0.45	-0.43	0.67
Pyhajarvi	-0.27	-0.07	0.79
Pyorealampi	-0.61	-0.29	0.64
Ristijarvi	-0.72	-0.25	0.77
Schleinsee	-2.57	-0.02	0.96
Siethenersee	-0.59	non-scaling	0.64
Tervalampi	-0.67	non-scaling	0.68

Table 4.1: Summary of scaling exponents

Lake	$\beta = 2H - 1$ error	$\alpha = 1 - \beta$ error	$\alpha = 2 - 2H$ error
Belauersee	0.96	0.53	0.17
Buchsee	0.11	na	na
C2-8	0.17	na	na
Deep	0.18	0.26	0.04
Degersee	1.84	1.27	0.11
Donard	0.07	na	na
Elk	0.02	0.5	0
Gosciaz	1.39	0.92	0.09
Hamelsee-a	0.89	0.69	0.04
Hamelsee-b	0.33	0.53	0.04
Heinalampi	1.01	0.46	0.29
Illmensee	0.18	na	na
Karhunpaanlampi	0.04	1.15	0.11
Meerfelder-a	0	0.9	0.02
Meerfelder-b	1.81	1.58	0.05
Muttelsee	0.18	na	na
Paajarvi	0.05	0.76	0.19
Paijanne	0.11	0.98	0.23
Pyhajarvi	0.31	0.8	0.35
Pyorealampi	0.33	0.68	0.43
Ristijarvi	0.18	0.53	0.21
Schleinsee	1.65	1.55	0.06
Siethenersee	0.31	na	na
Tervalampi	0.31	na	na

Table 4.2: Summary of scaling exponent relations.

4.2 Discussion

For lake sedimentation, the results suggest the dynamics of smaller scales, i.e., thinner varves, are connected to the dynamics of larger scales, i.e., thicker varves by a power law over all the resolvable orders of magnitude (see Table 4.1.). As such, the occurrence of thinner or thicker varves are likely to be followed by the occurrence of a thinner or thicker varves, respectively. The scaling exponents vary between ca. $H = 0.6$ to 0.9, and are significantly different from the white and red noise models. These results compare well with the values calculated by Hurst, [118] and Mandelbrot and Wallis [119], and with a range of other natural system dynamics, such as temperature, rainfall, topography, as well sedimentary deposits, e.g., marine shelf sediments, and turbidites. The value of the exponents indicate; (i) the underlying model is fGn, though this is unlikely to hold, as it is associated with Gaussian distributions, (ii) the persistence is weak, and (iii) the processes are stationary. Correlation results indicate the scaling exponents do not relate to any of the available physical parameters, (though β scales with γ_a, and similarly, H with actual τ, and α with actual τ) indicating scaling dynamics in sedimentation are a product of a complex interplay between numerous variables (see Figures 5.4. to 5.19.)

Comparisons between the scaling exponents indicate a range of relations (see Table 4.2.). For $\beta = 2H - 1$, Donard, Elk, Karhunpaanlampi, Meerfelder-a, and Paajarvi, show small errors, while the remaining lakes display large errors. For $\alpha = 1 - \beta$, only Deep shows a small error, while the remaining lakes display large errors. For $\alpha = 2 - 2H$, Deep, Degersee, Elk, Gosciaz, Hamelsee-a, Hamelsee-b., Karhunpaanlampi, Meerfelder-a, Meerfelder-b, and Schleinsee show small errors, while the remaining lakes display large errors. These results indicate that only α and H estimations are comparable.

The errors in the scaling exponent values comparisons relates to three main features. First, the established relationships between β, α, and H are only valid for a very specific model, i.e., fGn or fBm. So when the system dynamics diverge from this model, the relationship breaks down, as there is no theoretical reason for the scaling exponents to be controlled by a single underlying exponent, i.e., monoscaling.

Second, errors in scaling exponent relations involving β, are related to crossovers between scaling regimes, e.g., Belauersee, Degersee, and Schleinsee. This is related to power spectra generally considered to be less sensitive than the other methods that isolate scale invariance [61], [80], though the fluctuation analysis displays more smoothing than the autocorrelation and power spectra methods. As such, isolating crossovers in power spectra, in particular, fitting two straight lines is not an ideal statistical procedure, even though tests are available to assess statistical confidence [196]. However, we can confidently say that the crossovers observed in this study, within the range 100 yrs $\pm$ 20 yrs are statistically and physically significant. It is suggested the crossover represents a large scale change in system dynamics, possibly related to the timescales of operation of dominant climatic processes. Third, the most coherent results for all relations for all scaling exponents are from Elk lake, which is also the longest time series. Conversely, the most varied relations are from the shorter time series. There are exceptions to this general rule, but these results highlight the need for caution for invoking physical mechanisms when the actual reasons may be statistical artefacts. Nevertheless, from the body of results in this study it is thought the physical dynamics are robust.

The three most commonly implicated mechanisms for scaling are; random walk, (self-organised) critical phenomena, and multiscaling processes. In this study we have directly assessed random walk processes through the application of an AR(1) process (see Figure 4.16.). The results for β values for the actual data display notable variations from the AR(1) process, while the e-folding times display some similarities. Differences from the AR(1) process indicate the influence of the critical phenomena, and multiscaling processes. In addition, in the random walk analogy we assume the coin toss is a random process, i.e., unbiased (50/50). However, there are instances, when the coin is biased (70/30). Furthermore, the probabilities themselves can change as phenomena interact with each other, i.e., the probabilities themselves are non-stationary, and any probability becomes conditional upon surrounding events [202].

Implicating the mechanism of self-organised critically requires that what is external and internal with respect to varve formation is adequately defined. With the

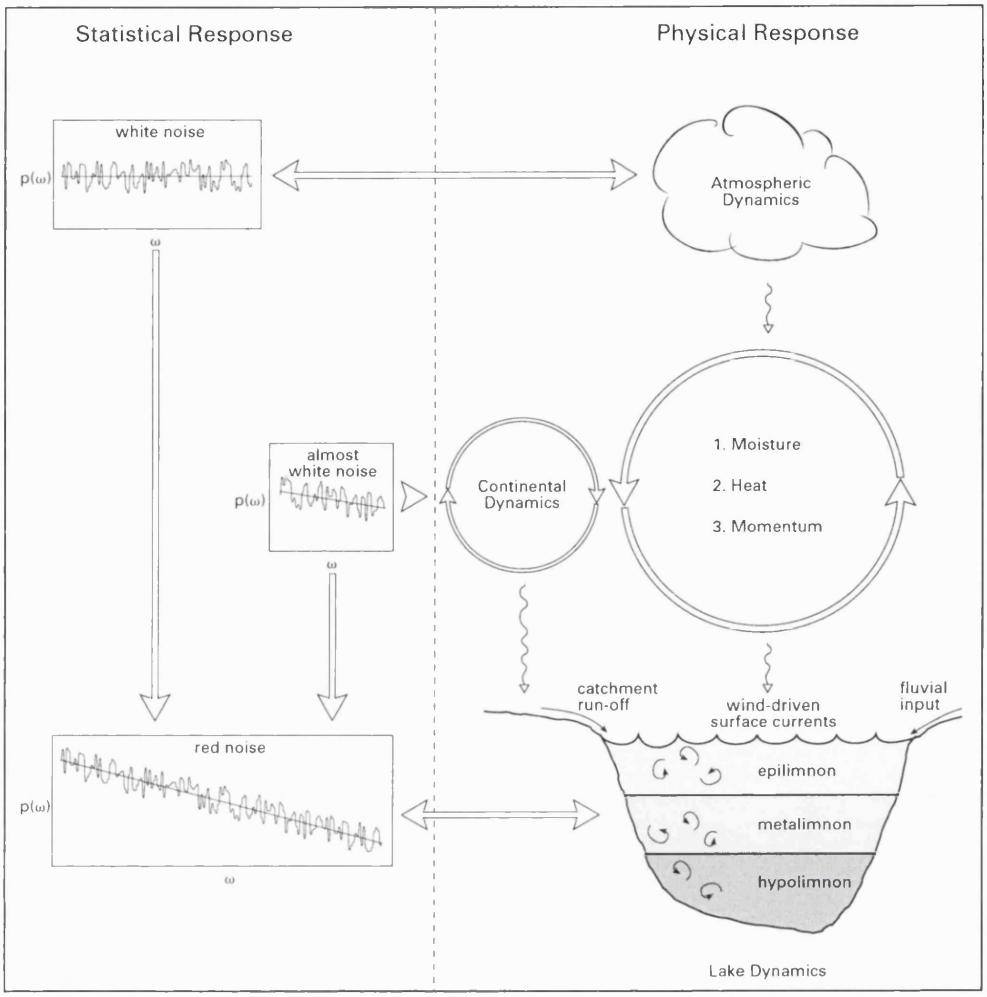

Figure 4.16: Schematic diagram illustrating the interaction of the atmosphere, continent and lakes, via random walk dynamics. As ocean-atmosphere interactions are the primary driving mechanism of global climate, the scaling signature is imprinted, by thermal and hydrological feedback mechanisms on all natural systems [197], [198]. In addition, there exists imprinting of scale invariant signatures from concomitant atmosphere-land processes [199], [200]. However, in this instance the form of the background spectrum will be almost white over a wide range of frequencies, due to equilibrium between the small thermal inertia (as compared to the oceans) of the continents with the thermal forcing from the atmosphere, effectively local forcing and local response [201]. Lake system dynamics also display independent elements of random walk processes, in particular Brownian motion.

exception of lakes C2-8 and Donard (which are composed of allochthonous particles) all of the lakes are characterised by varves composed of both allochthonous and autochthonous particles. This then means the lake is defined by the terrestrial catch-

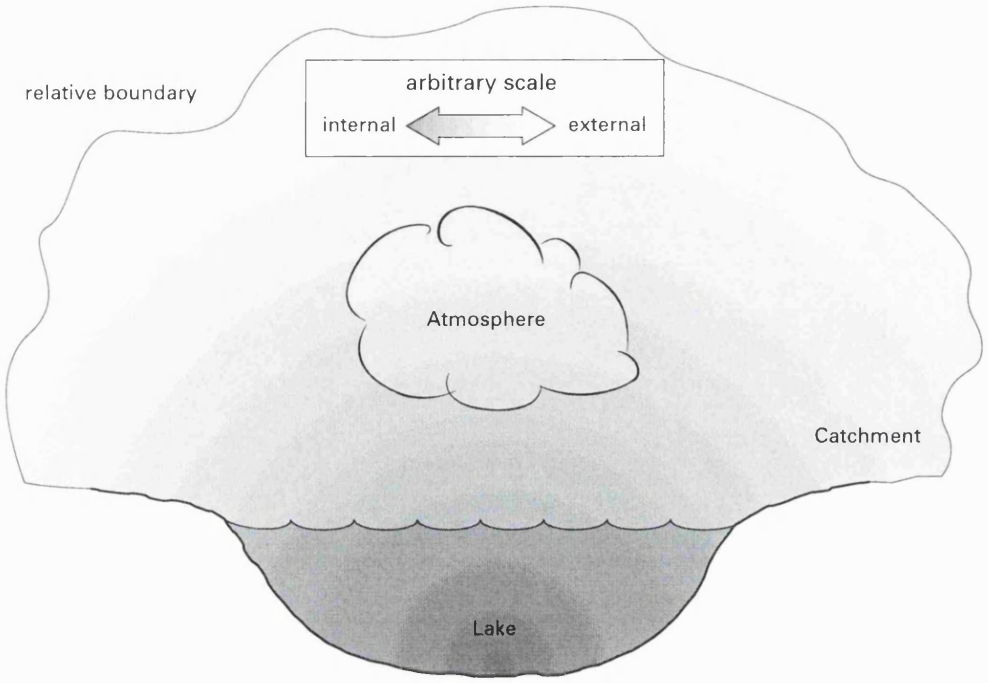

Figure 4.17: Schematic diagram illustrating the nature of a relative boundary in lake system dynamics.

ment and the atmospheric catchment. Although measurements are given for the terrestrial catchment, and it is this that provides the vast majority of allochthonous material, it is also highly likely there are particles derived from a greater source region. Similarly for atmospherically derived sediments, though less significant in terms of the overall composition, delineating the atmosphere is complicated by the fact that the "space" above the lake - catchment system is constantly changing in form. As such, we are forced to simply describe the concept of internal and thus, self-organised, to be represented by "local" processes. Thus, attempting to distinguish between which time-series (or parts of time series) are dominated by internal-self-organisational-endogenous changes and which by catchment-atmosphere-external-exogenous forcing is problematic (see Figure 4.17.).

Here we expand upon the discussion above by proposing a model for varve sedimentation encompassing processes associated with random walk, critical phenomena and multiscaling dynamics, and gamma and log-normal distributions (see Figure 4.18.).

Varves are derived from allochthonous particle loading from the catchment (via run-off and erosion, and fluvial input) and the atmosphere (via wind and precipitation), autochthonous bioactivity (via algal/diatom blooms), and calcite precipitation. Catchment dynamics, e.g., floods, display elements of randomness [203] and can be modelled as a nonlinear cascade of storage elements [204]. In addition, wind erosion and related saltation is characterised by cascades of intermittent bursts of activity, interspersed with periods of inactivity [205]. Overall, such catchment processes also play an integral role in multiplicative cascades of rainfields, which in turn affect catchment runoff and allochthonous loading [206]. Although it is conceviable in some open lakes, sediment delivery by groundwater process is considered unlikely for the lakes in this study, though such processes may impact on the over all fluid dynamics.

Phytoplankton dynamics also display notable random dynamics, as well as intermittent blooms [207] and particle trajectories, which are in part due to self-organisation mechanisms [208]. The lake water column is characterised by two components; the water molecules and the particles (allochthonous and autochthonous). These are distributed in particle rich, and particle poor regions [130].

Such particles are held up in suspension by a virtual threshold representing the water velocity. Deposition, the outcome of particle transport from the bulk of a flowing suspension to the sediment surface, occurs when water velocity is less than the threshold velocity (threshold crossing) required to keep the particles in suspension [209]. Generally, particle concentration is not dense, vis a vis fluid dynamics are passive. Random motions, i.e., Brownian motion of particles and molecules are initiated by thermal energy and an instability of a system parameter (velocity threshold) controlling particle flux (possibly after reaching a self-organised (critical) state). This diffusion mechanism smoothes irregularities in particle concentrations. This instability forces the properties of the system to accelerate away from a given previous state, i.e., the particles then move and change direction rapidly and independently of gravity and fluid flow [130], [173]. As the particles move through the water column, they drag the surrounding fluid and thus neighbouring particles, i.e., hydrodynamic interaction. This creates displacement, and ensures mixing, which is

small over short periods and large over long periods [210]. As such, particle rich and poor regions change position and velocity [211]. If this displacement esculates, it can provoke further instability in other clusters leading to an avalanche. This leads to entrainment of particles in fluxes to the lake bottom.

This process, effectively the formation of a varve laminae is random. It is suggested this process is analogous to the addition of random positive events leading to the gamma distribution. Here, each avalanche, and occurrence of a laminae is independent of the previous avalanche and laminae, respectively (but the "position" is not). These processes involve numerous biochemical and physical transformations [212],[213]. This causes constant changes in particle sizes, effective densities, settling rates, and surface areas, which attenuate the deposition rate [212], [213], [214].

It is suggested this process is analogous to the avalanche events in the archetypal SOC sandpile model. This model has already been applied in other sedimentation scenarios. For example, in fluvial bedload transport, the unidirectional and horizontal orientation of the water flow is effectively the slope. Similarly, for lakes, this water flow is unidirectional and in the vertical plane. Generally, the fast relaxation is controlled by slow particles, and the slow relaxation is controlled by the fast particles [215]. Some avalanches maybe transported as cascades by turbulent eddies of energetic flows in the boundary layers and isolated patches of the lake, e.g., in the hypolimnion [216] and metalimnon [217]. The growth and clustering of the avalanche stops when the probability of chain reaction expansion becomes less than the probability of its dampening. On a longer time, scale such relaxations occur due to a change in particle composition with the changing seasons. The length of the relaxation time in lake system will vary from lake to lake, and will dominantly reflect the hydrological setting and the efficiency of negative feedback mechanisms. It is suggested these physical processes, i.e., particle interaction behave intermittently as an on-off mechanism.

The amount of sediment formed and deposited as varves is a fraction of that which is available. This is analogous to fractionation processes and the observed log-normal distribution. For example; varve components of a biological origin, e.g., diatoms, will be a function of the amount of nutrients in the water column and the

amount of sunlight, i.e., photosynthetic processes, and thus the amount of deposited material will be a fraction of the biomass not recycled in the water column. Varve components of a physical origin will be a function of the wind speed, the amount of precipitation, and the amount of dust on the ground in the catchment, and or precipitation and rock type/vegetation. Varve components of a chemical origin will be a function of lake temperature and calcium carbonate concerntration.

While this model sets out the potential role of each of the three underlying mechanisms of scaling, and the log-normal and gamma distributions, relating statistical and physical quantities is difficult. Although we have specified the effects of specific mechanisms on particle formation and deposition, in reality, varve formation reflects a net balance of these dynamics, and as such, can be considered as a series of random depositional events, manifested as multiplicative cascades evolving towards and beyond (self-organised) critical states, effectively threshold systems with random (white noise) forcing on e.g., 3-4 different timescales.

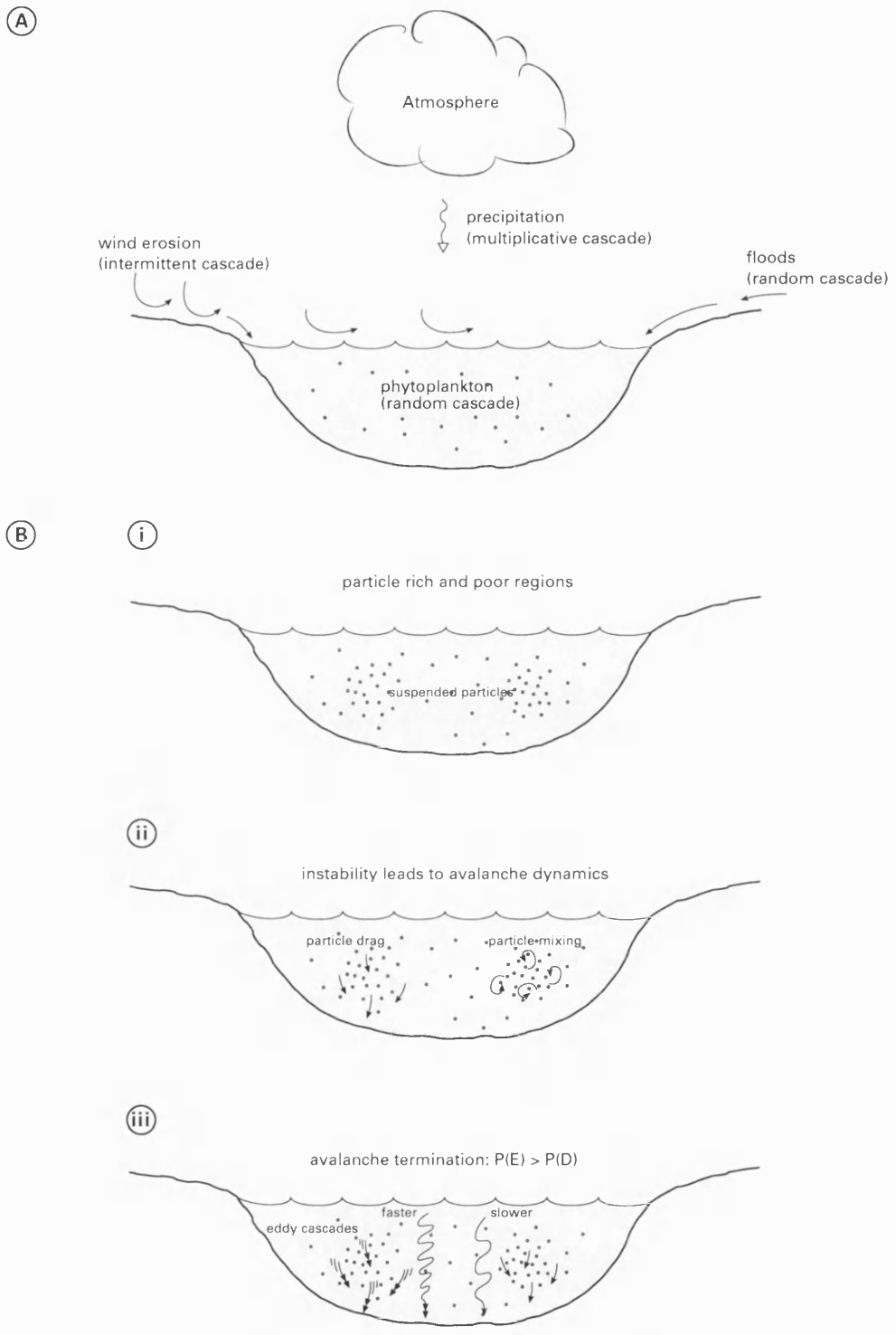

Figure 4.18: Schematic diagram illustrating the physical model of varve sedimentation. A. displays the interaction of the underlying scaling mechanisms in the formation of varve particles. B.i. to B. iii. displays the arrangement of suspended particles in particle rich and poor regions, which undergo movement when system instabilities exceed critical thresholds. Avalanche dynamics are characterised by eddy cascades.

Chapter 5

Temporal Signatures II

5.1 Introduction and Results

In this chapter we present the results of e-folding times calculated from the auto-correlation function, AR(1) model and waiting time analysis. Figures 5.1. to 5.3. display the waiting time distribution for the time series in this study. The x-axis is the thickness threshold, and the y-axis is the waiting time. The basic form of the distribution is shown in Figure 2.6., where a "typical" distribution with a constant mean, and the occurrence of extreme events in the form of thinner or thicker varves is represented by a "u-shaped" curve. For the lakes in this study this is the dominant distribution, e.g., Belauersee, Donard, Hamelsee-a, and Pyhajarvi. However, there are some variations on this form; (i) a low or non-existent thinner varve limb, e.g., Elk, and Meerfelder-b, (ii) a low or non-existent thicker varve limb, e.g., Heinalampi, Karhunpaanlampi, Meerfelder-a, Pyorelampi, and Tervalampi, and (iii) a centralised, or slightly skewed peak, e.g. Deep, Meerfelder-b, Paajarvi, and Paijanne. Figures 5.4. to 5.19. display the correlations between physical and statistical parameters for the lakes in this study.

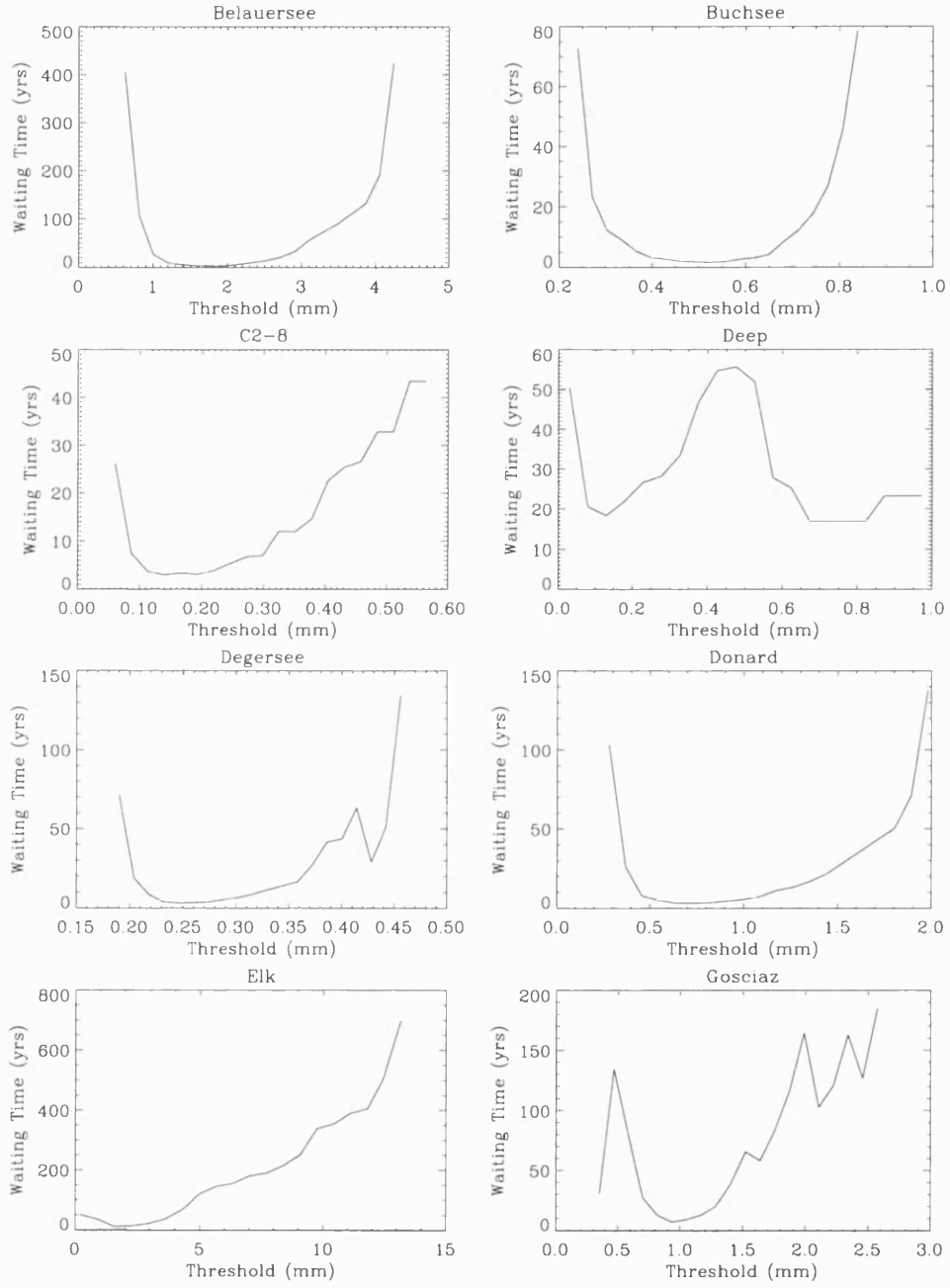

Figure 5.1: Figure illustrating the waiting time distribution for: Belauersee, Buchsee, C2-8, Deep, Degersee, Donard, Elk, and Gosciaz.

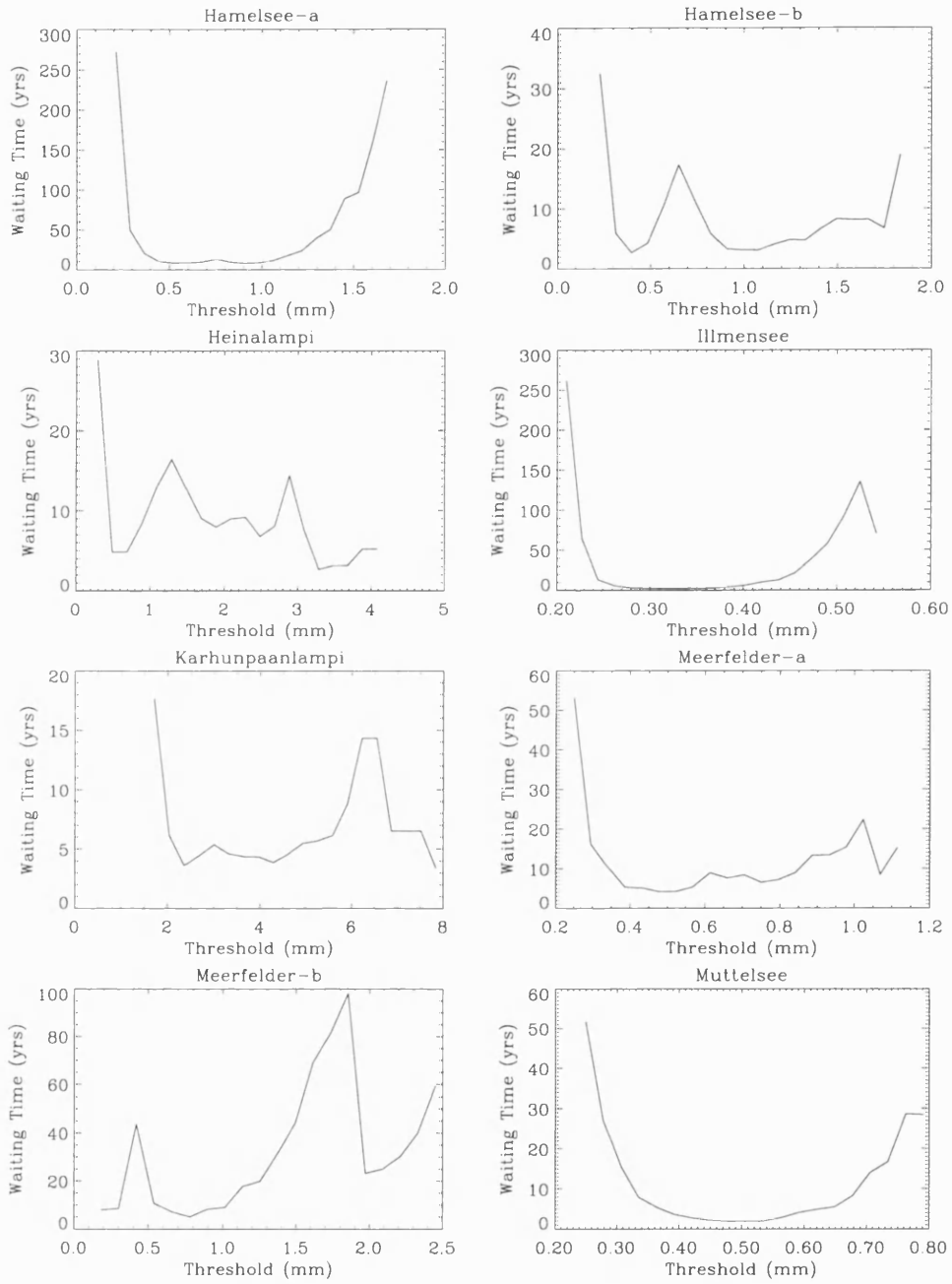

Figure 5.2: Figure illustrating the waiting time distribution for: Hamelesee-a, Hamelsee-b, Heinalampi, Illmensee, Karhunpaanlampi, Meerfelder-a, Meerfelder-b, and Muttelsee.

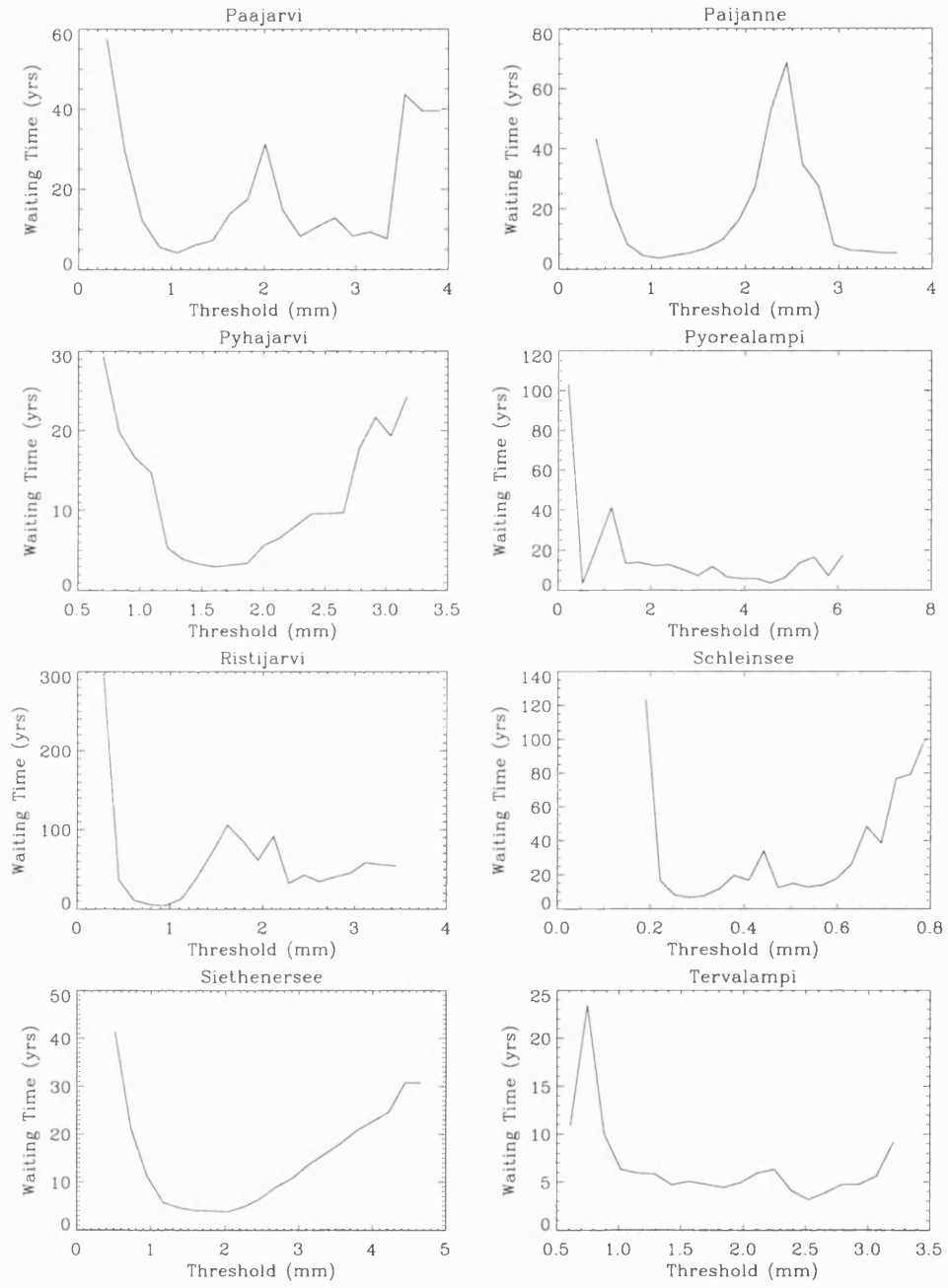

Figure 5.3: Figure illustrating the waiting time distribution for: Paajarvi, Paijanne, Pyhajarvi, Pyorealampi, Ristijarvi, Schleinsee, Siethenersee, and Tervalampi.

Lake	Lag-1 coeff.	ACF τ	AR(1) τ	ACF τ and AR(1) τ Diff.
Belauersee	0.93	7.7	13.9	6.2
Buchsee	0.91	na	11.5	na
C2-8	0.55	na	2.2	na
Deep	0.82	4.2	5.5	1.3
Degersee	0.97	4.4	31	26.6
Donard	0.87	na	7.5	na
Elk	0.87	3.9	7.8	3.9
Gosciaz	0.96	5.3	28	22.7
Hamelsee-a	0.93	12	14.3	2.3
Hamelsee-b	0.90	12.5	10.4	2.1
Heinalampi	0.80	1.7	5	3.3
Illmensee	0.96	na	23.2	na
Karhunpaanlampi	0.9	1.6	9.6	8
Meerfelder-a	0.93	2.3	15.2	12.9
Meerfelder-b	0.89	10.6	9.3	1.3
Muttelsee	0.92	na	11.9	na
Paajarvi	0.89	3.2	8.9	5.7
Paijanne	0.89	2.3	9.5	7.2
Pyhajarvi	0.91	15.2	10.8	4.4
Pyorealampi	0.89	3.5	9	5.5
Ristijarvi	0.94	3.9	15.6	11.7
Schleinsee	0.95	46	19.6	26.4
Siethenersee	0.87	na	7.4	na
Tervalampi	0.89	na	9.5	na

Table 5.1: Summary of autocorrelation and AR(1) e-folding times

Lake	Waiting Time τ_1	Waiting Time τ_2	WT τ_1 and ACF τ Diff.	WT τ_1 and AR(1) τ Diff.
Belauersee	15	410-430	7	1
Buchsee	7.5	70-80	na	4
C2-8	5	25-45	na	3
Deep	17.5	25-55	1	9
Degersee	10	70-140	10	21
Donard	10	100-140	na	3
Elk	50	50-700	46	40
Gosciaz	10	30-180	5	18
Hamelsee-a	15	230-280	3	1
Hamelsee-b	5	20-35	8	5
Heinalampi	5	5-30	3	0
Illmensee	10	140-260	na	13
Karhunpaanlampi	5	5-20	3	5
Meerfelder-a	7.5	15-55	5	8
Meerfelder-b	10	10-60	1	1
Muttelsee	5	30-50	na	7
Paajarvi	5	40-60	2	4
Paijanne	5	5-45	3	5
Pyhajarvi	5	25-30	10	6
Pyorealampi	10	20-100	6	1
Ristijarvi	15	50-300	12	1
Schleinsee	15	100-120	31	5
Siethenersee	5	30-40	na	2
Tervalampi	5	10-25	na	5

Table 5.2: Summary of waiting time e-folding times

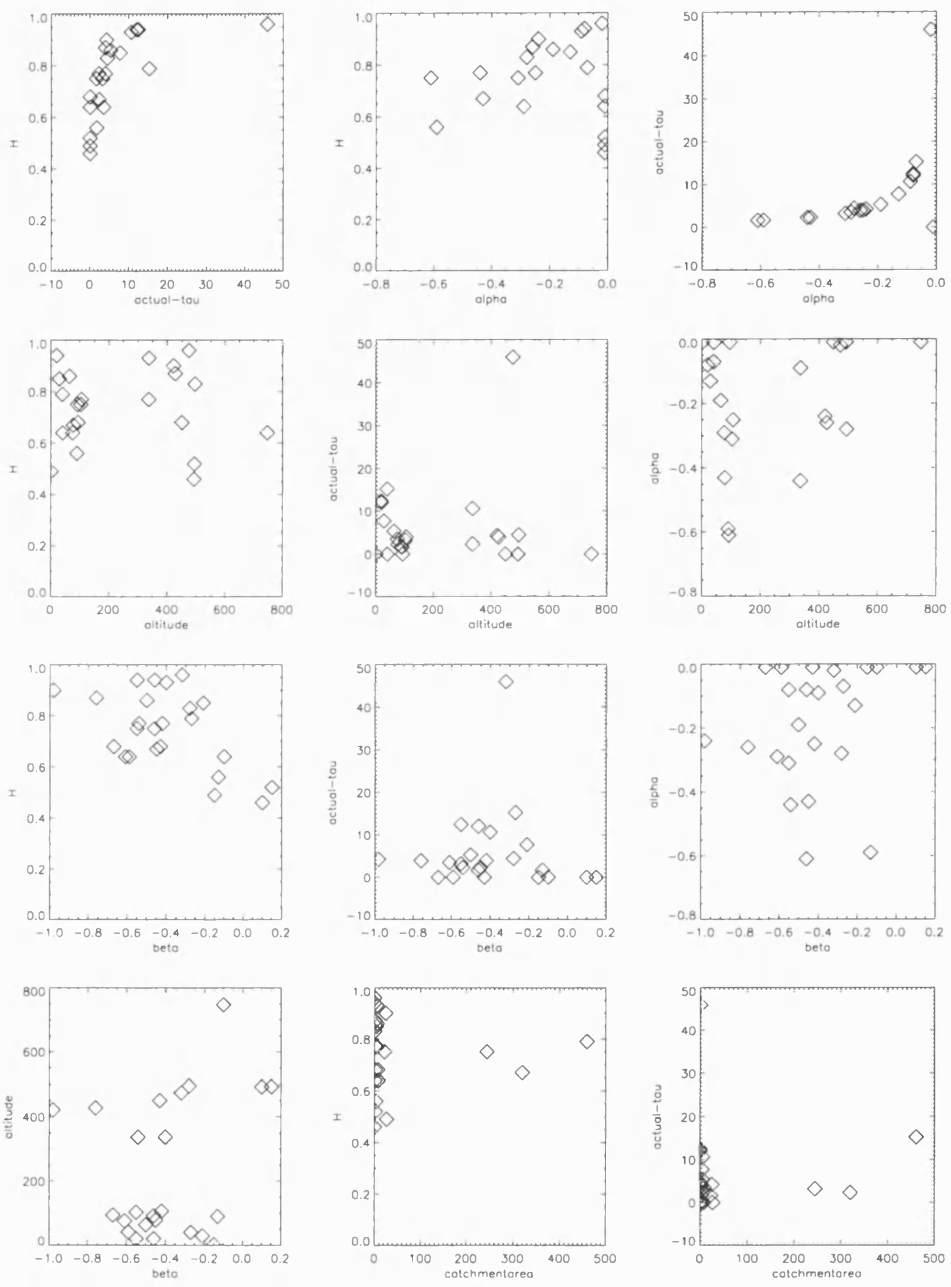

Figure 5.4: Figure illustrating the correlation between physical and statistical parameters

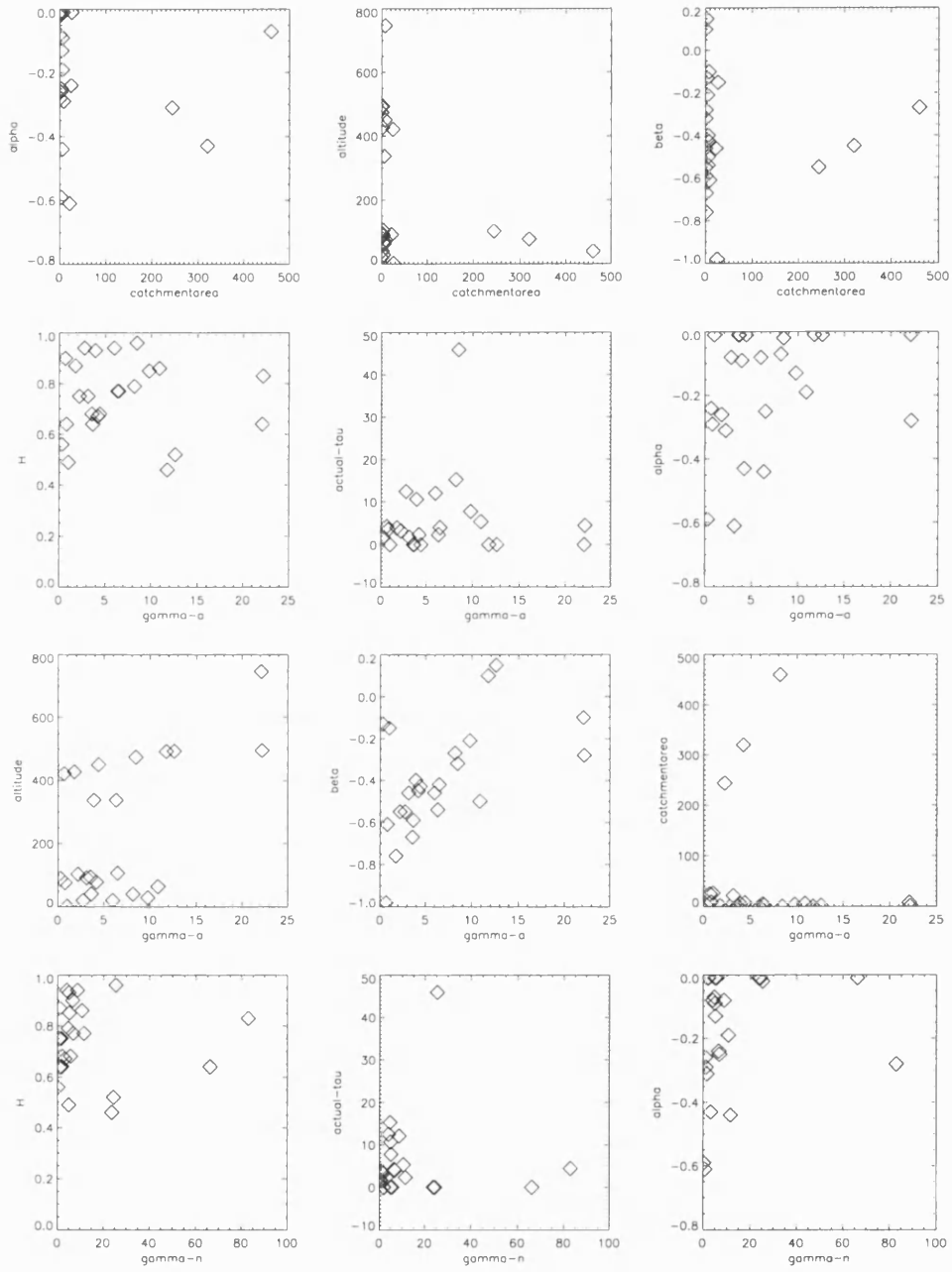

Figure 5.5: Figure illustrating the correlation between physical and statistical parameters

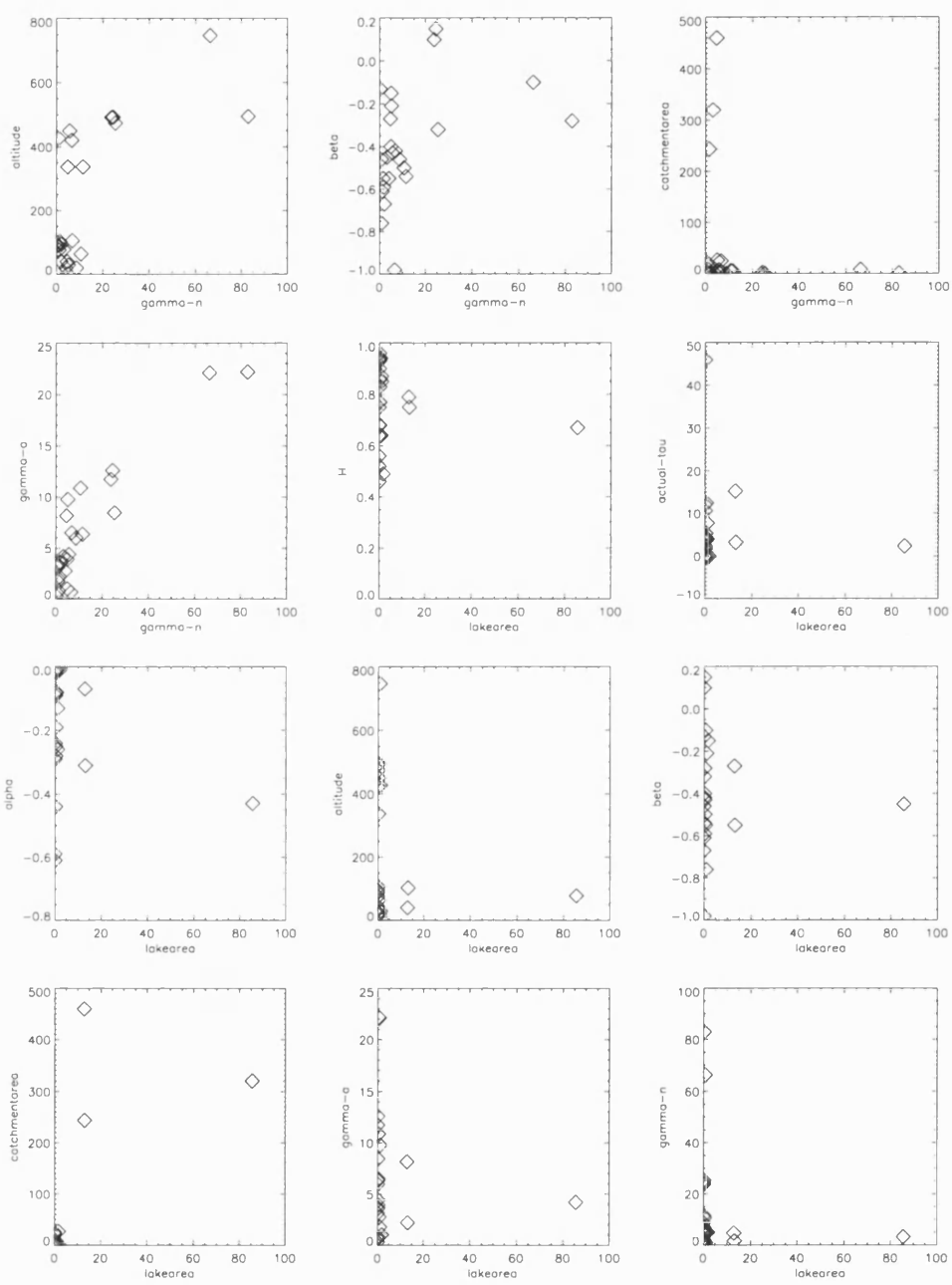

Figure 5.6: Figure illustrating the correlation between physical and statistical parameters

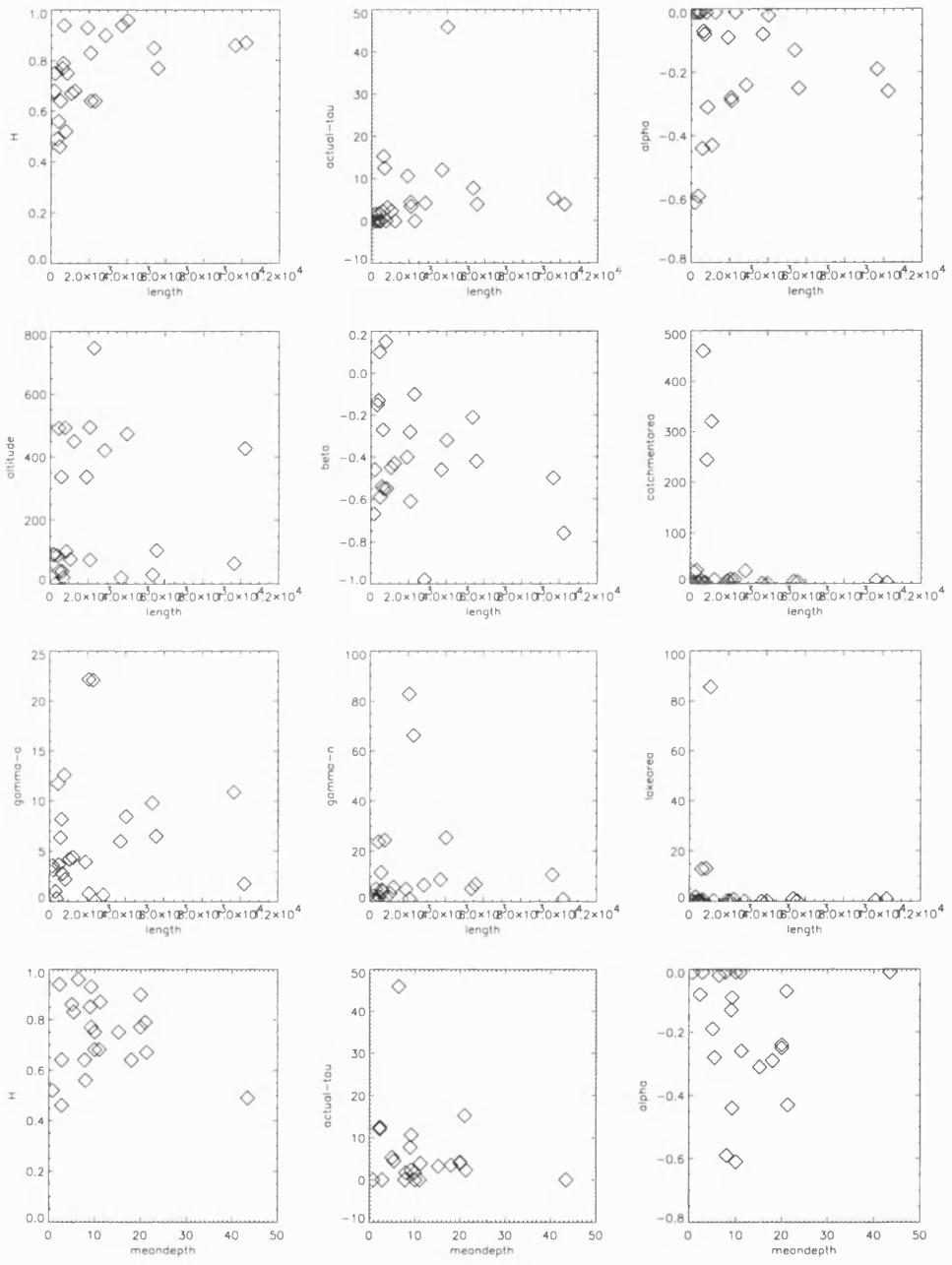

Figure 5.7: Figure illustrating the correlation between physical and statistical parameters

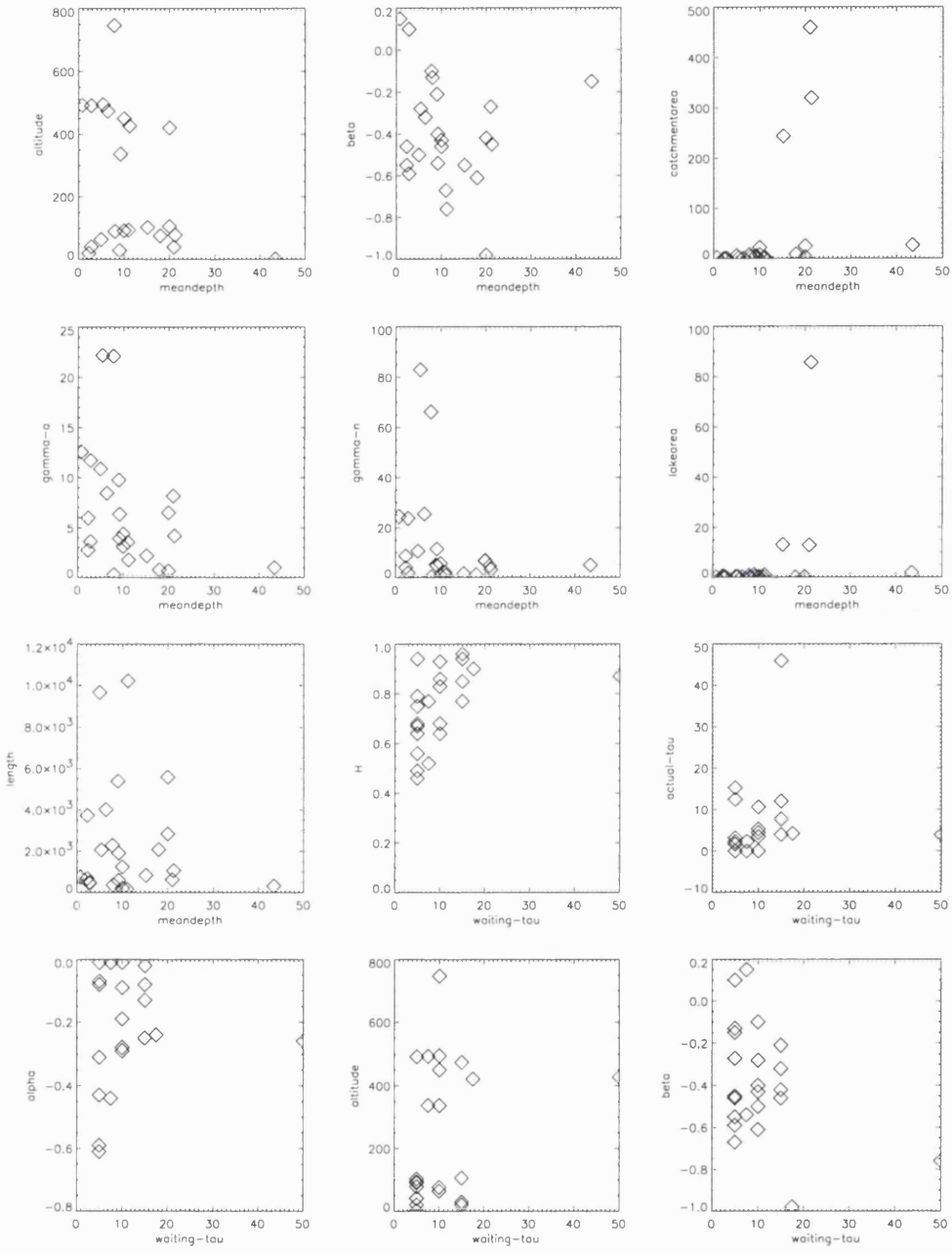

Figure 5.8: Figure illustrating the correlation between physical and statistical parameters

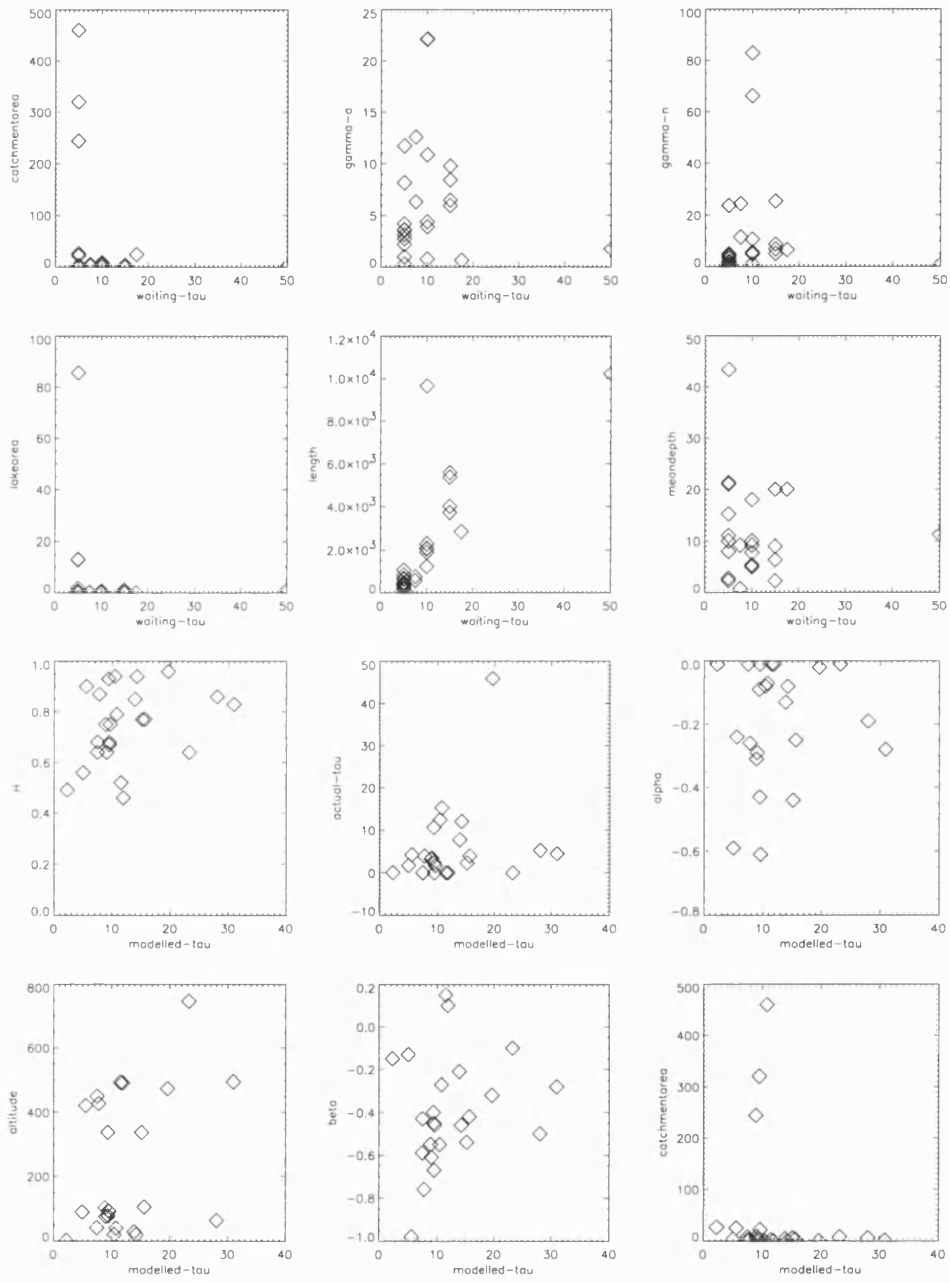

Figure 5.9: Figure illustrating the correlation between physical and statistical parameters

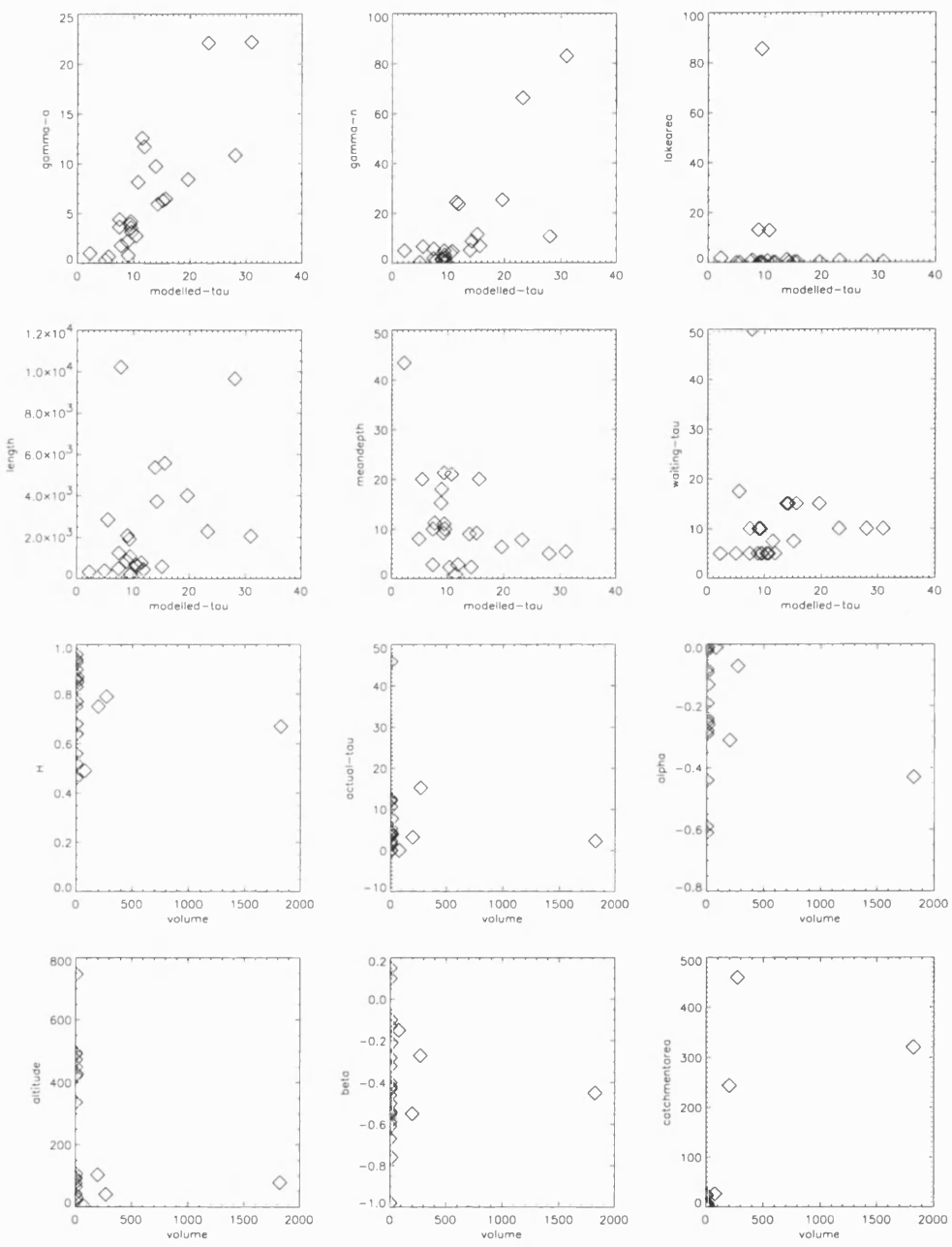

Figure 5.10: Figure illustrating the correlation between physical and statistical parameters

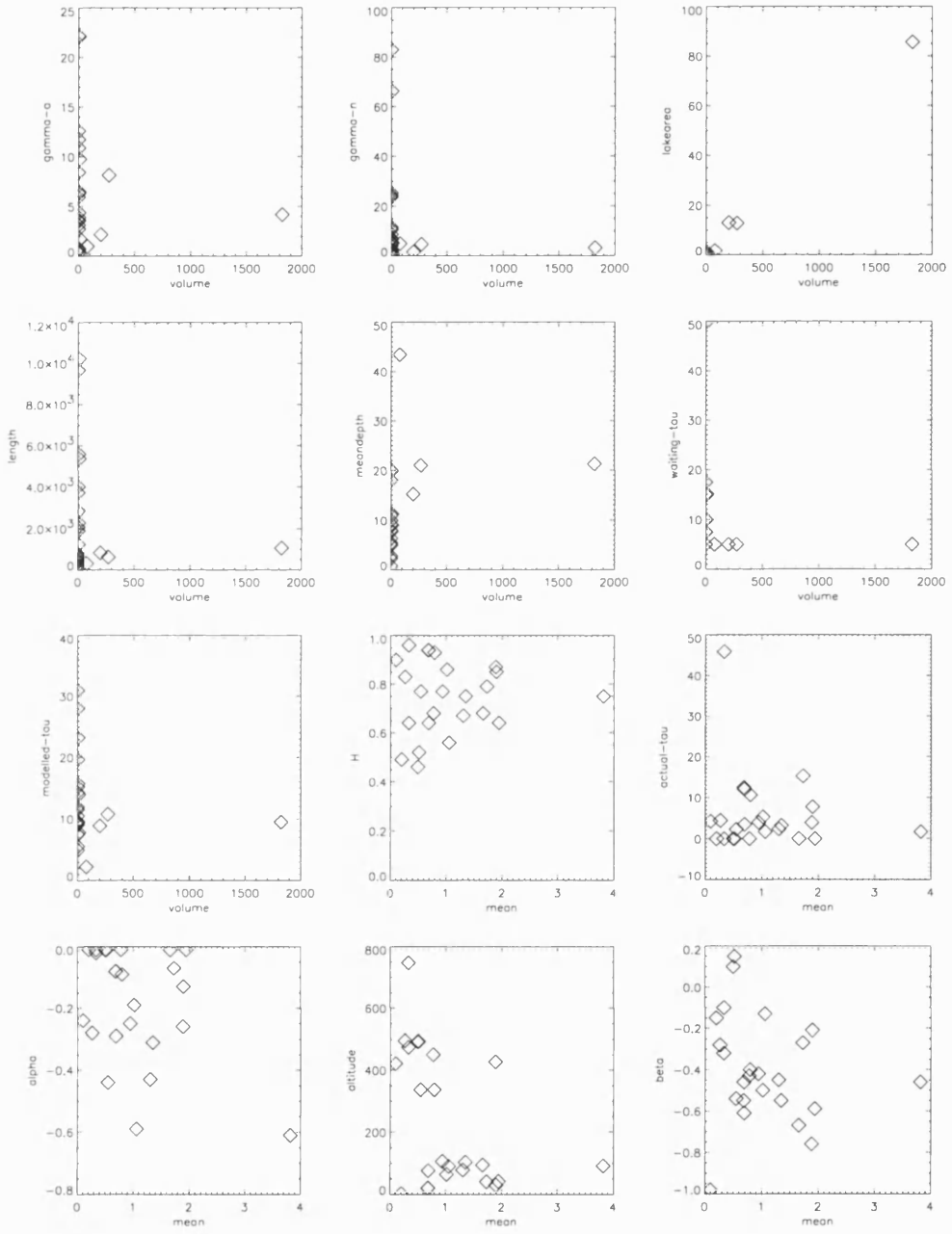

Figure 5.11: Figure illustrating the correlation between physical and statistical parameters

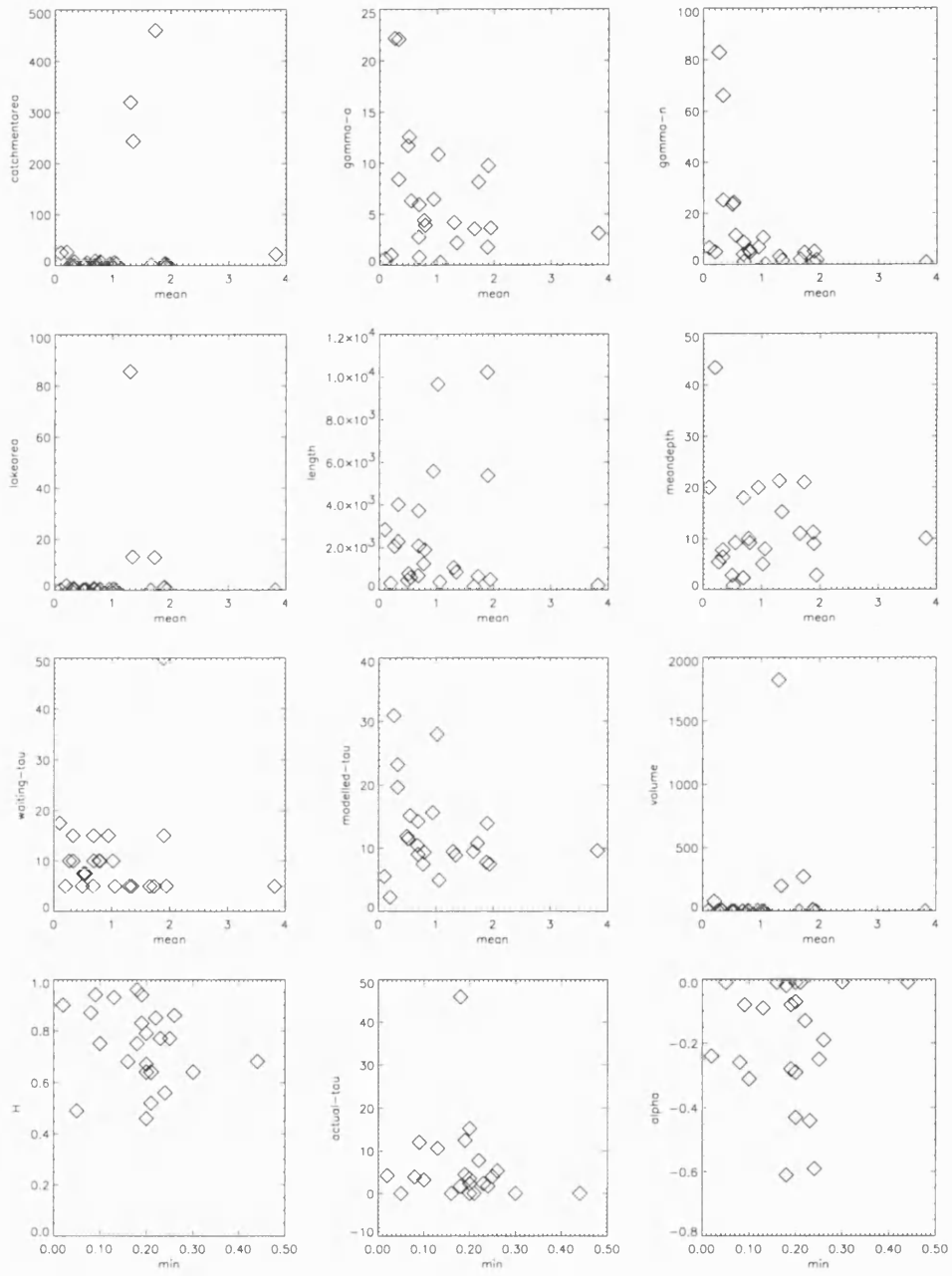

Figure 5.12: Figure illustrating the correlation between physical and statistical parameters

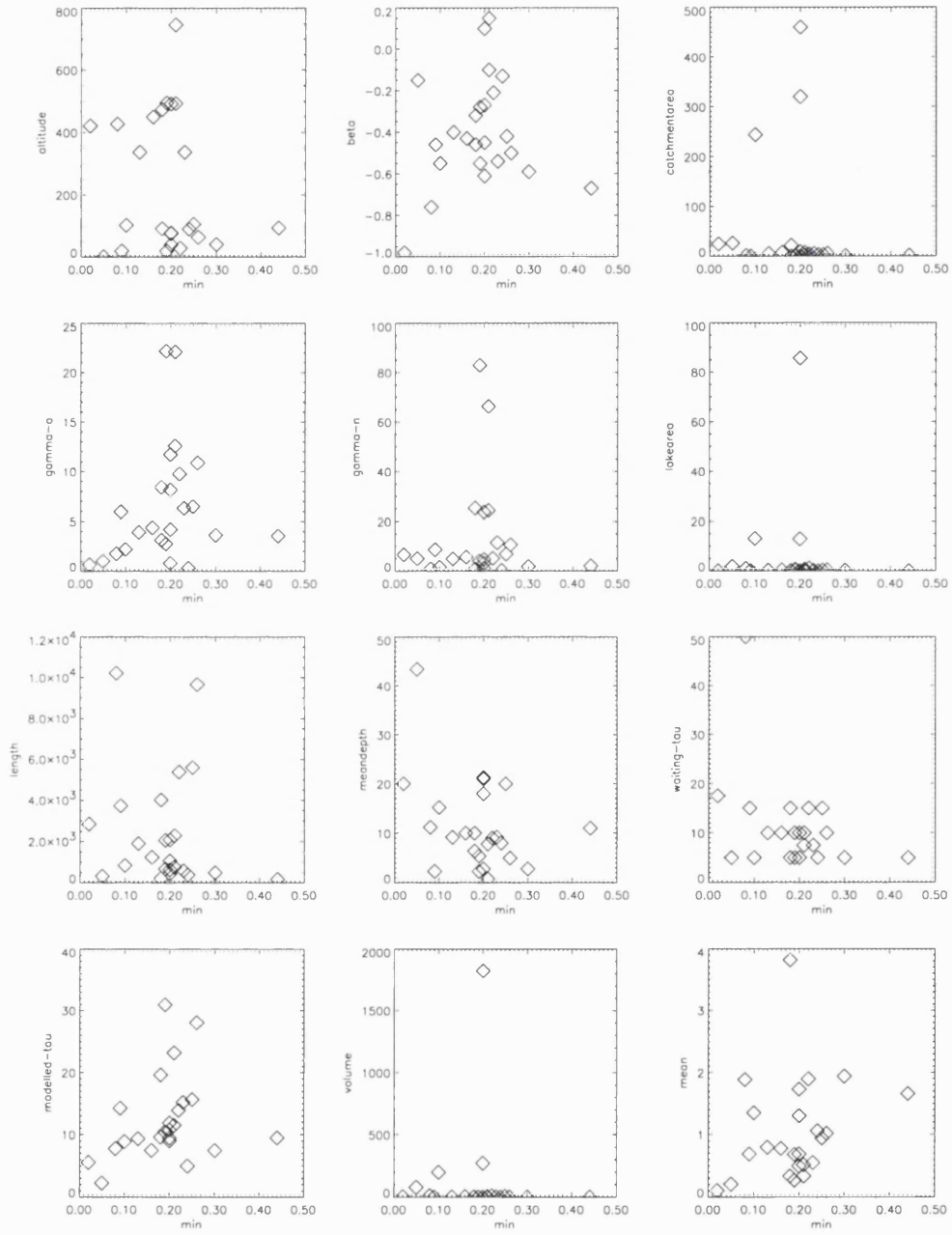

Figure 5.13: Figure illustrating the correlation between physical and statistical parameters

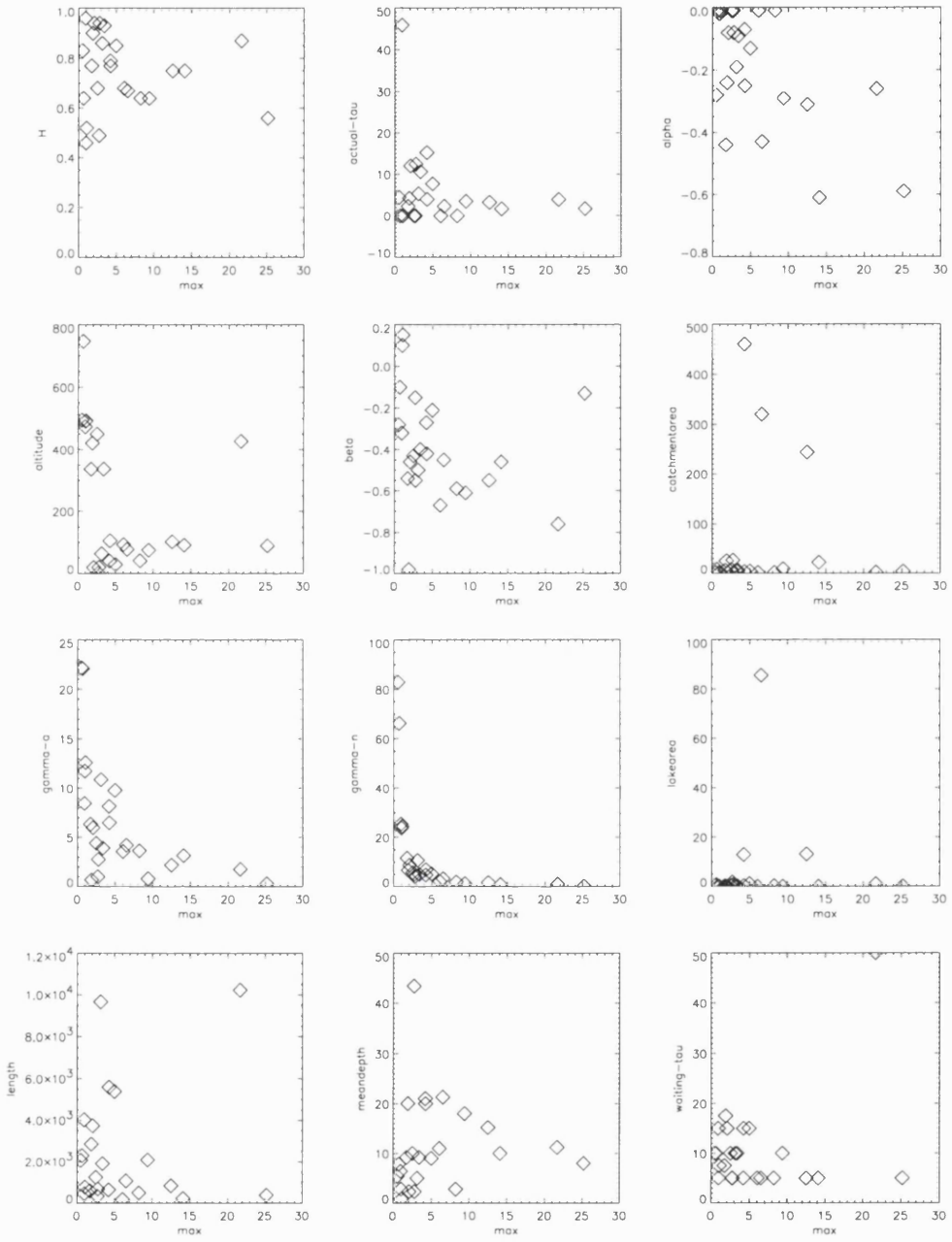

Figure 5.14: Figure illustrating the correlation between physical and statistical parameters

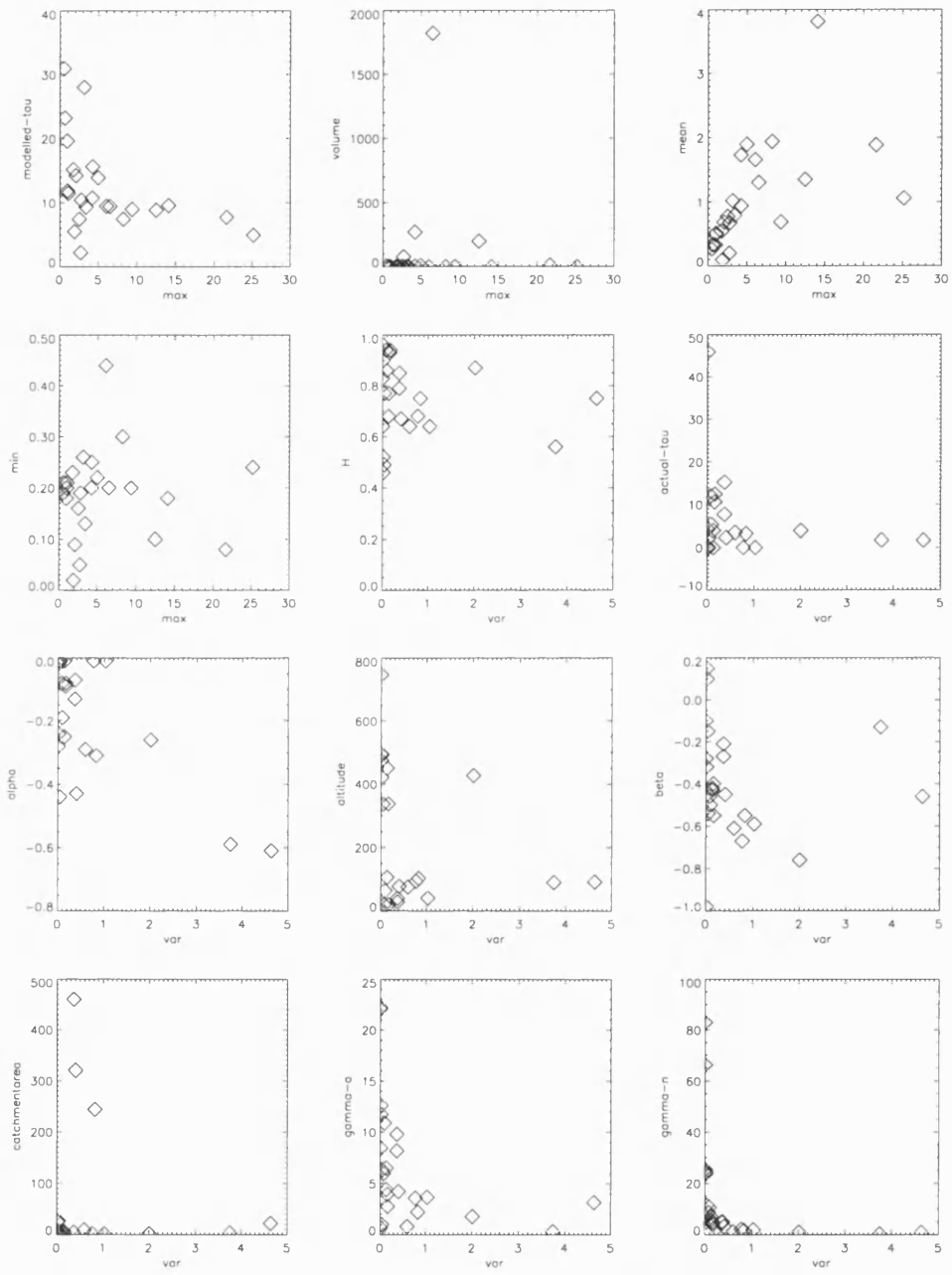

Figure 5.15: Figure illustrating the correlation between physical and statistical parameters

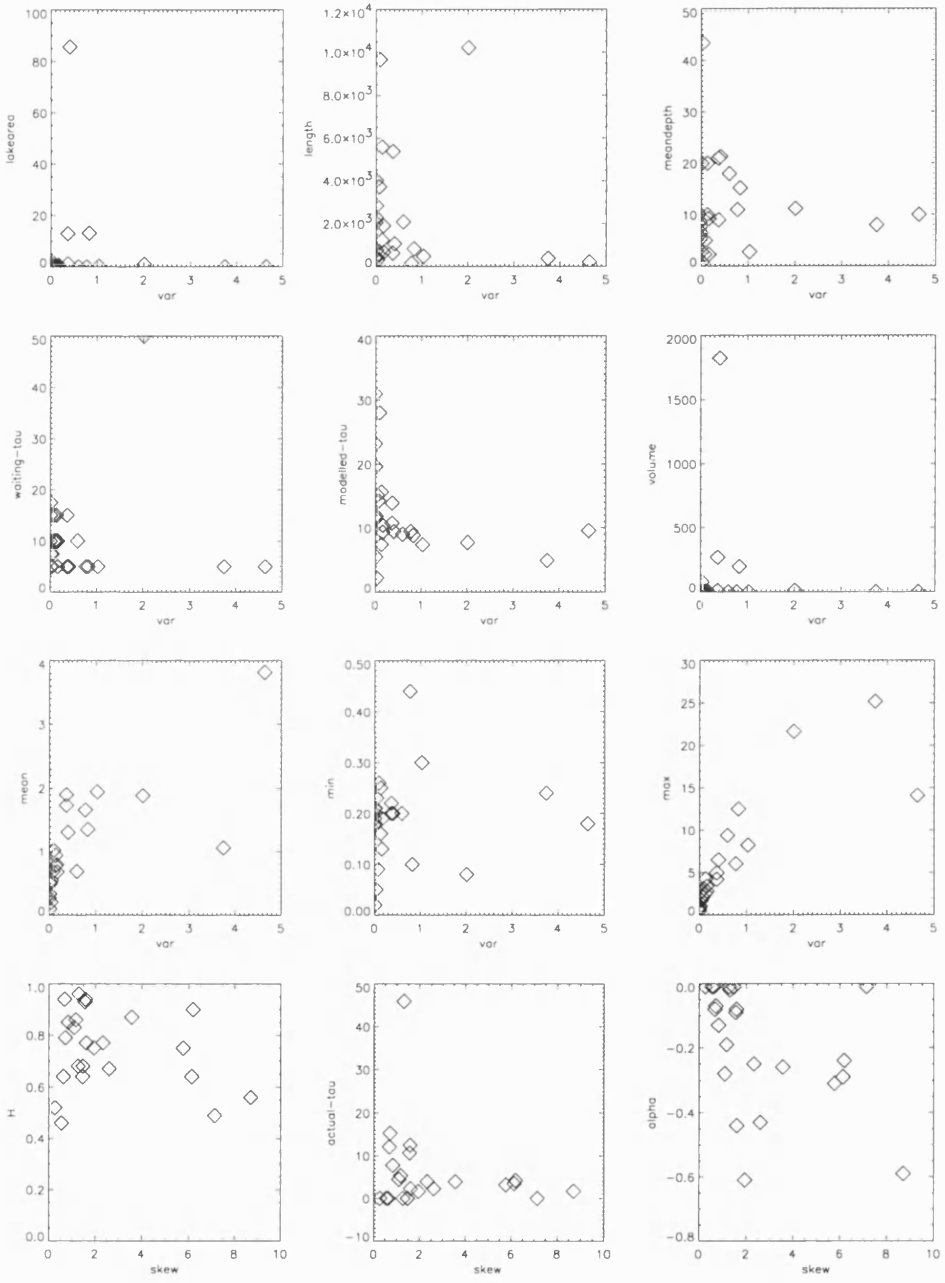

Figure 5.16: Figure illustrating the correlation between physical and statistical parameters

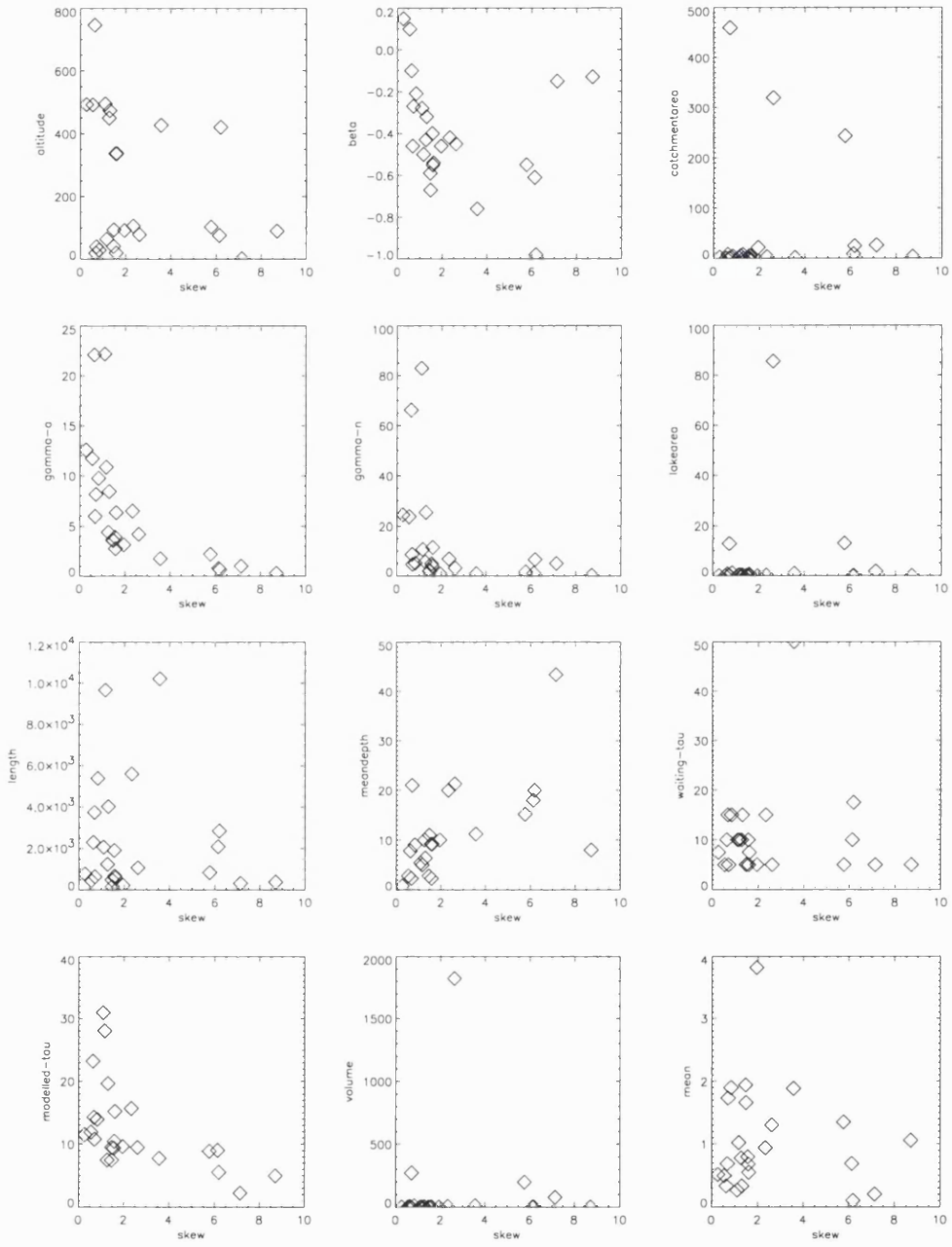

Figure 5.17: Figure illustrating the correlation between physical and statistical parameters

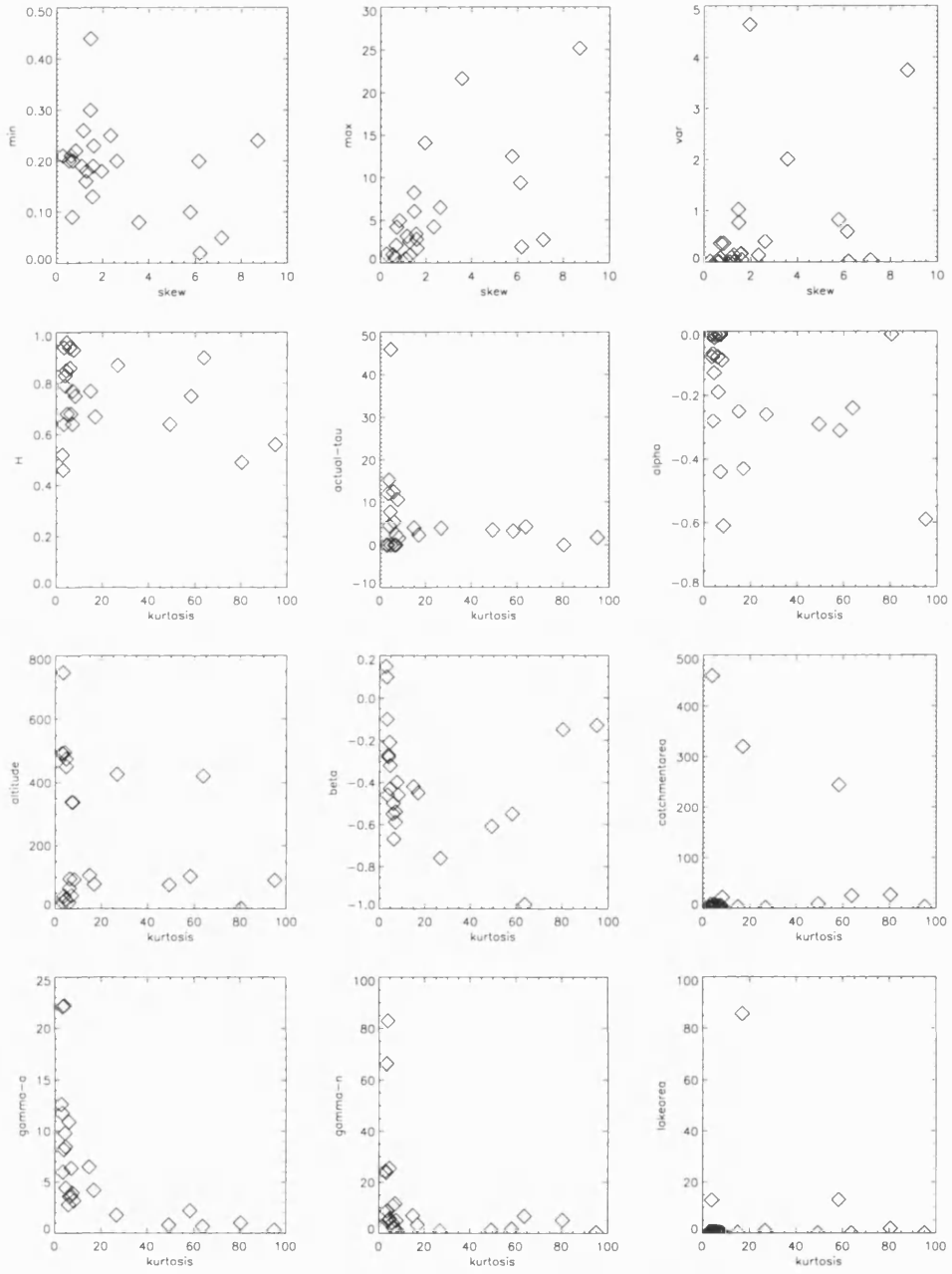

Figure 5.18: Figure illustrating the correlation between physical and statistical parameters

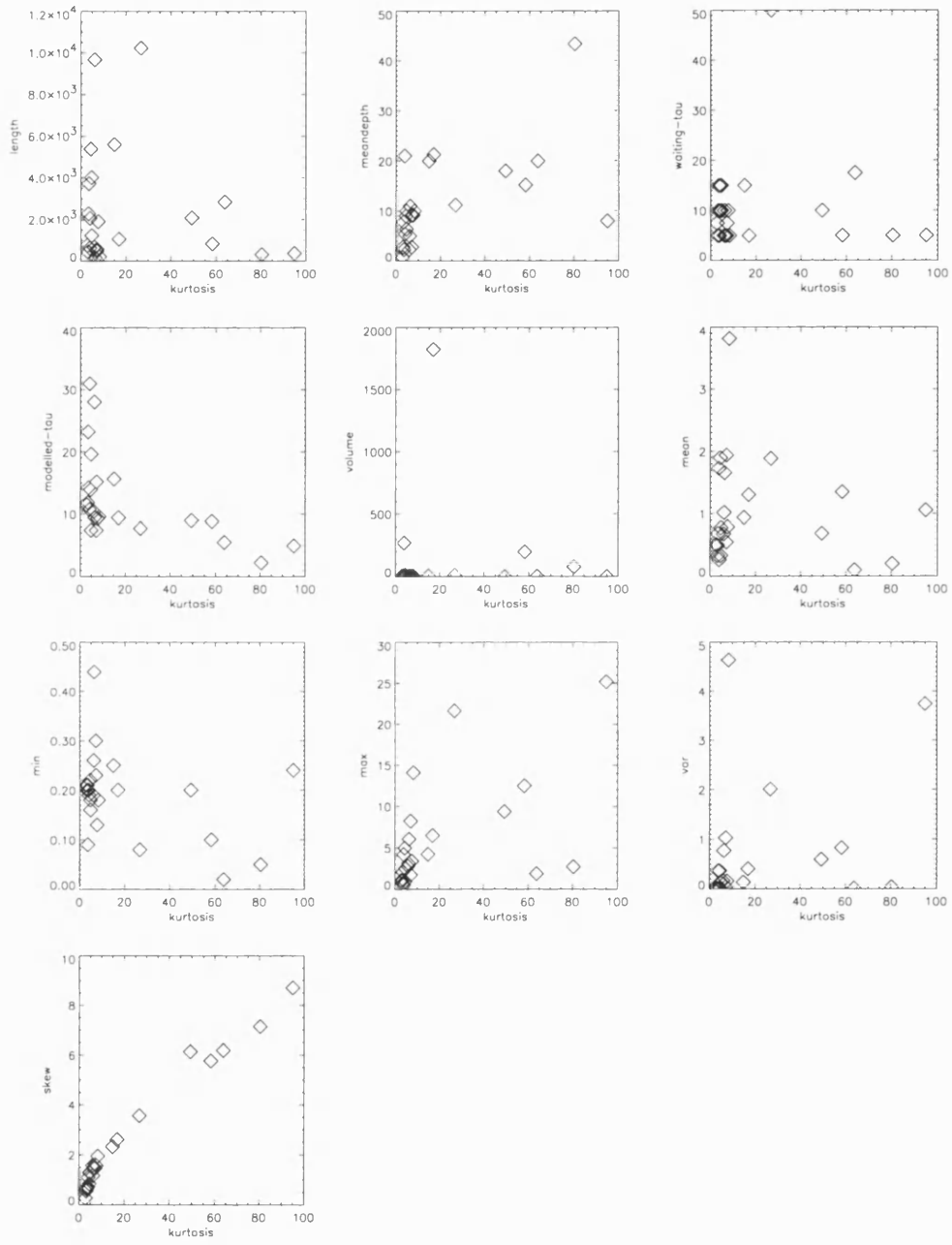

Figure 5.19: Figure illustrating the correlation between physical and statistical parameters

5.2 Discussion

Lake system dynamics are characterised by an e-folding time, τ, which is the time it takes for the system to reduce an imposed perturbation to a factor of $1/e$ of the perturbed value. The e-folding time can be estimated from both the actual data - autocorrelation function and waiting time analysis, and an AR(1) process (see Table 5.1.). Comparisons between the e-folding times of the AR(1) and the autocorrelation function reveal good fits (ca. $\leq$ 5 yrs) for; Belauersee, Deep, Elk, Hamelsee-a, Hamelsee-b, Heinalampi, Meerfelder-b, Paajarvi, Pyhajarvi, and Pyorelampi (see Table 5.1.). The waiting time results reveal the lakes are represented by two e-folding time "states" (see Figures 5.1. to 5.3. and Table 5.2.). State one (τ_1) represents the "main" part of the dynamics, and state two (τ_2) represents the "extreme" events. It should be emphasised that the terms "main" and "extreme" are descriptive, and do not indicate separate distributions (as already indicated by the probability distributions which indicate the extreme values are part of the distribution, and not outliers), as this would rule out the existence of self-affinity. Comparisons between the waiting time e-folding time for state one (τ_1) and the AR(1) e-folding time reveal good fits for; Belauersee, Buchsee, C2-8, Donard, Hamelsee-a, Hamelsee-b, Heinalampi, Karhunpaanlampi, Meerfelder-b, Paajarvi, Paijanne, Pyhajarvi, Pyorealampi, Ristijarvi, Schleinsee, Siethenersee, and Tervalampi, i.e., only Degersee, Elk, Gosciaz, and Illmensee are not comparable (see Table 5.2). Comparisons between the waiting time e-folding time for state one (τ_1) and the autocorrelation e-folding time reveal good fits for; Belauersee, Deep, Gosciaz, Hamelsee-a, Hamelsee-b, Heinalampi, Karhunpaanlampi, Meerfelder-a, Meerfelder-b, Paajarvi, Paijanne, and Pyorealampi, i.e., only Degersee, Elk, Pyhajarvi, Ristijarvi, and Schleinsee are not comparable (see Table 5.2.).

Correlation results indicate the e-folding times do not relate to any of the available physical parameters (though actual τ does relate to α (as expected), and H), indicating e-folding time dynamics in sedimentation are a product of a complex interplay between numerous variables (see Figures 5.4. to 5.19.). However, it should be noted that the autocorrelation function is only a measure of linear relationships,

and not a general measure of dependence, which we know is a feature of the system dynamics.

We suggest the e-folding time is nested within the overall scale invariant signature of lake sedimentation. Scale invariance indicates thin and thick varves are likely to be followed by thin and thick varves respectively. Switches exist between runs of thin and thick varves, with the length of these respective runs represented by the e-folding times, i.e., on decadal timescales.

Chapter 6

Spatial Signatures

6.1 Introduction and Results

In this chapter we present the results of correlation analysis. Figures 6.1. to 6.13. display the correlation between all lakes in this study for all overlaps. The x-axis is the running correlation, and the y-axis is the correlation coefficient. The results are notable for their lack of any significant correlation between any two lakes for any overlapping period (see Table 6.1.). The application of running correlation coefficients (with all coefficients < 0.5) confirms that lakes do not display any emergent correlation up to 30 yr timescales. Although the varve chronologies are considered robust enough for "shifting" with respect to each other, the averaging procedure was considered sufficient in order to isolate any spatial correlation features between the respective lakes.

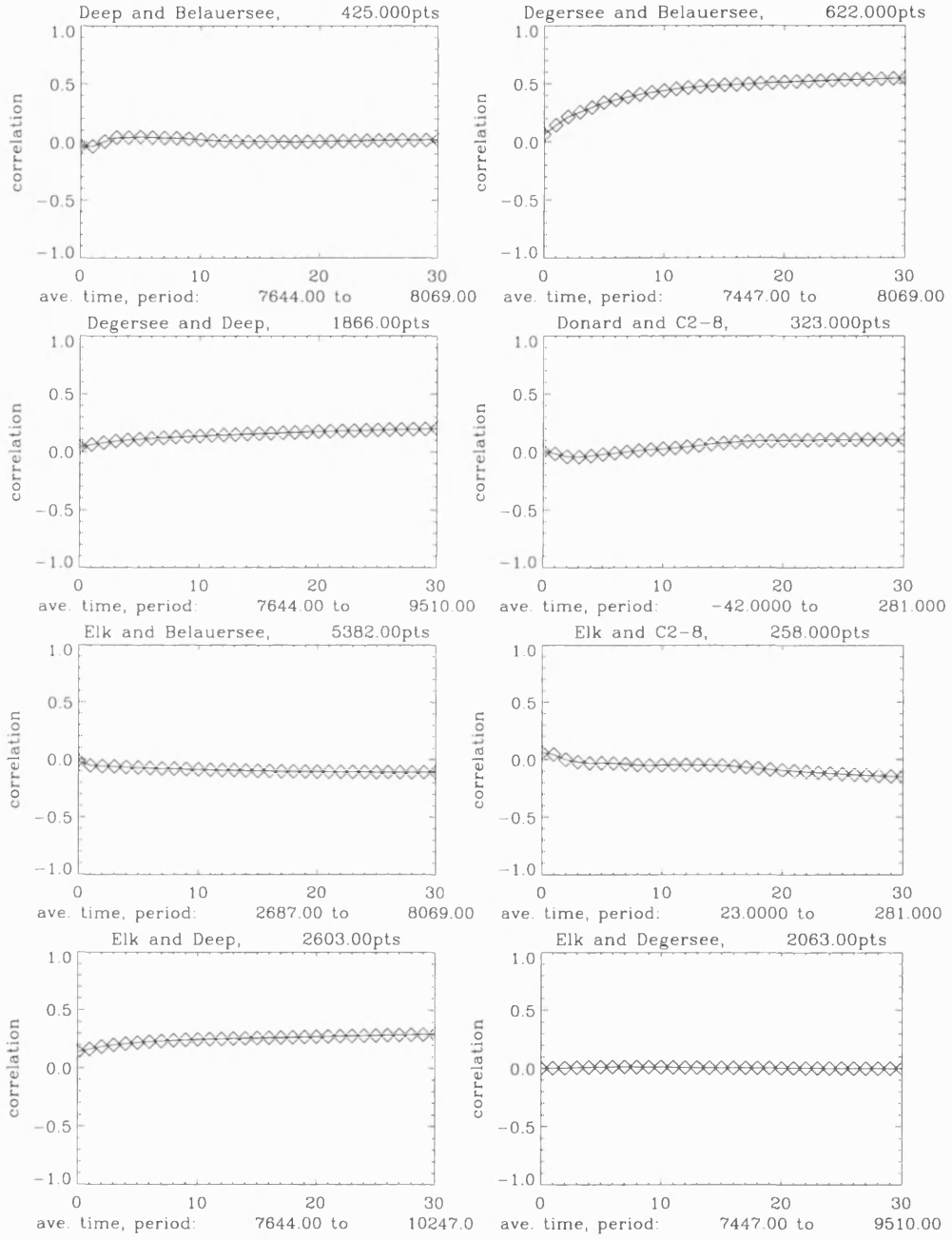

Figure 6.1: Figure illustrating the correlation between lakes.

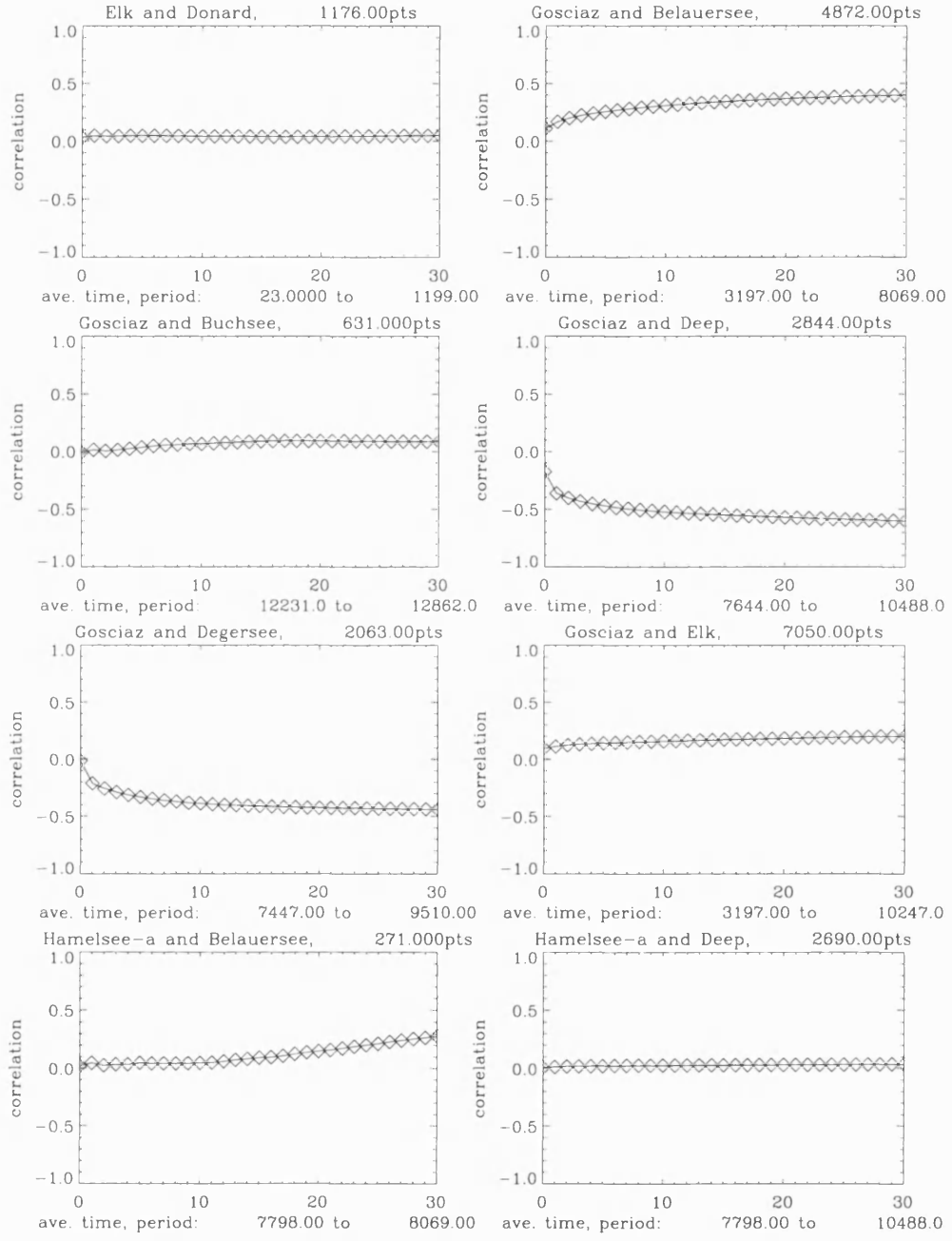

Figure 6.2: Figure illustrating the correlation between lakes.

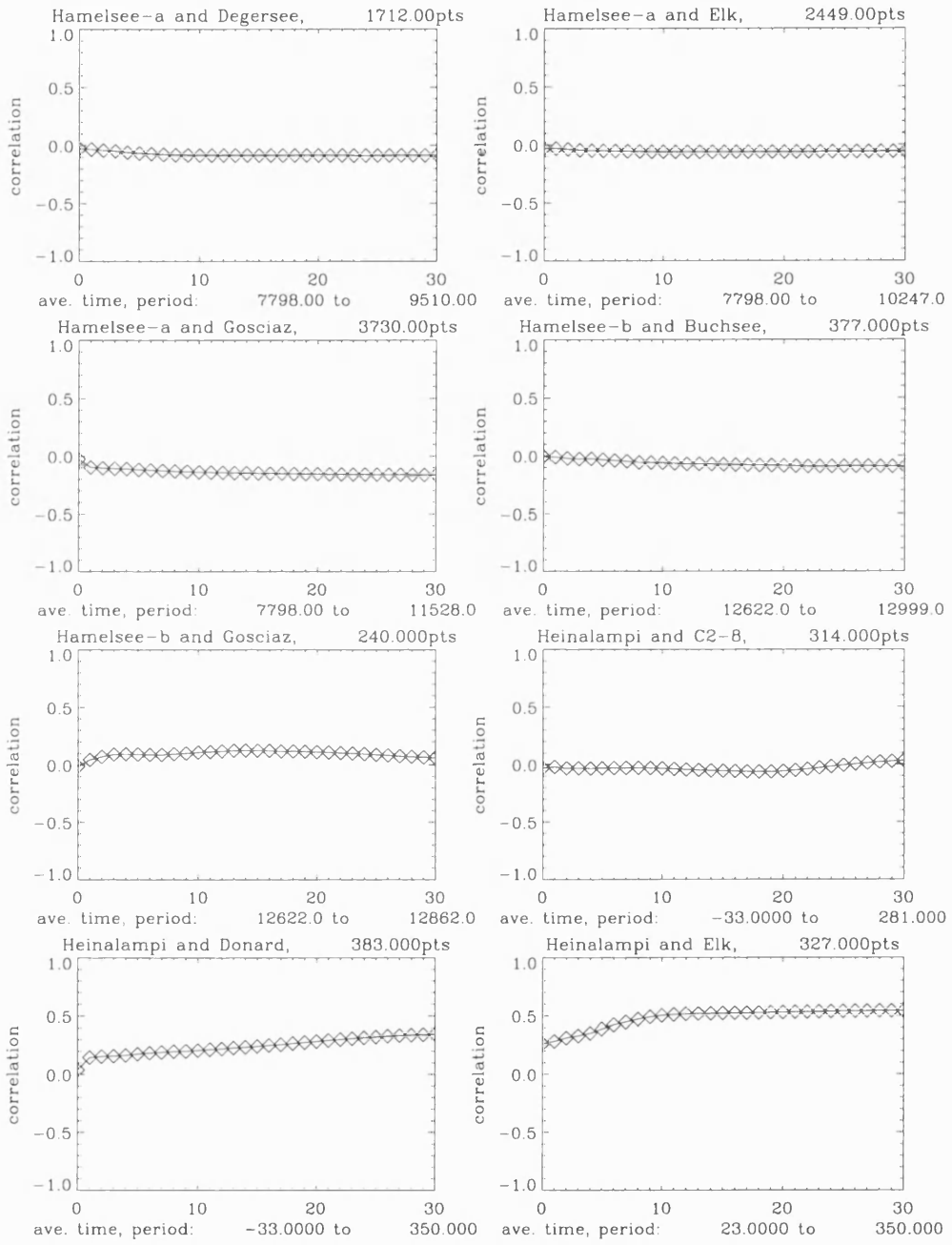

Figure 6.3: Figure illustrating the correlation between lakes.

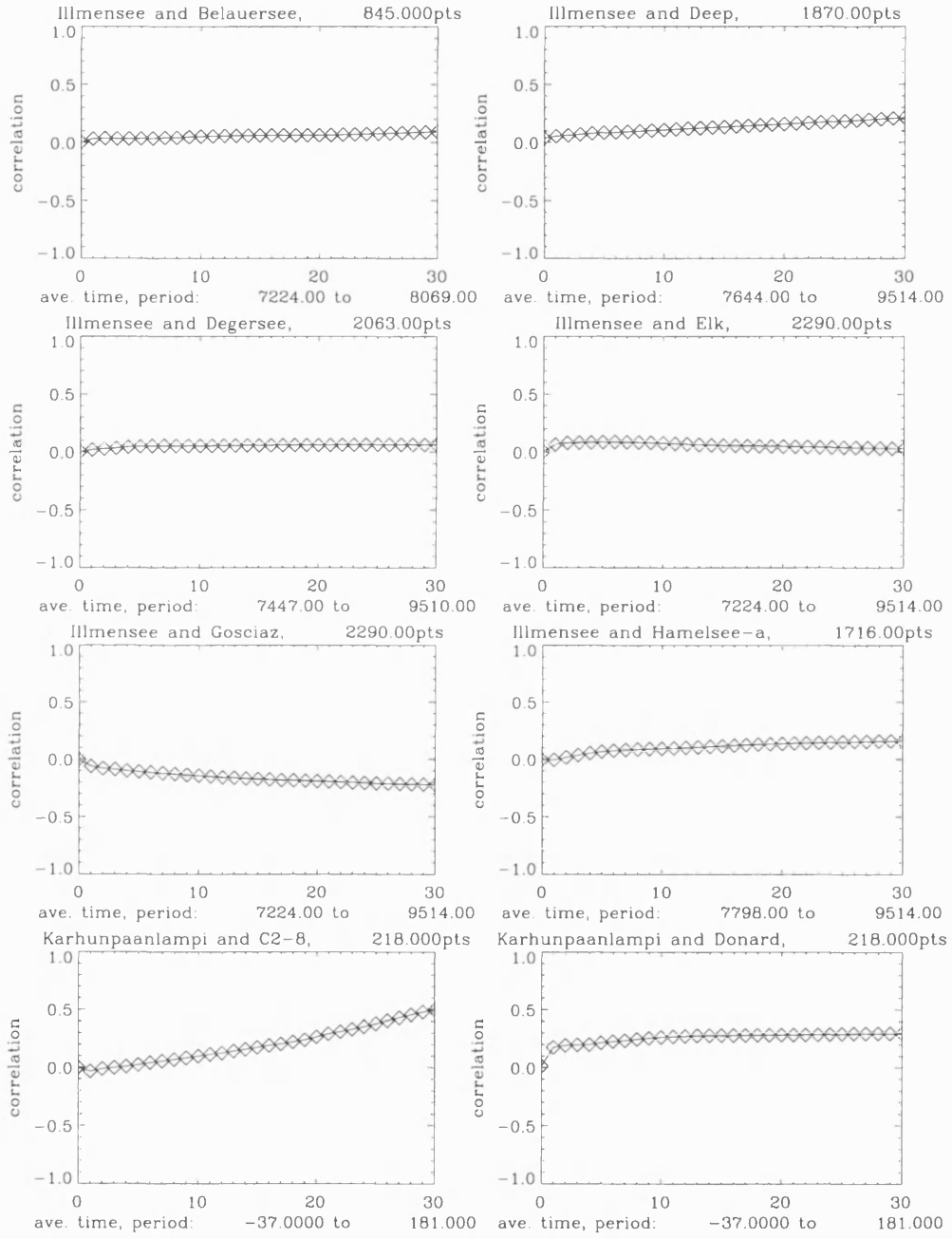

Figure 6.4: Figure illustrating the correlation between lakes.

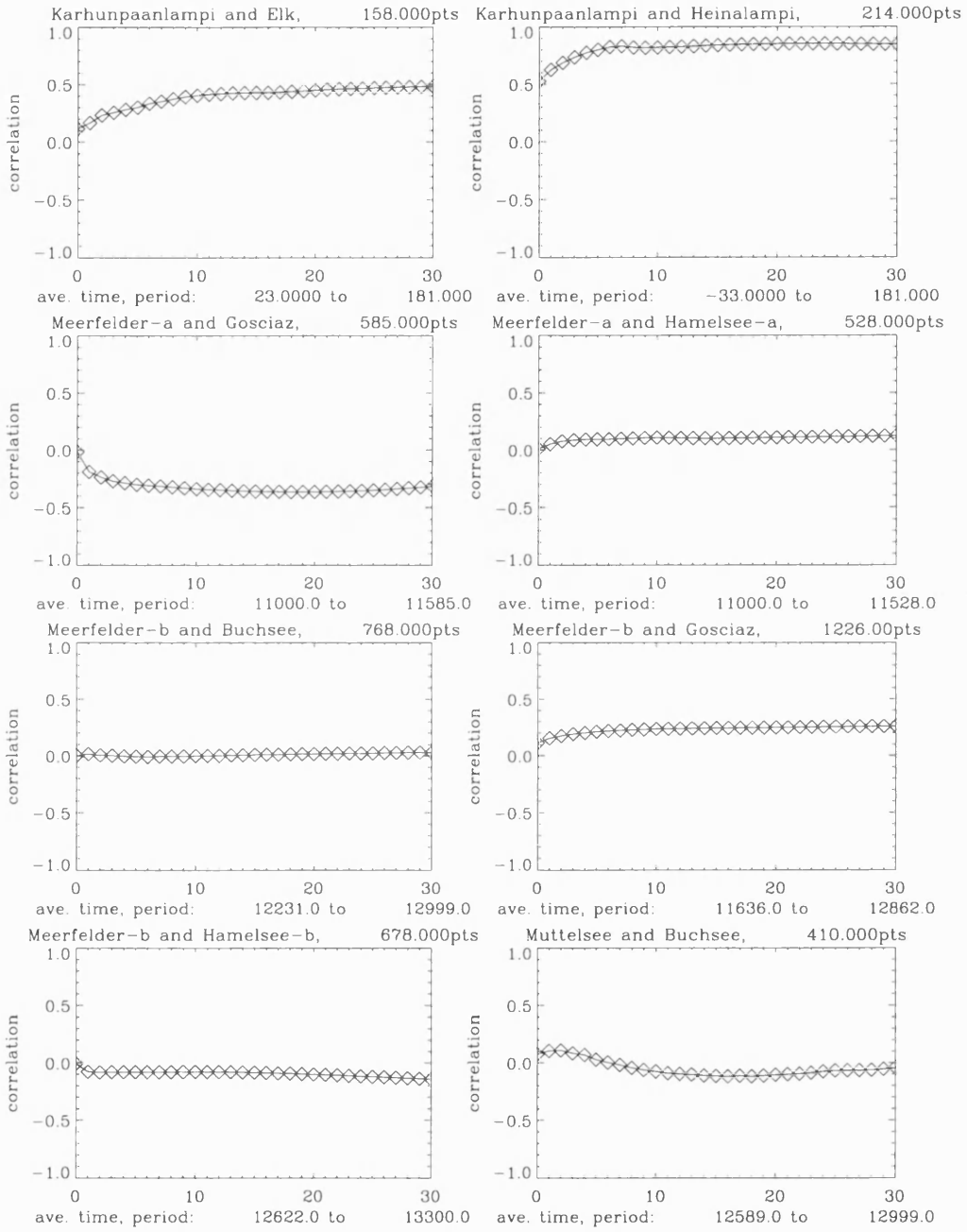

Figure 6.5: Figure illustrating the correlation between lakes.

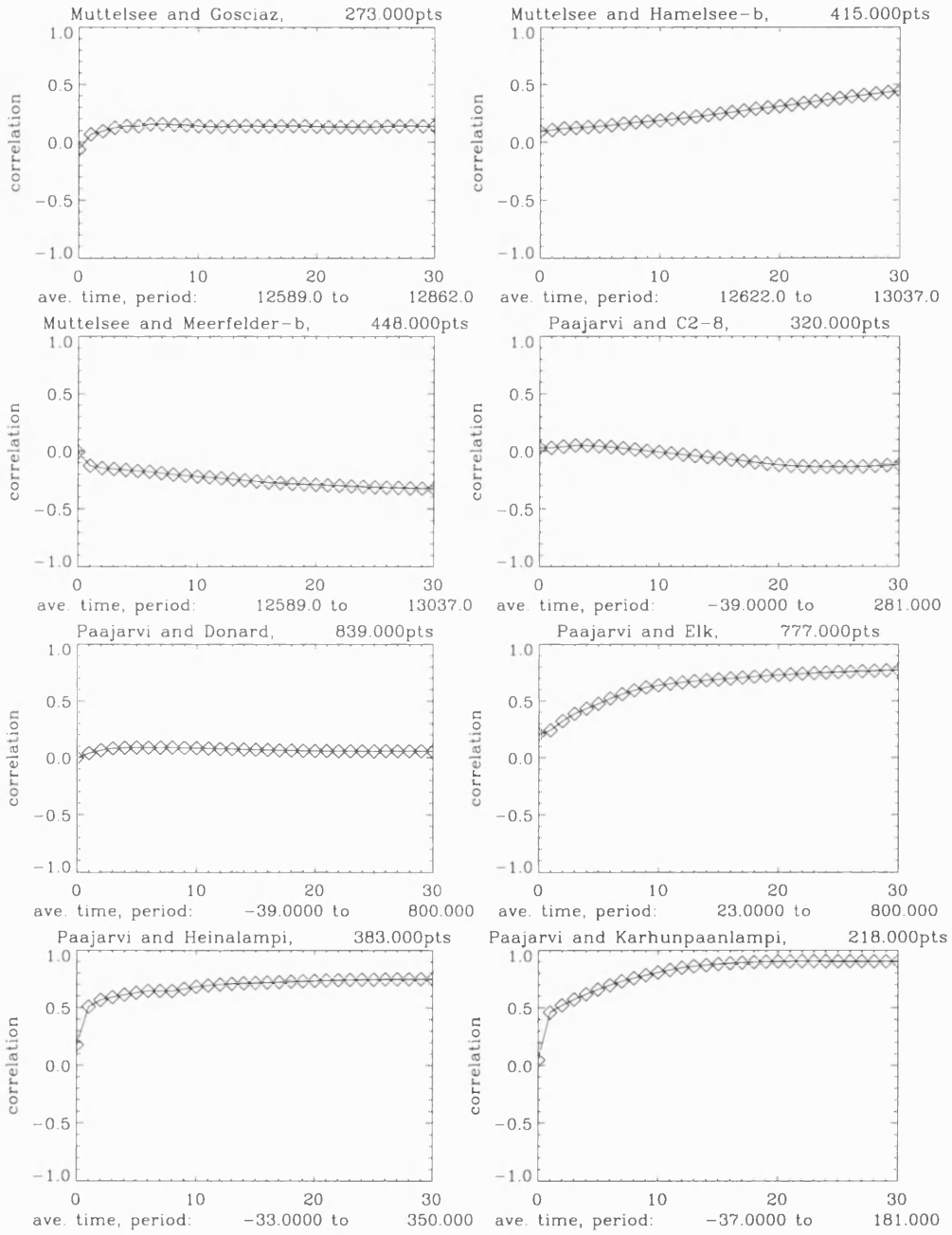

Figure 6.6: Figure illustrating the correlation between lakes.

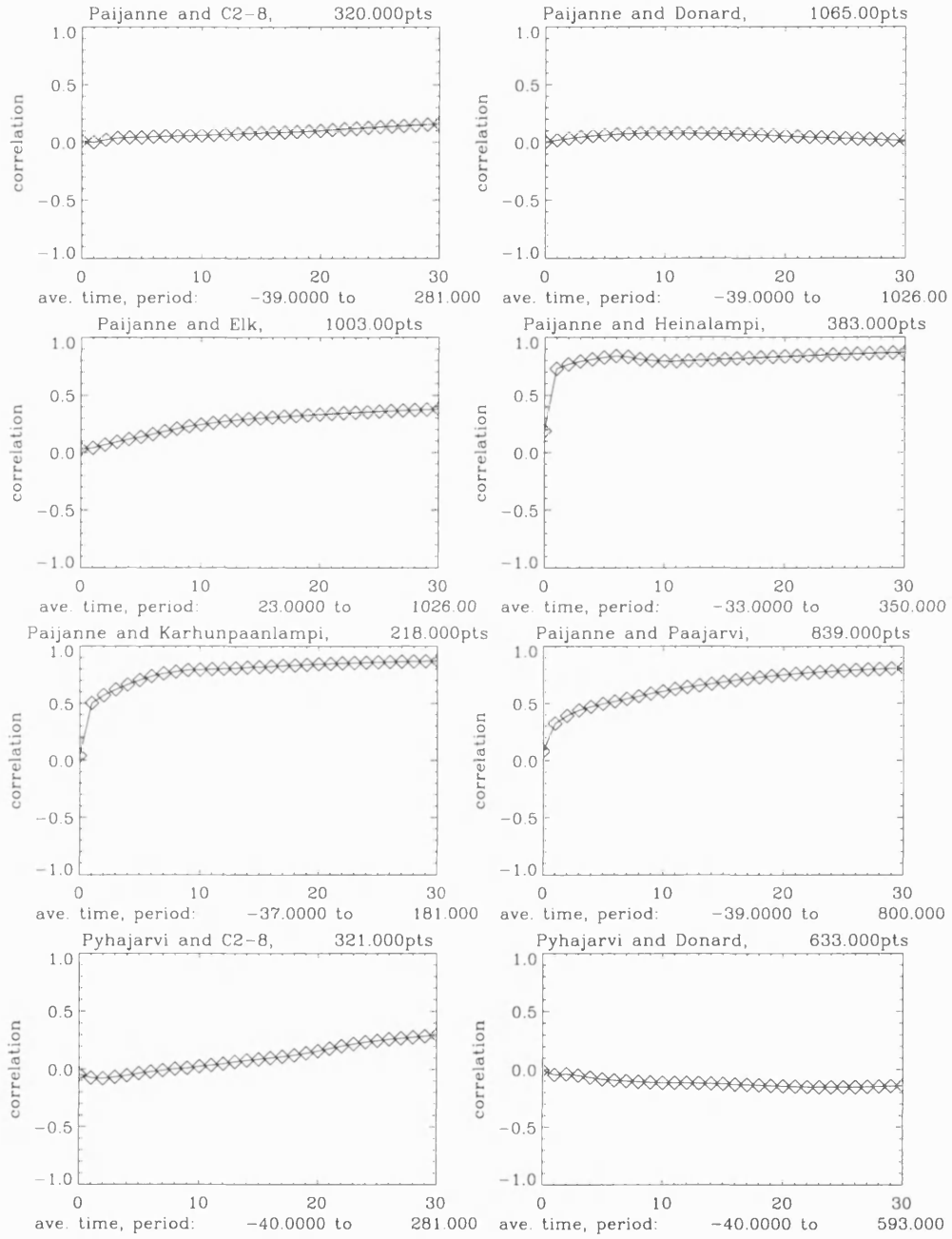

Figure 6.7: Figure illustrating the correlation between lakes.

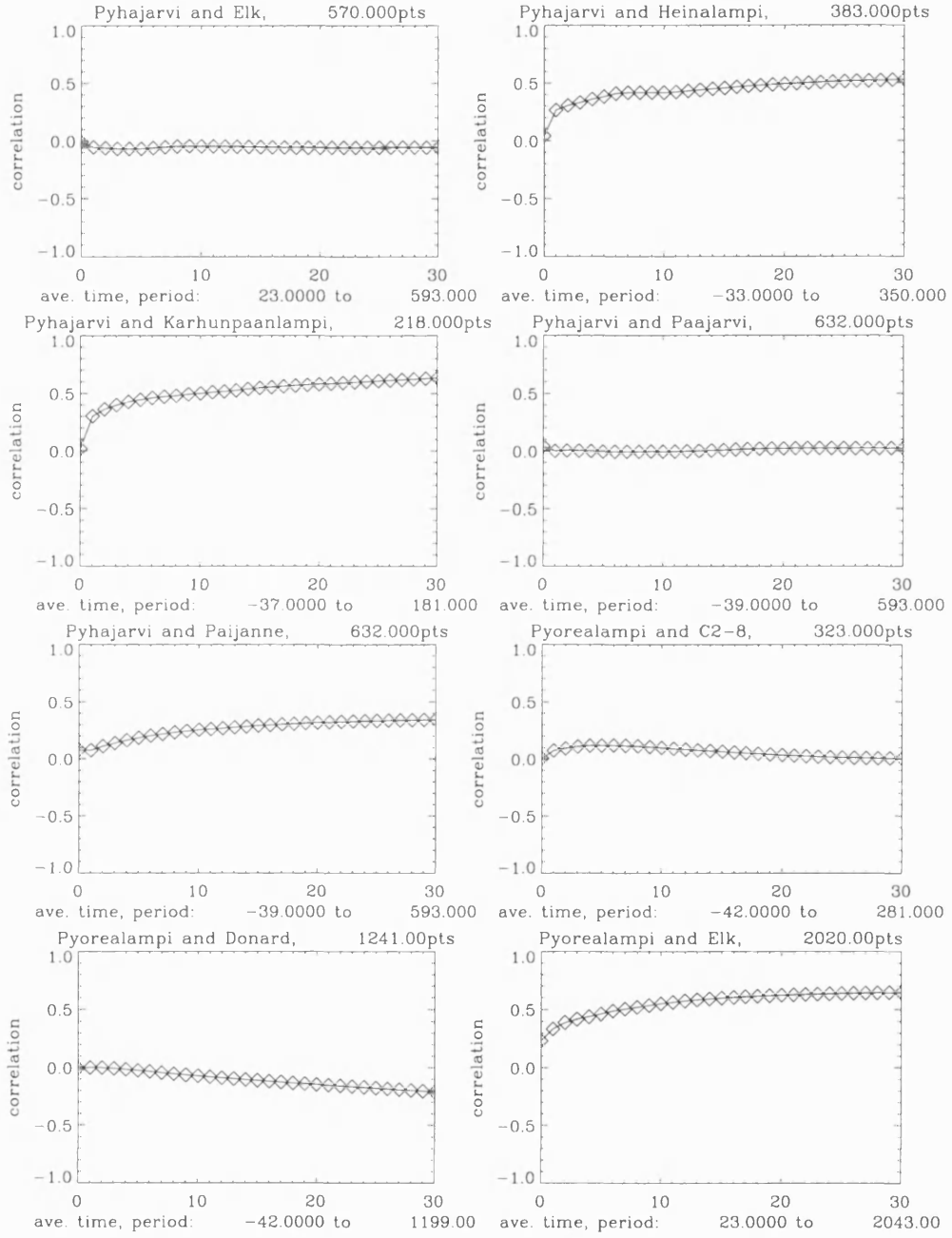

Figure 6.8: Figure illustrating the correlation between lakes.

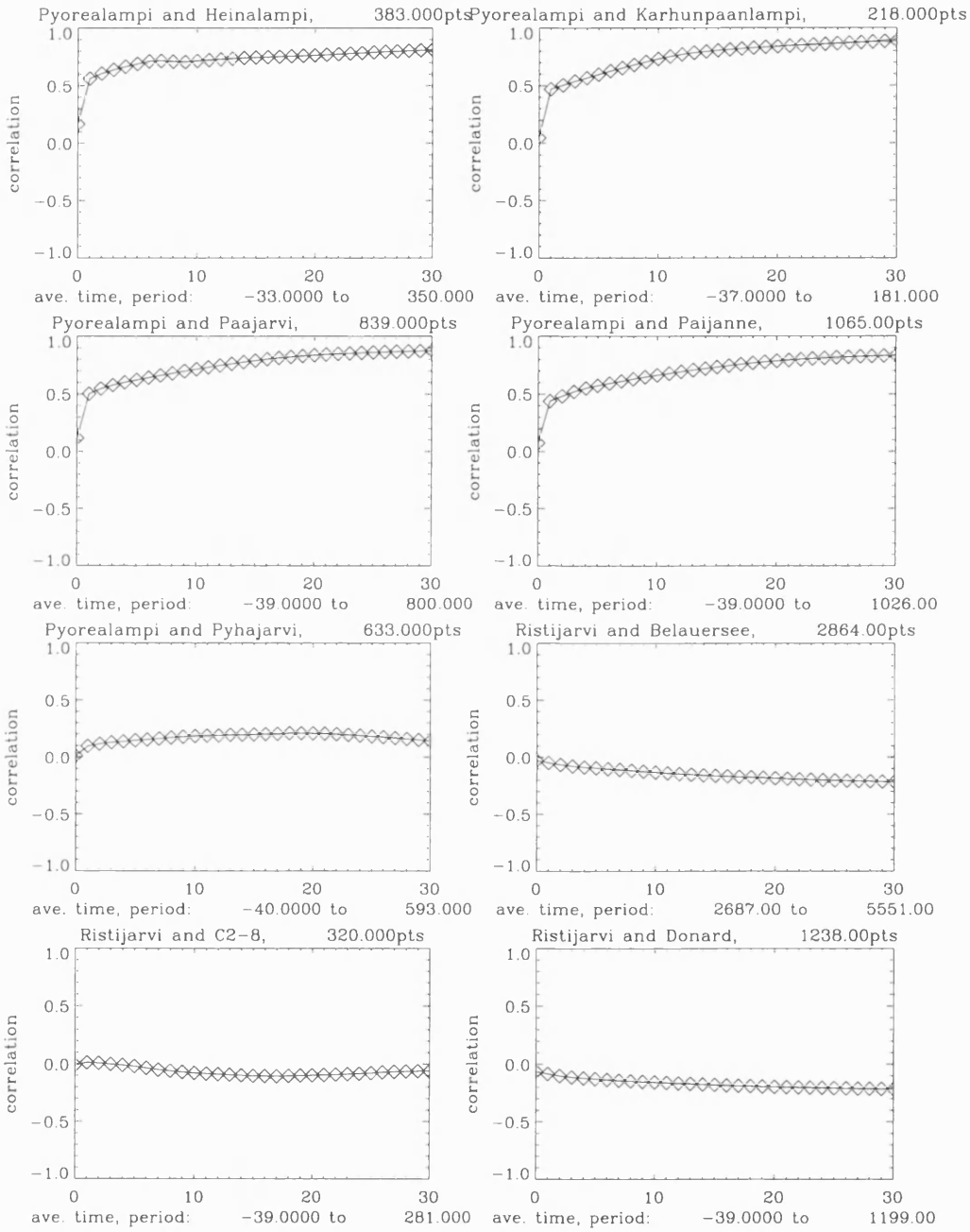

Figure 6.9: Figure illustrating the correlation between lakes.

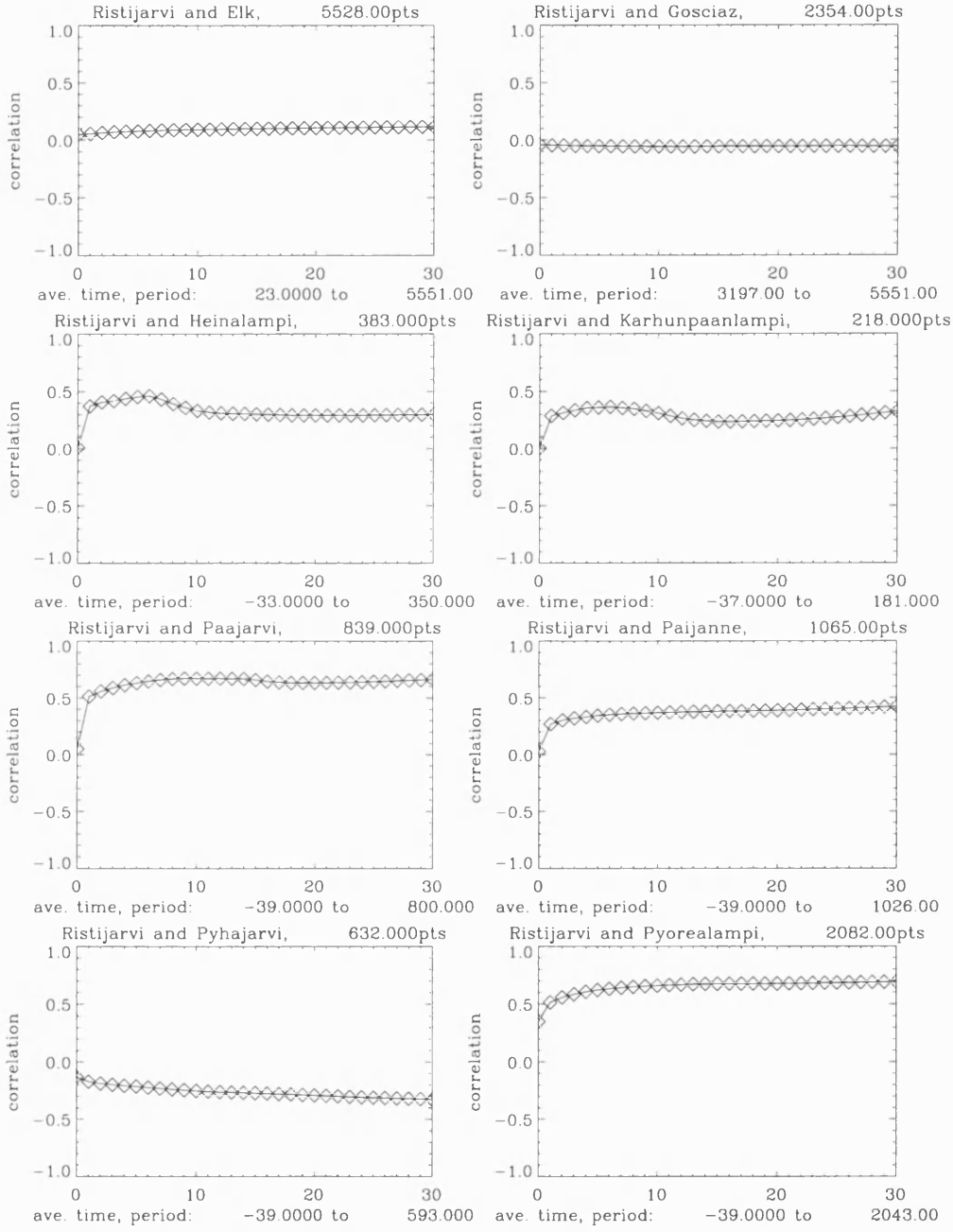

Figure 6.10: Figure illustrating the correlation between lakes.

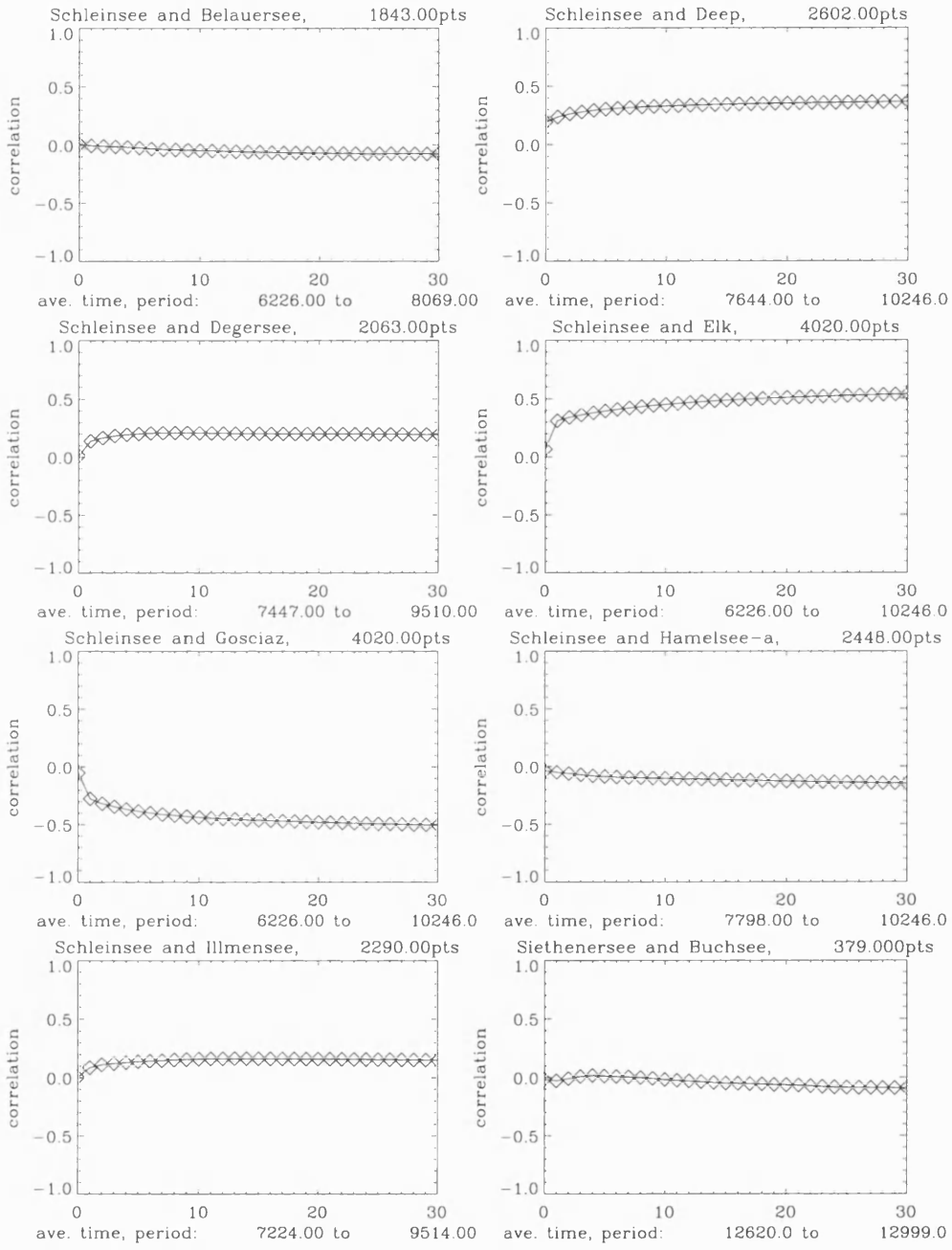

Figure 6.11: Figure illustrating the correlation between lakes.

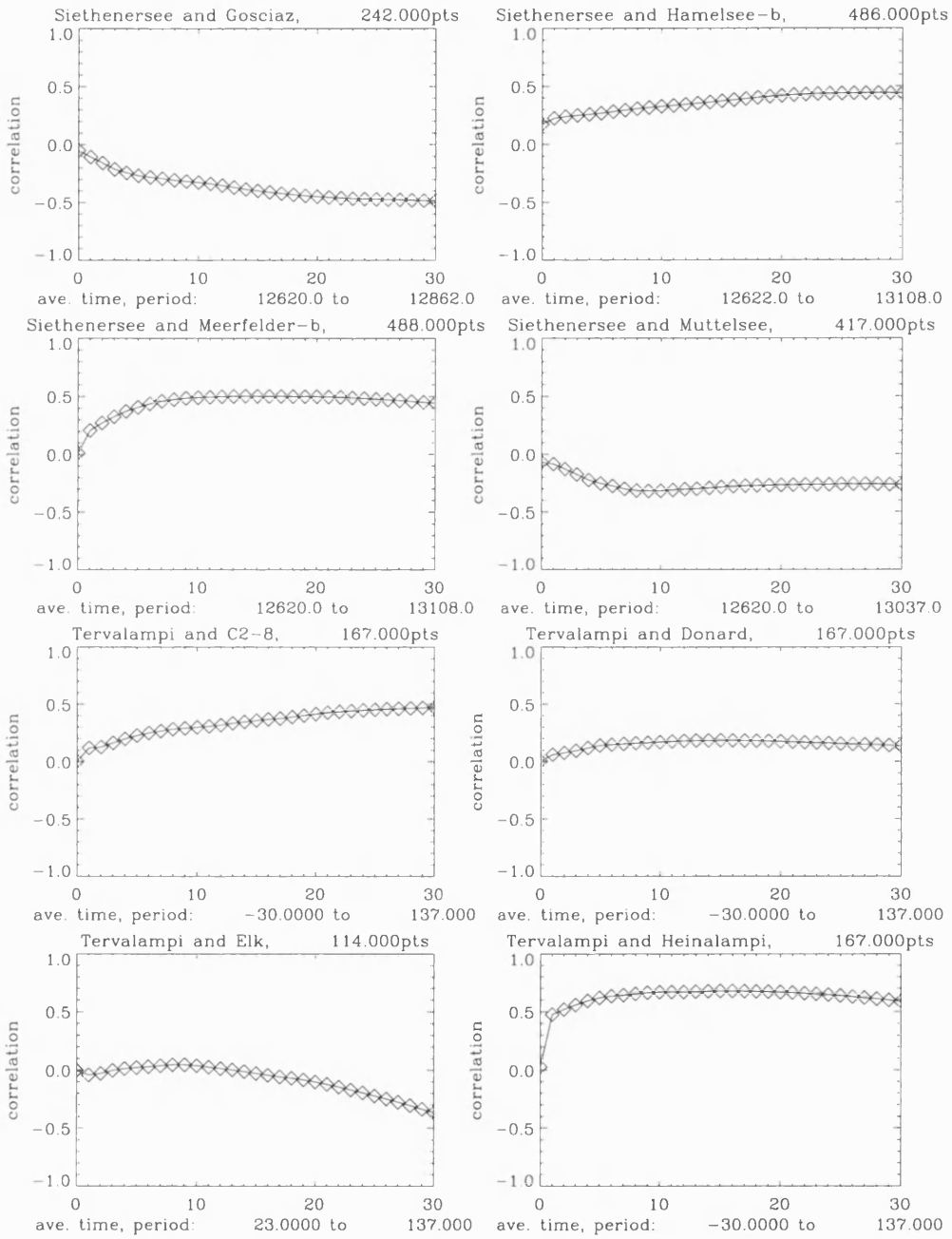

Figure 6.12: Figure illustrating the correlation between lakes.

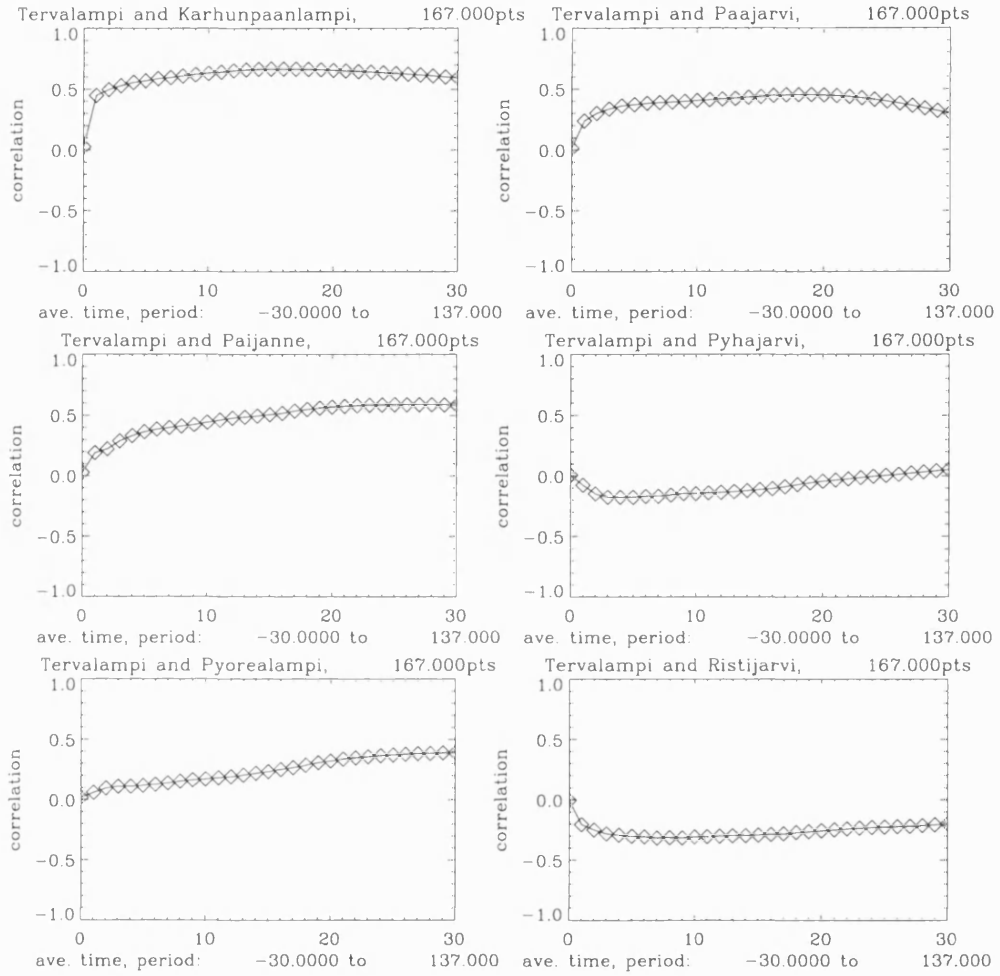

Figure 6.13: Figure illustrating the correlation between lakes.

Lake	Corr. Coeff. Zero Ave.	Interval cal yrs BP	N
Deep and Belauersee	-0.0350128	7644-8069	425
Degersee and Belauersee	0.0640525	7447-8069	622
Degersee and Deep	0.0402088	7644-9510	1866
Donard and C2-8	0.00369668	-42-281	323
Elk and Belauersee	-0.0130222	2687-8069	5382
Elk and C2-8	0.0606943	23-281	258
Elk and Deep	0.139101	7644-10247	2603
Elk and Degersee	-2.06540e-05	7447-9510	2063
Elk and Donard	0.0320639	23-1199	1176
Gosciaz and Belauersee	0.111223	3197-8069	4872
Gosciaz and Buchsee	-0.00831324	12231-12862	631
Gosciaz and Deep	-0.175283	7644-10488	2844
Gosciaz and Degersee	-0.0145055	7447-9510	2063
Gosciaz and Elk	0.0952644	3197-10247	7050
Hamelsee-a and Belauersee	0.0196612	7798-8069	271
Hamelsee-a and Deep	0.00656324	7798-10488	2690
Hamelsee-a and Degersee	-0.0261590	7798-9510	1712
Hamelsee-a and Elk	-0.0290768	7798-10247	2449
Hamelsee-a and Gosciaz	-0.0247818	7798-11528	3730
Hamelsee-b and Buchsee	-0.00514387	12622-12999	377
Hamelsee-b and Gosciaz	-0.0131458	12622-12862	240
Heinalampi and C2-8	-0.0301437	-33-281	314
Heinalampi and Donard	0.0382014	-33-350	383
Heinalampi and Elk	0.263113	23-350	327
Illmensee and Belauersee	0.00208083	7224-8069	845
Illmensee and Deep	0.0356838	7644-9514	1870
Illmensee and Degersee	0.00255218	7447-9510	2063
Illmensee and Elk	0.00282298	7224-9514	2290
Illmensee and Gosciaz	-0.00368775	7224-9514	2290
Illmensee and Hamelsee-a	-0.00356159	7798-9514	1716
Karhunpaanlampi and C2-8	-0.00126786	-37-181	218
Karhunpaanlampi and Donard	0.0120157	-37-181	218
Karhunpaanlampi and Elk	0.116284	23-181	158
Karhunpaanlampi and Heinalampi	0.526103	-33-181	214
Meerfelder-a and Gosciaz	-0.0136839	11000-11585	585
Meerfelder-a and Hamelsee-a	0.0101682	11000-11528	528
Meerfelder-b and Buchsee	-0.000693178	12231-12999	768
Meerfelder-b and Gosciaz	0.112002	11636-12862	1226
Meerfelder-b and Hamelsee-b	-0.00600459	12622-13300	678
Muttelsee and Buchsee	0.0750926	12589-12999	410
Muttelsee and Gosciaz	-0.0620800	12589-12862	273

Muttelsee and Hamelsee-b	0.0923195	12622-13037	415
Muttelsee and Meerfelder-b	-0.00519519	12589-13037	448
Paajarvi and C2-8	0.0296930	-39-281	320
Paajarvi and Donard	-0.00358361	-39-800	839
Paajarvi and Elk	0.204646	23-800	777
Paajarvi and Heinalampi	0.176403	-33-350	383
Paajarvi and Karhunpaanlampi	0.0467568	-37-181	218
Paijanne and C2-8	0.0133596	-39-281	320
Paijanne and Donard	0.000271392	-39-1026	1065
Paijanne and Elk	0.0325224	23-1026	1003
Paijanne and Heinalampi	0.187034	-33-350	383
Paijanne and Karhunpaanlampi	0.0391641	-37-181	218
Paijanne and Paajarvi	0.0814931	-39-800	839
Pyhajarvi and C2-8	-0.0432797	-40-281	321
Pyhajarvi and Donard	-0.00551690	-40-593	633
Pyhajarvi and Elk	-0.0104579	23-593	570
Pyhajarvi and Heinalampi	0.0433283	-33-350	383
Pyhajarvi and Karhunpaanlampi	0.0180312	-37-181	218
Pyhajarvi and Paajarvi	0.0400660	-39-593	632
Pyhajarvi and Paijanne	0.0780151	-39-593	632
Pyorealampi and C2-8	0.00496621	-42-281	323
Pyorealampi and Donard	-0.00624115	-42-1199	1241
Pyorealampi and Elk	0.233306	23-2043	2020
Pyorealampi and Heinalampi	0.166636	-33-350	383
Pyorealampi and Karhunpaanlampi	0.0466594	-37-181	218
Pyorealampi and Paajarvi	0.116179	-39-800	839
Pyorealampi and Paijanne	0.0749449	-39-1026	1065
Pyorealampi and Pyhajarvi	0.00972062	-40-593	633
Ristijarvi and Belauersee	-0.0297950	2687-5551	2864
Ristijarvi and C2-8	-0.0102971	-39-281	320
Ristijarvi and Donard	-0.0648289	-39-1199	1238
Ristijarvi and Elk	0.0472842	23-383	5528
Ristijarvi and Gosciaz	-0.0422843	3197-5551	2354
Ristijarvi and Heinalampi	0.00970136	-33-350	383
Ristijarvi and Karhunpaanlampi	0.00177404	-37-181	218
Ristijarvi and Paajarvi	0.0492664	-39-800	839
Ristijarvi and Paijanne	0.0277462	-39-1026	1065
Ristijarvi and Pyhajarvi	-0.132071	-39-593	632
Ristijarvi and Pyorealampi	0.350908	-39-2043	2082
Schleinsee and Belauersee	0.00766579	6226-8069	1843
Schleinsee and Deep	0.193926	7644-10246	2602
Schleinsee and Degersee	0.0108028	7447-9510	2063
Schleinsee and Elk	0.0664127	6226-10246	4020
Schleinsee and Gosciaz	-0.0519151	6226-10246	4020

Schleinsee and Hamelsee-a	-0.0368307	7798-10246	2448
Schleinsee and Illmensee	0.00417590	7224-9514	2290
Siethenersee and Buchsee	-0.0159285	12620-12999	379
Siethenersee and Gosciaz	-0.0509975	12620-12862	242
Siethenersee and Hamelsee-b	0.174996	12622-13108	486
Siethenersee and Meerfelder-b	0.0115702	12620-13108	488
Siethenersee and Muttelsee	-0.0676871	12620-13037	417
Tervalampi and C2-8	0.00382035	-30-137	167
Tervalampi and Donard	0.00179619	-30-137	167
Tervalampi and Elk	-0.00197707	23-137	114
Tervalampi and Heinalampi	0.0268803	-30-137	167
Tervalampi and Karhunpaanlampi	0.0266018	-30-137	167
Tervalampi and Paajarvi	0.0130138	-30-137	167
Tervalampi and Paijanne	0.0275445	-30-137	167
Tervalampi and Pyhajarvi	0.00659414	-30-137	167
Tervalampi and Pyorealampi	0.0170036	-30-137	167
Tervalampi and Ristijarvi	-0.00572710	-30-137	167

Table 6.1: Summary of spatial correlation coefficients

6.2 Discussion

Lake to lake spatial correlations relates to a dynamic interplay between lake and atmospheric spatiotemporal and lake specific processes. As lakes are spatially limited systems, any correlation between them is dependent on the action of atmospheric processes. Within the atmosphere spatial correlation emerges as scales become larger and longer. This relates to the smoothing action of heat and moisture reservoirs in atmospheric circulation (see Figure 6.14.). As such, the observed lack of correlation indicates the air masses surrounding the lakes do not extend to any other lake, and as such are neither large enough to; smooth out local scale dynamics, nor teleconnect such dynamics to other lakes. In addition, the lack of correlation indicates the temporal smoothing is insufficient to smooth out local scale dynamics.

It also possible that the lack of correlation relates to "internal" lake processes. Lakes operate on timescales slower than the atmosphere, where inertia exists between their respective thermal regimes (see fig 4.16) [201] (e.g., during a 24 hour period, surface waters will be characterised by warm and cold temperatures, while deeper waters will not display the same range, if at all). As such, the thermal structure of lakes tends to react less to fast short term fluctuations than to slow long term fluctuations, i.e., acting as a low pass filter [218]. This implies that lakes are not physically capable spatial correlation on faster timescales, but are on longer timescales.

Looking in more detail at the lake sedimentation processes, the waiting time analysis indicates lake system dynamics can be broadly partitioned into two broad categories; the "main" component (state one, τ_1) of system dynamics operates on decadal timescales, while the "extreme" component (state two, τ_2) of system dynamics operates on longer timescales up to and beyond centennial scales. This indicates that as the timescale of the extreme events are individual to each lake, and if they are part of a regime shift, then it is unlikely lakes will be correlated, and correlation may be expected to emerge once extreme dynamics have been smoothed, i.e., up to and beyond centennial scales.

This individualism can also be extended to a lesser extent to the "main" system

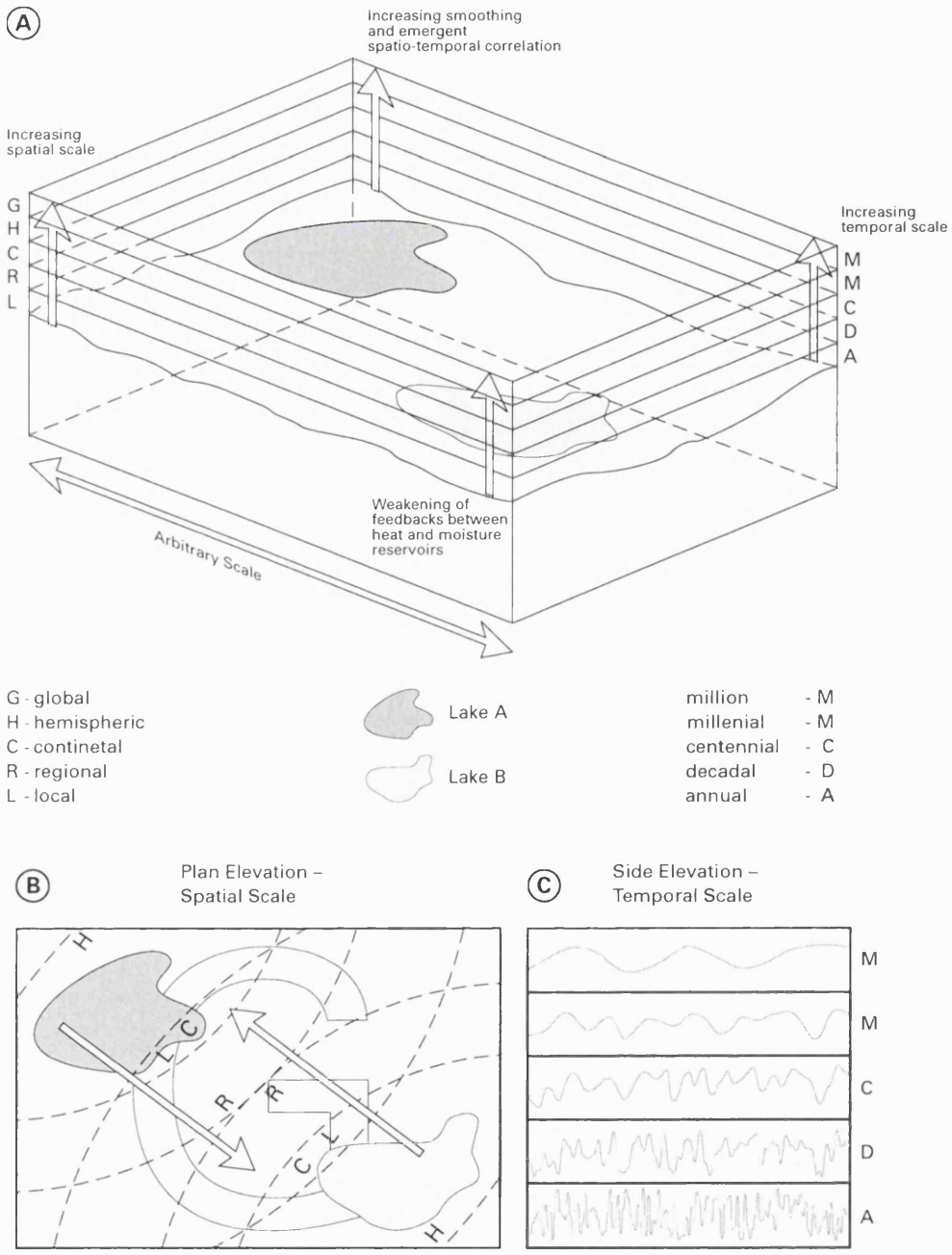

Figure 6.14: Schematic diagram illustrating the concepts of spatiotemporal scaling. A., B. and C. display the importance of linked spatiotemporal processes in the emergence of correlation as scales increase.

dynamics, as the correlation between statistical and physical parameters revealed no significant relations (see Figures 5.4. to 5.19.), even without taking into consid-

eration other correlation limiting site specific factors (e.g., local moisture balance, local hydrological balance, bedrock lithology, vegetation, catchment geomorphology, and open or closed status, all of which interact nonlinearly).

Furthermore, the poor inter-site correlation may relate to the formation of allochthonous and autochthonous particles. If we look at the origin of the sediments comprising the varves, with the exception of lakes C2-8 and Donard, which are purely allochthonous, the composition is mixed allochthonous and autochthonous. As such, at each site we have site specific dynamics in terms of allochthonous loading, where can assume these dynamics introduce greater site specific variation into the varve structure than the autochthonous particles.

Finally, in terms of the type of proxy used in this study, that of varve thickness, we would anticipate distinct variations in each lake (in contrast to more primary recorders of climate dynamics such as microfossils and various isotopes), as a multitude of complex processes affect the range of particles forming a varve.

By invoking the AR(1) process, a null hypothesis can be suggested for expected timescales of emergent correlation (see Figure 6.15.). The e-folding time for an AR(1) process, depends on $\lambda - 1$, the feedback term, where $\tau = 1/\lambda$, and k, the lake thermal regime, essentially stronger feedback is associated with a shorter e-folding time, and weaker feedback with a longer e-folding time. The magnitude of λ is governed by radiative processes in the atmosphere [219] (see Figure 6.16.). Effectively, we would expect the time it takes for smoothing to create emergent spatial correlation to be the same as that for a system, based on an AR(1) process to reach $1/e$ ($= 0.37$) of the perturbed value. That the e-folding times in this study are on decadal timescales and the emergent correlation is not, generally relates to the partial application of the AR(1) (and the role of (self-organised) critical phenomena and multiscaling) to describe system dynamics, and more specifically, to the nonlinear dependence of the e-folding time on the local feedback term ($-\lambda y_n$).

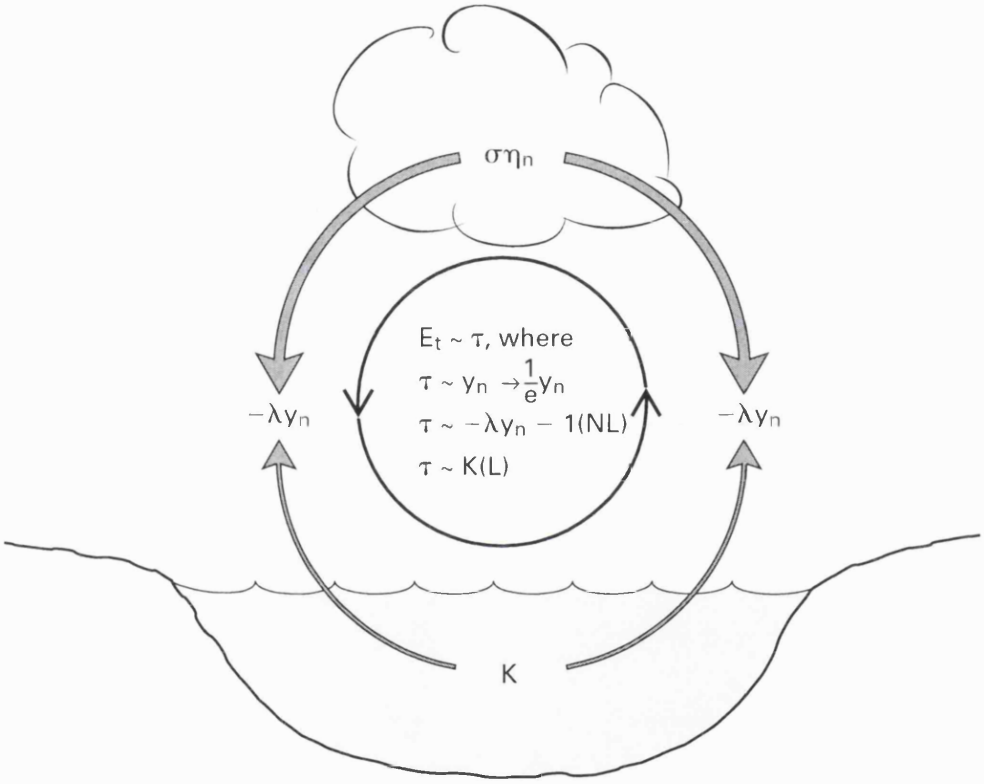

Figure 6.15: Schematic diagram illustrating the concepts of spatial correlation with respect to an AR(1) model. If lake system dynamics are represented by an AR(1) process, then spatial correlation should emerge when $\sigma\eta_n$ forces y_n to a state $1/ey_n$. Nonlinear - NL, and Linear - L.

Chapter 7

Conclusions

7.1 Summary

In this study we have applied both reductionist and holistic approaches to describe the dynamics of lake systems, in particular sedimentation and varve formation. Below we present the main conclusions of this study.

- Lake sedimentation can be considered in terms of the quantity and stratigraphic position of a sedimentary deposit. The statistical signature of the quantity of a sedimentary deposit is non-scaling. Probability density functions, and cumulative distribution functions indicate this is represented by gamma and log-normal processes, i.e., the addition and multiplication of random variables. Phase portraits, exceedence probability analysis (which indicates some parts of the distribution are non-scaling), and power spectra, autocorrelation functions, fluctuation analysis, indicate the stratigraphic position of a sedimentary deposit is represented by a scaling signature. Crossovers occur in the power spectra on ca. 100 yrs timescales for some lakes, indicating the possible presence of changes in dominant timescales of large scale climatic processes. This scaling signature occurs over all the resolvable orders of magnitude. This indicates the dynamics of thinner varves are connected to the dynamics of thicker varves by a power law distribution. As such, the occurrence of thinner varves is likely to be followed by thinner varves, and similarly for thicker varves.

- Scaling exponents are in the range $H = 0.6$ to 0.9, and compare well with other natural system dynamics, but show limited compatibility with each other. This may relate to; (i) statistical - fitting best fit lines to estimate scaling exponents, sensitivity of method or length of the time series, or (ii) physical - indicator of divergence from fGn, i.e., not just a random walk, but also critical phenomena and multiscaling signatures. This is corroborated by the scaling exponents themselves which differ significantly from archetypal scaling (and random walk) null hypothesis - AR(1) process. Implicating self-organising processes in lake processes demands a definition of internal and external processes, but in lake systems these can only be considered as relative boundaries. A physical model is proposed based on all three underlying mechanisms of power law, gamma, and log-normal distributions. Effectively, lakes are threshold systems with random forcing on different timescales.

- The e-folding time for the actual autocorrelation function and the model AR(1) are similar for several lakes. In addition, the e-folding time of the waiting time distribution is represented by two states, one for "main" dynamics, and another for "extreme" dynamics. The e-folding time for the main state is comparable in some cases with the e-folding time of the autocorrelation and AR(1), suggesting it is these dynamics that are best represented by a random walk process on decadal timescales. The lakes displaying notable differences essentially confirm the importance of considering the other underling mechanisms of scaling, i.e., critical phenomena and multiscaling. The e-folding time is nested within the overall scale invariant mechanisms, whereby switches between "runs" of thin and thin or thick and thick varves occur on decadal timescales, as indicated by the e-folding time.

- Multiple correlation between physical (e.g., volume, area, depth, etc) and physical (variance, e-folding times, scaling exponents, etc) parameters reveals few significant relations. Interestingly, these relations involve only the statistical values and none of the physical parameters, suggesting that at least for single combinations there is no direct link between a physical and statistical param-

eter. It is unlikely these relations provide further insight into lake system dynamics, except to confirm the individualistic nature of lake systems.

- Spatial correlation between lakes is very weak, in unshifted direct and averaged correlations between respective lakes. This relates to the limited spatial and temporal smoothing by atmospheric processes. In addition, lakes operate on timescales slower than the atmosphere, as such, the thermal regime of lakes respond more to slow long processes rather than faster short term processes. Furthermore, as noted above, the timescales of extreme system dynamics are different in every lake (as opposed to the main dynamics, which occur on similar decadal timescales, as such correlation is unlikely when such events occur. Variation in the actual components, i.e., allochthonous and/or autochthonous, of such extreme layers is also likely to dilute any correlation. As such, emergent correlation can be expected when these processes have been smoothed out, which is indicated as up to and beyond centennial scales (and beyond the resolution of this study, due to the length of the time series).

  As such, lake systems are temporally universal and spatially individualistic, whereby at any one time, the proportions of thinner and thinner, and thicker and thicker varves are on a "run", so the processes are the same, as indicated by the scaling signature. Whereas, the lack of spatial correlation indicates that these proportions are not the same in all lakes.

7.2 Future Work

There is much scope for future work based on the results of this study, but perhaps the two of particular interest, would firstly be to assess the validity of the proposed model for varve sedimentation based on random walk, critical phenomena, and multiscaling dynamics, by analysing a range of limnological time series, e.g., particle size, velocity, etc, and secondly to assess the nature of spatiotemporal correlation between lake systems, by analysing a range of other (palaeo)climatic parameters, e.g., tree rings, ice cores, etc.

Bibliography

[1] Von Bertalanffy, L. 1950 An outline of general systems theory. British Journal of Philosophical Science. 1 134-165.

[2] Von Bertalanffy, L. 1968 General Systems Theory. Braziller, New York. pp 289.

[3] Laszlo, E. 1972 Introduction to Systems Philosophy: Toward a Paradigm of Contemporary Thought. Harper and Row, New York. pp 328.

[4] Laszlo, E. 1997 The Systems View of the World: A Holistic Vision for Our Time. Hampton Press, New Jersey. pp 103.

[5] Nielsen, S.N. 2000 Thermodynamics of an ecosystem interpreted as a hierarchy of embedded systems. Ecological Modelling. 135 (2-3) 279-289.

[6] Li, B.-L. 2000 Why is the holistic approach becoming so important in landscape ecology? Landscape and Urban Planning. 50 (1-3) 27-41.

[7] Strahler, A.N. 1952 Dynamic basis for geomorphology. Geological Society America Bulletin. 63 117-142.

[8] Strahler, A.N. 1980 Systems theory in general geography. Physical Geography. 1 1-27.

[9] Chorley, R.J. 1962 Geomorphology and general systems theory. U.S. Geological Survey Professional Paper. 500-B 1-10.

[10] Scheidegger, A.E. 1992 Limitations of the system approach in geomorphology. Geomorphology. 5 (3-5) 213-217.

[11] Phillips, J.D. 1992 Nonlinear dynamical systems in geomorphology: Revolution or evolution. Geomorphology. 5 219-229.

[12] Dearing, J.A., and Zolitschka, B. 1999 System dynamics and environmental change: An exploratory study of Holocene lake sediments at Holzmaar, Germany. The Holocene. 9 (5) 531-540.

[13] Chorley, R.J. and Kennedy, B.A. 1971 Physical Geography. Prentice Hall, London. pp 370.

[14] Glansdorff, P., and Prigogine, I. 1971 Thermodynamics of Structure, Stability and Fluctuations. Wiley, New York. pp 126.

[15] Nicolis, G., and Prigogine, I. 1977 Self-Organization in Non-Equilibrium Systems. Wiley, New York. pp 491.

[16] Jorgensen, S.E., Mejer, H., Nielsen, S.N. 1998 Ecosystem as self-organizing critical systems. Ecological Modelling. 111 (2-3) 261-268.

[17] Sole, R.V., Manrubia, S.C., Benton, M., Kauffman, S., Bak, P. 1999 Criticality and scaling in evolutionary ecology. Trends in Ecology and Evolution. 14 (4) 156-160.

[18] O'Neill, R.V., De Angelis, D.L., Waide, J.B., Allen, T.H.F. 1986 A hierarchical concept of ecosystems. Monographs in Population Ecology 23. Princeton University Press. pp 262.

[19] Perry, D.A. 1995 Self-organising systems across scales. Trends in Ecology and Evolution. 10 (6) 241-244.

[20] Valentine, J.W., and May, C.L. 1996 Hierarchies in biology and paleontology. Palaeobiology. 22 (1) 23-33.

[21] Peterson, G.D. 2000 Scaling ecological dynamics: Self-organisation, hierarchical structure, and ecological resilience. Climatic Change. 44 (3) 291-309.

[22] Toussaint, O, Schneider, E.D. 1998 The thermodynamics and evolution of complexity in biological systems. Comparative Biochemistry and Physiology A. Molecular and Integrative Physiology. 120 (1) 3-9.

[23] Haken, H. 1978 Synergetics. Springer-Verlag, Berlin. pp 371.

[24] Prigogine, I. 1980 From Being to Becoming. W.H. Freeman and Co. San Francisco. pp 272.

[25] Haken, H. 1997 Visions of synergetics. International Journal of Bifurcation and Chaos. 7 (9) 1927-1951.

[26] Koestler, A. The Ghost in the Machine. Hutchinson, London. pp 203.

[27] White, I.D., Mottershead, D.N., Harrison, S.J. 1992 Environmental Systems: An Introductory Text. Chapman and Hall, London. pp 616.

[28] Schumm, S.A. 1979 Geomorphic thresholds: The concept and its application. Transactions of the Institute of British Geographers. 4 485-515.

[29] Coates, D.R., and Vitek, J.D. 1980 Perspectives on geologic thresholds. In: Thresholds in Geomorphology. Coates, D.R., and Vitek, J.D. (eds.). Allen and Unwin, Boston. pp 498.

[30] Chappell, J. 1983 Thresholds and lags in geomorphologic changes. Australian Geographer. 15 (6) 357-366.

[31] Dearing, J. Nonlinear environmental change and the lake sediment record. In prep.

[32] Allen, J.R.L. 1974 Reaction, relaxation and lag in natural sedimentary systems: General principles, examples and lessons. Earth Science Reviews. 10 263-342.

[33] Park, C. 2001 The Environment. Principles and Applications. Routledge, UK. pp 695.

[34] Dorlas, T.C. 1999 Statistical Mechanics: Fundamentals and Model Solutions. Institute of Physics, Bristol. pp 273.

[35] Ditlevsen, P.D. Characteristics of Natural Systems. In prep.

[36] http://www.endeav.org/evolut/text/denbig1/denbig1e.htm.

[37] Prigogine, I. 1955 Introduction to Thermodynamics of Irreversible Processes. Wiley, New York. pp 119.

[38] Eigen, M. 2000 Natural selection: a phase transition? Biophysical Chemistry. 85 (2-3) 101-123.

[39] Jorgensen, S.E., Patten, B.C., Straskraba, M. 2000 Ecosystems emerging: 4. Growth. Ecological Modelling. 126 (2-3) 249-284.

[40] Nicolis, C. 1995 Predictability of the atmosphere and climate: Towards a dynamical review. In: Space and Time Scale Variability and Interdependencies in Hydrological Processes. Feddes, R.A. (ed.). Cambridge University Press. pp 193.

[41] Gardiner, C.W. 1985 Handbook of Stochastic Methods. Springer-Verlag, Berlin. pp 442.

[42] Peixoto, J.P., and Oort, A.H. 1992 Physics of Climate. American Institute of Physics. pp 520.

[43] Kay, J.J., Regier, H.A., Boyle, M., Francis, G. 1999 An ecosystem approach for sustainability: Addressing the challenge of complexity. Futures. 31 (7) 721-742.

[44] Huggett, R.J. 1988 Dissipative systems: Implications for geomorphology. Earth Surface Processes and Landforms. 13 45-49.

[45] Lorenz, E.N. 1990 Can chaos and intransitivity lead to interannual variability? Tellus. 42A 378-389.

[46] Lorenz, E.N. 1969 The predictability of a flow which possesses many scales of motion. Tellus. 21 289-307.

[47] Yasunari, T., and Seki, Y. 1992 Role of the Asian monsoon on the interannual variability of the global climate system. Journal of the Meteorological Society of Japan. 70 (1B) 177-189.

[48] Paillard, D. 1998 The timing of Pleistocene glaciations from a simple multiple-state climate model. Nature. 391 378-381.

[49] May, R. M. 1972 Thresholds and break-points in ecosystems with a multiplicity of stable states. Nature. 269 471-477.

[50] Deevey, E. S. 1984 Stress, strain and stability of lacustrine ecosystems. In: Lake Sediments and Environmental History. Haworth, E.Y. and Lund, J.W.G., (eds.). Leicester University Press. pp 411.

[51] Tavakol, R.K. 1978 Is the sun almost intransitive? Nature. 276 802-803.

[52] Mearns, L.O., Katz, R.W., Schneider, S.H. 1984 Extreme high temperature events: Changes in their probabilities with changes in mean temperature. Journal of Climate and Applied Meteorology. 23 1601-1613.

[53] Katz, R.W., and Brown, B.G. 1992 Extreme events in a changing climate: Variability is more important than averages. Climatic Change. 21 289-302.

[54] Slaymaker, O., and Spencer, T. 1998 Physical Geography and Global Environmental Change. Longman, UK. pp 292.

[55] Brunsden, D. 2001 A critical assessment of the sensitivity concept in geomorphology. Catena 42 (2-4) 99-123.

[56] Clifford, N.J., and McClatchey, J. 1996 Identifying the timescales of environmental change: The instrumental record. In: Timescales and Environmental Change. Driver, T.S. and Chapman, G.P. (eds.). Routledge, London. pp 275.

[57] Meehl, G.A., Karl, T., Easterling, D.R., Changnon, S., Pielke, R., Changnon, D., Evans, J., Groisman, P.Y., Knutson, T.R., Kunkel, K.E., Mearns, L.O., Parmesan, C., Pulwarty, R., Root, T., Sylves, R.T., Whetton, P., Zwiers, F. 2000 An introduction to trends in extreme weather and climate events: Observations, socioeconomic impacts, terrestrial ecological impacts, and model projections. Bulletin of the American Meteorological Society. 81 (3) 413-416.

[58] Bradley, R.S. 1999 Palaeoclimatology: Reconstructing Climates of the Quaternary. Academic Press, San Diego. pp 610.

[59] Wanner, H., Rickli, R., Salvisberg, E., Schmutz, C.M., Schuepp, M. 1997 Global climate change and variability and its influence on alpine climate - concepts and observations. Theoretical and Applied Climatology. 58 221-243.

[60] Mandelbrot, B.B. 1982 The Fractal Geometry of Nature. W. H. Freeman and Co., San Francisco. pp 468.

[61] Davis, A., Marshak, A., Wiscombe, W., Cahalan, R. 1996 Scale invariance of liquid water distributions in marine stratocumulus. Part I: Spectral properties and stationarity issues. Journal of Atmospheric Sciences. 53 (11) 1538-1558.

[62] Bak, P., and Paczuski, M. 1995 Complexity, contingency, and criticality. Proceedings of the National Academy of Science. 92 6689-6696.

[63] Tsonis, A.A. 1998 Fractality in nature. Science. 279 1614-1615.

[64] Turcotte, D.L. 1994 Modelling geomorphic processes. Physica D. 77 (1-3) 229-237.

[65] Plotnick, R.E., and Prestegaard, K.L. 1995 Fractal and multifractal models and methods in stratigraphy. In: Fractals in Petroleum Geology and Earth Processes. Barton, C.G., and La Pointe, P.R. (eds.). Plenum Press, New York. pp 179.

[66] Stanley, H.E., Amaral, L.A.N., Buldyrev, S.V., Goldberger, A.L., Havlin, S., Leschhorn, H., Maass, P., Makse, H.A., Peng, C.K., Salinger, M.A., Stanley, M.H.R., Viswanathan, G.M. 1996 Scaling and universality in animate and inanimate systems. Physica A. A231 20-48.

[67] Turcotte, D. 1992 Fractals and Chaos in Geology and Geophysics. Cambridge University Press. pp 221.

[68] Koscielny-Bunde, E., Bunde, A., Havlin, S., Roman, H.E., Goldreich, Y., Schellnhuber, H.J. 1998 Indication of a universal persistence law governing atmospheric variability. Physical Review Letters. 81 (3) 729-732.

[69] Fox, C.G. 1989 Empirically derived relationships between fractal dimension and power law form frequency spectra. PAGEOPH. 131 (1-2) 211-239.

[70] Higuchi, T. 1990 Relationship between the fractal dimension and the power law index for a time series: a numerical investigation. Physica D. 46 254-264.

[71] Gomes da Silva, L.M., and Turcotte, D.L. 1994 A comparison between Hurst and Hausdorff measures derived from fractional time series. Chaos, Solutions and Fractals. 4 (12) 2181-2192.

[72] Vassilicos, J.C. 1993 Fractals in Turbulence. In: Wavelets, Fractals, and Fourier Transforms. Farge, M., Hunt, J.C.R., and Vassilicos, J.C. (eds). 325-341.

[73] Drummond, C.N. 1997 A persistent fractional noise model of stratigraphic organisation in turbidite successions. Recent Research Developments in Geology. 1 13-25.

[74] Schwarzacher, W. 2000 Repetitions and cycles in stratigraphy. Earth Science Reviews. 50 (1-2) 51-75.

[75] Janosi, I.M., and Vattay, G. 1992 Soft turbulent state of the atmospheric boundary layer. Physical Review A. 46 (10) 6386-6389.

[76] Talkner, P., and Weber, R.O. 2000 Power spectrum and detrended fluctuation analysis: Application to daily temperatures. Physical Review E. 62 (1) 150-160.

[77] Lovejoy, S., and Schertzer, D. 1986 Scale invariance in climatological temperatures and the local spectral plateau. Annales Geophysique. Series B. Terrestrial and Planetary Physics. 4 (4) 401-409.

[78] Pelletier, J.D. 1997 Analysis and modelling of the natural variability of climate. Journal of Climate. 10 1331-1342.

[79] Sonechkin, D.M. 1998 Climate dynamics as a nonlinear Brownian motion. International Journal of Bifurcation and Chaos. 8 (4) 799-803.

[80] Tsonis, A.A., Roebber, P.J., Elsner, J.B. 1998 A characteristic timescale in the global temperature record. Geophysical Research Letters. 25 2821-2823.

[81] Kiely, G., and Ivanova, K. 1999 Multifractal analysis of hourly precipitation. Physics and Chemistry of the Earth. Part B. Hydrology, Oceans and Atmosphere. 24 (7) 781-786.

[82] Tessier, Y., Lovejoy, S., Hubert, P., Schertzer, D., Pecknold, S. 1996 Multifractal analysis and modelling of rainfall and river flows and scaling, causal transfer functions. Journal of Geophysical Research. 101 (D21) 26,427-26,440.

[83] Fraedrich, K., and Larnder, C. 1993. Scaling regimes of composite rainfall time series. Tellus. 45A 289-298.

[84] Pelletier, J.D. and Turcotte, D.L. 1997 Long range persistence in climatological and hydrological time series: Analysis, modelling and application to drought hazard assessment. Journal of Hydrology. 203 198-208.

[85] Stephenson, D.B., Kumar, K.R., Doblas-Reyes, F.J., Royer, J.F., Chauvin, E., Pezzulli, S. 1999 Extreme daily rainfall events and their impact on ensemble forecasts of the Indian monsoon. Monthly Weather Review. 127 (9) 1954-1966.

[86] Sharma, T.C. 1996 Simulation of the Kenyan longest dry and wet spells and the largest rain-sums using a Markov model. Journal of Hydrology. 178 55-67.

[87] Lana, X., and Burgueno, A. 2000 Statistical distribution and spectral analysis of rainfall anomalies for Barcelona (NE Spain). Theoretical and Applied Climatology. 66 211-227.

[88] Bodri, L. 1993 Some long-run properties of climatic records. Fractals. 1 (3) 601-605.

[89] Duan, J.F., Selker, J., Grant, G.E. 1998 Evaluation of probability density functions in precipitation models for the Pacific Northwest. Journal of the American Water Resources. 34 (3) 617-627.

[90] Schmidt, G.M., Smajstrla, A.G., Zazueta, F.S. 1996 Parametric uncertainty in stochastic precipitation models: wet day. Transactions of the ASAE. 39 (6) 2093-2103.

[91] Vattay, G., and Harnos, A. 1994 Scaling behaviour in daily air humidity fluctuations. Physical Review Letters. 73 (5) 768-771.

[92] Tsonis, A.A., Roebber, P.J., Elsner, J.B. 1999 Long-range correlations in the extratropical atmospheric circulation: Origins and implications. Journal of Climate. 12 1534-1541.

[93] Oreopoulos, L., and Davies, R. 1998 Plane parallel albedo biases from satellite observations. Part II: Parameterisations for bias removal. Journal of Climate. 11 933-944.

[94] Khvorostyanov, V.I., and Curry, J.A. 1999 Toward the theory of stochastic condensation in clouds. Part II: Analytical solutions of the gamma-distribution type. Journal of the Atmospheric Science. 56 3997-4013.

[95] Andrade, J.S., Wainer, I., Filho, J.M., Moreira, J.E. 1995 Self-organised criticality in the El Nino Southern Oscillation. Physica A. 215 331-338.

[96] Alexander, M.A., and Penland, C. 1996 Variability in a mixed layer ocean model driven by stochastic atmospheric forcing. Journal of Climate. 9 (10) 2425-2442.

[97] Wunsch, C. 1999 The interpretation of short climate records, with comments on the North Atlantic and Southern Oscillations. Bulletin of the American Meteorological Society. 80 (2) 245-255.

[98] Cronise, R.J., Noever, D.A., Brittain, A. 1996 Self-organised criticality in closed ecosystems: Carbon dioxide fluctuations in Biosphere 2. International Journal of Climatology. 16 (5) 597-602.

[99] Ditlevsen, P.D., Svensmark, H., Johnsen, S. 1996 Contrasting atmospheric and climate dynamics of the last-glacial and Holocene periods. Nature. 379 810-812.

[100] Schmitt, F., Lovejoy, S., Schertzer, D. 1995 Multifractal analysis of the Greenland ice-core project climate data. Geophysical Research Letters. 22 (13) 1689-1692.

[101] Marsh, N.D., and Ditlevsen, P.D. 1997 Observation of atmospheric and climate dynamics from a high resolution ice core record of a passive tracer over the last glaciation Journal of Geophysical Research. 102 (D10) 11,219-11,224.

[102] Pandey, G., Lovejoy, S., Schertzer, D. 1998 Multifractal analysis of daily flows including extremes for basins of five to two million square kilometres, one day to 75 years. Journal of Hydrology. 208 62-81.

[103] Ivanov, S. 1996 Variability of sedimentary sequence: Numerical modelling of the deposition erosion process. Geologische Rundschau. 85 (1) 12-18.

[104] Stolum, H.H. 1991 A fractal index of reservoir heterogeneity. American Association of Petroleum Geologists. AAPG Bulletin. 75 (3) p 677.

[105] Diedrich, N.W., and Wilkinson, B.H. 1999 Depositional cyclicity in the Lower Devonian Helderberg Group of New York State. Journal of Geology. 107 (6) 643-658.

[106] Wilkinson, B.H., Diedrich, N.W., Drummond, C.N., Rothman, E.D. 1998 Michigan hockey, meteoric precipitation, and rhythmicity of accumulation on peritidal carbonate platforms. Geological Society of America Bulletin. 110 (8) 1075-1093.

[107] Wilkinson, B.H., Drummond, C.N., Rothman, E.D., Diedrich, N.W. 1997 Stratal order in peritidal carbonate sequences. Journal of Sedimentary Research. 67 (6) 1068-1082.

[108] Wilkinson, B.H., Diedrich, N.W., Drummond, C.N., Rothman, E.D. 1999 Poisson processes of carbonate accumulation on Palaeozoic and Holocene platforms. Journal of Sedimentary Research. 69 (2) 338-350.

[109] Drummond, C. N., and Wilkinson, B. H. 1993 Aperiodic accumulation of cyclic peritidal carbonate. Geology. 21 (11) 1023-1026.

[110] Hiscott, R., Coella, A., Perard, P., Lovell, M., Mancinverno, A 1992 Sedimentology of deep-water volcanic clastics, Oligocene Izu-Bonin forearc basin, based on formation microscanar images. In: Proceedings of the Ocean Drilling Program Scientific Results. Volume 126. College Station, Texas.

[111] Rothman, D.H., Grotzinger, J.P., Flemings, P. 1994 Scaling in turbidite deposition. Journal of Sedimentary Research. A64 (1) 59-67.

[112] Beattie, P.D., and Dade, W.B. 1996 Is scaling in turbidite deposition consistent with forcing by earthquakes? Journal of Sedimentary Research. 66 (5) 909-915.

[113] Winkler, W., and Gawenda, P. 1999 Distinguishing climatic and tectonic forcing of turbidite sedimentation, and the bearing on turbidite bed scaling: Palaeocene-Eocene of northern Spain. Journal of the Geological Society. 156 791-800.

[114] Rothman, D.H. and Grotzinger, J.P. 1995 Scaling properties of gravity-driven sediments. Nonlinear Processes in Geophysics. 2 178-185.

[115] Drummond, C.N. 1999 Bed-thickness structure of multi-sourced ramp turbidites: Devonian Brallier Formation, Central Appalacian Basin. Journal of Sedimentary Research. 69 (1) 115-121.

[116] Murray, C.J. 1996 Statistical analysis of bed thickness patterns in a turbidite section from the Great Valley Sequence, Cache Creek, Northern California. Journal of Sedimentary Research. 66 (5) 900-908.

[117] Talling, P. 2001 On the frequency distribution of turbidite thickness. In press.

[118] Hurst, H.E. 1951 Long-term storage capacity of reservoirs. Transactions of the American Society of Civil Engineers. 116 770-799.

[119] Mandelbrot, B.B., and Wallis, J.R. 1969 Some long-run properties of geophysical records. Water Resources Research. 5 (2) 321-340.

[120] Crowley, K.D., Duchon, C.E., Rhi, J. 1986 Climate record in varved sediments of the Eocene Green River Formation. Journal of Geophysical Research. 91 (D8) 8637-8647.

[121] Rittenour, T.M., Brigham-Grette, J., Mann, M.E. 2000 El Nino-like climate teleconnections in New England during the late Pleistocene. Science. 288 1039-1042.

[122] Kondolf, G.M., and Adhikari, A. 2000 Weibull vs. log-normal distributions for fluvial gravels. Journal of Sedimentary Research. 70 (3) 456-460.

[123] Richards, A., Phipps, P., Lucas, N. 2000 Possible evidence for underlying nonlinear dynamics in steep-faced glaciodeltaic progradational successions. Earth Surface Processes and Landforms. 25 1181-1200.

[124] Sly, P.G. 1978. Sedimentary processes in lakes. In: Lerman, A. (ed.), Lakes Chemistry, Geology, and Physics. Springer-Verlag, Berlin. pp 363.

[125] Hakanson, L., and Jansson, M. 1983. Principles of lake sedimentology. Springer-Verlag, Berlin. pp 316.

[126] Fritz, S. 1996 Palaeolimnological records of climatic change in North America. Limnology and Oceanography. 41 (5) 882-889.

[127] Talbot, M.R. and Allen, P.A. 1996 Lakes. In: Sedimentary Environments: Processes, Facies and Stratigraphy. Reading, H.G. (ed.). Blackwell Science, Oxford. pp 688.

[128] Spiegel, R.H., and Imberger, J. 1987 Mixing processes relevant to phytoplankton dynamics in lakes. New Zealand Journal of Marine and Freshwater Research. 21 (3) 361-377.

[129] Hostetler, S.W. 1995. Hydrological and thermal response of lakes to climate: Description and modelling. In: Physics and Chemistry of Lakes. Lerman, A., Imboden, D. and Gat, J. (eds.). Springer-Verlag, Berlin. pp 351.

[130] Weilenmann, U., O' Melia, C.R., Stumm, W., 1989 Particle transport in lakes: Models and measurements. Limnology and Oceanography. 34 (1) 1-18.

[131] O'Sullivan, P.E. 1983 Annually laminated lake sediments and the study of Quaternary environmental changes - a review. Quaternary Science Reviews. 1 245-313.

[132] Lotter, A.F., and Birks, H.J.B. 1997 The separation of the influence of nutrients and climate on the varve time series of Baldegersee, Switzerland. Aquatic Sciences. 59 (4) 362-375.

[133] Zolitschka, B. 1996 High resolution lacustrine sediments and their potential for palaeoclimatic reconstruction. In: Climatic Variations and Forcing Mechanisms of the Last 2000 years. Jones, P.D., Bradley, R.S and Jouzel, J., (eds.). NATO ASI Series Vol. 141. Springer-Verlag, Berlin. pp 649.

[134] Beer, J., and Sturm, M. 1995 Dating of lake and Loess sediments. Radiocarbon 37 (1) 81-86.

[135] Saarnisto, M. 1986 Annually laminated lake sediments. In: Handbook of Holocene Palaeoecology and Palaeohydrology. Berglund, B.E. (ed). Wiley and Sons, Chichester. pp 869.

[136] Renberg, I. 1982 Varved lake sediments - geochronological records of the Holocene. Geologiska Foreningens i Stockholm Forhandlingar. 104 275-279.

[137] Slawinski, D. 1998 Varved lake sediments of mid-western North America, indicators of cyclic climate change. Masters thesis. University of Minnesota. pp 122.

[138] Simola, H. 1990 Structural elements in varved lake sediments. laminated sediments. In: Geological Society of Finland, special paper 14. Saarnisto, M, and Kahra, A. (eds.). pp 113.

[139] Oldfield, F. 1983 Man's impact on the environment: Some recent perspectives. Geography. 68 245-256.

[140] Lamoureux, S. 2000 Five centuries of interannual sediment yield and rainfall-induced erosion in the Canadian High Arctic recorded in lacustrine varves. Water Resources Research. 36 (1) 309-318.

[141] Ohlendorf, C., Niessen, F., Weissert, H. 1997 Glacial varve thickness and 127 years of instrumental climate data: A comparison. Climatic Change. 36 391-411.

[142] Itkonen, A., and Salonen, V.P. 1994 The response of sedimentation in three varved lacustrine sequences to air temperature, precipitation and human impact. Journal of Paleolimnology. 11 323-332.

[143] Desolges, J.R. 1994 Varve deposition and the sediment yield record at three small lakes of the Southern Canadian Cordillera. Arctic and Alpine Research. 26 (2) 130-140.

[144] Hardy, D.R., Bradley, R.S., Zolitschka, B. 1996 The climatic signal in varved sediments from Lake C2, northern Ellesmere Island, Canada. Journal of Palaeolimnology. 16 227-238.

[145] Hughen, K.A., Overpeck, J.T., Anderson, R.F. 2000 Recent warming in a 500-year palaeotemperature record from varved sediments, Upper Soper Lake, Baffin Island, Canada. The Holocene. 10 (1) 9-19.

[146] Zolitschka, B. 1998 A 14,000 year sediment yield record from western Germany based on annually laminated sediments. Geomorphology. 22 1-17.

[147] Anderson, N.J., Odgaard, B.V., Segerstrom, U. Renberg, I. 1996 Climate-lake interactions recorded in varved sediments from a Swedish boreal forest lake. Global Change Biology. 2 399-405.

[148] Agterberg, F.P., and Banerjee, I. 1969 Stochastic model for the deposition of varves in glacial Lake Barlow-Ojibway, Ontario, Canada. Canadian Journal of Earth Sciences. 6 625-652.

[149] Shumway, R.H., and Verosub, K.L. 1992 State space modelling of palaeoclimatic time series. Abstracts Volume. 5th international meeting on statistical climatology. 139-144.

[150] Young. R., Walanus, A., Goslar, T. 2000 Auto-correlation analysis in search of short-term patterns in varve data from sediments of Lake Gosciaz, Poland. Boreas. 29 (3) 251-260.

[151] Personal Communications with Dr. Josef Merkt.

[152] Personal Communications with Dr. Heikki Simola.

[153] Personal Communications with Dr. Achim Brauer.

[154] Merkt, J., Muller, H., Knabe, W., Muller, P., Weiser, T. 1993 The early Holocene Saksunarvatn tephra found in lake sediments in NW Germany. Boreas. 22 93-100.

[155] Hajdas, I., Ivy, S.D., Beer, J., Bonani, G., Imboden, D., Lotter, A.F., Sturm, M., Suter, M. 1993 AMS radiocarbon dating and varve chronology of Lake Soppensee: 6000 to 12,000 C^{14} years BP. Climate Dynamics. 9 107-116.

[156] Pisias, N.G., and Mix, A.C. 1988 Aliasing of the geologic record and the search for long-period Milankovitch cycles. Palaeoceanography. 3 (5) 613-619.

[157] Sprenger, A., and ten Kate, W.G. 1993 Cross Spectral analysis of two late Berriasian rhythmic limestone-marl successions in SE Spain and SE France favours orbital control. Geologie en Mijnbouw. 72 69-83.

[158] Minobe, S. 1999 Resonance in bidecadal and pentadecadal climate oscillations over the North Pacific: Role in climatic regime shifts. Geophysical Research Letters. 26 (7) 855-858.

[159] Von Storch, H., and Zwiers, F. 1998 Statistical Analysis in Climate Research. Cambridge University Press. pp 425.

[160] Ditlevsen, P.D. 1999 A note on climate statistics and stochastic climate modelling. http://www.gfy.ku.dk/ pditlev/publications.html.

[161] Priestly, M.B. 1995 A short history of time series. In: Application of Time Series Analysis in Astronomy and Meteorology. Rao, T.S., Priestly, M.B., and Lessi, O. (eds.) Chapman and Hall, London. pp 350.

[162] Viswanathan, G.M., Afanasyev, V., Buldyrev, S.V., Murphy, E.J., Prince, P.A., Stanley, H.E. 1996 Levy flight search patterns of wandering albatrosses. Nature. 381 413-415.

[163] Feller, W. 1967 An Introduction to Probability Theory. Wiley, New York. pp 626.

[164] Acheson, D. 1997 From Calculus to Chaos. An Introduction to Dynamics. Oxford University Press. pp 269.

[165] Railsback, L.B. 1999 Evaluation of spacing of stylolites and its implications for self-organisation of pressure dissolution. Journal of Sedimentary Research. 68 (1) 2-7.

[166] Feder, J. 1991 Fractal time-series and fractional Brownian motion. In: Spontaneous Formation of Space-Time Structures and Criticality. Riste, T. and Sherrington, D. (eds.). Kluwer Acedemic Publishers. pp 446.

[167] Newman M 2000 Applied mathematics - The power of design. Nature. 405 412-413.

[168] Sarachik, E.S., Winton, M., Yin, F.L. 1996 Mechanisms for decadal-to-centenial climate variability. In: Decadal Climate Variability Dynamics and Predictability. Anderson, D.L.T., and Willebrand, J. (eds.). NATO ASI Series Vol I 44. Springer-Verlag, Berlin. pp 504.

[169] Dodds, P.S., and Rothman, D.H. 2000 Scaling, universality, and geomorphology. Annual Review of Earth and Planetary Sciences. 28 571-610.

[170] Hasselmann, K. 1976 Stochastic climate models Part I. Theory. Tellus. 28 (6) 473-484.

[171] Bak, P., Tang, C., and Wiesenfeld, K., 1987 Self-organised criticality: An explanation of 1/f Noise. Physical Review Letters. 59 (4) 381-384.

[172] Stanley, H.E. 2000 Scale Invariance and universality: Organizing principles in complex systems. Physica A. 281 60-68.

[173] Stolum, H.H. 1997 Fluctuations at the self-organised critical state. Physical Review E. 56 (6) 6710-6718.

[174] Marsan, D., Schertzer, D.N., Lovejoy, S. 1996 Causal space-time multifractal processes: Predictability and forecasting of rain fields. Journal of Geophysical Research. 101 (D21) 26,333-26,346.

[175] Plotnick, R.E., and Sepkoski, J.J. 2001 A multiplicative multifractal model for originations and extinctions. Palaeobiology. 27 (1) 126-139.

[176] Schertzer, D., and Lovejoy, S. 1997 Universal multifractals do exist!: Comments on "A statistical analysis of mesoscale rainfall as a random cascade". Journal of Applied Meteorology. 36 1296-1303.

[177] Ivanov, P.C., Amaral, L.A.N., Goldberger, A.L., Havlin, S., Rosenblum, M.G., Struzik, Z.R., Stanley, H.E. 1999 Multifractality in human heartbeat dynamics. Nature. 399 461-465.

[178] Mann, M.E., and Lees, J.M. 1996 Robust estimation of background noise and signal detection in climatic time series. Climatic Change. 33 409-445.

[179] Ruelle, D. 1989 Deterministic chaos: The science and the fiction. Proceedings of the Royal Society of London. 427 241-248.

[180] Nicolis, G., and Deams, D. 1998 Probabilistic and thermodynamic aspects of dynamical systems. Chaos. 8 (2) 311-320.

[181] Chatfield, C. 1996 The Analysis of Time Series. Chapman and Hall, London. pp 283.

[182] http://stommel.tamu.edu/ baum/paleo/ocean/node10.html.

[183] Takens, F. 1981 Detecting strange attractors in fluid turbulence In: Dynamical Systems and Turbulence, Warwick. D., Rand, D., and Young, L.-S. (eds.). Springer-Verlag, Berlin. pp 366.

[184] Schwarzacher, W. 1993. Cyclostratigraphy and the Milankovitch Theory. Developments in Sedimentology 52. Elsevier, Amsterdam. pp 225.

[185] Tsonis, A.A., and Elsner, J.B. 1989 Chaos, strange attractors, and weather. Bulletin of the American Meteorological Society. 70 (1) 14-23.

[186] May, R.M. 1976 Simple mathematical models with very complicated dynamics. Nature. 261 459-467.

[187] Sornette, D. 1998 Linear stochastic dynamics with nonlinear fractal properties. Physica A. 250 (1-4) 295-314.

[188] Stone, L., and Ezrati, S. 1996 Chaos, cycles and spatiotemporal dynamics in plant ecology. Journal of Ecology. 84 279-291.

[189] Parthasarathy, S., and Guemez, J. 1998 Synchronisation of chaotic metapopulations in a cascade of coupled logistic map models. Ecological Modelling. 106 (1) 17-25.

[190] Jin, F.-F., Neelin, J.D., Ghil, M. 1994 El Nino on the devil's staircase: Annual subharmonic steps to chaos. Science. 264 70-72.

[191] Tziperman, E., Stone, L., Cane, M., Jarosh, H. 1994 El Nino chaos: Overlapping of resonances between the seasonal cycle and the Pacific ocean-atmosphere oscillator. Science. 264 72-74.

[192] Rial, J.A., and Anaclerio, C.A. 2000 Understanding nonlinear responses of the climate system to orbital forcing. Quaternary Science Reviews. 19 (17-18) 1709-1722.

[193] Prokoph, A., Fowler, A.D., Patterson, R.T. 2001 Evidence for periodicity and nonlinearity in a high resolution fossil record of long-term evolution. Geology 28(10) 867-870.

[194] Rohani, P., Miramontes, O., Hassell, M.P. 1994 Quasiperiodicity and chaos in population models. Proceedings of the Royal Society of London. Part B. Biological Sciences. 258 (1351) 17-22.

[195] Sornette, D. 2000 Critical Phenomena in Natural Sciences. Chaos, Fractals, Self-organisation and Disorder: Concepts and Tools. Springer-Verlag, Heidelberg. pp 432.

[196] Main, I.G., Leonard, T., Papasouliotis, O., Hatton, C.G., Meredith, P.G. 1999 One slope or two? Detecting statistically significant breaks of slope in geophysical data, with application to fracture scaling relationships. Geophysical Research Letters. 26 (18) 2801-2804.

[197] Latif, M., and Barnett, T.P. 1994 Causes of decadal climate variability over the North Pacific and North America. Science. 266 634-637.

[198] Grotzner, A., Latif, M., Barnett, T.P. 1998 A decadal climate cycle in the North Atlantic ocean as simulated by the ECHO coupled GCM. Journal of Climate. 11 (5) 831-847.

[199] Wang, J.F., Bras, R.L., Entekhabi, D. 1997 Structure in fluctuations of large-scale soil moisture climate due to external random forcing and internal feedbacks. Stochastic Hydrology and Hydraulics. 11 (2) 95-114.

[200] Rodriguez-Iturbe, I., D'Odorico, P., Rinaldo, A. 1998 Possible self-organising dynamics for land-atmosphere interaction. Journal of Geophysical Research. 103 (D18) 23,071-23,077.

[201] Manabe, S., and Stouffer, R.J. 1997 Climate variability of a coupled ocean-atmosphere-land surface model: Implication for the detection of global warming. Bulletin of the American Meteorological Society. 78 (6) 1177-1185.

[202] Popper, K. R. 1990 A World of Propensities. Thoemass, Bristol. pp 51.

[203] Malard, F., Tockner, K., Ward, J.V. 2000 Physico-chemical heterogeneity in a glacial riverscape. Landscape Ecology. 15 (8) 679-695.

[204] Szilagyi, J., and Parlange, M.B. 1999 A geomorphology-based semi-distributed watershed model. Advances in Water Resources. 23 (2) 177-187.

[205] Stout, J.E., and Zobeck, T.M. 1997 Intermittent saltation. Sedimentology. 44 (5) 959-970.

[206] Deidda, R. 1999 Multifractal analysis and simulation of rainfall fields in space. Physics and Chemistry of the Earth. Part B. Hydrology, Oceans and Atmosphere. 24 (1-2) 73-78.

[207] Hamels, I., Sabbe, K., Muylaert, K., Barranguet, C., Lucas, C., Herman, P., and Vyverman, W. 1998 Organisation of microbenthic communities in intertidal estuarine flats, a case study from the Molenplaat (Westerschelde estuary, The Netherlands). European Journal of Protistology. 34 (3) 308-320.

[208] Rojo, C., Ortega-Mayagoitia, E., Rodrigo, M.A., Alvarez-Cobelas, M. 2000 Phytoplankton structure and dynamics in a semiarid wetland, the National Park "Las Tablas de Daimiel" (Spain). Archiv Fur Hydrobiologie. 148 (3) 397-419.

[209] Rasmussen, J.B., Rowan, D.J. 1997 Wave velocity thresholds for fine sediment accumulation in lakes, and their effect on zoobenthic biomass and composition. Journal of the North American Benthological Society. 16 (3) 449-465.

[210] Weitz, D.A. 1997 Diffusion in a different direction. Nature. 390 233-234.

[211] Tory, E.M. 2000 Stochastic sedimentation and hydrodynamic diffusion. Chemical Engineering. 80 (1-3) 81-89.

[212] Lick, W., Huang, H., Jespen, R. 1993 Flocculation of fine-grained sediments due to differential settling. Journal of Geophysical Research. 98 (C6) 10,279-10,288.

[213] Bloesch, J., and Wehrli, B. 1995. Formation of natural sediment records. EAWAG news. 38 E 10-12.

[214] Yiantsios, S.G., Karabelas, A.J. 1998 The effect of gravity on the deposition of micron-sized particles on smooth surfaces. International Journal of Multiphase Flow. 24 (2) 283-293.

[215] Miguel, M.C., and Pastor-Satorras, R. 2001 Velocity fluctuations and hydrodynamic diffusion in sedimentation. Europhysics Letters. 54 (1) 45-50.

[216] Gbah, M.B., Rao, Y.R., Murthy, R.C. 2001 Turbulent exchange characteristics in the hypolimnon layer of Lake Ontario. Nordic Hydrology. 32 (1) 13-28.

[217] Saggio, A., and Imberger., J. 2001 Mixing and turbulent fluxes in the metalimnon of a stratified lake. Limnology and Oceanography. 46 (2) 392-409.

[218] Livingstone, D.M. 1991 The diel oxygen cycle in three subaloine Swiss streams. Archiv Fur Hydrobiologie. 120 (4) 457-479.

[219] Ramanathan, V., Callis, L., Cess, R., Hansen, J., Isaksen, I., Kuhn, W., Lacis, A., Luther, F., Mahlman, J.D., Reck, R., Schlesinger, M. 1987 Climate-chemical interactions and effects of changing atmospheric trace gases. Reviews of Geophysics. 25 (7) 1441-1482.